STRUCTURE AND CHEMISTRY OF SULFUR TETRAFLUORIDE

JAMES T. GOETTEL
B.Sc., University of Alberta, 2011

A Thesis
Submitted to the School of Graduate Studies
of the University of Lethbridge
in Partial Fulfilment of the
Requirements for the Degree
MASTER OF SCIENCE

Department of Chemistry and Biochemistry
University of Lethbridge
LETHBRIDGE, ALBERTA, CANADA

ABSTRACT

Sulfur tetrafluoride was shown to be a useful reagent in preparing salts of $Re^{VII}O_2F_4^-$, $I^{V}OF_4^-$, and $I^{VII}O_2F_4^-$. Sulfur tetrafluoride reacts with oxo-anions in acetonitrile or anhydrous HF (aHF) via fluoride-oxide exchange reactions to quantitatively form oxide fluoride salts, as observed by Raman and ^{19}F NMR spectroscopy. Pure $Ag[ReO_2F_4]$ as well as the new CH_3CN coordination compounds $[Ag(CH_3CN)_2][ReO_2F_4]$ and $[Ag(CH_3CN)_4][ReO_2F_4]\bullet CH_3CN$ were prepared. The latter was characterized by single-crystal X-ray diffraction. The reaction of $[N(CH_3)_4]IO_3$ with SF_4 in acetonitrile gave the new $[N(CH_3)_4][IOF_4]$ salt.

Sulfur tetrafluoride forms Lewis acid-base adducts with pyridine and its derivatives, i.e., 2,6-dimethylpyridine, 4-methylpyridine and 4-dimethylaminopyridine, which have recently been identified in our lab. In the presence of HF, the nitrogen base in the SF_4 base reaction systems is protonated, which can formally be viewed as solvolysis of the SF_4•base adducts by HF. The resulting salts have been studied by Raman spectroscopy and X-ray crystallography. Crystal structures were obtained for pyridinium salts: $[HNC_5H_5^+]F^-\bullet SF_4$, $[HNC_5H_5^+]F^-[HF_2^-]\bullet 2SF_4$; 4-methylpyridinium salt: $[HNC_5H_4(CH_3)^+]F^-\bullet SF_4$, $[HNC_5H_4(CH_3)^+][HF_2^-]$; 2,6-dimethylpyridinium salt: $[HNC_5H_3(CH_3)_2^+]_2[SF_5^-]F^-\bullet SF_4$; 4-dimethylaminopyridinium salts: $[HNC_5H_4N(CH_3)_2^+]_2[SF_5^-]F^-\bullet CH_2Cl_2$, $[NC_5H_4N(CH_3)_2^+][HF_2^-]\bullet 2SF_4$; and the 4,4'-bipyridinium salts: $[HNH_4C_5{-}C_5H_4N^+]F^-\bullet 2SF_4$, $[HNH_4C_5{-}C_5H_4NH^{2+}]2F^-\bullet 4SF_4$. These structures exhibit a surprising range of bonding modalities between SF_4 and fluoride and provide an extensive view of SF_4 in the solid state.

For the first time, the solid-state structure of SF_4 was elucidated by single-crystal X-ray diffraction. The structure can best be described as a network with weak intermolecular S---F contacts formed exclusively by the axial fluorines that exhibit more ionic character. A similar structural motif was found in the novel $[HNC_5H_3(CH_3)_2^+]_2[SF_5^-]F^-\bullet 4SF_4$ salt which contains layers of SF_4.

Adduct formation of SF_4 with oxygen-bases was observed for the first time. These $SF_4\bullet$*O*-base adducts ($SF_4\bullet OC_4H_8$, $SF_4\bullet(OC_4H_8)_2$, $SF_4\bullet(CH_3OCH_2)_2$, $SF_4\bullet(O{=}C_5H_8)_2$) were synthesized, isolated, and characterized at low temperatures. The structures were elucidated by X-ray crystallography and Raman spectroscopy. The characterization of the $SF_4\bullet$ketone adduct ($SF_4\bullet O{=}C_5H_4$) is of great significance, since SF_4 can serve as a fluorinating agent towards carbonyl groups. These adducts offer the first extensive view of dative O---S(IV) bonds.

ACKNOWLEDGEMENTS

I would like to thank my supervisor, Prof. Michael Gerken, for his superior mentorship during the past few years. Michael always provided me with the highest quality equipment and reagents, and gave me the freedom to explore a wide range of chemistry. His expertise, enthusiasm, dedication, and overall professionalism made him the ultimate supervisor for me.

I would like to thank the other members of my committee, Prof. Paul Hayes and Prof. Paul Hazendonk, for taking the time out of their busy schedules, especially considering the time commitment associated with newborns!

I would like to thank my external examiner, Prof. Jennifer Love, for traveling a great distance for my defence, and for her time spent reviewing my Thesis.

I am grateful to Kris and Heinz Fischer for all their hard work in maintaining our instruments and especially for fixing the X-ray diffractometer. I am grateful to Tony Montina for fixing the NMR spectrometer.

I would like to thank all the members of the Gerken group, Praveen, Tyler, Rudy, Nathan, and Doug, for support and friendship in and outside of the lab. Special thanks to Nathan, who helped with the research presented in Chapter 4 and was a pleasure to supervise.

Thank you to the members of the Hayes group, for unofficially adopting me as one of their own. Special thanks to Breanne Kamenz, who made this adoption possible and for keeping me well informed and to Kevin Johnson for his helpful advice.

I would like to thank my friends for the fun and enjoyment that contributed to my great work-life balance.

I wish to thank my girlfriend, Boram Kim, for emotional support, care and companionship.

Finally I would like the thank my family and my parents, Mark Goettel and Karen Toohey, who have provided financial support, insightful advice, and a loving and caring environment.

TABLE OF CONTENTS

1 Introduction 1

1.1 Sulfur Fluorides 1

1.2 Sulfur Tetrafluoride Chemistry 7

1.2.1 Lewis-Acid and Fluoride-Ion Donor Properties 7

1.2.2 Sulfur Tetrafluoride as Reagent in Organic Chemistry. 9

1.3 Sulfur Fluoride Substituents in Organic and Inorganic Chemistry 13

1.3.1 Pentafluorosulfonyl Substituent, SF_5 13

1.3.2 SF_x (x = 2-4) 15

1.3.3 Sulfur Fluorides as Ligands in Transition Metal Chemistry 16

1.4 Goals of Present Research 17

2 Experimental 28

2.1 General Methods 28

2.2 Purification and Preparation of Starting Materials 31

2.2.1 Purification of Anhydrous HF, SF_4, Acetonitrile 31

2.2.2 Oxo-Anions Salts 32

2.2.3 Nitrogen Bases 32

2.2.4 Purification of Toluene, Diethyl Ether, Pentane, THF 33

2.2.5 Purification of CH_2Cl_2, $CFCl_3$, CF_2Cl_2 33

2.3 Preparation of Oxide Fluoride Salts 33

2.3.1 Preparation of $[Ag(CH_3CN)_x][ReO_2F_4]$ where (x = 0, 2, 4) 33

2.3.2 Preparation of $KReO_2F_4$ 34

2.3.3 Preparation of $K[IO_2F_4]$ 34

2.3.4 Preparation of $[N(CH_3)_4][IOF_4]$ 35

2.4 Preparation of Hydrolysis Products of SF_4•Nitrogen Base Adducts by HF 36

2.4.1 Preparation of $[HNC_5H_5^+]F^-$•SF_4 36

2.4.2 Preparation of $[HNC_5H_5^+][HF_2^-]$•$2SF_4$ 36

2.4.3 Preparation of $[HNC_5H_4(CH_3)^+]F^-$•SF_4 37

2.4.4 Preparation of $[HNC_5H_3(CH_3)_2^+]_2[SF_5^-]F^-$•$SF_4$ 37

2.4.5 Preparation of $[HNC_5H_4N(CH_3)_2^+][HF_2^-]$•$2SF_4$ 38

2.4.6 Preparation of $[HNC_5H_4N(CH_3)_2^+]_2[SF_5^-]F^-$•$CH_2Cl_2$ 38

2.4.7 Preparation of $[HNH_4C_5{-}C_5H_4N^+]F^-$•$2SF_4$ 39

2.4.8 Preparation of $[HNH_4C_5{-}C_5H_4NH^{2+}]2F^{-}{\bullet}4SF_4$ 39
2.4.9 Crystal Structure of $[HNC_5H_4(CH_3)^{+}]HF_2^{-}$ 40
2.5 Solid-State Structure of SF_4 40
2.5.1 Synthesis of $[HNC_5H_3(CH_3)_2^{+}]_2F^{-}[SF_5^{-}]{\bullet}4SF_4$ 40
2.5.2 X−Ray Crystallography of Neat SF_4 41
2.5.3 X−Ray Crystallography of SF_4 from CF_2Cl_2 41
2.6 SF_4 Oxygen Base Adducts 41
2.6.1 Preparation of the $SF_4{\bullet}OC_4H_6$ Adduct 41
2.6.2 Preparation of the $SF_4{\bullet}(OC_4H_6)_2$ Adduct 42
2.6.3 Preparation of the $SF_4{\bullet}(CH_3OCH_2)_2$ Adduct 42
2.6.4 Preparation of the $SF_4{\bullet}(O{=}C_5H_8)_2$ 43
2.6.5 Attempted Preparation of $SF_4{\bullet}OEt_2$ 43
2.6.6 Attempted Preparation of SF_4•acetylacetone 43
2.6.7 Attempted Preparation of SF_4•4-methylcyclohexanone 43
2.7 Single Crystal X-ray Diffraction 44
2.7.1 Low-Temperature Crystal Mounting 44
2.7.1.1 Special Cases 45
2.7.2 Data Collection 46
2.7.3 Solution and Refinement of Structures 46
2.7.3.1 Special Cases 48
2.8 Vibrational Spectroscopy 49
2.9 NMR Spectroscopy 49
3 Sulfur Tetrafluoride as a Fluorinating Agent Towards Main-Group and Transition-Metal Oxo-Anions. 51
3.1 Introduction 51
3.2 Results and Discussion 53
3.2.1 Synthesis 53
3.2.2 $[Ag(CH_3CN)_4][ReO_2F_4]{\bullet}CH_3CN$, $[Ag(CH_3CN)_x]ReO_2F_4$ (where x = 0, 2) 54
3.2.2.1 Raman Spectroscopy 54
3.2.2.2 X-ray Crystallography 58
3.2.3 $K[IO_2F_4]$ 62

3.2.3.1 X-ray Crystallography 63
3.2.4 $[N(CH_3)_4][IOF_4]$ 63
3.2.4.1 Raman Spectroscopy 63
3.3 Summary and Conclusions 66
4 Solvolysis Products of SF_4•Nitrogen Base Adducts by HF 69
4.1 Introduction 69
4.2 Results and Discussion 70
4.2.1 General Synthetic Approach 70
4.2.2 Pyridine-HF-SF_4 System 73
4.2.2.1 X−ray Crystal Structures of $[HNC_5H_5^+]F^-$•SF_4 and $[HNC_5H_5^+]HF_2^-$•$2SF_4$. 73
4.2.2.2 Raman Spectroscopy 80
4.2.3 4-Methylpyridine-HF-SF_4 System 83
4.2.3.1 X−ray Crystal Structures of $[HNC_5H_4(CH_3)^+]F^-$•SF_4 and $[HNC_5H_4(CH_3)^+]HF_2^-$ 83
4.2.3.2 Raman Spectroscopy 87
4.2.4 2,6-Dimethylpyridine-HF-SF_4 System 89
4.2.4.1 X-ray Crystal Structure of $[HNC_5H_3(CH_3)_2^+]_2[SF_5^-]F^-$•$SF_4$ 90
4.2.4.2 Raman Spectroscopy 94
4.2.5 The 4-Dimethylaminopyridine-HF-SF_4 System 95
4.2.5.1 X−ray Crystal Structures of $[HNC_5H_4N(CH_3)_2^+][HF_2^-]$•$2SF_4$ and $[HNC_5H_4N(CH_3)_2^+]_2[SF_5^-]F^-$•$CH_2Cl_2$ 95
4.2.5.2 Raman Spectroscopy 102
4.2.6 The 4,4'-Bipyridyl-HF-SF_4 System 107
4.2.6.1 X−ray Crystal Structures of $[HNH_4C_5{-}C_5H_4N^+]F^-$•$2SF_4$ and $[HNH_4C_5{-}C_5H_4NH^{2+}]2F^-$•$4SF_4$ 107
4.2.6.2 Raman Spectroscopy 114
4.3 Summary and Conclusion 118
5 Structure of Sulfur Tetrafluoride in the Solid State 123
5.1 Introduction 123

5.2 Results and Discussion 125
5.2.1 $[HNC_5H_3(CH_3)_2^+]_2[SF_5^-]F^- \bullet 4SF_4$ 125
5.2.1.1 X-ray crystallography 126
5.2.1.2 Raman Spectroscopy 133
5.2.2 Solid State Structure of SF_4 136
5.3 Summary and Conclusion 140
6 Sulfur Tetrafluoride Oxygen-Base Adducts 143
6.1 Introduction 143
6.2 Results and Discussion 143
6.2.1 Synthesis and Properties 143
6.2.2 Crystal Structure of $SF_4 \bullet OC_4H_6$ and $SF_4 \bullet (OC_4H_6)_2$ 147
6.2.3 Raman Spectroscopy of $SF_4 \bullet OC_4H_6$ and $SF_4 \bullet (OC_4H_6)_2$ 153
6.2.4 Crystal Structure of $SF_4 \bullet (CH_3OCH_2)_2$ 157
6.2.5 Raman Spectroscopy of $SF_4 \bullet (CH_3OCH_2)_2$ 160
6.2.6 Crystal Structure of $SF_4 \bullet (O{=}C_5H_8)_2$ 163
6.2.7 Raman Spectroscopy of $SF_4 \bullet (O{=}C_5H_8)_2$ 166
6.3 Summary and Conclusion 170
7 Summary and Directions for Future Work 175
7.1 Conclusions 175
7.2 Directions for Future Work 176

LIST OF FIGURES

Figure 1 ^{19}F NMR assignment of $FSSF_3$.....2
Figure 1.2 The structures of the lower sulfur fluorides: SF_2, SF_3SF, FSSF, and SSF_2..3
Figure 1.3 The structures of the higher sulfur fluorides: SF_4, SF_6, and S_2F_{10}. 4
Figure 1.4 The structures of some common fluorinating agent replacements for SF_4.10
Figure 2.1 Glass vacuum line system equipped with J. Young PTFE/glass stopcocks, a Heise gauge (Adapted from Jared Nieboer's M.Sc. Thesis).....29
Figure 2.2 Metal vacuum system; (A) MKS type 626A capacitance manometer (0-1000 Torr), (B) MKS Model PDR-5B pressure transducers (0-10 Torr), (C) 3/8-in. stainless-steel high-pressure valves (Autoclave Engineers, 30VM6071), (D) 316 stainless-steel cross (Autoclave Engineers, CX6666), (E) 316 stainless-steel L-piece (Autoclave Engineers, CL6600), (F) 316 stainless steel T-piece (Autoclave engineers, CT6660), (G) 3/8-in o.d., 1/8-in. i.d. nickel connectors, (H) 1/8-in o.d., 1/8-in. i.d. nickel tube. (from Jared Nieboer's M.Sc. thesis).....30
Figure 2.3 Low-temperature crystal mounting setup, consisting of a 10.5-L Dewar, equipped with a foam stopper, a glass nitrogen inlet, a silvered glass cold nitrogen outlet with an 11-cm long aluminum trough (2-cm o.d.). (Adapted from Jared Nieboer's M.Sc. thesis).....45
Figure 3.1 Raman spectra of $AgReO_2F_4$ salts with varying amounts of CH_3CN. 55
Figure 3.2 Thermal ellipsoid plot of $[Ag(CH_3CN)_4][ReO_2F_4]\bullet CH_3CN$. Thermal ellipsoids are set to 50% probability.....61
Figure 3.3 Raman spectrum of $[N(CH_3)_4][IOF_4]$. Asterisks (*) denote bands arising from the FEP sample tube. Daggers (†) denote bands arising from the $[N(CH_3)_4^+]$ cation.....64
Figure 4.1 Drawings of the nitrogen-bases studied with SF_4/HF mixtures. 72
Figure 4.2 Thermal ellipsoid plot of the $[HNC_5H_5^+]F^-\bullet SF_4$ chain with thermal ellipsoids set to 50% probability.....77
Figure 4.3 Thermal ellipsoid plot of the $[HNC_5H_5^+][HF_2^-]\bullet 2SF_4$ double chain. The fluorines bound to S(1A), S(2A) and S(1B) are omitted for clarity. Thermal ellipsoids are set to 50% probability. 78
Figure 4.4 Raman spectrum of $[HNC_5H_5^+][HF_2^-]\bullet 2SF_4$. Asterisks (*) denote bands arising from the FEP sample tube.....81

Figure 4.5 Thermal ellipsoid plot of the dimer present in the crystal structure of $[HNC_5H_4(CH_3)^+]F^-•SF_4$. Thermal ellipsoids are at 50% probability. 86
Figure 4.6 Thermal ellipsoid plot of the $[HNC_5H_4(CH_3)^+]HF_2^-$ ion pair. Thermal ellipsoids are at 50% probability.....87
Figure 4.7 Raman spectrum of $[HNC_5H_4(CH_3)^+]F^-•SF_4$. Asterisks (*) denote bands arising from the FEP sample tube.....89
Figure 4.8 Thermal ellipsoid plot of $[HNC_5H_3(CH_3)_2^+]_2F^-•SF_4[SF_5^-]$; a) the $[HNC_5H_3(CH_3)_2^+]_2F^-•SF_4$ moiety and b) the disordered SF_5^- anion. Thermal ellipsoids are at 50% probability.....93
Figure 4.9 Thermal ellipsoid plot of the $[HNC_5H_4N(CH_3)_2^+][HF_2^-]•2SF_4$ double chain. Thermal ellipsoids are at 50% probability. 99
Figure 4.10 Thermal ellipsoid plot of $[HNC_5H_4N(CH_3)_2^+]_2[SF_5^-]F^-•CH_2Cl_2$, excluding the SF_5^- anion. Thermal ellipsoids are at 50% probability. 101
Figure 4.11 Thermal ellipsoid plot of the SF_5^- anion in $HNC_5H_4N(CH_3)_2^+]_2[SF_5^-]F^-•CH_2Cl_2$. Thermal ellipsoids set at 50% probability. ...102
Figure 4.12 Raman spectrum of $[HNC_5H_4N(CH_3)_2^+][HF_2^-]•2SF_4$. Asterisks (*) denote bands arising from the FEP sample tube.....103
Figure 4.13 Raman spectrum of $[HNC_5H_4N(CH_3)_2^+]_2[SF_5^-]F^-•CH_2Cl_2$. Asterisks (*) denote bands arising from the FEP sample tube.....103
Figure 4.14 Thermal ellipsoid plot of $[HNH_4C_5–C_5H_4N^+]F^-•2SF_4$ Thermal ellipsoids are at 50% probability.....110
Figure 4.15 Thermal ellipsoid plot of $[HNH_4C_5–C_5H_4NH^{2+}]2F^-•4SF_4$ with thermal ellipsoids set at 50% probability.....112
Figure 4.16 Thermal ellipsoid plot of $[HNH_4C_5–C_5H_4NH^{2+}]2F^-•4SF_4$ packed along the *c*-axis. Thermal ellipsoids are set to 50% probability.....113
Figure 4.17 Raman spectra of $[HNH_4C_5–C_5H_4N^+]F^-•2SF_4$ (top) and $[HNH_4C_5–C_5H_4NH^{2+}]2F^-•4SF_4$ (bottom). Asterisks (*) denote bands arising from the FEP sample tube. 115
Figure 5.1 Proposed structures of SF_4 from reference 9.....124
Figure 5.2 Thermal ellipsoid view along the *a*-axis of the packing of $[HNC_5H_3(CH_3)_2^+]_2F^-[SF_5^-]•4SF_4$. Thermal ellipsoids are set at 50 % probability. ..129
Figure 5.3 Thermal ellipsoid plot of the $[HNC_5H_3(CH_3)_2^+]_2F^-$---$SF_4$ moiety. Thermal ellipsoids are set at 50 % probability. 130

Figure 5.4 Thermal ellipsoid plot of the SF_5^- anion in $[HNC_5H_3(CH_3)_2^+]_2F^-[SF_5^-]\bullet 4SF_4$. Thermal ellipsoids are set at 50 % probability. ..130
Figure 5.5 Thermal ellipsoid plot of the coordination environment about the SF4 molecules in the X-ray crystal structure of $[HNC_5H_3(CH_3)_2^+]2F^-[SF_5^-]\bullet 4SF_4$; thermal ellipsoids are drawn at the 50% probability level. 132
Figure 5.6 Raman spectra of (a) $[HNC_5H_3(CH_3)_2^+]_2F^-[SF_5^-]\bullet 4SF_4$ in FEP tubing and (b) of solid SF_4 in a Pyrex glass 5-mm NMR tube recorded at –100 °C and –135 °C, respectively, using 1064-nm excitation. Asterisks (*) denote signals arising from the FEP sample tube. Bands attributed to the 2,6-dimethylpyridinium cation and to the SF_5^- anion are denoted by (†) and (§), respectively. 136
Figure 5.7 Thermal Ellipsoid Plot of the asymmetric unit of SF_4. Thermal Ellipsoids are set to 50% probability. 137
Figure 5.8 Thermal Ellipsoid Plot of the TeF_4 chain. Thermal ellipsoids are set at 50% probability. 139
Figure 5.9 Thermal ellipsoid plot of SeF_4, showing contacts to adjacent SeF_4 molecules. Thermal ellipsoids are set to 50% probability. 140
Figure 6.1 Structures of the oxygen-bases that form Lewis acid-base adducts with SF_4. 144
Figure 6.2 Structure of Oxygen-bases that were studied and for which no SF_4 adducts could be isolated. 146
Figure 6.3 Thermal ellipsoid plot of the $(SF_4\bullet OC_4H_6)_2$ dimer; thermal ellipsoids are set at 50% probability. 150
Figure 6.4 Thermal ellipsoid plots of the four crystallographically unique $SF_4\bullet(OC_4H_8)_2$ moieties within the asymmetric unit. 152
Figure 6.5 Raman spectra of a) $SF_4\bullet OC_4H_6$, b) $SF_4\bullet(OC_4H_6)_2$, and c) OC_4H_6 (room temperature). Asterisks (*) denote bands arising from the FEP sample tube. 154
Figure 6.6 Thermal ellipsoid plot of the $SF_4\bullet(CH_3OCH_2)_2$ adduct; thermal ellipsoids are set at 50% probability. 158
Figure 6.7 View along the *c*-axis of the thermal ellipsoid plot of $SF_4\bullet(CH_3OCH_2)_2$. Thermal ellipsoids set at 50% probability. 159
Figure 6.8 Raman Spectrum of $SF_4\bullet(CH_3OCH_2)_2$ (top) and neat 1,2-dimethoxyethane (bottom). Asterisks (*) denote bands arising from the FEP sample tube. 161

Figure 6.9 Thermal ellipsoid plot of the SF_4•$(O=C_5H_8)_2$ adduct; thermal ellipsoids are set at 50% probability. 165
Figure 6.10 Raman spectra of SF_4•$(O=C_5H_8)_2$ (top) and neat cyclopentanone ($O=C_5H_8$) (bottom). Asterisks (*) denote bands arising from the FEP sample tube. 167

LIST OF TABLES

Table 1.1 Properties of the known sulfur fluorides. 7
Table 2.1 X-ray Crystal Structures and Selected Acquisition Parameters. 48
Table 3.1 Raman Frequencies (cm^{-1}) and Tentative Assignments of $[Ag(CH_3CN)_4]$-ReO_2F_4•CH_3CN, $[Ag(CH_3CN)_2]ReO_2F_4$, $AgReO_2F_4$, and CH_3CN. 56
Table 3.2 Crystal Data Collection Parameters and Results of $[Ag(CH_3CN)_4][ReO_2F_4]$•CH_3CN. 59
Table 3.3 Selected Bond Lengths (Å) and Angles (deg.) of $[Ag(CH_3CN)_4][ReO_2F_4]$•CH_3CN. 60
Table 3.4 Raman Frequencies (cm^{-1}) and Tentative Assignments of $[N(CH_3)_4][IOF_4]$. 65
Table 4.1 Crystal Data Collection Parameters and Results of $[HNC_5H_5^+]F^-$•SF_4 and $[HNC_5H_5^+]HF_2^-$•$2SF_4$ 74
Table 4.2 Bond Lengths (Å), Contacts (Å), and Angles (deg.) of $[HNC_5H_5^+]F^-$•SF_4. 75
Table 4.3 Bond Lengths (Å), Contacts (Å), and Angles (deg.) of $[HNC_5H_5^+][HF_2^-]$•$2SF_4$. 76
Table 4.4 Raman Frequencies (cm^{-1}) and Tentative Assignments of $[HNC_5H_5^+][HF_2^-]$•$2SF_4$. 82
Table 4.5 Crystal Data Collection Parameters and Results of $[HNC_5H_4(CH_3)^+]F^-$•SF_4 and $[HNC_5H_4(CH_3)^+][HF_2^-]$. 84
Table 4.6 Bond Lengths (Å), Contacts (Å), and Angles (deg.) of $[HNC_5H_4(CH_3)^+]F^-$•SF_4. 85
Table 4.7 Bond Lengths (Å), Contacts (Å), and Angles (deg.) of $[HNC_5H_4(CH_3)^+]HF_2^-$. 85
Table 4.8 Raman Frequencies (cm^{-1}) and Tentative Assignments of $[HNC_5H_4(CH_3)^+]F^-$•SF_4. 88
Table 4.9 Crystal Data Collection Parameters and Results of $[HNC_5H_3(CH_3)_2^+]_2[SF_5^-]F^-$•$SF_4$. 91

Table 4.10 Bond Lengths (Å), Contacts (Å), and Angles (deg.) of $[HNC_5H_3(CH_3)_2^+]_2[SF_5^-]F^-\bullet SF_4$. 92
Table 4.11 Crystal Data Collection Parameters and Results of $[HNC_5H_4N(CH_3)_2^+][HF_2^-]\bullet 2SF_4$ and $[HNC_5H_4N(CH_3)_2^+]_2[SF_5^-]F^-\bullet CH_2Cl_2$. 96
Table 4.12 Selected Bond Lengths (Å), Contacts (Å), and Angles (deg.) of $[HNC_5H_4N(CH_3)_2^+][HF_2^-]\bullet 2SF_4$ 97
Table 4.13 Selected Bond Lengths (Å), Contacts (Å), and Angles (deg.) of $[HNC_5H_4N(CH_3)_2^+]_2[SF_5^-]F^-\bullet CH_2Cl_2$ 98
Table 4.14 Raman Frequencies (cm^{-1}) and Tentative Assignments of $[HNC_5H_4N(CH_3)_2^+][HF_2^-]\bullet 2SF_4$. 104
Table 4.15 Raman Frequencies (cm^{-1}) and Tentative Assignments of $[HNC_5H_4N(CH_3)_2^+]_2[SF_5^-]F^-\bullet CH_2Cl_2$. 105
Table 4.16 Crystal Data Collection Parameters and Results of $[HNH_4C_5{-}C_5H_4N^+]F^-\bullet 2SF_4$ and $[HNH_4C_5{-}C_5H_4NH^{2+}]2F^-\bullet 4SF_4$ 108
Table 4.17 Selected Bond Lengths (Å), Contacts (Å), and Angles (deg.) of $[HNH_4C_5{-}C_5H_4N^+]F^-\bullet 2SF_4$. 109
Table 4.18 Selected Bond Lengths (Å), Contacts (Å), and Angles (deg.) of $[HNH_4C_5{-}C_5H_4NH^{2+}]2F^-\bullet 4SF_4$. 109
Table 4.19 Raman Frequencies (cm^{-1}) and Tentative Assignments of $[HNH_4C_5{-}C_5H_4N^+]F^-\bullet 2SF_4$. 116
Table 4.20 Raman Frequencies (cm^{-1}) and Tentative Assignments of $[HNH_4C_5{-}C_5H_4NH^{2+}]2F^-\bullet 4SF_4$. 118
Table 5.1 Crystal Data Collection Parameters and Results of $[HNC_5H_3(CH_3)_2^+]_2[SF_5^-]F^-\bullet 4SF_4$ and SF_4. 127
Table 5.2 Selected Bond Lengths (Å), Contacts (Å), and Angles (deg.) of $[HNC_5H_3(CH_3)_2^+]2F^-[SF_5^-]\bullet 4SF_4$ 128
Table 5.3 Experimental Raman frequencies and Tentative Assignments for $[HNC_5H_3(CH_3)_2^+]_2F^-[SF5^-]\bullet_4SF_4$. 134
Table 5.4 Bond Lengths (Å), Contacts (Å), and Angles (deg.) of SF_4. 138
Table 6.1 Crystal Data Collection Parameters and Results of $SF_4\bullet OC_4H_8$, $SF_4\bullet(OC_4H_8)_2$, $SF_4\bullet(CH_3OCH_2)_2$, and $SF_4\bullet O{=}C_5H_8$ 147

Table 6.2 Selected Bond Lengths (Å), Contacts (Å), and Angles (°) of SF_4•OC_4H_6. 148
Table 6.3 Selected Bond Lengths (Å), Contacts (Å), and Angles (°) of SF_4•$(OC_4H_6)_2$. 149
Table 6.4 Raman Frequencies (cm^{-1}) and Tentative Assignments of SF_4•OC_4H_6, OC_4H_6, and SF_4. 155
Table 6.5 Raman Frequencies (cm^{-1}) and Tentative Assignments of SF_4•$(OC_4H_6)_2$, OC_4H_6, and SF_4. 156
Table 6.6 Selected Bond Lengths (Å), Contacts (Å), and Angles (°) of SF_4•$(CH_3OCH_2)_2$ 158
Table 6.7 Raman Frequencies (cm^{-1}) and Tentative Assignments of SF_4•$(CH_3OCH_2)_2$, $(CH_3OCH_2)_2$, and SF_4 162
Table 6.8 Selected Bond Lengths (Å), Contacts (Å), and Angles (°) of SF_4•$(O{=}C_5H_8)_2$ 164
Table 6.9 Raman Frequencies (cm^{-1}) and Tentative Assignments of SF_4•$(O{=}C_5H_8)_2$ (−107 °C), $O{=}C_5H_8$, and SF_4 168
Table 6.10 Selected Structural and Vibrational Data in isolated SF_4•*O*-Base Adducts. 172

LIST OF ABREVIATIONS AND SYMBOLS

General

ax	axial
eq	equatorial
FEP	copolymer of perfluoroethylene and perfluoropropylene
Kel-F	chlorotrifluoroethylene
NMR	nuclear magnetic resonance
THF	tetrahydrofuran
DFT	density functional theory
o.d.	outside diameter
Ph	phenyl
VSEPR	valence shell electron pair repulsion
aHF	anhydrous hydrogen fluoride
PTFE	polytetrafluoroethylene

Nuclear Magnetic Resonance

δ	chemical shift
J	scalar coupling constant in Hertz
ppm	parts per million
TMS	tetramethylsilane
T	tesla

X-ray Crystallography

a, b, c,α, β, γ	cell parameters
V	cell volume
λ	wavelength
Z	molecules per unit cell
μ	absorption coefficient
R_1	conventional agreement index
wR_2	weighted agreement index
GooF	goodness of fit

1 Introduction

1.1 Sulfur Fluorides

Sulfur forms several binary fluorides, namely SF_2, F_3SSF, S_2F_2, SF_4, SF_6 and S_2F_{10}.[1] All of these sulfur fluorides can be prepared by direct combination of elemental sulfur with elemental fluorine at varying concentrations and temperatures.[1] Due to the high reactivity, low boiling points, and/or difficulties in handling these compounds, extensive computational studies have been reported to elucidate the molecular geometries and to fully understand the electronic structures.[2-6] Sulfur difluoride and disulfur difluoride are thermally unstable and remain laboratory curiosities.[1] Sulfur difluoride is only stable as a highly dilute gas,[7] and exists as dimeric SF_3SF in the liquid and solid state.[8] Sulfur difluoride is prepared by the reaction of SCl_2 vapour with metal fluorides (AgF, KF, HgF_2) at high temperatures (150 to 160 °C) under vacuum (<10 Torr) (see Equation 1.1.1).[9]

$$SCl_2 + HgF_2 \rightarrow SF_2 + HgCl_2 \qquad (1.1.1)$$

The bent geometry (see Figure 1.2) of the monomer was determined by gas-phase infrared[7] and microwave[10] spectroscopy, and matrix-isolation vibrational spectroscopy.[11] The four ^{19}F NMR spectroscopic signals of $FSSF_3$ (see Figure 1.1) in the liquid phase at −53.2 (F_1), −5.7 (F_2), 26.3 (F_3), and 204.1 (F_4) ppm ($^2J_{12}$ = 86.3, $^2J_{13}$ = 32.8, $^2J_{23}$ = 32.2, $^3J_{14}$ = 40.2, $^3J_{24}$ = 156.0, and $^3J_{34}$ = 63.5 Hz) confirmed the existence of the asymmetric dimer, as well as determined the connectivity of the atoms.[8,12]

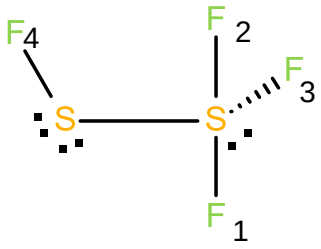

Figure 1.1 ^{19}F NMR spectroscopic assignment of $FSSF_3$

An electron diffraction study provided bond lengths and angles of F_3SSF (see Figure 1.2).[13] The dimer decomposes above −75 °C into sulfur tetrafluoride, S_8, and other allotropes of sulfur (see Equation 1.1.2).

$$F_3SSF \rightarrow SF_4 + {}^{1}/_{n}\, S_n \qquad (1.1.2)$$

Small amounts of HF can catalyze the decomposition of F_3SSF into SF_4 and FSSF instead of SF_4 and elemental sulfur (see Equation 1.1.3a and 1.1.3b).[1]

$$SF_3SF + HF \rightarrow SF_4 + HSF \qquad (1.1.3a)$$

$$SF_2 + HSF \rightarrow FSSF + HF \qquad (1.1.3b)$$

Disulfur difluoride exists as two isomers, difluorosulfane (FSSF) and thiothionyl fluoride (SSF_2), with SSF_2 being the more stable isomer at room temperature. Both isomers are prepared in a similar fashion to sulfur difluoride except disulfur dichloride (ClSSCl) is used in place of sulfur dichloride and a temperature range of 120 to 165 °C is used (see Equation 1.1.4).[14]

$$ClSSCl + MF \rightarrow S_2F_2 + MCl \quad (\text{where M = Ag, K, Hg}) \qquad (1.1.4)$$

At higher temperatures (165 °C), SSF_2 is the main product. An alternative method of preparing disulfur difluoride is by the reaction of nitrogen trifluoride with elemental sulfur (see Equation 1.1.5).[15]

$$NF_3 + {}^{3}/_{8}\, S_8 \rightarrow S_2F_2 + NSF \qquad (1.1.5)$$

The structures of FSSF and SSF_2 were elucidated using a combination of microwave,[16] infrared,[11] and ^{19}F NMR[8] spectroscopies (see Figure 1.2).

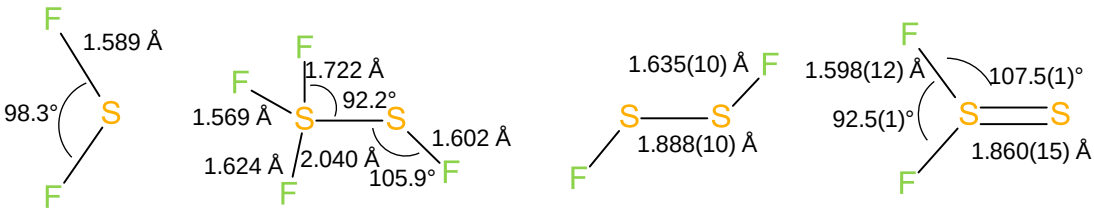

Figure 1.2 The structures of the lower sulfur fluorides: SF_2, SF_3SF, FSSF, and SSF_2

Sulfur tetrafluoride, sulfur hexafluoride and disulfur decafluoride have been commercially available, but in recent times, only sulfur hexafluoride is easily obtainable. Sulfur tetrafluoride is a highly toxic and reactive gas at room temperature. It is a selective fluorinating agent, which has been used extensively in organic chemistry (see Section 1.2.2). In contrast to the lower sulfur fluorides, sulfur tetrafluoride is thermally stable up to very high temperatures (500 to 1000 °C), with only 1% being converted to SF_6 (see Equation 1.1.6) in this temperature range.[17]

$$3\ SF_4 \quad \rightleftharpoons \quad 2\ SF_6 + S \qquad (1.1.6)$$

Sulfur tetrafluoride exhibits a disphenoidal (seesaw) molecular geometry in the gas and liquid phases (see Figure 1.3). The structure has been well studied in the gas phase by electron diffraction,[18,19] microwave,[20] infrared,[21-23] and ^{19}F NMR[24] spectroscopies and has been the subject of computational studies.[4,5] The structure in the liquid phase has been studied by variable temperature ^{19}F NMR,[4] Raman, and infrared spectroscopy.[25] Significantly less information has been reported on the structure in the solid state.[26] Using miniature zone-melting techniques, the crystal

structure of SF_4 has previously been reported to be severely disordered and no discernible structure could be determined.[27]

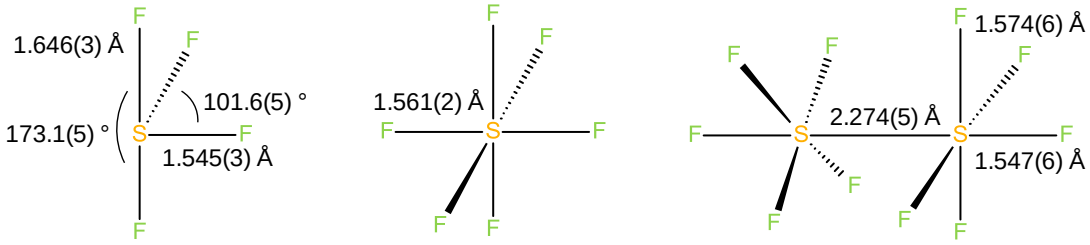

Figure 1.3 The structures of the higher sulfur fluorides: SF_4, SF_6, and S_2F_{10}.

Sulfur tetrafluoride can be prepared by fluorination of elemental sulfur suspended in $CFCl_3$ at −78 °C with 100% elemental fluorine[28] or by direct fluorination of molten sulfur between 120 to 200 °C with 10% fluorine in nitrogen.[29] It can also be conveniently prepared in the laboratory by reaction of SCl_2 and Cl_2 with metal fluorides, such as NaF, KF, CoF_2, between 200 and 300 °C (see Equation 1.1.7).[30]

$$SCl_2 + Cl_2 + 4\ NaF \rightarrow SF_4 + 4\ NaCl \quad (1.1.7)$$

Sulfur tetrafluoride is extremely moisture sensitive and reacts with water producing HF and thionyl fluoride (see Equation 1.1.8). Thionyl fluoride can further react with water to produce HF and sulfur dioxide (see Equation 1.1.9).

$$SF_4 + H_2O \rightarrow 2\ HF + SOF_2 \quad (1.1.8)$$

$$SOF_2 + H_2O \rightarrow 2\ HF + SO_2 \quad (1.1.9)$$

Hydrogen fluoride can readily be separated from SF_4 by distillation at low temperatures (<−80 °C) and by the use of HF scavengers (NaF), but the reactivity,

melting point (−100 °C), and boiling point of SOF_2 (−44 °C) and SF_6 (−50 °C sublimation) make their separation from SF_4 difficult. One method of purifying SF_4 is by the formation of adducts with Lewis acids (BF_3) (see Equation 1.1.10), removal of SOF_2 and SF_6 from the solid adduct, and then substitution of SF_4 with a base such as diethyl ether (see Equation 1.1.11).[31]

$$SF_4 + BF_3 \rightarrow SF_3BF_4 \quad (1.1.10)$$

$$SF_3BF_4 + Et_2O \rightarrow Et_2O{\bullet}BF_3 + SF_4 \quad (1.1.11)$$

Sulfur hexafluoride is an extremely inert and dense gas at room temperature. Inhalation of SF_6 depresses the vibrational frequency of one's voice, as opposed to the well-known effect of helium, which increases the vibrational frequency of one's voice. Although SF_6 is non-toxic, it can sometimes contain toxic impurities (e.g. S_2F_{10}), therefore inhalation of SF_6 is not recommended. Due to the high density of the gas, light objects, such as aluminum boats, can float on gaseous SF_6. Approximately 8,000 tons of SF_6 is produced annually (2000), and approximately 75% of the annual production is used as dielectric gas in the electric power industry and an inert gas for the magnesium industry.[32] Although sulfur hexafluoride is generally inert, it can react with lithium generating large amounts of heat, which have been used in closed Rankine-cycle propulsion systems (see Equation 1.1.12).[33]

$$SF_6 + 8\ Li \rightarrow Li_2S + 6\ LiF \quad (1.1.12)$$

Sulfur hexafluoride has octahedral geometry (see Figure 1.3) and has extensively been characterized by Raman,[34,35] infrared,[35-37] photoelectron,[38] and ^{19}F NMR[39] spectroscopies and by electron[40] and neutron[41-43] diffraction techniques.

Disulfur decafluoride is a moisture stable, volatile, extremely toxic liquid at room temperature, and had been considered for use as a war gas in WWII.[44] Under

exclusion of moisture and air, it can be stored at room temperature. In 1934 it was isolated and its basic physical properties and reactivity were characterized.[45] Disulfur decafluoride slowly decomposes above 150 °C into SF_4 and SF_6 in a two-step mechanism (see Equation 1.1.12a/b).[46]

$$S_2F_{10} \rightleftharpoons 2\ SF_5\ (\text{fast}) \qquad (1.1.12a)$$

$$2SF_5 \rightleftharpoons SF_6 + SF_4\ (\text{slow}) \qquad (1.1.12b)$$

Disulfur decafluoride is obtained as a by-product of SF_6 synthesis. It can be prepared in the laboratory by photolysis of SF_5Br[47] (Equation 1.1.13) or by photochemical reduction of SF_5Cl (Equation 1.1.14) with H_2 gas.[48]

$$2\ SF_5Br \rightleftharpoons S_2F_{10} + Br_2 \qquad (1.1.13)$$

$$2\ SF_5Cl + H_2 \rightleftharpoons S_2F_{10} + HCl \qquad (1.1.14)$$

The structure of disulfur decafluoride was initially characterized by infrared spectroscopy.[49] In 1953, an electron diffraction study of the gas provided the metric parameters.[50] In 1989, a reinvestigation of the gas-phase structure of S_2F_{10} by electron diffraction revised the bond lengths.[51] Infrared,[52] Raman,[52] and ^{19}F NMR[53] spectroscopy have since been used to characterize liquid S_2F_{10}. Despite the fact that disulfur decafluoride is a liquid at room temperature and freezes at a moderate temperature of −53 °C, there is a dearth of information reported on its structural characterization in the solid state. Infrared and Raman spectroscopy were performed on the neat solid[54] at liquid nitrogen temperatures and matrix-isolation vibrational spectroscopy was performed on the solid in an argon matrix at 8 K.[55] Computational chemistry has been used to determine the electronic structure[56] and thermochemistry[57] of S_2F_{10} as well as structural properties[58] of the potential anion, $S_2F_{11}^-$.

Table 1.1 Properties of the known sulfur fluorides.

	SF_2	F_3SSF	FSSF	SSF_2	SF_4	SF_6	S_2F_{10}
m.p. (°C)	−	−	−133	−164.6	−121.5	−63.9	−53
b.p. (°C)	−	−75[a] (decomp.)	15	−10.6	−40.4	−50.8	30
Δ_fH_{298} (kJ/mol)[a]	−21.6	−	−349	−385	−46.3	−48.6	−1903[c]
Vap. Press. (atm)	−	−	1.46[d]	3.47[e]	9.52	21.8	0.888
^{19}F (ppm) gas[b]	−167	54.9 7.0 −24.7 −211.1	−128.8	77.8	93 34.2	54.9	54.0
^{19}F (ppm) liquid[b]	−	53.2 5.7 −26.3 −204.1	−123.2	79.0	88.4 34.1	53.2	51.5 to 56.5

[a] From: Seel, F. *Advan. Inorg. Chem. Radiochem.* **1974**, *16*, 297-333.
[b] From: Gombler, W.; Schaebs, J.; Willner, H. *Inorg. Chem.* **1990**, *29*, 2697-2698.
[c] From: Irikura, K. K. *J. Chem. Phys.* **1995**, *103*, 10162-10168.
[d] From: Brown, R.; Burden, F.; Pez, G. *Chem. Commun.* **1965**, 277b-278.
[e] From: Seel, F.; Budenz, R. *Chem. Ber.* **1965**, *98*, 251-258.

1.2 Sulfur Tetrafluoride Chemistry

1.2.1 Lewis-Acid and Fluoride-Ion Donor Properties

Sulfur tetrafluoride can act as a fluoride-ion donor towards strong Lewis acids forming SF_3^+ salts (see Equation 1.2.1/1.2.2).

$$SF_4 + AF_5 \rightarrow SF_3^+AF_6^- \quad \text{(where A = P, As, Sb, Pt, Ir, Os)} \qquad (1.2.1)$$

$$SF_4 + BF_3 \rightarrow SF_3^+BF_4^- \qquad (1.2.2)$$

Robinson and Bartlett first reported the reaction of SF_4 with the Lewis acids, BF_3, PF_5, AsF_5 and SbF_5 and suggested a simple Lewis acid-base interaction between sulfur and the Lewis acid.[59,60] Cotton and George reported that such an interaction through the sulfur was unlikely, and the compounds were either fluorine-

bridged or ionic.[61] Gillespie *et al.* characterized the BF_3, PF_5, AsF_5 and SbF_5 adducts using Raman, infrared, and ^{19}F NMR spectroscopy, and conductivity measurements.[62] The Raman and infrared spectra contained signals associated with SF_3^+ and the respective anions (BF_4^-, PF_6^-, AsF_6^-, and SbF_6^-). Conductivity measurements of SF_3BF_4 and SF_3SbF_6, in anhydrous HF solvent, gave similar values as their respective potassium salts, indicating the presence of ionic species in solution. The low-temperature ^{19}F NMR spectra exhibited two distinct resonances, attributable to the SF_3^+ cation and the counter anion. All their data support the ionic model.[62] Crystal structures of SF_3BF_4,[63] SF_3AsF_6,[63] and $SF_3(HF)SbF_6$,[64] have since been reported. Two sulfur tetrafluoride molecules can react with one GeF_4 molecule to form the $(SF_3)_2GeF_6$ salt, which was also characterized by X-ray crystallography.[65] In these crystal structures, the SF_3^+ cation adopts a trigonal pyramidal geometry and has three contacts with fluorides on the anion (S---$FGeF_5^{2-}$ = 2.420(1)[x2] and 2.367(2) Å; S---FBF_3^- = 2.593(3) and 2.624(2)[x2] Å). Sulfur tetrafluoride reacts with the sulfonyl hypohalites, ($ClOSO_2F$, $BrOSO_2F$, and $ClOSO_2CF_3$), to form thermally unstable $[SF_3^+][FSO_3^-]$ and $[SF_3^+][CF_3SO_3^-]$ salts and the covalently bonded *cis*/*trans*-$SF_4(Cl)OSO_2F$ and *trans*-$SF_4(Cl)OSO_2CF_3$ compounds, as shown by Raman and ^{19}F NMR spectroscopy.[66]

Sulfur tetrafluoride can act as a Lewis acid towards fluoride. It can accept a fluoride from strong fluoride-ion donors such as $[N(CH_3)_4]F$ and CsF, forming the SF_5^- anion (see Equation 1.2.3).[67,68]

$$SF_4 + CsF \quad \rightarrow \quad Cs^+SF_5^- \qquad (1.2.3)$$

These salts dissociate into SF_4 and their respective fluoride salt when heated. The vapour pressure of SF_4 above $[N(CH_3)_4]SF_5$ is 2-3 Torr at 25 °C, 7 Torr at 38 °C and

19 Torr at 60 °C.[67] The Rb^+ and Cs^+ salts of the SF_5^- anion have since been characterized by vibrational spectroscopy, and the SF_5^- anion has been studied by computational means.[69-71] The crystal structures of $Rb[SF_5]$,[69] $Cs_6[SF_5]_4[HF_2]_2$,[69] and $[Cs(18\text{-crown-}6)_2][SF_5]$[72] have confirmed the expected square pyramidal geometry of the SF_5^- anion. The structures, however, exhibit relatively large uncertainties in bond lengths (Rb^+ and Cs^+ salts) and are disordered ($[Cs(18\text{-crown-}6)_2^+]$.

The Lewis acidity of SF_4 towards nitrogen bases was first reported by Muetterties *et al.* in 1959, suggesting the formation of adducts with pyridine and triethylamine.[31,73] This claim was based on crude vapour pressure measurements, mass balance and ^{19}F NMR spectroscopy data. In a matrix-isolation study it was claimed that the formation of 1:1 adducts occurred between SF_4 and ammonia, pyridine, acetone, and methylamine.[74] Recently, SF_4 adducts with pyridine,[75] 4-methylpyridine,[75] 2,6-dimethylpyridine,[75] and triethylamine[76] were unambiguously characterized by Raman spectroscopy, computational studies, and ^{19}F NMR spectroscopy (see Equation 1.2.4).[64]

$$SF_4 + N(C_2H_5)_3 \rightleftharpoons SF_4{\bullet}N(C_2H_5)_3 \qquad (1.2.4)$$

Crystal structures of $SF_4{\bullet}NC_5H_5$,[75] $SF_4{\bullet}NC_5H_5(CH_3)$,[75] $SF_4{\bullet}NC_5H_5(N(CH_3)_2$,[75] and $SF_4{\bullet}N(C_2H_5)_3$[76] provided the experimental geometries and metric parameters for these adducts.

1.2.2 Sulfur Tetrafluoride as Reagent in Organic Chemistry.

In organic chemistry, sulfur tetrafluoride has been used to convert OH, C=O, and COOH groups into CF, CF_2, and CF_3 groups, respectively.[77] These reactions are generally carried out in high-pressure stainless-steel autoclaves. Depending on the

reactivity of the substrate, reaction temperatures ranging from −78 to 300 °C have been employed. In recent years the use of sulfur tetrafluoride has declined due to the difficulties associated with handling this gaseous and toxic compound. Replacements include diethylaminosulfur trifluoride (DAST),[78] Ishikawa's reagent,[79] and aminodifluorosulfinium salts[80] (see Figure 1.4).

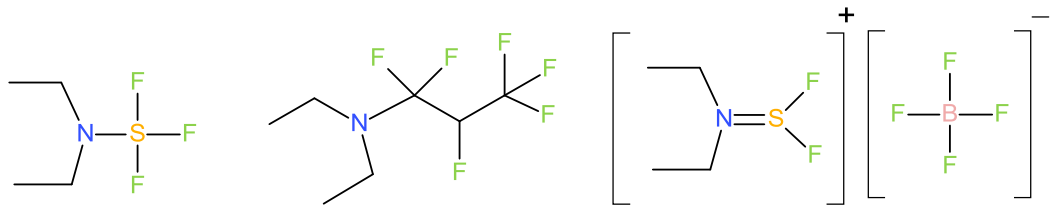

Figure 1.4 The structures of some common fluorinating agent replacements for SF_4.

Sulfur tetrafluoride generally requires catalytic or sometimes molar equivalents of HF for fluorination reactions to occur.[81] Traces of HF are inevitably present in the reaction mixture due to hydrolysis of SF_4 by moisture. Spectral and conductivity investigations of SF_4 in anhydrous HF solvent suggest the existence of ionic species SF_3^+ and HF_2^-, in SF_4/HF systems (see Equation 1.2.5) .[62]

$$SF_4 + HF \quad \rightleftharpoons \quad SF_3^+ + HF_2^- \qquad (1.2.5)$$

The currently accepted mechanism for the reaction of SF_4 with carbonyl groups involves the electrophilic attack of the oxygen atom by the SF_3^+ cation to form an oxygen-sulfur bonded intermediate.[1] This intermediate undergoes intramolecular rearrangement and eliminates thionyl fluoride to give the fluorocarbenium ion, which can then be attacked by bifluoride to generate CF_2 and regenerate HF (Equation 1.2.6).

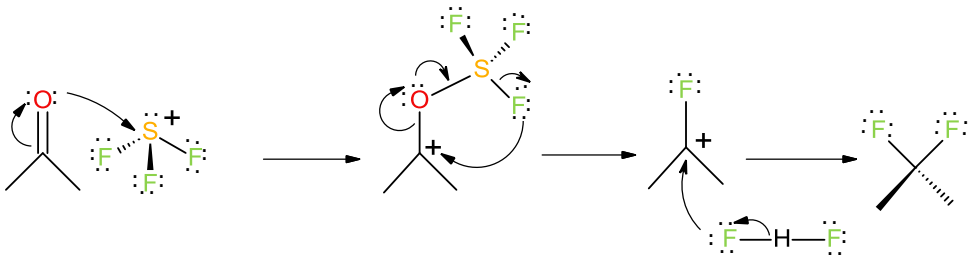

(1.2.6)

The fluorocarbenium ion can electrophilically attack the oxygen on a second carbonyl compound which leads to the formation of fluoroethers as by-products.[82] The fluorocarbenium cation can be trapped with aromatic hydrocarbons in the reaction of SF_4 with haloacids. For example, the reaction of SF_4 with $CHCl_2COOH$ in the presence of p-xylene affords $ArCF_2CH_2Cl$[83] and haloacetones.[84]

The reaction of SF_4 with substrates containing hydroxyl groups, is generally much faster than substrates containing carbonyl groups. The proposed mechanism for the reaction of SF_4 with hydroxyl groups involves the formation of the alkoxysulfur trifluoride (Equation 1.2.7), which can then act as a fluoride-ion donor towards HF to form $ROSF_2^+$ (Equation 1.2.8), containing the excellent leaving group, OSF_2. The $ROSF_2^+$ then undergoes a substitution reaction with fluoride (or bifluoride) (Equation 1.2.9). Dmowski *et al.* suggest the mechanism can either be S_N1 in the case of structures that form carbenium ions, or S_N2 in primary or secondary alkyl compounds,[85,86] whereas Baum *et al.* propose an internal (S_Ni) displacement mechanism.[87]

$$ROH + SF_3^+ \rightarrow ROSF_3 + H^+ \quad (1.2.7)$$

$$ROSF_3 + HF \rightarrow ROSF_2^+ + HF_2^- \quad (1.2.8)$$

$$ROSF_2^+ + F^- \rightarrow RF + SOF_2 \quad (1.2.9)$$

Certain fluorination reactions require the addition of hydrogen fluoride scavengers (MF, organic nitrogen bases) in the reaction mixture. For example, tertiary amides react with SF_4 in the presence of trace HF yielding acyl or aryl fluorides and trifluoromethyl compounds, by undergoing N−C bond cleavage. In the presence of a HF scavenger, the fluorination of the carbonyl group proceeds with good yields (see Equation 1.2.10).[88]

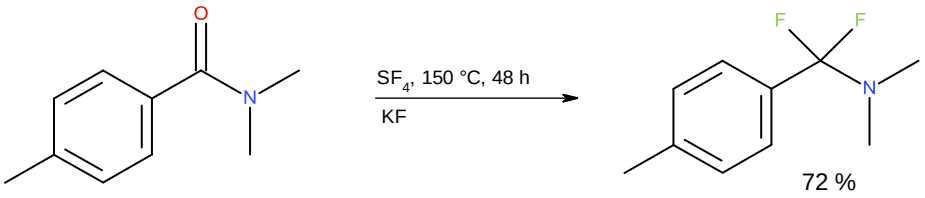

(1.2.10)

Alkyl alcohols, with a non-fluorinated aromatic substituent, react with SF_4 to give polymerized products. In the presence of triethylamine or pyridine, the fluorination of the hydroxyl group takes place (Equation 1.2.11).[89]

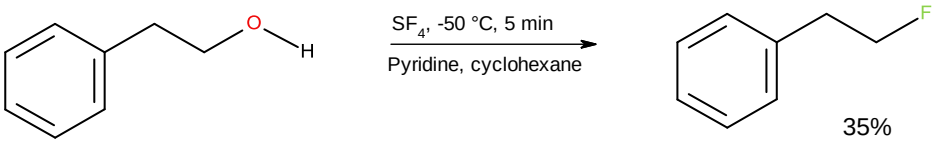

(1.2.11)

To the best of my knowledge, no mechanism has been reported on the fluorination of organic carbonyl and hydroxyl groups with SF_4 under basic conditions. The formation of SF_3^+ under basic conditions is extremely unlikely, therefore a different mechanism is probable.

1.3 Sulfur Fluoride Substituents in Organic and Inorganic Chemistry

1.3.1 Pentafluorosulfonyl Substituent, SF_5

Renewed interest in SF_5 as a substituent used in organic compounds is taking place.[90,91] The substituent has shown great promise in synthesizing high-performance polymers, energetic materials, and liquid crystals, because SF_5 is very electron withdrawing, lipophilic, chemically inert and has more steric bulk when compared to other fluorinated organic groups such as CF_3.[92,93] The pentafluorosulfanyl substituent was discovered accidentally in 1950, when attempting to synthesize CF_3SF by reaction of CH_3SF with CoF_3 at 250 to 275 °C, produced CF_3SF_5.[94] Aliphatic SF_5 compounds can be prepared in low yields (10 to 30%) by electrochemical fluorination or by direct fluorination of thiols, thioethers, and other sulfur containing compounds.[95-97] Pentafluorosulfanyl chloride (SF_5Cl) and bromide (SF_5Br) have been proven to be useful reagents in the introduction of SF_5 groups into organic compounds. Direct addition of SF_5X (X = Cl, Br) across double and triple bonds of alkenes and alkynes is a convenient method of synthesizing aliphatic compounds containing the SF_5 substituent.[98] (see Equation 1.3.1)

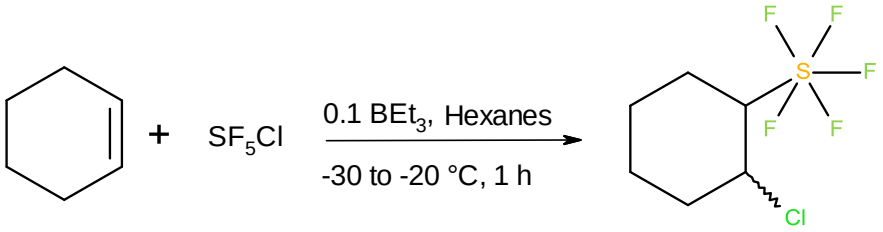

(1.3.1)

Studies suggest that the reaction proceeds via a radical mechanism, in which SF_5Cl first dissociates into $\bullet SF_5$ and $\bullet X$ radicals.[99] The production of these radicals can be increased photochemically, thermally, or by use of a radical initiator such as

BEt_3.[100] A competing side reaction is the addition of Cl−F instead of Cl−SF_5 (see Equation 1.3.2).

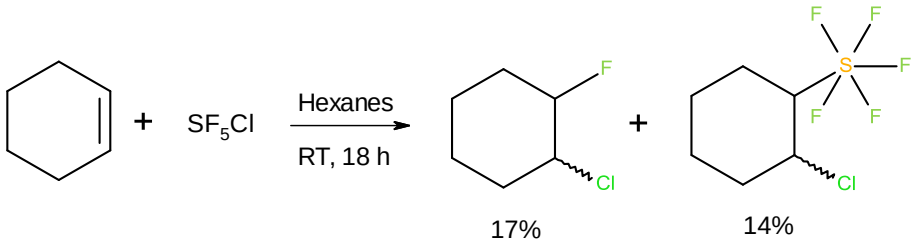

(1.3.2)

In contrast to aliphatic pentafluorosulfonyl compounds there are very few reported synthetic methods for preparing aromatic compounds containing the SF_5 substituent.[101] The direct fluorination of aryl sulfides in acetonitrile at −5 °C, with elemental fluorine (10% F_2/N_2 v/v) produces aryl pentafluorosulfides in a yield of 40%.[102] More recently, a new method has been developed to synthesize arylsulfur pentafluorides in high yields.[103] The reaction of diaryl disulfides with a mixture of chlorine and potassium fluoride affords two equivalents of arylsulfur chlorotetrafluoride (see Equation 1.3.3). Treatment of the arylsulfur chlorotetrafluoride with a fluoride source, such as such as ZnF_2, HF, and Sb(III/V) fluorides affords the pentafluorosulfonyl arene.

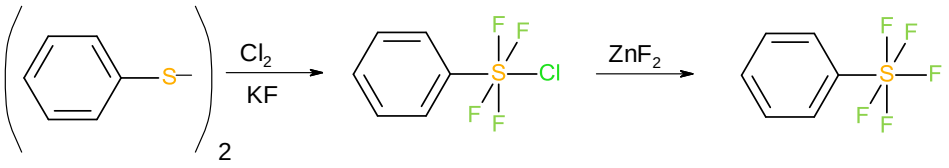

(1.3.3)

1.3.2 SF_x (x = 2-4)

Compounds containing the SF_x group have a wide range of reactivity and potential uses.[104] The following is a small sample of some interesting compounds which have been reported. Compounds containing S(IV) or S(VI) are common, in which the SF_x group is attached to carbon, or other main-group elements such as nitrogen or oxygen. The reaction of SF_4 with varying amounts of trimethylsilyl amines produces a large range of compounds containing N-S(IV)F_x (where x = 2, 3) substituents, which have been very useful as fluorinating agents (see Equation 1.3.4).[105]

$$xR_2N{-}SiMe_3 + SF_4 \rightarrow (R_2N)_x{-}SF_{4-x} + xFSiMe_3 \quad \text{(where x = 1, 2)} \qquad (1.3.4)$$

If three equivalents of $R_2N{-}SiMe_3$ are used the $[(R_2N)_3S^+][Me_3SiF_2^-]$ salt will form, which is a useful source of fluoride ions. In the above reaction, when R is ethyl and a one-to-one molar ratio of reactants is used, diethylaminosulfur trifluoride (DAST) is produced, which is a popular, commercially available fluorinating agent (see Figure 1.4).

A large range of aryloxysulfur(IV) fluorides, which contain O-S(IV)F_x (where x = 1, 2, 3) substituents, have been synthesized and characterized by ^{19}F NMR spectroscopy and mass spectrometry.[106] These compounds are formed by the reaction between aryl silyl ethers and sulfur tetrafluoride (see Equation 1.3.5).

$$xArOSiMe_3 + SF_4 \rightarrow (ArO)_xSF_{4-x} + xMe_3SiF \quad \text{(where x = 1, 2, 3)} \qquad (1.3.5)$$

Selective fluorination of sulfur on organic compounds is a common method of producing various SF_x moieties. Aryl and alkyl sulfur trifluorides can be prepared by fluorination of disulfides with AgF_2 (see Equation 1.3.6).

$$(R{-}S{-})_2 + 6AgF_2 \rightarrow 2\,RSF_3 + 6AgF \qquad (1.3.6)$$

The fluorination of a sulfurane ($S\{C_6H_4C(CF_3)_2O\}$) with BrF_3 produced a *trans*-difluorosulfurane ($SF_2\{C_6H_4C(CF_3)_2O\}$) if a 2/3rd BrF_3 molar equivalency is used, and the *cis*-difluorosulfurane if excess BrF_3 was used.[107] Alkylidene sulfur difluorides ($R_2C{=}SF_2$) can be prepared by an addition-elimination reaction (see Equation 1.3.7).

$$F_3C{-}CH{=}CF_2 + SF_4 \rightarrow (F_3C)_2C{=}SF_2 + HF \qquad (1.3.7)$$

Alkylidene sulfur tetrafluorides (R-C=SF_4) can be prepared by elimination of halo-fluorides from $FS_5CBr(CH_3)CF_3$ or by isomerization of $F_5S{-}CH{=}C{=}O$.[108,109] These compounds can then be further dehydrofluorinated to produce R-C≡SF_3 compounds, which are unstable.[110] An alkylidene sulfur difluoride oxide was synthesized by the hydrolysis of an alkylidene sulfur tetrafluoride (see Equation 1.3.8).[104]

$$O{=}CF{-}CH{=}SF_4 + H_2O \rightarrow O{=}CF{-}CH{=}SF_2{=}O + 2HF \qquad (1.3.8)$$

1.3.3 Sulfur Fluorides as Ligands in Transition Metal Chemistry

In 1969, Stocks *et al.* reported that the reaction between SF_5Cl and *trans*-stilbenebis(triphenylphosphine)platinum(0) forms $(PPh_3)_2PtClSF_5$, the first metal complex to contain a sulfur fluoride directly bonded to a metal.[111] The only evidence provided for the existence of this structure were physical properties and infrared absorptions at 316 cm^{-1} (Pt-Cl) and at 891 cm^{-1} attributed to SF_5. Holloway *et al.* reported that SF_4 oxidatively adds to Vaska-type complexes forming $(PR_3)_2IrXFSF_3$ (where R = Me, Et, Ph and X = Cl, Br, I) complexes (see Equation 1.3.9).[112]

$$SF_4 + Cl_2(CO)(PEt_3)_2Ir(I) \rightarrow F(SF_3)Cl_2(CO)(PEt_3)_2Ir \quad (1.3.9)$$

The reaction between SF_4 and $Ir(CO)Cl(PEt_3)_2$ occurs rapidly in CD_2Cl_2 at −73 °C to form $Ir(CO)ClF(PEt_3)_2SF_3$, the only reported instance of SF_3 as a ligand. These compounds were identified by ^{19}F and ^{31}P NMR spectroscopy and further characterized by partial elemental analysis, by their infrared spectra, and by incomplete single-crystal X-ray diffraction. It was also reported that tellurium tetrafluoride oxidatively adds to rhodium analogues of Vaska's complex.[113] More recently, computational methods have been used to study the stability of SF_3 ligands attached to metal carbonyl compounds.[114] This study suggests that SF_3 bonded to first-row transition-metal carbonyls would be disfavoured over SF_2 and F addition for certain complexes (($V(CO)_5$, $Mn(CO)_4$, $Co(CO)_3$, $Ir(CO)_3$)), whereas the opposite is favoured in other compounds ($Cr(CO)_5$, $Fe(CO)_4$, and $Ni(CO)_3$).[114]

1.4 Goals of Present Research

One of the original goals of this thesis was to expand the chemistry of sulfur fluorides as ligands in transition-metal chemistry. The first goal was to replicate the findings of Stocks *et al.* and Holloway *et al.* by synthesizing the only reported compounds containing sulfur fluoride ligands, i. e., $(PPh_3)_2PtClSF_5$ and $Ir(CO)ClF(PEt_3)_2SF_3$, respectively, and provide structural information for these complexes. Unfortunately, attempts at replicating their results and isolating sulfur fluoride complexes proved to be challenging. Reactions of sulfur tetrafluoride and sulfur pentafluoride chloride with a multitude of metal complexes gave no conclusive

results. The use of SF_4 in some of these reactions led to the study of the structure of SF_4, the use of SF_4 as a reagent in inorganic chemistry, and the behavior of SF_4 as a Lewis acid.

Since SF_4 has been extensively used in synthetic organic chemistry, the use of SF_4 as a fluorinating agent towards inorganic oxo-anions under ambient conditions was investigated. At high temperatures and pressures, the reactions of sulfur tetrafluoride with inorganic oxides yield fluorides,[115] but under ambient conditions, it is not known to what degree fluorination will take place. The reported synthesis of high-oxidation-state main-group and transition-metal oxide fluorides generally uses reagents such as xenon hexafluoride or krypton difluoride which are not commercially available. The use of sulfur tetrafluoride as a fluorinating agent may provide an alternative cost-effective route to oxide fluorides.

Another goal of the present study is to further elucidate structure and bonding of sulfur tetrafluoride in the solid state and explore the interaction of sulfur tetrafluoride with fluoride. At low temperatures it may be possible to isolate and characterize the actual fluorinating agents which are present in nitrogen-base sulfur tetrafluoride mixtures that have been used to fluorinate ketone and hydroxyl groups in organic compounds. Reaction mechanisms have been proposed for the fluorination of organic substrates in the presence of HF, but not in the presence of organic bases.

The conclusive solid-state structure of SF_4 has not been reported prior to this work. Reports on the structure of SF_4 in the solid state varied widely, some suggesting disorder, dimers, or chains. Full characterization of this important binary main group fluoride is long overdue. With the use of low-temperature crystal mounting techniques, the X-ray crystal structure of neat SF_4 may be obtained and

will provide a conclusive picture of SF_4 in the solid state. This fundamental data would be beneficial to both theoretical and experimental chemists.

The synthesis and characterization of SF_4-Lewis base adducts will be extended from the nitrogen-bases to the oxygen-bases. The SF_4-oxygen-base adducts are expected to be unstable at ambient temperature. For their isolation and characterization, low-temperature techniques have to be employed, especially low-temperature mounting techniques for X-ray crystallography. Lewis acid-base adducts between oxygen and sulfur are rare, dioxane•SO_3 adducts being the only reported S-OR_2 adducts studied by X-ray crystallography.[116] To the best of my knowledge, there has yet to be a S(IV)-OR_2 adduct.

References

(1) Seel, F. *Advan. Inorg. Chem. Radiochem.* **1974**, *16*, 297-333.

(2) Leiding, J.; Woon, D. E.; Dunning, T. H. *J. Phys. Chem. A* **2012**, *116*, 1655-1662.

(3) Lee, E. P. F.; Mok, D. K. W.; Chau, F.T.; Dyke, J. M. *J. Chem. Phys.* **2006**, *125*, 104304/104301-104304/104313.

(4) Pavone, M.; Barone, V.; Ciofini, I.; Adamo, C. *J. Chem. Phys.* **2004**, *120*, 9167-9174.

(5) Oberhammer, H.; Shlykov, S. A. *Dalton Trans.* **2010**, *39*, 2838-2841.

(6) Steudel, Y.; Steudel, R.; Wong, Ming W.; Lentz, D. *Eur. J. Inorg. Chem.* **2001**, *2001*, 2543-2548.

(7) Deroche, J. C.; Bürger, H.; Schulz, P.; Willner, H. *J. Mol. Spectros.* **1981**, *89*, 269-275.

(8) Seel, F.; Budenz, R.; Gombler, W. *Chem. Ber.* **1970**, *103*, 1701-1708.

(9) Seel, F.; Heinrich, E.; Gombler, W.; Budenz, R. *Chimia* **1969**, *23*, 73-74.

(10) Johnson, D. R.; Powell, F. X. *Science* **1969**, *164*, 950-951.

(11) Haas, A. W., H. *Ber. Bunsenges. Phys. Chem.* **1978**, *82*, 24.

(12) Gombler, W.; Schaebs, J.; Willner, H. *Inorg. Chem.* **1990**, *29*, 2697-2698.

(13) Carlowitz, M. V.; Oberhammer, H.; Willner, H.; Boggs, J. E. *J. Mol. Struc.* **1983**, *100*, 161-177.

(14) Seel, F.; Gölitz, H. D. *Z. Anorg. Allg. Chem.* **1964**, *327*, 32-50.

(15) Glemser, O.; Biermann, U.; Knaak, J.; Haas, A. *Chem. Ber.* **1965**, *98*, 446-450.

(16) Davis, R. W. *J. Mol. Spectros.* **1986**, *116*, 371-383.

(17) Smith, W. C.; Engelhardt, V. A. *J. Am. Chem. Soc.* **1960**, *82*, 3838-3840.

(18) Ewing, V. C.; Sutton, L. E. *Trans. Farad. Soc.* **1963**, *59*, 1241-1247.

(19) Kimura, K.; Bauer, S. H. *J. Chem. Phys.* **1963**, *39*, 3172-3178.

(20) Tolles, W. M.; Gwinn, W. D. *J. Chem. Phys.* **1962**, *36*, 1119-1121.

(21) Dodd, R. E.; Woodward, L. A.; Roberts, H. L. *Trans. Faraday Soc.* **1956**, *52*, 1052-1061.

(22) Raffael, K. D.; Smith, D. M. *J. Mol. Spectros.* **2002**, *214*, 21-27.

(23) Raffael, K. D.; Smith, D. M.; Newnham, D. A. *J. Mol. Spectros.* **2003**, *218*, 108-113.

(24) Spring, C. A.; True, N. S. *J. Am. Chem. Soc.* **1983**, *105*, 7231-7236.

(25) Christe, K. O.; Curtis, E. C.; Schack, C. J.; Pilipovich, D. *Inorg. Chem.* **1972**, *11*, 1679-1682.

(26) Berney, C. V. *J. Mol. Struc.* **1972**, *12*, 87-97.

(27) Mootz, D.; Korte, L. *Z. Naturforsch., B: Anorg. Chem., Org. Chem.* **1984**, *39B*, 1295-1299.

(28) Naumann, D.; Padma, D. *Z. Anorg. Allg. Chem.* **1973**, *401*, 53-56.

(29) Fedorova, A.N.; Dromov, G.A.; Antonova, E.I.; Antipenko, G.L. U.S.S.R. Pat., 823 276, 1981.

(30) Tullock, C. W.; Fawcett, F. S.; Smith, W. C.; Coffman, D. D. *J. Am. Chem. Soc.* **1960**, *82*, 539-542.

(31) Muetterties, E. L.; U.S. Patent 2,729,663: **1959**.

(32) Smythe, K. D. In *Proceedings of" Conference on SF_6 and the Environment: Emission Reduction Strategies", November* 2000, p 2-3.

(33) Rhein, R. A. *Lithium combustion: a review*, DTIC Document, 1990.

(34) Gullikson, C. W.; Nielsen, J. R.; Stair Jr, A. T. *J. Mol. Spectros.* **1957**, *1*, 151-154.

(35) Goyal, S.; Schutt, D. L.; Scoles, G. *Phys. Rev. Lett.* **1992**, *69*, 933-936.

(36) Lagemann, R. T.; Jones, E. A. *J. Chem. Phys.* **1951**, *19*, 534-536.

(37) Brunet, H.; Perez, M. *J. Mol. Spectros.* **1969**, *29*, 472-477.

(38) Frost, D. C.; McDowell, C. A.; Sandhu, J. S.; Vroom, D. A. *J. Chem. Phys.* **1967**, *46*, 2008-2009.

(39) Gillespie, R. J.; Quail, J. W. *J. Chem. Phys.* **1963**, *39*, 2555-2557.

(40) Bartell, L. S.; Doun, S. K. *J. Mol. Struc.* **1978**, *43*, 245-249.

(41) Taylor, J. C.; Waugh, A. B. *J. Solid State Chem.* **1976**, *18*, 241-246.

(42) Cockcroft, J. K.; Fitch, A. N. *Z. Kristallogr. Kristallgeo.* **1988**, *184*, 123-145.

(43) Strauss, G.; Zweier, H.; Bertagnolli, H.; Bausenwein, T.; Todheide, K.; Chieux, P. *J. Chem. Phys.* **1994**, *101*, 662-671.

(44) Jones, J. P.; Wagner, E. N. *Poision Gas Proliferation: Paradox, Politics, and Law*, 1992; Vol. 15.

(45) Denbigh, K. G.; Whytlaw-Gray, R. *J. Chem. Soc.* **1934**, 1346-1352.

(46) Benson, S. W.; Bott, J. *Int. J. Chem. Kinet.* **1969**, *1*, 451-458.

(47) Winter, R.; Nixon, P. G.; Gard, G. L. *J. Fluorine Chem.* **1998**, *87*, 85-86.

(48) Nyman, F.; Roberts, H. L. *J. Chem. Soc.* **1962**, 3180-3183.

(49) Edelson, D. *J. Am. Chem. Soc.* **1952**, *74*, 262.

(50) Harvey, R. B.; Bauer, S. H. *J. Am. Chem. Soc.* **1953**, *75*, 2840-2846.

(51) Oberhammer, H. *J. Mol. Struc.* **1989**, *192*, 171-175.

(52) Dodd, R.; Woodward, L.; Roberts, H. *Trans. Faraday Soc.* **1957**, *53*, 1545-1556.

(53) Harris, R. K.; Packer, K. J. *J. Chem. Soc.* **1962**, *0*, 3077-3082.

(54) Wilmshurst, J. K.; Bernstein, H. J. *Can. J. Chem.* **1957**, *35*, 191-201.

(55) Smardzewski, R. R.; Noftle, R. E.; Fox, W. B. *J. Mol. Spectros.* **1976**, *62*, 449-457.

(56) Novak, I. *Inorg. Chim. Acta* **1991**, *181*, 81-83.

(57) Irikura, K. K. *J. Chem. Phys.* **1995**, *103*, 10162-10168.

(58) Gutsev, G. L. *Zh. Fiz. Khim.* **1992**, *66*, 1820-1827.

(59) Robinson, N. B. a. P. L. *Chem. & Ind.* **1956**, 1351.

(60) Bartlett, N.; Robinson, P. L. *J. Chem. Soc.* **1961**, 3417-3425.

(61) Cotton, F. A.; George, J. W. *J. Inorg. Nucl. Chem.* **1958**, *7*, 397-403.

(62) Azeem, M.; Brownstein, M.; Gillespie, R. J. *Can. J. Chem.* **1969**, *47*, 4159-4167.

(63) Gibler, D. D.; Adams, C. J.; Fischer, M.; Zalkin, A.; Bartlett, N. *Inorg. Chem.* **1972**, *11*, 2325-2329.

(64) Chaudhary, P., M.Sc. Thesis, Lethbridge, Alta.: University of Lethbridge, Dept. of Chemistry and Biochemistry, 2011.

(65) Mallouk, T. E.; Rosenthal, G. L.; Mueller, G.; Brusasco, R.; Bartlett, N. *Inorg. Chem.* **1984**, *23*, 3167-3173.

(66) O'Brien, B. A.; DesMarteau, D. D. *Inorg. Chem.* **1984**, *23*, 644-648.

(67) Tunder, R.; Siegel, B. *J. Inorg. Nucl. Chem.* **1963**, *25*, 1097-1098.

(68) Tullock, C.; Coffman, D.; Muetterties, E. *J. Am. Chem. Soc.* **1964**, *86*, 357-361.

(69) Bittner, J.; Fuchs, J.; Seppelt, K. *Z. Anorg. Allg. Chem.* **1988**, *557*, 182-190.

(70) Drullinger, L. F.; Griffths, J. E. *Spectrochim. Acta A* **1971**, *27*, 1793-1799.

(71) Christe, K. O.; Curtis, E. C.; Schack, C. J.; Pilipovich, D. *Inorg. Chem.* **1972**, *11*, 1679-1682.

(72) Clark, M.; Kellen-Yuen, C.; Robinson, K.; Zhang, H.; Yang, Z.-Y.; Madappat, K.; Fuller, J.; Atwood, J.; Thrasher, J. *Eur. J. Solid State Inorg. Chem.* **1992**, *29*, 809-833.

(73) Muetterties, E. L. *J. Am. Chem. Soc.* **1960**, *82*, 1082-1087.

(74) Sass, C. S.; Ault, B. S. *J. Phys. Chem.* **1985**, *89*, 1002-1006.

(75) Goettel, J. T.; Chaudhary, P.; Hazendonk, P.; Mercier, H. P. A.; Gerken, M. In *95th Canadian Chemistry Conference* Calgary, Alberta, Canada 2012, Abstract #353.

(76) Goettel, J. T.; Chaudhary, P.; Hazendonk, P.; Mercier, H. P. A.; Gerken, M. *Chem. Commun.* **2012**, *48*, 9120–9122.

(77) Smith, W. C. *Angew. Chem. Int. Ed. Engl.* **1962**, *1*, 467-475.

(78) Hudlický, M. In *Organic Reactions*; John Wiley & Sons, Inc.: 2004.

(79) Takaoka, A.; Iwakiri, H.; Ishikawa, N. *Bull. Chem. Soc. Jpn.* **1979**, *52*, 3377-3380.

(80) L'Heureux, A.; Beaulieu, F.; Bennett, C.; Bill, D. R.; Clayton, S.; LaFlamme, F.; Mirmehrabi, M.; Tadayon, S.; Tovell, D.; Couturier, M. *J. Org. Chem.* **2010**, *75*, 3401-3411.

(81) Dmowski, W.; Kolinski, R. *Pol. J. Chem.* **1978**, *52*, 547; *Chem. Abstr.* **1978**, *89*, 41906.

(82) Wojciech, D.; Ryszard, A. K. *Pol. J. Chem.* **1978**, *52*, 71-85.

(83) Wielgat, J.; Domagała, Z. *J. Fluorine Chem.* **1982**, *20*, 785-789.

(84) Wielgat, J.; Domagała, Z.; Koliński, R. *J. Fluorine Chem.* **1987**, *35*, 643-652.

(85) Kollonitsch, J.; Marburg, S.; Perkins, L. *J. Org. Chem.* **1975**, *40*, 3808-3809.

(86) Kollonitsch, J.; Marburg, S.; Perkins, L. M. *J. Org. Chem.* **1979**, *44*, 771-777.

(87) Baum, K. *J. Am. Chem. Soc.* **1969**, *91*, 4594-4594.

(88) Dmowski, W. *Pol. J. Chem.* **1982**, *56*, 1369.

(89) Schaefer, T.; Rowbotham, J. B.; Parr, W. J.; Marat, K.; Janzen, A. F. *Can. J. Chem.* **1976**, *54*, 1322-1328.

(90) Thayer, A. M. *Chem. Eng. News* **2006**, *84*, 27-32.

(91) Kirsch, P.; Röschenthaler, G. V. Functional Compounds Based on Hypervalent Sulfur Fluorides. In *Current Fluoroorganic Chemistry*, Soloshonok, V. A.; Mikami, A.; Yamazaki, T.; Welch, J. T.; Honek, J. F., Eds.; ACS Symposium Series 949; American Chemical Society: Washington, DC, 2007, Ch. 13; pp 221-243.

(92) Dolbier, W. R. *Jr.Chimica Oggi* **2003**, *21*, 66-69.

(93) Sheppard, W. A. *J. Am. Chem. Soc.* **1962**, *84*, 3072-3076.

(94) Silvey, G. A.; Cady, G. H. *J. Am. Chem. Soc.* **1950**, *72*, 3624-3626.

(95) Clifford, A. F.; El-Shamy, H. K.; Emeleus, H. J.; Haszeldine, R. N. *J. Chem. Soc.* **1953**, *0*, 2372-2375.

(96) Hoffmann, F. W.; Simmons, T. C.; Beck, R. B.; Holler, H. V.; Katz, T.; Koshar, R. J.; Larsen, E. R.; Mulvaney, J. E.; Rogers, F. E.; Singleton, B.; Sparks, R. S. *J. Am. Chem. Soc.* **1957**, *79*, 3424-3429.

(97) Huang, H. N.; Lagow, R. J.; Roesky, H. *Inorg. Chem.* **1991**, *30*, 789-794.

(98) Winter, R. W.; Dodean, R. A.; Gard, G. L. SF_5-Synthons: Pathways to Organic Derivatives of SF_6. In *Fluorine-Containing Synthons*, Soloshonok, V. A., Ed.; ACS Symposium Series 911; American Chemical Society: Washington, DC, 2005, Ch. 4, pp 87-118.

(99) Berry, A. D.; Fox, W. B. *J. Org. Chem.* **1978**, *43*, 365-367.

(100) Dolbier Jr, W. R.; Aït-Mohand, S.; Schertz, T. D.; Sergeeva, T. A.; Cradlebaugh, J. A.; Mitani, A.; Gard, G. L.; Winter, R. W.; Thrasher, J. S. *J. Fluorine Chem.* **2006**, *127*, 1302-1310.

(101) Sipyagin, A. M.; Bateman, C. P.; Tan, Y.-T.; Thrasher, J. S. *J. Fluorine Chem.* **2001**, *112*, 287-295.

(102) Bowden, R. D.; Comina, P. J.; Greenhall, M. P.; Kariuki, B. M.; Loveday, A.; Philp, D. *Tetrahedron* **2000**, *56*, 3399-3408.

(103) Umemoto, T.; Garrick, L. M.; Saito, N. Beilstein *J. Org. Chem.* **2012**, *8*, 461-471.

(104) Seppelt, K. *Angew. Chem. Int. Ed. Engl.* **1991**, *30*, 361-374.

(105) Middleton, W.; Bingham, E. *J. Org. Chem.* **1980**, *45*, 2883-2887.

(106) Darragh, J. I.; Hossain, S. F.; Sharp, D. W. A. *J. Chem. Soc., Dalton Trans.* **1975**, *0*, 218-221.

(107) Michalak, R. S.; Martin, J. C. *J. Am. Chem. Soc.* **1982**, *104*, 1683-1692.

(108) Krügerke, T.; Buschmann, J.; Kleemann, G.; Luger, P.; Seppelt, K. *Angew. Chem. Int. Ed. Engl.* **1987**, *26*, 799-801.

(109) Buschmann, J.; Koritsanszky, T.; Kuschel, R.; Luger, P.; Seppelt, K. *J. Am. Chem. Soc.* **1991**, *113*, 233-238.

(110) Poetter, B.; Seppelt, K.; Simon, A.; Peters, E. M.; Hettich, B. *J. Am. Chem. Soc.* **1985**, *107*, 980-985.

(111) Kemmitt, R. D. W.; Peacock, R. D.; Stocks, J. *J. Chem. Soc. D* **1969**, 554.

(112) Cockman, R. W.; Ebsworth, E. A. V.; Holloway, J. H. *J. Am. Chem. Soc.* **1987**, *109*, 2194-2195.

(113) Ebsworth, E. A. V.; Holloway, J. H.; Watson, P. G. *J. Chem. Soc., Chem. Commun.* **1991**, 1443-1444.

(114) Deng, J.; Wang, C.; Li, Q.-s.; Xie, Y.; King, R. B.; Schaefer, H. F. *Inorg. Chem.* **2011**, *50*, 2824-2835.

2 Experimental

Caution: Anhydrous HF (aHF) is toxic and highly corrosive. Exposure to aHF will cause severe burns. Sulfur tetrafluoride is highly toxic and corrosive. At room temperature, the pressure in the reactor will be close to 10 atmospheres, and therefore there is a danger of overpressurization. Reactions between SF_4 and water are highly exothermic. The reactions should be performed on small scales at low temperatures.

2.1 General Methods

The chemistry presented in this thesis requires strict exclusion of oxygen and moisture due to the extremely reactive nature of the compounds used throughout this work. All operations were carried out under rigorously dried and strictly inert atmospheres, by the use of glass and metal vacuum lines, and a dry box (Omni Lab, Vacuum Atmospheres). Edwards two-stage direct-drive RV8 vacuum pumps were used for the metal and glass vacuum lines, and the antechambers of the glove box. Vacuum on the glass (ca. 10^{-5} Torr) and metal lines (ca. 10^{-4} Torr) were verified by a mercury McCleod gauge (Labconco). Nitrogen (Praxair), was passed through a column containing anhydrous calcium sulfate (cobalt chloride indicator), and activated 4Å molecular sieves. Ultra-high-purity (5.0) argon (Praxair) was used without further purification.

Pyrex-glass vacuum lines, equipped with grease-free 6-mm J. Young glass stopcocks with PTFE barrels, were used to manipulate volatiles which do not react with glass (see Figure 2.1). Heise gauges (model CC, 0-1000 mmHg, beryllium/copper Bourdon tube, Dresser Instruments) were used to measure pressures inside the glass

manifold. The final vacuum was monitored by Varian model 801 thermocouple gauges connected to the vacuum lines between the liquid nitrogen traps and the vacuum pumps.

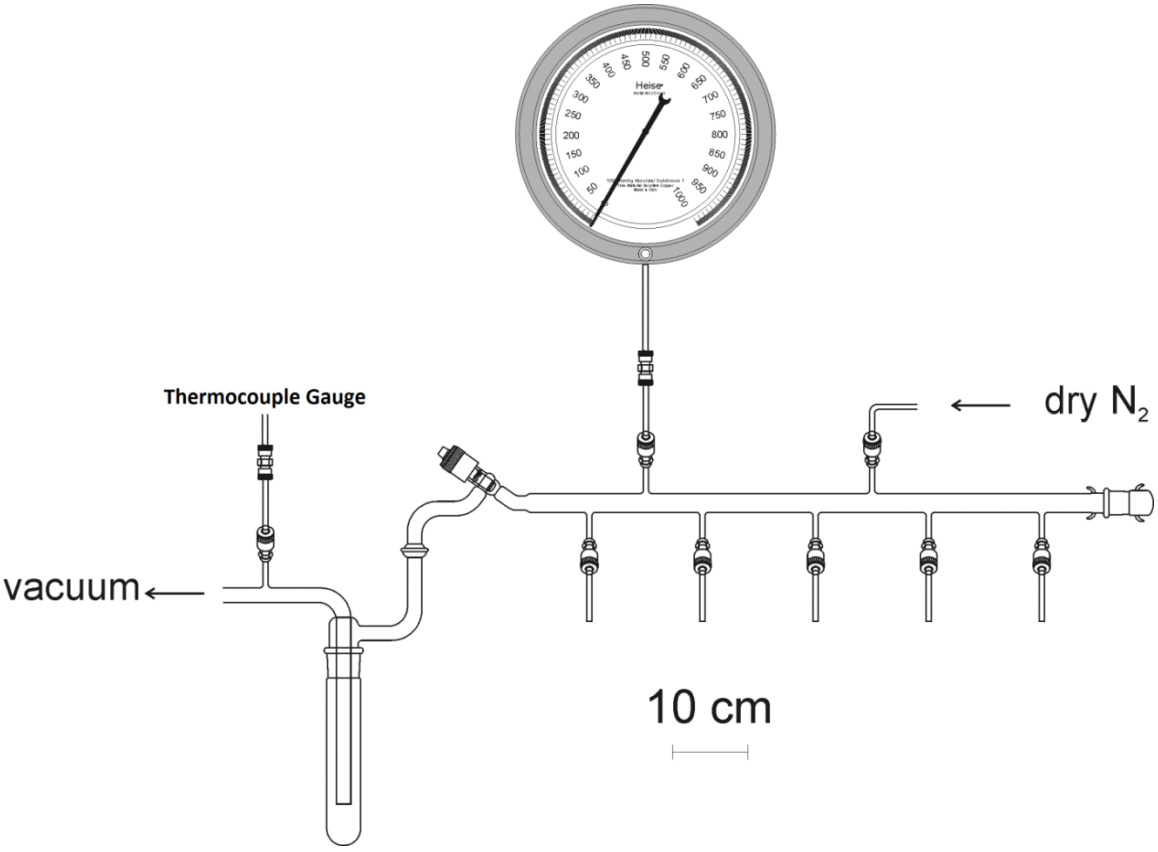

Figure 2.1 Glass vacuum line system equipped with J. Young PTFE/glass stopcocks, a Heise gauge (Adapted from Jared Nieboer's M.Sc. Thesis).

A metal line constructed from nickel, 316 stainless-steel, and equipped with 316 stainless steel valves and fittings (Autoclave Engineers Inc.), PTFE, and FEP, was used to manipulate volatiles which react with glass (see Figure 2.2). Three vacuum pumps were connected to the metal line; two pumps for fine vacuum connected to small towers of activated charcoal, and one roughing pump connected to a fluoride/fluorine trap consisting of a stainless-steel cylinder (75-cm length, 17-cm outer diameter) packed with soda lime absorbent (EMD, 4 mesh). The fine vacuum pumps provided high vacuum to

each respective side of the metal line. The roughing vacuum provided a method of removal and disposal of volatile reactive fluorinated compounds for both sides of the metal lines. Pressures were measured using Baratron capacitance manometers (MKS, Type 626A, effective range 0-1000 mmHg) having inert wetted surfaces constructed of Inconel, connected to digital readouts.

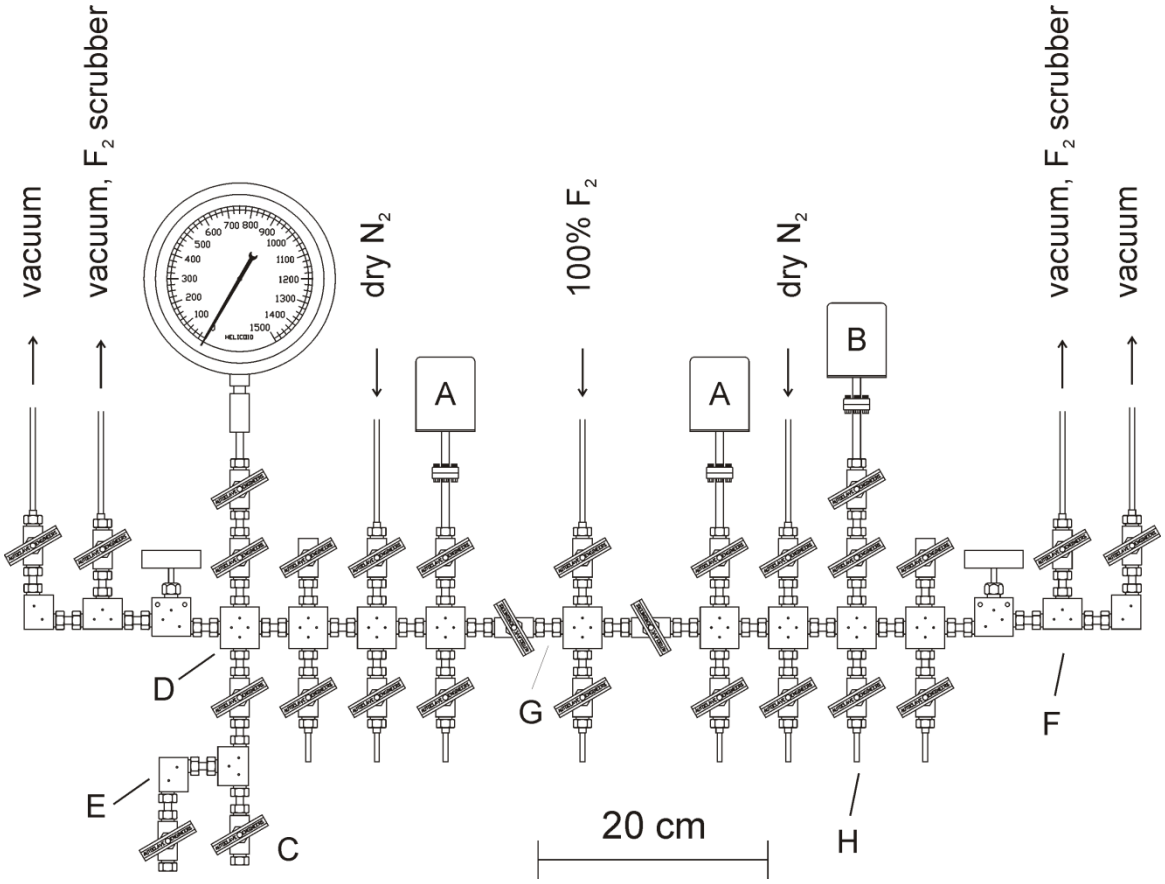

Figure 2.2 Metal vacuum system; (A) MKS type 626A capacitance manometer (0-1000 Torr), (B) MKS Model PDR-5B pressure transducers (0-10 Torr), (C) 3/8-in. stainless-steel high-pressure valves (Autoclave Engineers, 30VM6071), (D) 316 stainless-steel cross (Autoclave Engineers, CX6666), (E) 316 stainless-steel L-piece (Autoclave Engineers, CL6600), (F) 316 stainless steel T-piece (Autoclave engineers, CT6660), (G) 3/8-in o.d., 1/8-in. i.d. nickel connectors, (H) 1/8-in o.d., 1/8-in. i.d. nickel tube. (from Jared Nieboer's M.Sc. thesis).

All preparative work involving reactive fluorinated compounds was carried out in 4-mm, ¼-in., or ¾-in. o.d. FEP reactors which were heat sealed at one end and affixed to either Kel-F or stainless-steel valves by means of a 45° and 33° flare, respectively. The FEP reactors were rinsed with acetone, checked for leaks and dried under dynamic vacuum overnight on a glass vacuum line. The reactors were then passivated with pure fluorine gas at a pressure greater than 1 atm overnight, and backfilled with nitrogen. The reactors were weighed underneath using a Sartorius Ag Göttingen balance, with a suspended copper wire.

Raman spectroscopy was performed on samples in ¼-in. or 4-mm FEP reactors, 5-mm glass tubes equipped with a J-Young valves, or Pyrex-glass melting-point capillaries. The Pyrex-glass melting-point capillaries were loaded in the dry box and sealed with Kel-F grease. They were then heat-sealed outside of the glove box using a standard natural-gas Bunsen burner.

Nuclear magnetic resonance (NMR) spectroscopy was performed in sealed 4-mm FEP tubes, inserted into standard 5-mm glass NMR tubes. The 4-mm FEP tubes were sealed under dynamic vacuum with a heat gun, while the contents remained cooled at −196 °C.

2.2 Purification and Preparation of Starting Materials

2.2.1 Purification of Anhydrous HF, SF_4, Acetonitrile

Anhydrous hydrogen fluoride (Air Products) was stored at room temperature in a nickel storage vessel equipped with a monel (Autoclave Engineers) valve. Hydrogen fluoride was pre-dried with fluorine gas in a ¾-in. o.d. FEP vessel equipped with a stainless-steel valve. The vessel was evacuated and backfilled with approximately 900 Torr of pure fluorine gas. The vessel was agitated periodically for two weeks. Volatiles

were pumped off below −80 °C. The HF was then vacuum distilled onto potassium hexafluoronickelate(IV) in a ¾-in o.d. FEP vessel and backfilled with nitrogen.

Sulfur tetrafluoride (Ozark-Mahoning Co.) was purified by passing the gas through a column of activated charcoal. Traces of thionyl fluoride and sulfur hexafluoride were present in the sulfur tetrafluoride, but did not interfere with the chemistry.

Acetonitrile (Sigma-Aldrich) was purified according to the literature procedure reported by Winfield.[1] It was then vacuum distilled and stored on freshly activated 4Å molecular sieves.

2.2.2 Oxo-Anions Salts

Tetramethylammonium iodate was prepared by neutralization of an aqueous solution of $[N(CH_3)_4][OH]$ (Fluka, 95.0%) with a stoichiometric amount of an aqueous solution of HIO_3 (BDH) as previously described.[2] Potassium periodate (Sigma, 99.8%), potassium perrhenate (Strem, 99%), and silver perrhenate (Strem, 99%) were used as received.

2.2.3 Nitrogen-Bases

Both 4-dimethylaminopyridine (Sigma, 99%) and 4,4’-bipyridyl (Sigma, 98%) were dried under vacuum at ambient temperatures and brought into the glove box. Pyridine was vacuum distilled onto CaH_2. 4-Methylpyridine (Sigma, 99%) was distilled onto freshly cut sodium, and stirred overnight, and subsequently distilled into dry glass vessels equipped with J-Young valves. 2,6-Dimethylpyridine (Sigma, 99%) was used as received.

2.2.4 Purification of Toluene, Diethyl Ether, Pentane, THF

The solvents were dispensed directly from an MBraun dry solvent system into a dry glass flask equipped with a J-Young valve. The solvents were then freeze-thaw degassed and vacuum distilled onto freshly cut sodium, potassium, or a liquid sodium potassium alloy. THF was refluxed with benzophenone and sodium, and then distilled onto freshly cut sodium. Diethyl ether, was vacuum distilled onto freshly cut sodium and stirred for three days, followed by vacuum distillation onto freshly activated 4Å molecular sieves. Pentane was vacuum distilled onto liquid Na/K alloy. Toluene was first vacuum distilled onto activated molecular sieves, however, reactions using this toluene led to hydrolysis products, which suggested that it was insufficiently dried. The toluene was then distilled onto a Na/K alloy and sonicated for several hours.

2.2.5 Purification of CH_2Cl_2, $CFCl_3$, CF_2Cl_2

Dichloromethane was dispensed from a dry solvent system, and then vacuum distilled onto freshly activated 4A molecular sieves. Trichlorofluoromethane was vacuum distilled onto calcium hydride, and vacuum distilled into a dry, evacuated flask. Difluorodichloromethane (Synquest Labs Inc.) was used as received.

2.3 Preparation of Oxide Fluoride Salts

2.3.1 Preparation of $[Ag(CH_3CN)_x][ReO_2F_4]$ where (x = 0, 2, 4)

Inside the dry box, 0.053 g (0.15 mmol) of $AgReO_4$ was loaded into a ¼-in. o.d. FEP tube equipped with a Kel-F valve. Excess acetonitrile (0.388 g, 5.96 mmol) was vacuum distilled onto the solid $AgReO_4$. The reactor was agitated at room temperature to completely dissolve the solid. Excess SF_4 (0.23 g, 2.1 mmol) was vacuum distilled onto the frozen mixture at –196 °C. After warming and agitation at 0 °C, a pale yellow

solution was obtained. Slow cooling to –40 °C led to the formation of large plate-like crystals. Volatiles were removed under dynamic vacuum at –40 °C. These crystals ($[Ag(CH_3CN)_4][ReO_2F_4]\bullet CH_3CN$) were characterized by low-temperature Raman spectroscopy (see Table 3.1) and X-ray crystallography. Placing the crystals under dynamic vacuum afforded a cream coloured powder ($[Ag(CH_3CN)_2][ReO_2F_4]$) which was characterized by room temperature Raman spectroscopy (see Table 3.1). Heating the powder to approximately 60 °C under dynamic vacuum resulted in a loss of mass, and a fine light yellow powder ($Ag[ReO_2F_4]$) which was characterized by Raman spectroscopy (see Table 3.1). ^{19}F NMR (CH_3CN, 20 °C, unlocked, 282.4 MHz, δ [ppm]): –54.0 (t, $F_{c,t}$), –63.7 (t, ($F_{c,c}$), $^2J_{Fax-Feq}$ = 87 Hz.

2.3.2 Preparation of $KReO_2F_4$

Inside the dry box, 0.064 g (0.22 mmol) of $KReO_4$ was loaded into a 4-mm o.d. FEP tube equipped with a Kel-F valve. Approximately 0.05 mL of acetonitrile was vacuum distilled onto the solid $KReO_4$, and the mixture was agitated. Only a very small portion of the $KReO_4$ dissolved at room temperature. A large excess of sulfur tetrafluoride was vacuum distilled into the reactor. The reactor was warmed to room temperature and cautiously agitated. The mixture was left at room temperature overnight. A pale yellow solid formed. Volatiles were removed from −40°C to room temperature, leaving 69 mg of a pale yellow solid (approximately 55% yield). ^{19}F NMR (CH_3CN, 20 °C, unlocked, 282.4 MHz, δ [ppm]): –52.8 (t, $F_{c,t}$), –74.9 (t, $F_{c,c}$), $^2J_{Fax-Feq}$ = 90 Hz.

2.3.3 Preparation of $K[IO_2F_4]$

Inside the dry box, 0.081 g (0.35 mmol) of KIO_4 was loaded into a ¼-in. o.d. FEP tube equipped with a Kel-F valve. Approximately 0.1 mL of aHF was vacuum distilled onto

the solid, which partially dissolved the solid. Excess SF_4 was vacuum distilled onto the frozen mixture at –196 °C. Warming the reaction mixture to ambient temperature caused the remaining solid to dissolve upon agitation, yielding a clear colourless solution. The solvent was removed under dynamic vacuum at –78 °C, yielding 0.094 g (0.34 mmol) of colourless crystalline powder. ^{19}F NMR (HF, 20 °C, unlocked, 282.4 MHz, δ [ppm]): 64.4 (F_{trans}). Raman (cm^{-1}): 1078(4), (unidentified impurity); 875(2), (*cis* $\nu_{as}(IO_2)$; 856(19), (*cis* $\nu_{sym}(IO_2)$); 819(100), (*trans* $\nu_{sym}(IO_2)$); 797(2), (KIO_4); 609(13), (*cis* $\nu_{sym}(IF_{2eq})$); 577(41), (*trans* $\nu_{sym}(IF_4)_{in\ phase}$); 397(24), (*cis* $\delta_{sciss}(IO_2)$); 381(37), (*trans* $\delta(OIF_4O)$; 333(10), (*cis* $\nu_{torsion}(IO_2)$); 260(9), (*trans* $\nu_s(IF_4)_{in\ plane}$)).

2.3.4 Preparation of $[N(CH_3)_4][IOF_4]$

Inside the dry box, 0.072 g (0.29 mmol) of $[N(CH_3)_4][IO_3]$ was loaded into a ¼-in. o.d. FEP tube equipped with a Kel-F valve. Excess acetonitrile (0.563 g, 8.90 mmol) was vacuum distilled onto the solid $[N(CH_3)_4][IO_3]$. The reactor was agitated at room temperature, and only a small amount of solid dissolved. Excess SF_4 was distilled onto the frozen mixture at –196 °C. Warming to –40 °C caused the evolution of gas, and the solution to turn pale yellow. Warming and agitation at room temperature caused the solution to turn a light orange. Large thin plates were obtained when the solution was cooled to −30 °C. The plates were characterized by Raman spectroscopy (see Table 3.1), ^{19}F NMR spectroscopy and single crystal X-ray crystallography. The volatiles were transferred to a 4-mm o.d. FEP reactor at –80 °C. ^{19}F NMR (HF, 20 °C, unlocked, 282.4 MHz, δ [ppm]): 10.6

2.4 Preparation of Hydrolysis Products of SF_4•Nitrogen Base Adducts by HF

2.4.1 Preparation of $[HNC_5H_5^+]F^-$•SF_4

Pyridine (0.014 g, 0.18 mmol) was distilled into a ¼-in. FEP reactor. Sulfur tetrafluoride (0.057 g, 0.52 mmol) was vacuum distilled at −196 °C. The reactor was warmed to −80 °C and agitated to form a clear colourless solution. The excess SF_4 was removed by pumping at −75 °C for 2 hours, yielding colourless solid SF_4•NC_5H_5. Approximately 0.05 mL of toluene, which had been apparently insufficiently dried over molecular sieves, was vacuum distilled into the reactor at −196 °C. The reactor was warmed to −60 °C; gas evolution was observed as the adduct dissolved. The reactor was placed in a cryo-bath at −80 °C. Large colourless crystalline needles formed overnight. The crystals were characterized by X-ray crystallography.

2.4.2 Preparation of $[HNC_5H_5^+][HF_2^-]$•$2SF_4$

Water (0.013 g, 0.72 mmol) was syringed into a ¼-in. FEP reactor, followed by vacuum distillation of pyridine (0.109 g, 1.38 mmol) at −196 °C. A large excess of SF_4 (ca. 0.04 g, 4 mmol) was distilled at −196 °C. The reactor was warmed slightly to the melting point of SF_4, and the vigorous reaction was quenched by cooling in liquid nitrogen to control the reaction rate. After no further reaction was observed, the reactor was allowed to warm to room temperature, resulting in a clear colourless solution. Slow cooling to −90 °C resulted in crystal formation. Excess SF_4 and SOF_2 were pumped off at −90 °C. The product was characterized by low-temperature Raman spectroscopy (see Table 4.4) and X-ray crystallography.

2.4.3 Preparation of $[HNC_5H_4(CH_3)^+]F^-\bullet SF_4$

In an open atmosphere, water (0.019 g, 1.05 mmol) was syringed into a ¼-in o.d. FEP reactor and thoroughly degassed. After vacuum distillation of 4-methylpyridine (0.185 g, 1.99 mmol), SF_4 (0.65 g, 6.4 mmol) was transferred *in vacuo* at −196 °C onto the H_2O and 4-methylpyridine. The reactor was warmed slightly to the melting point of SF_4, and quenched by cooling in liquid nitrogen to control the reaction rate. After no further reaction was observed, the reactor was allowed to warm to room temperature, resulting in a clear colourless solution. Slow cooling to −20 °C resulted in crystal formation. Excess SF_4 and SOF_2 were pumped off at −90 °C, yielding a colourless crystalline solid. The product was characterized by low-temperature Raman spectroscopy (see Table 4.8) and X-ray crystallography.

2.4.4 Preparation of $[HNC_5H_3(CH_3)_2^+]_2[SF_5^-]F^-\bullet SF_4$

Method 1: After 2,6-dimethylpyridine (0.047 g, 0.44 mmol) was syringed into a ¼-in. FEP reactor, excess sulfur tetrafluoride (ca. 1 g, 9 mmol) was distilled at −196 °C. The reactor was warmed to −80 °C and the reactants mixed. The mixture was placed under dynamic vacuum at −85 °C until a 1:1 mole ratio of SF_4 : 2,6-dimethylpyridine was obtained. Approximately 0.05 mL of toluene containing traces of water was distilled onto the adduct at −196 °C. Upon melting of the toluene, the adduct dissolved and gas evolution was observed. Large plate-like crystals were obtained by cooling from −60 to −80 °C. A large plate (0.212 × 0.461 × 0.734 mm^3) was affixed to the tip of a glass fiber and mounted on the X-ray diffractometer.

Method 2: Water (0.005 g, 0.3 mmol) was syringed into a ¼-in. FEP reactor followed by syringing of 2,6-dimethylpyridine (0.086 g, 0.80 mmol) into the reactor. Subsequently, SF_4 (0.375 g, 3.47 mmol) was vacuum distilled at −196 °C onto the frozen. The mixture

was warmed slightly and liquid nitrogen was used to quench the vigorous reaction. The reaction mixture was warmed to −45 °C and mixed, resulting in a clear colourless solution. Slow cooling to −85 °C resulted in growth of clear colourless crystals. Excess SF_4 and SOF_2 were removed at −90 °C under dynamic vacuum. The crystals were characterized by X-ray crystallography.

2.4.5 Preparation of $[HNC_5H_4N(CH_3)_2^+][HF_2^-]\bullet 2SF_4$

Inside a dry box, 4-dimethylaminopyridine (0.026 g, 0.21 mmol) was transferred to a ¼-in. FEP reactor. Water (0.002 g, 0.1 mmol) was micro-syringed into the reactor, followed by distillation of an excess of SF_4 (ca. 0.04 mL, 0.7 mmol) at −196 °C. The reactor was slowly warmed to 3 °C, resulting in a clear colourless solution. Slow cooling to −20 °C resulted in the formation of large needles. Further cooling to −40 °C caused the crystals to grow considerably. Excess SF_4 and SOF_2 were removed between −97 and −87 °C, which caused precipitation of a white powder. A large needle, out of many needles, was selected out of a pile of low density colourless powder, and cut into a block (0.202 × 0.216 × 0.524 mm^3), and then affixed to the end of a cryo-loop for characterization by X-ray crystallography. The product was also characterized by low-temperature Raman spectroscopy (see Table 4.14).

2.4.6 Preparation of $[HNC_5H_4N(CH_3)_2^+]_2[SF_5^-]F^-\bullet CH_2Cl_2$

Inside a dry box, 4-dimethylaminopyridine (0.023 g, 0.19 mmol) was transferred to a ¼-in. FEP reactor. A large excess of SF_4 (ca. 0.04 mL, 0.7 mmol) was vacuum distilled at −196 °C onto the 4-dimethylaminopyridine, and the reactor was stored at −70 °C in a cryo-bath. Approximately 0.05 mL of CH_2Cl_2, which apparently contained moisture, was distilled onto the mixture and the reactor was agitated and warmed to −60

°C, resulting in a clear colourless solution. Removal of volatiles under dynamic vacuum at −80 °C resulted in large needles, with a small amount of yellow powder. The product was characterized by low-temperature Raman spectroscopy (see Table 4.15) and X-ray crystallography.

2.4.7 Preparation of $[HNH_4C_5{-}C_5H_4N^+]F^-{\bullet}2SF_4$

Inside a dry box 4,4'-bipyridyl (0.022 g, 0.14 mmol) was added to a ¼-in. FEP reactor. Water (0.001 g, 0.06 mmol) was micro-syringed into the reactor. A large excess of SF_4 (ca. 0.04 mL, 0.7 mmol) was distilled at −196 °C. The reactor was warmed to −80 °C which caused the brown solid 4,4'-bipyridyl to turn colourless. Further warming resulted in a clear pale yellow solution. Slow cooling resulted in growth of large needles. Volatiles were pumped off at −70 °C. A fragment of a needle (0.088 × 0.146 × 0.336 mm^3) was affixed onto a cryo-loop and mounted onto the diffractometer. The product was characterized by low-temperature Raman spectroscopy (see Table 4.19) and X-ray crystallography.

2.4.8 Preparation of $[HNH_4C_5{-}C_5H_4NH^{2+}]2F^-{\bullet}4SF_4$

Inside a dry box, 4,4'-bipyridyl (0.009 g, 0.06 mmol) was added to a 1.4-in. FEP reactor. Water (0.001 g, 0.06 mmol) was micro-syringed into the reactor. A large excess of SF_4 (ca. 0.1 mL) was distilled at −196 °C. Subsequent warming of the reactor to room temperature caused a portion of the colourless solid to dissolve, but the solubility was relatively low. Slow cooling to −80 °C, resulted in the formation of large needles. Excess SF_4 and SOF_2 were pumped off at −90 °C. The product was characterized by low-temperature Raman spectroscopy (see Table 4.20) and X-ray crystallography.

2.4.9 X-ray Crystal Structure of $[HNC_5H_4(CH_3)^+]HF_2^-$

After distillation of 4-methylpyridine (0.073 g, 0.78 mmol) into a ¼-in. FEP reactor, SF_4 (0.23 g, 2.1 mmol) was transferred *in vacuo* onto the frozen solid. A slow reaction proceeded at −80 °C, dissolving the solid yielding a clear colourless solution. Volatiles were removed at −75 °C. The reactor only contained 0.4 mmol of SF_4 after removal of volatiles. The reactor was accidentally warmed to room temperature, causing the solid to melt and form a colourless yellow liquid. Toluene, containing traces of H_2O, was distilled onto the solid at −196 °C. While the solid dissolved, gas evolved at −60 °C. The reactor was heat-sealed under vacuum and stored in the cryo-bath at −80 °C for crystal growth. Large needles formed, which, when mounted on the diffractometer, had very weak reflections. A needle (0.090 × 0.162 × 0.348 mm^3) was affixed onto a cryo-loop dipped in perfluorinated oil (Fomblin Z-25) at −80 °C.

2.5 Solid-State Structure of SF_4

2.5.1 Synthesis of $[HNC_5H_3(CH_3)_2^+]_2F^-[SF_5^-]\bullet 4SF_4$

Water (0.016 g, 0.89 mmol) was injected into a ¼-in. FEP reactor equipped with a Kel-F valve using a micro syringe, followed by transfer of 2,6-dimethylpyridine (0.176 g, 1.64 mmol) into the ¼-in. FEP reactor using a syringe in a dry-nitrogen-filled glove bag. A large excess of SF_4 was vacuum-distilled onto the frozen mixture at –196 °C. Upon melting of SF_4 at –120 °C, a vigorous reaction occurred, causing a white insoluble precipitate to form. Warming the reaction mixture to 0 °C formed a clear colourless solution. Slow cooling of this solution to –85 °C led to the formation of large needle-like crystals. Excess SF_4 was partially removed under dynamic vacuum at –95 °C, yielding 0.69 g of a white solid, i.e., $[HNC_5H_3(CH_3)_2^+]_2F^-[SF_5^-] \bullet 4SF_4$ with small amounts of

residual SF_4. The product was characterized by low-temperature Raman spectroscopy (see Table 5.3) and X-ray crystallography.

2.5.2 X−Ray Crystallography of Neat SF_4

Sulfur tetrafluoride (0.015 g, 1.4 mmol) was vacuum distilled into a ¼-in. FEP reactor. Crystals were grown by slowly cooling the liquid SF_4 to –150 °C in the ¼-in. FEP reactor placed inside an aluminium cold trough. After the temperature stabilized, the FEP tube was cut approximately 6 cm above the frozen SF_4. A Pasteur pipette was used to remove some crystals. A suitable crystal ($0.063 \times 0.075 \times 0.117$ mm^3) was affixed to a nylon cryo-loop coated in Fomblin Z-15 perfluorinated oil. Crystals were mounted at low temperature under a stream of dry cold nitrogen as described below.

2.5.3 X−Ray Crystallography of SF_4 from CF_2Cl_2

Sulfur tetrafluoride (0.034 g, 3.1 mmol) was vacuum distilled in a ¼-in. FEP reactor. Approximately 0.1 mL of CF_2Cl_2 was vacuum distilled on top of the solid SF_4. Upon melting, two distinct layers were observed. Agitation caused the liquids to mix, forming a homogeneous solution. Cooling of the solution to –131.8 °C (pentane cold bath) and reducing the volume of CF_2Cl_2 under dynamic vacuum led to the formation of plate-like crystals. The FEP was cut in a cold trough, and the crystals were removed using a Pasteur pipette. A suitable plate ($0.135 \times 0.149 \times 0.173$ mm^3) was affixed to a ball of Fomblin Z-15 perfluorinated oil on a nylon cryo-loop, off the end of the pipette tip.

2.6 SF_4 Oxygen Base Adducts

2.6.1 Preparation of the SF_4•OC_4H_6 Adduct

An equimolar amount of tetrahydrofuran (0.233 g, 3.23 mmol) and SF_4 (0.35 g 3.2 mmol) were condensed into a ¼-in. FEP reactor. Warming to −80 °C yielded a solution.

Slow cooling caused the solution to freeze at −99 °C. Alternatively, an excess SF_4 can be used and the sample can be placed under dynamic vacuum at −90 °C until a 1:1 mixture is obtained. The clear colourless solid melts at approximately −95 °C. The product was characterized by low-temperature Raman spectroscopy (see Table 6.4) and X-ray crystallography.

2.6.2 Preparation of the $SF_4•(OC_4H_6)_2$ Adduct

Tetrahydrofuran (0.172 g, 2.39 mmol) and subsequently SF_4 (0.13 g, 1.2 mmol) were vacuum distilled into a ¼-in. FEP reactor. Warming to −80 °C yielded a homogeneous mixture. Slow cooling caused the solution to freeze at −106 °C. The solid melted at approximately −100 °C into a clear colourless solution. The product was characterized by low-temperature Raman spectroscopy (see Table 6.5) and X-ray crystallography.

2.6.3 Preparation of the $SF_4•(CH_3OCH_2)_2$ Adduct

1,4-Dimethoxyethane (0.037 g, 0.41 mmol) was pipetted into a ¼-in. FEP reactor. Excess SF_4 (0.231 g, 2.14 mmol) was vacuum distilled onto the frozen 1,4-dimethoxyethane at −196 °C. The reactor was warmed to approximately −60 °C and agitated in order to dissolve the 1,4-dimethoxyethane. The clear colourless liquid was placed under dynamic vacuum at −90 °C to remove excess SF_4. Slow cooling of the clear colourless solution caused the sample to crystallize at −100 °C. The solid (81 mg, 0.41 mmol) melted at approximately −83 °C. The product was characterized by low-temperature Raman spectroscopy (see Table 6.7) and X-ray crystallography.

2.6.4 Preparation of the $SF_4•(O=C_5H_8)_2$

Cyclopentanone (20 mg, 0.24 mmol) was pipetted into a ¼-in. FEP reactor. Sulfur tetrafluoride (26 mg, 0.24 mmol) was vacuum distilled onto the frozen cyclopentanone at −196 °C. The reactor was warmed to −50 °C and vigorously agitated until a clear colourless solution was obtained. The reactor was slowly cooled to −100 °C at which point it slowly crystallized. The colourless crystalline solid melted at approximately −63 °C. The product was characterized by low-temperature Raman spectroscopy (see Table 6.9) and X-ray crystallography.

2.6.5 Attempted Preparation of $SF_4•OEt_2$

An equimolar amount of diethyl ether and SF_4 were distilled into a ¼-in. FEP reactor. The mixture froze when it was slowly cooled to approximately −145 °C.

2.6.6 Attempted Preparation of SF_4•acetylacetone

Acetylacetone (39mg, 0.39 mmol), was pipetted into a ¼-in. FEP reactor and degassed using the freeze-pump-thaw method. Sulfur tetrafluoride (51 mg, 0.47 mmol) was vacuum distilled onto the acetylacetone and the reactor was warmed to −60 °C and agitated, until a clear colourless solution was obtained. The reactor was placed under dynamic vacuum at −80 °C for approximately one hour, when clear colourless plates formed. Raman spectroscopy showed signals of neat acetylacetone and liquid SF_4.

2.6.7 Attempted Preparation of SF_4•4-methylcyclohexanone

4-Methylcyclohexanone (58 mg, 0.52 mmol) was pipetted into a ¼-in. FEP reactor and degassed using the freeze-pump-thaw method. Sulfur tetrafluoride (55 mg, 0.52 mmol) was vacuum distilled onto the frozen 4-methylcyclohexanone at −196 °C. The

mixture was warmed to −80°C and agitated to form a clear colourless solution. The mixture was slowly cooled and froze at approximately −120 °C.

2.7 Single Crystal X-ray Diffraction

2.7.1 Low-Temperature Crystal Mounting

Low-temperature crystal mounting was used for thermally unstable and moisture-sensitive crystals. (Figure 2.3) The temperature of the trough was measured with a copper-constantan thermocouple and adjusted to the appropriate temperature (between −70 and −150 °C) before the samples were introduced to the trough. For dry samples containing crystals in FEP tubes (4 mm or ¼-in.), the FEP tube was cut under a stream of dry nitrogen while maintaining the crystals at −78 °C in packed dry ice. The crystals were then transferred into the metal trough that had previously been cooled to approximately −80 °C. Alternatively, the samples in the FEP tubes were removed from an ethanol cold bath (below −80 °C), quickly wiped to remove the ethanol, and placed in the cold trough. The FEP tube was then cut at the end of the trough with scissors, and the crystals could be removed using a glass pipette or by inverting the FEP tube with tweezers. For wet samples, the cut FEP tubes were manipulated in the cold trough, at temperatures just above the freezing point of the solvent. Solvents were removed using a combination of glass pipettes, and capillary action of Kimwipes®. For extra sensitive crystals, the crystals were removed with the tip of a glass pipette and were directly affixed onto either a glass fiber, or a nylon cryo-loop dipped in inert perfluorinated polyethers, Fomblin Z-25 or Z-15 (Ausimont Inc.). The use of a round FEP tray, inside the trough, was also used to manipulate crystals which decomposed on contact with the metal troughs.

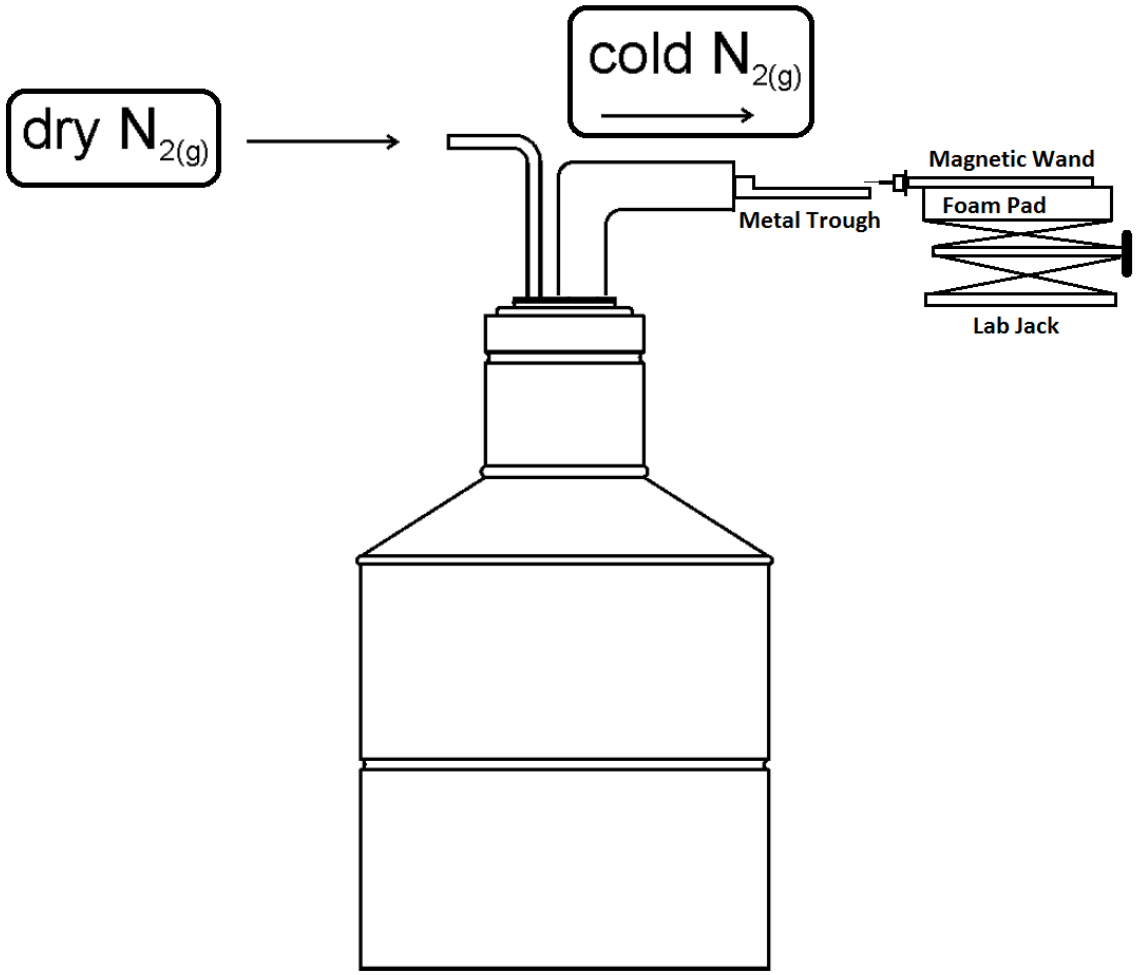

Figure 2.3 Low-temperature crystal mounting setup, consisting of a 10.5-L Dewar, equipped with a foam stopper, a glass nitrogen inlet, a silvered glass cold nitrogen outlet with an 11-cm long aluminium trough (2-cm o.d.). (Adapted from Jared Nieboer's M.Sc. thesis)

2.7.1.1 Special Cases

$[HNC_5H_5^+][HF_2^-]$•$2SF_4$: When the clumps were cut apart, nice clear colourless crystals could be observed, which turned opaque within 5 to 10 seconds. These opaque crystals did not diffract. The temperature in the cold trough was lowered to approximately −90 °C and the temperature of the diffractometer cold stream was lowered to −130 °C. A

large clump was broken apart, and a single crystal (0.077 × 0.117 × 0.290 mm^3) was mounted and transferred as quickly as possible.

$[HNC_5H_4N(CH_3)_2^+]_2[SF_5^-]F^-•CH_2Cl_2$: The error associated with this structure is relatively high. This is most likely because the crystal was an extremely thin needle and gave weak reflections, even with a relatively long exposure time of 120 s. In addition, the SF_5^- anion is disordered over two positions which increases the degree of error associated with the refined metrical parameters, thus increasing the overall uncertainties.

$[HNH_4C_5–C_5H_4NH^{2+}]2F^-•4SF_4$: A large needle was mounted onto the diffractometer, in which the cryo-stream was set at −100 °C. The crystal decomposed over the time span of approximately one minute. The cryo-stream was lowered to −120 °C and a thin, long needle (0.079 × 0.084 × 0.581 mm^3) was mounted.

2.7.2 Data Collection

Crystal structures were collected at temperatures at temperatures ranging from −120 to −173 °C on a Bruker AXS X-ray diffractometer. The Apex II 4K charge-coupled device (CCD) area detector was positioned 6.120 cm away from the crystal. The Kα radiation (λ = 0.71073 Å) of a Mo source X-ray tube was used with a graphite monochrometer. Cell reduction was carried out using the Program *SAINT*[3] which applied Lorentz and polarization corrections to three-dimensionally integrated diffraction spots.

2.7.3 Solution and Refinement of Structures

Calculations were performed using the *SHELXTL-plus v.6.14* package[4] for structure determination, refinement and molecular graphics. The program SADABS[5] was used for scaling of diffraction data, the application of a decay correction, and a multi-scan absorption correction. *Mercury 2.4* aided in the visualization of packing and

intermolecular interactions.[6] *Xprep* was used to confirm the unit cell dimensions and the Bravais crystal lattice. *Platon* was used to check for higher symmetry.[7] Crystal structures were solved using direct methods, Patterson methods, or dual space methods. The structures were minimized by least squares refinement based on the square of the structure factors, F^2 (equivalent to intensity, I). Atom positions were refined anisotropically and the extinction coefficient was calculated for the crystal structure. If the error in the extinction coefficient was on the same order of magnitude as the extinction coefficient, it was omitted. Both residual values, R_1 based on F and the weighted residual values wR_2 based on F^2, are available in the structure refinement tables along with the goodness of fit (*GooF*). They represent the following equations:

$R_1 = \frac{\sum||F_o| - |F_c||}{\sum|Fo|}$ The conventional R-factor based upon the structure factor.

$wR_2 = \sqrt{\frac{\sum\left[w(F_o^2 - F_c^2)^2\right]}{\sum\left[w(F_o^2)^2\right]}}$ The weighted R-factor based on the square of the structure factors

$Goof = \sqrt{\frac{\sum[w(F_o^2 - F_c^2)]}{(n-p)}}$ The *GooF* (goodness of fit) is based upon intensity where n is the number of reflections and p is the number of parameters refined.

Experimental details of each crystal data set are listed in Table 2.1 and the cif files are available on the attached CD.

Table 2.1 X-ray Crystal Structures and Selected Acquisition Parameters.

Sample Code	Compound	T (°C)	Size (mm^3)	Exposure Time (s)
MG12035	$[Ag(CH_3CN)_4][ReO_2F_4]$	−120	0.09 × 0.23 × 0.41	40
MG12077	$K[IO_2F_4]$	−120	0.15 × 0.10 × 0.05	40
MG12063	$[N(CH_3)_4][IO_2F_4]$	−120	0.04 × 0.33 × 0.34	40
MG11019	$[HNC_5H_5^+]F^-•SF_4$	−120	0.32 × 0.36 × 1.38	10
MG12051	$[HNC_5H_5^+]HF_2^-•2SF_4$	−130	0.08 × 0.12 × 0.29	60
MG12072	$[HNC_5H_4(CH_3)^+]F^-•SF_4$	−120	0.16 × 0.23 × 0.28	45
MG12078	$[HNC_5H_4(CH_3)^+]HF_2^-$	−120	0.09 × 0.16 × 0.35	50
MG11020	$[HNC_5H_3(CH_3)_2^+]_2[SF_5^-]F^-•SF_4$	−120	0.70 × 0.46 × 0.20	20
MG12071	$[HNC_5H_4N(CH_3)_2^+][HF_2^-]•2SF_4$	−120	0.20 × 0.22 × 0.52	40
MG12074	$[HNC_5H_4N(CH_3)_2^+]_2[SF_5^-]F^-•CH_2Cl_2$	−120	0.08 × 0.086 × 0.37	120
MG120176	$[HNH_4C_5{-}C_5H_4N^+]F^-•2SF_4$	−120	0.09 × 0.15 × 0.34	45
MG12086	$[HNH_4C_5{-}C_5H_4NH^{2+}]2F^-•4SF_4$	−120	0.08 × 0.08 × 0.58	120
MG12107	$[HNC_5H_3(CH_3)_2^+]_2[SF_5^-]F^-•4SF_4$	−140	0.16 × 0.19 × 0.58	40
MG12097	SF_4	−173	0.06 × 0.075 × 0.12	30
MG12088	$SF_4•OC_4H_8$	−140	0.15 × 0.31 × 0.50	5
MG13029	$SF_4•(OC_4H_8)_2$	−150	0.22 × 0.19 × 0.10	40
MG13024	$SF_4•(CH_3OCH_2)_2$	−145	0.67 × 0.20 × 015	40
MG13026	$SF_4•(O{=}C_5H_8)_2$	−150	0.27 × 0.16 × 0.12	40

2.7.3.1 Special Cases

$[Ag(CH_3CN)_4][ReO_2F_4]•CH_3CN$: Using the *RLATT* program, multiple crystal domains were observed in the reciprocal lattice. The largest domain was selected, and the other reflections discarded.

$[HNC_5H_3(CH_3)_2^+]_2[SF_5^-]F^-•SF_4$ and $[HNC_5H_4N(CH_3)_2^+]_2[SF_5^-]F^-•CH_2Cl_2$: After refinement of each structure, residual electron density was observed around some fluorine atoms in the SF_5^- anion, which suggested that the SF_5^- anion occupied two separate orientations. The site occupancy factor between these two orientations was set as a free variable, which suggested a 70-to-30% occupancy for $[HNC_5H_3(CH_3)_2^+]_2[SF_5^-]F^-•SF_4$ and a 80-to-20% for $[HNC_5H_4N(CH_3)_2^+]_2[SF_5^-]F^-•CH_2Cl_2$. Similarity restraints were used to set the bond lengths and angles (SAME), and thermal ellipsoids (SIMU) of the two orientations of the SF_5^- anion, as they are assumed to be equal. The SF_5^- anions are joined by a fixed pivot point, i.e., the axial fluorine for $[HNC_5H_3(CH_3)_2^+]_2[SF_5^-]F^-•SF_4$ and one of the equatorial fluorines for $[HNC_5H_4N(CH_3)_2^+]_2[SF_5^-]F^-•CH_2Cl_2$.

SF_4: The program *ROTAX* was used to find the twin law (0 −1 0 −1 0 0 0 0 −1). After the twin law was implemented, the structure was refined as usual.

$SF_4•(OC_4H_6)_2$: The program *Cell Now* was used to determine the two separate crystal domains. Both domains were integrated together and an hkl.4 file was created. TWINABS[8] was used to process the data, and structure was solved using direct methods.

2.8 Vibrational Spectroscopy

Raman spectra were recorded on a Bruker RFS 100 FT Raman spectrometer with a quartz beam splitter, a liquid-nitrogen cooled Ge detector, and R-496 low-temperature accessory. The actual usable Stokes range was 50 to 3500 cm^{-1}. The 1064-nm line of a Nd:YAG laser was used for excitation of the sample. The Raman spectra were recorded at temperatures ranging from –142 °C to 20 °C with a spectral resolution ranging from 1 to 4 cm^{-1} using laser powers ranging from 50 to 300 mW. Samples were recorded in Pyrex-glass mp capillaries and NMR tubes, 4-mm and ¼-in. FEP tubes.

2.9 NMR Spectroscopy

NMR spectra were recorded unlocked on a 300.13 MHz (7.0486 T) Bruker Advance II NMR spectrometer equipped with a variable temperature, two channel BBFO probe. The ^{19}F, ^{1}H, and ^{13}C NMR spectra were referenced at room temperature to external samples of neat $CFCl_3$ {^{19}F} and TMS {^{1}H and ^{13}C). All NMR spectra were recorded on sealed 4-mm FEP tubes inserted into standard 5-mm glass NMR tubes.

References

(1) Winfield, J. M. *J. Fluorine Chem.* **1984**, *25*, 91-98.

(2) Gerken, M.; Mack, J. P.; Schrobilgen, G. J.; Suontamo, R. J. *J. Fluorine Chem.* **2004**, *125*, 1663-1670.

(3) Bruker; Apex2 and Saint-plus. Bruker AXS Inc.: Madison, W., USA, 2006.

(4) Sheldrick, G. M. 6.14 ed.; Bruker AXS INC.: Madison, Wisconsin, USA, 2003

(5) G. M. Sheldrick, *SADABS*, Version 2007/4; Bruker AXS Inc.; Madison, WI, 2007.

(6) Cambridge Crystallographic Data Centre, *Mercury 2.4*, 2013.

(7) Spek, A.L. *Acta Cryst.* **2009**, *D65*, 148-155.

(8) Bruker. *TWINABS.* Bruker AXS Inc., Madison, Wisconsin, USA, 2001.

3 Sulfur Tetrafluoride as a Fluorinating Agent Towards Main-Group and Transition-Metal Oxo-Anions.

3.1 Introduction

Sulfur tetrafluoride has extensively been used as a fluorinating agent in organic chemistry.[1] The usefulness of SF_4 in inorganic chemistry has been explored for converting metal oxides to fluorides at high temperatures and pressures.[2] For example, Bi_2O_3, TiO_2, U_3O_8, and HgO are fluorinated by SF_4 to BF_3 (Equation. 3.1), TiF_4, UF_6, and HgF_2, respectively.

$$Bi_2O_3 + 3\ SF_4 \rightarrow 2\ BiF_3 + 3\ SOF_2 \quad (3.1)$$

Main-group oxides and sulfides also react with SF_4 to produce fluorides (SnS_2 to SnF_4 and FeS_2 to FeF_2) and oxide fluorides (P_4O_{10} to POF_3) (see Equations 3.2 and 3.3, respectively).

$$SnS_2 + SF_4 \rightarrow SnF_4 + {}^3/_8\ S_8 \quad (3.2)$$

$$P_4O_{10} + 6\ SF_4 \rightarrow 4\ POF_3 + 6\ SOF_2 \quad (3.3)$$

Sulfur tetrafluoride will generally lose two of its fluorines when reacting with oxides, but loses all four of its fluorines when reacting with sulfides. Very little has been reported on the use of SF_4 as a fluorinating agent towards oxo-anions of main-group and transition-metal elements in high oxidation states.[3] A large number of oxide-fluoride anions have been synthesized and characterized.[4] The $ReO_2F_4^-$ anion was first synthesized in 1955 by Peacock from the reaction of excess BrF_3 with metal perrhenate salts (see Equation 3.4).[5]

$$3\ ReO_4^- + 4\ BrF_3 \rightarrow 3\ ReO_2F_4^- + 3\ O_2 + 2\ Br_2 \quad (3.4)$$

The reaction required extensive heating under vacuum to remove excess unreacted BrF_3 and the Br_2 by-product. Another method of synthesizing the $ReO_2F_4^-$ anion is through the reaction of ReO_2F_3 with fluoride salts, such as LiF and $[N(CH_3)_4]F$.[6] The Li^+ and $N(CH_3)_4^+$ salts of $ReO_2F_4^-$ were characterized by Raman and ^{19}F NMR spectroscopy as well as X-ray crystallography.[6] Neutral ReO_2F_3 can be prepared by the reaction of Re_2O_7 with XeF_6 in anhydrous HF. Holloway *et al.* report that $KReO_4$ does not react with anhydrous HF at room temperature, whereas Seppelt *et al.* report the reaction yields $ReO_2F_4^-$. Another paper mentions the formation of ReO_3F in the reaction of $KReO_4$ with anhydrous HF.[7-9] These rhenium species are in equilibrium with each other in aHF, therefore, a large excess of aHF is required to produce $ReO_2F_4^-$ and the yields are low.

Previous syntheses of the IOF_4^- anion used the reaction of IF_5 with a metal fluoride and iodate, or the hydrolysis of the IF_6^- anion.[10] The previous reactions also produced the $IO_2F_2^-$ anion, besides IOF_4^-, which are difficult to separate. Although the crystal structure of the $Cs[IOF_4]$ salt has been reported, the quality is poor.[11] The $IO_2F_4^-$ anion was previously synthesized by the repeated reaction of IO_4^- with aHF over long periods of time.[10] An alternative route is the reaction of IO_2F_3 with $[N(CH_3)_4]F$ in acetonitrile, but this route is hazardous since detonations have occurred during this reaction.[12] Both of these methods of preparing the $IO_2F_4^-$ anion produced mixtures of *trans* and *cis* isomers.[12]

3.2 Results and Discussion

3.2.1 Synthesis

The reactions of sulfur tetrafluoride with oxo-anions of Re^{VII}, I^{VII}, and I^{V} were studied using Raman and NMR spectroscopy, as well as X-ray crystallography. No reaction between $AgReO_4$, $KReO_4$, KIO_4 or $[N(CH_3)_4]IO_3$ and neat SF_4 was observed at room temperature even with sonication. The reaction between $AgReO_4$ and SF_4 proceeds when acetonitrile is used as a solvent at temperatures between −40 and 20 °C (see Equation 3.5).

$$AgReO_4 + 2\ SF_4 \quad \rightarrow \quad Ag[ReO_2F_4] + 2\ SOF_2 \qquad (3.5)$$

The reaction also proceeds with $KReO_4$, but due to the poor solubility of $KReO_4$ in acetonitrile, more solvent and longer reaction times are required for the reaction to proceed to completion. At low temperatures, the silver salt contains acetonitrile coordinated to the silver cation. Crystals of $[Ag(CH_3CN)_4][ReO_2F_4]\bullet CH_3CN$ were grown at low temperature containing four CH_3CN ligands coordinated to Ag^+ and one a "free" solvent per asymmetric unit (*vide infra*). The CH_3CN can be partially removed under dynamic vacuum at room temperature presumably yielding $[Ag(CH_3CN)_2][ReO_2F_4]$, and fully removed upon heating to 60 °C under vacuum, as shown by Raman spectroscopy. Peacock reported that $Ag[ReO_2F_4]$ is a darker coloured salt than the other metal salts of $ReO_2F_4^-$, which must have been due to contamination, since the salt obtained in the present study was a light cream-coloured solid.[5] The $Ag[ReO_2F_4]$ salt has only been characterized by its physical properties, and crude elemental analysis.[5]

The reaction between $[N(CH_3)_4]IO_3$ and SF_4 in acetonitrile quantitatively yields the new IOF_4^- salt, $[N(CH_3)_4][IOF_4]$ at room temperature (see Equation 3.6).

When the orange solution is cooled from room temperature to −30 °C, large plates crystallize from the reaction mixture.

$$[N(CH_3)_4][IO_3] + 2\ SF_4 \rightarrow [N(CH_3)_4][IOF_4] + 2\ SOF_2 \quad (3.6)$$

When the volatiles were removed at −80 °C, the reaction mixture became clear and colourless. The rest of the volatiles were removed between −80 and −30 °C leaving clear colourless plate-like crystals.

No reaction occurred between KIO_4 and SF_4 in acetonitrile. A slurry of KIO_4 in anhydrous HF reacted with SF_4 to form a clear colourless solution at 0 °C. (Equation 3.7) When the volatiles were removed at −78 °C, a white solid remained with clear colourless crystals.

$$KIO_4 + 2\ SF_4 \rightarrow K[IO_2F_4] + 2\ SOF_2 \quad (3.7)$$

3.2.2 $[Ag(CH_3CN)_4][ReO_2F_4]\bullet CH_3CN$, $[Ag(CH_3CN)_x]ReO_2F_4$ (where x = 0, 2)

3.2.2.1 Raman Spectroscopy

The Raman spectra of $[Ag(CH_3CN)_4][ReO_2F_4]\bullet CH_3CN$ and $[Ag(CH_3CN)_x]ReO_2F_4$ (where x = 0, 2) are depicted in Figure 3.1. The Raman frequencies and tentative assignments are listed in Table 3.1. The signals associated with the acetonitrile moieties were assigned based on previous assignments made by Reedijk *et al.*[13] The signals associated with $ReO_2F_4^-$ anion were assigned based on the previous assignments made by Schrobilgen *et al.*,[6] who used computational techniques to aide in the assignment of the vibrational modes.

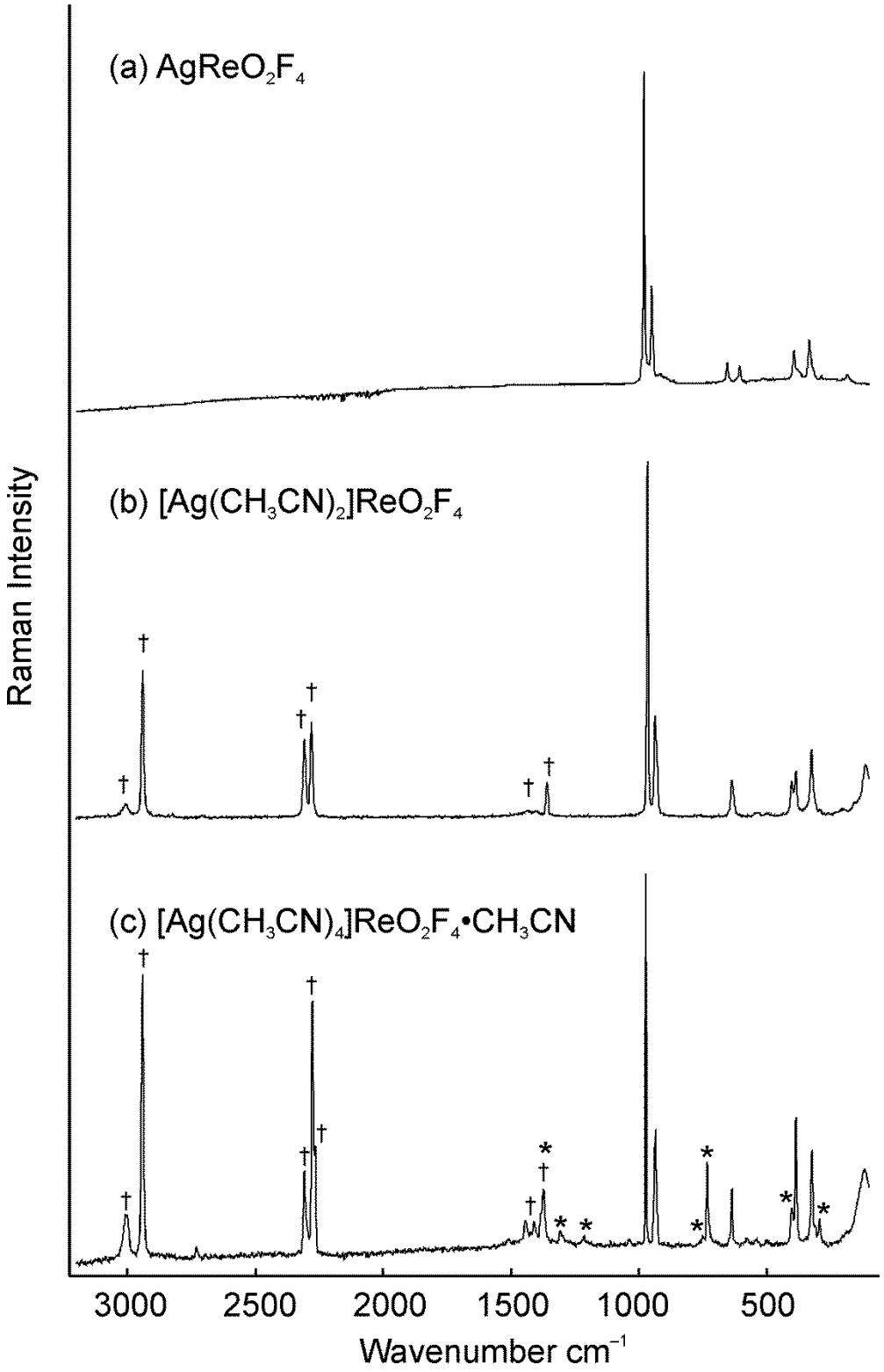

Figure 3.1 Raman spectra of $AgReO_2F_4$ salts with varying amounts of CH_3CN. Asterisks (*) denote bands arising from the FEP sample tube. Daggers (†) denote bands arising from the CH_3CN.

Table 3.1 Raman Frequencies (cm^{-1}) and Tentative Assignments of $[Ag(CH_3CN)_4]$-$ReO_2F_4 \bullet CH_3CN$, $[Ag(CH_3CN)_2]ReO_2F_4$, $AgReO_2F_4$, and CH_3CN.

$[Ag(CH_3CN)_4][ReO_2F_4]$ $\bullet CH_3CN$[a]	$[Ag(CH_3CN)_2]$ $[ReO_2F_4]$[b]	$Ag[ReO_2F_4]$	CH_3CN	Tentative Assignment
3007(13)	3006(3)		3001(6)	ν_{as}(C−H)
2941(76)	2940(42)		2943(100)	ν_s(C−H)
			2888(2)	Combination bands
			2847(2)	
2730(5)			2732(3)	
2308(23)	2308(23)		2293(6)	
2276(70)	2281(28)			C≡N stretch
2266(30)			2253(60)	
			2204(1)	Combination band
1443(5)			1443(3)	
1410(4)			1416(1)	$\delta_{as}(CH_3)$
	1360(11)		1375(6)	$\delta_s(CH_3)$
1038(1)				
973(100)	967(100)	981(100)		$\nu_s(ReO_2)$
939(28)	938(29)	951(32)		$\nu_{as}(ReO_2)$
934(33)			919(20)	ν(C−C)
636(16)	637(11)	655(7)		$\nu_s(ReF_2c,c + ReF_2c,t)$
		607(6)		$\nu_{as}(ReF_2c,c)$
402(10)	403(10)		380(10)	δ(C−C≡N)
387(35)[b]	387(14)	394(9)		$\delta_{sciss}(ReO_2)$
324(26)	326(19)	334(13)		Sym comb of *cis/trans* ReF_2 scissor
	115(15)	187(3)		antisym comb of *cis/trans* ReF_2 scissor

[a] Signals from the FEP sample tube were observed at FEP: 1373(15), 1307(2), 1216(1), 733(23), 387(35), 294(6) cm^{-1}. [b] Acquired in glass m.p. capillary.

The Raman spectrum of $[Ag(CH_3CN)_4][ReO_2F_4]\bullet CH_3CN$ contains signals associated with both free and coordinated acetonitrile, as well as the $ReO_2F_4^-$ anion. The most intense band at 973(100) cm^{-1} can be assigned to the $\nu_s(ReO_2)$ mode and is at the same frequency as that found in the previously reported Cs^+ and $N(CH_3)_4^+$ salts.[6] This suggests no significant anion-cation interactions. The $\nu_{as}(ReO_2)$ mode can be assigned to the band at 939(28) cm^{-1}, which is also at the exact same frequency as the band previously reported for Cs^+ and $N(CH_3)_4^+$ salts. The ν_s(C−H) mode has remained essentially unshifted at 2941(76) cm^{-1} relative to that of neat liquid CH_3CN (2943(100) cm^{-1}).[13] In contrast to the un-shifted ν_s(C−H) mode, the C≡N stretch has been significantly shifted to a higher frequency of 2276(70) cm^{-1} from 2253(60) cm^{-1} found in neat liquid CH_3CN, reflecting the coordination to the silver cation. The increase in the C≡N stretching frequency of acetonitrile upon complexation with metal cations is a well-studied phenomenon.[13] In addition to coordinate CH_3CN, the "free" CH_3CN gives rise to a second C≡N stretching band at 2266(30) cm^{-1}.

After allowing the sample to warm to room temperature under dynamic vacuum, the signals associated with acetonitrile decreased in relative intensities. The relative intensity of the ν(C−H) mode (2940(42) cm^{-1}) is significantly lower, while the frequency is unchanged compared to the Raman band for $[Ag(CH_3CN)_4]ReO_2F_4\bullet CH_3CN$. The C≡N stretch (2281(28) cm^{-1}) has been shifted to an even higher frequency than for the previous salt (2276(70) cm^{-1}), exhibiting a larger complexation shift than the tetraacetonitrile complex. No other C≡N stretching band at a lower frequency was observed, suggesting the removal of the "free" CH_3CN at room temperature. The $\nu_s(ReO_2)$ mode (967(100) cm^{-1}) is shifted to a slightly lower frequency. The lower intensity of the signals associated with CH_3CN,

and the change in the frequencies of the signals associated with the $ReO_2F_4^-$ anion suggests a change in symmetry of the $[Ag(CH_3CN)_x^+]$ cation, but it is difficult to predict the exact nature of the coordination. The low frequency of the $\nu_s(ReO_2)$ mode suggests that there is no significant interaction with the cation, as the frequency of this band shifts to higher wavenumbers as the cation becomes more Lewis acidic (987 cm^{-1} for K^+, 1011 cm^{-1} for Na^+).[6] Since a linear coordination about Ag^+ is commonly observed,[14] the nature of this salt is likely $[Ag(CH_3CN)_2][ReO_2F_4]$.

The Raman spectrum of $Ag[ReO_2F_4]$ only contains peaks associated with the $ReO_2F_4^-$ moiety. The most intense band at 981(100) cm^{-1} was assigned to the $\nu_s(ReO_2)$ mode, which is at a higher frequency relative to the salts which contain CH_3CN coordinated to Ag^+, suggesting cation-anion interactions. This is corroborated with the significant increase in frequency of the $\nu_{as}(ReO_2)$ mode from 938(29) cm^{-1} ($[Ag(CH_3CN)_2][ReO_2F_4]$), to 951(32) cm^{-1} in $Ag[ReO_2F_4]$. The Raman spectrum most closely resembles that of the previously reported potassium salt.[6]

3.2.2.2 X-ray Crystallography

Large plates quickly formed when a mixture of $AgReO_4$, SF_4, and CH_3CN was cooled from 0 °C to −40 °C. The correct unit cell was found to be orthorhombic, with multiple twinning. Details of data collection parameters and crystallographic information for $[Ag(CH_3CN)_4][ReO_2F_4]\bullet CH_3CN$ are given in Table 3.2. Important bond lengths, angles and contacts are listed in Table 3.3.

Table 3.2 Crystal Data Collection Parameters and Results of $[Ag(CH_3CN)_4][ReO_2F_4]•CH_3CN$.

Compound	$[Ag(CH_3CN)_4][ReO_2F_4]•CH_3CN$
File Code	MG12035
Empirical Formula	$H_{15}C_{20}N_5O_2F_4AgRe$
Formula weight, g mol^{-1}	1715.38
Temperature, K	153
Wavelength, Å	0.71073
Crystal System	Orthorhombic
Space Group	$Pmn2_1$
Unit Cell Dimensions	a = 13.420(7) Å b = 8.861(4) Å c = 8.879(4) Å
Volume	1055.7(9)
Z	4
Density (calculated), g cm^3	2.039
Crystal Size, mm^3	0.09 × 0.23 × 0.41
Theta Range for data collection	28.2 to 2.3
Reflections Collected	12385
Independent Reflections	2695
Data/Restraints/Parameters	2695/0/16
Goodness-of-fit on F^2	1.22
Refine Diff $\Delta\rho$max e $Å^{-3}$	5.08
Refine Diff $\Delta\rho$min e $Å^{-3}$	−2.75
R_1, $I > 2\sigma(I)$[a]	0.064
wR_2 (F^2)[a]	0.183

[a] $R_1 = \Sigma||F_o| - |F_c||/\Sigma|F_o|$; w$R_2 = [\Sigma w(F_o^2 - Fc^2)^2/\Sigma w(F_o^4)]^{1/2}$.

Table 3.3 Selected Bond Lengths (Å) and Angles (deg.) of $[Ag(CH_3CN)_4][ReO_2F_4]\bullet CH_3CN$.

Bond Lengths, Å			
Ag1−N1	2.308(11)	Ag1−N3	2.267(19)
Ag1−N1^{i}	2.308(11)	Ag1−N2	2.214(17)
Re2−O6^{i}	1.668(11)	Re2−O6	1.668(11)
Re2−F1^{i}	1.919(8)	Re2−F1	1.919(8)
Re2−F3	1.929(10)	Re2−F2	1.873(12)
Bond Angles, (deg.)			
N1−Ag1−N1^{i}	104.3(6)	N2−Ag1−N1	115.6(4)
N3−Ag1−N1	108.8(4)	N2−Ag1−N1^{i}	115.6(4)
N3−Ag1−N1^{i}	108.8(4)	N2−Ag1−N3	103.7(6)
O6^{i}−Re2−O6	99.2(8)	F3−Re2−O6	92.2(4)
F1^{i}−Re2−O6^{i}	89.8(5)	F3−Re2−F1^{i}	85.4(4)
F1^{i}−Re2−O6	170.9(4)	F3−Re2−F1	85.4(4)
F1−Re2−O6	89.8(5)	F2−Re2−O6^{i}	96.6(5)
F1−Re2−O6^{i}	170.9(4)	F2−Re2−O6	96.6(5)
F1^{i}−Re2−F1	81.3(5)	F2−Re2−F1^{i}	84.2(4)
F3−Re2−O6^{i}	92.2(4)	F2−Re2−F1	84.2(4)
		F2−Re2−F3	166.3(5)

Symmetry code: (i) −*x*+1, *y*, *z*.

The structure consists of well separated $ReO_2F_4^-$ anions, which adopt the *cis*-conformation, and a silver cation coordinated by four acetonitrile ligands, forming a tetrahedral geometry around silver (see Figure 3.2).

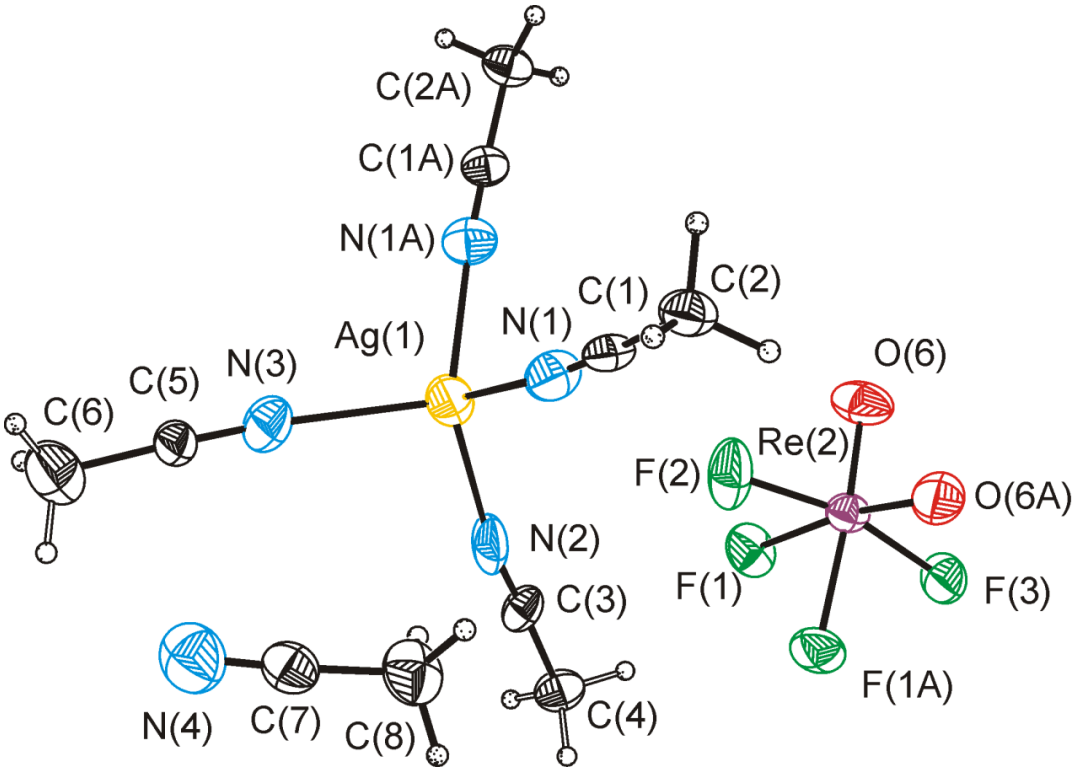

Figure 3.2 Thermal ellipsoid plot of $[Ag(CH_3CN)_4][ReO_2F_4]\bullet CH_3CN$. Thermal ellipsoids are set to 50% probability.

An additional "free" acetonitrile co-crystallizes in this salt. The *cis*-$ReO_2F_4^-$ anion adopts a distorted octahedral geometry, in which the axial fluorines are pushed towards the equatorial fluorines. The ReF_{2ax} moieties lie along a mirror plane, and therefore the equatorial Re−O bonds, as well as the Re−F_{eq} bonds, are crystallographically equivalent. The bond lengths agree well with those of the previously reported Li^+ salt. The Li^+ cation has six Li---F (2.04(3) to 2.108(7) Å)

contacts in an octahedral geometry.[6] For the $[Ag(CH_3CN)_4][ReO_2F_4]\bullet CH_3CN$ salt no significant cation-anion contacts are observed, since acetonitrile molecules separate the cations from the anions. The limited number of crystal structures which contain four acetonitriles coordinated to Ag(I) cations, contain counter-anions which are weakly coordinating, such as BF_4^-.[15]

The Re−O bonds (1.668(11) Å) are significantly shorter than the $Re-F_{eq}$ (1.919(8) Å) and the $Re-F_{ax}$ bonds (1.929(10), 1.873(12) Å). These values agree with the $Li[ReO_2F_4]$ salt ($Re-F_{eq}$ = 1.867(8) Å and $Re-F_{ax}$ = 2.002(7) Å), except for the distortion of one of $Re-F_{ax}$ bonds.[6] The *cis*-dioxo arrangement is favored in Re(VII) oxide-fluoride species and has been studied in depth by vibrational and ^{19}F NMR spectroscopies.[6,16]

3.2.3 $K[IO_2F_4]$

The Raman frequencies and tentative assignments for this known salt are listed in the experimental chapter. The Raman frequencies and intensities agree very well with what has previously been reported by Gillespie and Krasznai,[17] Boatz *et al.*,[12] and Christe *et al.*[18] The Raman spectrum contains signals associated with both the *cis* and *trans*-$IO_2F_4^-$ anion. The assignment of the signals for the two isomers are based on the previous assignments made by Boatz *et al.* for the $N(CH_3)_4^+$ and Cs^+ salts, who were able to separate the two stereoisomers.[12]

3.2.3.1 X-ray Crystallography

The crystal structure of the *trans*-$IO_2F_4^-$ anion has only recently been reported as the $(PPh_4)^+$ salt.[19] The structure of $K[IO_2F_4]$ crystals grown during this study was solved in the monoclinic space group *Cc*. The asymmetric unit contains two $IO_2F_4^-$ moieties, one that exhibits severe rotational disorder in the equatorial plane, and one appears to suffer from substitutional disorder. Both iodine anions appear to have octahedral geometries. It is likely that the *cis/trans*-isomers co-crystallized, but no conclusive structural information could be obtained.

3.2.4 $[N(CH_3)_4][IOF_4]$

Large thin plates were obtained when a solution of $[N(CH_3)_4][IOF_4]$ in acetonitrile was cooled to −30 °C. These plates gave an intense diffraction pattern. The structure was solved in the tetragonal $I\bar{4}2m$ space group. The asymmetric unit contained two well separated tetramethylammonium cations adopting tetrahedral geometries, and disordered anions. These anions are arranged as tetramers. The disorder of these tetramers could not be modeled in a chemically sensible way.

3.2.4.1 Raman Spectroscopy

The Raman spectrum of $[N(CH_3)_4][IOF_4]$ at room temperature is depicted in Figure 3.3. The Raman frequencies and tentative assignments are listed in Table 3.4. The spectrum contains signals associated with the $N(CH_3)_4^+$ cation and the IOF_4^- anion. The bands associated with the $N(CH_3)_4^+$ moiety were assigned based on previous assignments of other tetramethylammonium salts.[20] The bands associated

with the IOF_4^- anion were assigned based on the assignments for the previously reported $Cs[IOF_4]$ salt.[10]

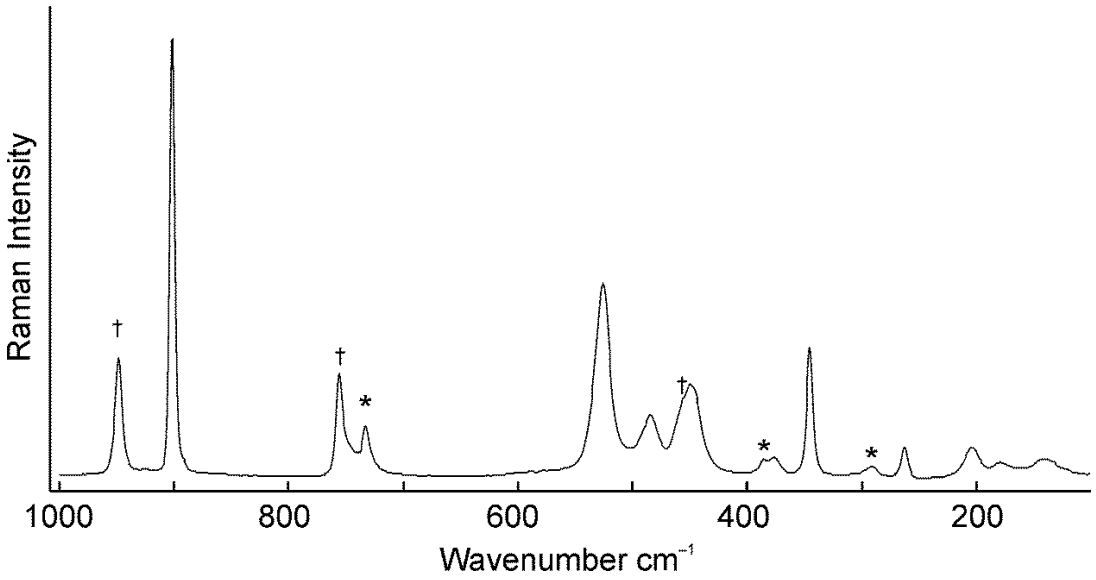

Figure 3.3 Raman spectrum of $[N(CH_3)_4][IOF_4]$. Asterisks (*) denote bands arising from the FEP sample tube. Daggers (†) denote bands arising from the $[N(CH_3)_4^+]$ cation.

The most intense band in the Raman spectrum at 901(100) cm^{-1} can be assigned to the ν(I−O) mode, and is in good agreement with that of the $Cs[IOF_4]$ salt (888 cm^{-1}). The in-phase ν_s (IF_4) mode was assigned to the band at 526(45) cm^{-1} and is in good agreement with the $Cs[IOF_4]$ salt (533 cm^{-1}).

Table 3.4 Raman Frequencies (cm^{-1}) and Tentative Assignments of $[N(CH_3)_4][IOF_4]$.

$[N(CH_3)_4][IOF_4]$	$CsIOF_4$[b]	Assignment
3039(25)		C−H stretch
2980(11)		
2960(23)		
2920(9)		
2882(5)		
2811(6)		
1531(1)		CH_3 deformation
1497(2)		
1470(33)		
1464(24)		
1412(7)		
1286(4)		C−N stretching modes
1175(6)		
1070(2)		
948(28)		$N(CH_3)_4^+$
901(100)	888 vs	ν(I−O)
756(24)		$\nu_s(NC_4)$
526(45)	533 vs	$\nu_s(IF_4)$ in phase
484(15)	485 s	$\nu_{as}(IF_4)$
449(22)	475 m	$\nu_s(IF_4)$ out of phase
376(5)		$\delta_s(NC_4)$
345(28)	365 ms	$\delta(OF_4)$ wag
263(7)	273 w	$\delta_s(IF_4)$ umbrella
204(8)	214 w	$\delta_s(IF_4)$ in plane
180(3)		
143(4)	124 w	$\delta_{as}(IF_4)$ in plane

[a] Signals from the FEP sample tube were observed at: 1380(3), 1214(1), 733(13), 526(overlap), 385(5), 291(3) cm^{-1}.
[b] From reference 10.

3.3 Summary and Conclusions

The reaction of transition-metal and main-group oxo-anions with SF_4 conveniently formed Re^{VII}, I^{VII}, and I^{V} oxide fluoride anions. These reactions occur in acetonitrile or anhydrous HF and give quantitative yields in a single step. The byproducts and solvents are easily removed under dynamic vacuum at low temperatures, or in the case of the $[Ag(CH_3CN)_x]^+$ cation, upon mild heating. The $Ag[ReO_2F_4]$ salt was characterized by Raman spectroscopy for the first time. Although the $Ag[ReO_2F_4]$ salt had been previously prepared, it had only been characterized by crude elemental analysis. The new $[Ag(CH_3CN)_4][ReO_2F_4]\bullet CH_3CN$ salt was characterized by low-temperature Raman and X-ray crystallography. The new $[N(CH_3)_4][IOF_4]$ salt was synthesized and characterized by Raman spectroscopy.

References

(1) Dmowski, W. Introduction of Fluorine Using Sulfur Tetrfluoride and Analogs In *Organo-Fluorine Compounds*; Baasner, B.; Hagemann, H.; Tatlow, J. C., Eds.; Methods of Organic Chemistry, Houben-Weyl, Vol. E10a; Thieme: Stuttgart, 2000; Ch. 8, pp. 321-431.

(2) Oppegard, A. L.; Smith, W. C.; Muetterties, E. L.; Engelhardt, V. A. *J. Am. Chem. Soc.* **1960**, *82*, 3835-3838.

(3) Smith, W. C.; Engelhardt, V. A. *J. Am. Chem. Soc.* **1960**, *82*, 3838-3840.

(4) Gerken, M.; Mercier, H. P. A.; Schrobilgen, G. J. Syntheses and Structures of the Oxide Fluorides of the Main-Group and Transition Metal Elements In *Advanced Inorganic Fluorides*; Nakajima, T.; Zemva, B., Eds.; Tressaud, A., Elsevier: Lausanne, 2000, Ch. 5, pp. 117-174.

(5) Peacock, R. D. *J. Chem. Soc.* **1955**, 602-603.

(6) Casteel, W. J.; Dixon, D. A.; LeBlond, N.; Lock, P. E.; Mercier, H. P. A.; Schrobilgen, G. J. *Inorg. Chem.* **1999**, *38*, 2340-2358.

(7) Brisdon, A. K.; Holloway, J. H.; Hope, E. G. *J. Fluorine Chem.* **1998**, *89*, 35-37.

(8) Supeł, J.; Marx, R.; Seppelt, K. *Z. Anorg. Allg. Chem.* **2005**, *631*, 2979-2986.

(9) Selig, H.; El-Gad, U. *J. Inorg. Nucl. Chem.* **1973**, *35*, 3517-3522.

(10) Milne, J. B.; Moffett, D. M. *Inorg. Chem.* **1976**, *15*, 2165-2169.

(11) Ryan, R. R.; Asprey, L. B. *Acta Crystallogr. B* **1972**, *28*, 979-981.

(12) Boatz, J. A.; Christe, K. O.; Dixon, D. A.; Fir, B. A.; Gerken, M.; Gnann, R. Z.; Mercier, H. P. A.; Schrobilgen, G. J. *Inorg. Chem.* **2003**, *42*, 5282-5292.

(13) Reedijk, J.; Zuur, A. P.; Groeneveld, W. L. *Recl. Trav. Chim. Pays-Bas* **1967**, *86*, 1127-1137.

(14) Shoeib, T.; El, A. H.; Siu, K. W. M.; Hopkinson, A. C. *J. Phys. Chem. A* **2001**, *105*, 710-719.

(15) Aly, A.; Walfort, B.; Lang, H. *Z. Kristallogr. - New Cryst. Struct.* **2004**, *219*, 489-491.

(16) Kuhlmann, W.; Sawodny, W. *J. Fluorine Chem.* **1977**, *9*, 341-357.

(17) Gillespie, R. J.; Krasznai, J. P. *Inorg. Chem.* **1977**, *16*, 1384-1392.

(18) Christe, K. O.; Wilson, R. D.; Schack, C. J. *Inorg. Chem.* **1981**, *20*, 2104-2114.

(19) Christe, K. O.; Haiges, R. In *21st Winterfluorine Conference* St. Petersburg, Florida, Abstract IL-6, 2013.

(20) Kabisch, G. *J. Raman Spectrosc.* **1980**, *9*, 279-285.

4 Solvolysis Products of SF_4•Nitrogen Base Adducts by HF

4.1 Introduction

The fluoride anion is very different from the other halide anions as it has a significantly larger charge-to-radius ratio. Fluoride is a strong base, closely resembling hydroxide, which can be used as a base in a wide variety of organic reactions.[1,2] Fluoride is usually solvated in solutions and in salts with large counter cations reducing its basicity. Unsolvated, "naked", fluoride is a strong base that, for example, can deprotonate CH_3CN at room temperature.[3] Sulfur tetrafluoride reacts with anhydrous $[N(CH_3)_4]F$, a naked fluoride source, to form the $[N(CH_3)_4^+][SF_5^-]$ salt, which was first reported in 1963.[4] The Rb^+ and Cs^+ salts of the SF_5^- anion have since been prepared and characterized by vibrational spectroscopy.[5-7] Only three crystal structures have been reported containing the SF_5^- anion: $Rb[SF_5]$,[5] $Cs_6[SF_5]_4[HF_2]_2$,[8] and $[Cs(18\text{-crown-}6)_2][SF_5]$.[8] The SF_5^- anion adopts a square pyramidal configuration in which the equatorial fluorines have similar S−F bond lengths.

Sulfur tetrafluoride acts as a Lewis acid towards nitrogen-bases, i.e., pyridine, 4-methylpyridine, 2,6-dimethylpyridine, 4-dimethylaminopyridine, and triethylamine, to form 1:1 adducts that are stable below −40 °C.[9] These adducts exhibit N---S(IV) dative bonds ranging from 2.141(2) to 2.5140(18) Å. The $S{-}F_{eq}$ bond opposite of the nitrogen base is significantly elongated. The Raman signals of both the nitrogen base and SF_4 are shifted in these adducts, which agree well with adduct formation and the longer $S{-}F_{eq}$ bonds compared to SF_4.

Both anhydrous hydrogen fluoride (aHF) and SF_4 are used as fluorinating agents in organic chemistry. Due to the difficulties associated with handling aHF, a mixture of pyridine and HF is often used.[10] Mixtures of pyridine with varying amounts of HF (C_5H_5N•*n*HF, where *n* = 1, 2, 3, 4) have been structurally characterized by X-ray crystallography.[11] The N−H bond distance decreases from 1.34 Å in C_5H_5N•HF to 0.87 Å in C_5H_5N•4HF. This trend is accompanied by an increase of the N(H)---F distance from 2.472 Å for C_5H_5N•HF to 2.793 Å for C_5H_5N•4HF. This can be explained by the decrease in Lewis basicity as the size of the polyfluoride anion ($H_nF^-_{n+1}$ where *n* = 1, 2, 3, 4) increases. Sulfur tetrafluoride almost always contains traces of HF due to the presence of moisture and HF is sometimes purposely added to the reaction mixture. Several mechanisms have been proposed for the fluorination of carbonyl and hydroxyl groups by SF_4 containing HF in the reaction mixture (see Introduction). In contrast to the acidic conditions of fluorination using SF_4/HF mixtures, certain carbonyl, and hydroxyl containing molecules, are fluorinated with SF_4 in the presence of bases, such as triethylamine, pyridine, or KF.[12,13] To the best of my knowledge, no mechanism has been reported on the fluorination of organic carbonyl and hydroxyl groups with SF_4 under basic conditions. Therefore, the study of the SF_4-HF-nitrogen-base reaction system may help in expanding our knowledge about species present in such reactions.

4.2 Results and Discussion

4.2.1 General Synthetic Approach

Initial attempts to recrystallize adducts between SF_4 and nitrogen-bases (pyridine, 4-methylpyridine, and 2,6-dimethylpyridine) from toluene, which was

apparently insufficiently dried, afforded large needle-like crystals. These crystals proved to be $[HNC_5H_5^+]F^-\bullet SF_4$, $[HNC_5H_4(CH_3)^+]HF_2^-$, and $[HNC_5H_3(CH_3)_2^+]_2[SF_5^-]F^-\bullet SF_4$. Such salts were subsequently targeted by reactions of nitrogen bases, HF, and excess SF_4.

Reactions of pyridine with excess aHF and sulfur tetrafluoride gave a multitude of products which were difficult to isolate, containing a range of polyfluoride anions. The products often did not contain SF_4 as shown by Raman spectroscopy. Attempts at measuring equimolar amounts of HF to pyridine, while excluding H_2O, proved to be exceedingly difficult. The use of stoichiometric amounts of water as a reagent, added with the help of a microsyringe, to generate HF *in situ,* was shown to be a successful preparative route. (Equation 1)

$$SF_4 + H_2O \quad \rightarrow \quad SOF_2 + 2HF \qquad (1)$$

A typical reaction contained 4 mg of water, 50 mg of base, and 0.2 g of SF_4. Scales as large as 20 mg of water, 200 mg of base and 0.7 g of SF_4 were also employed. The nitrogen-bases used in these syntheses were pyridine and some of its derivatives, i.e., 4-methylpyridine, 2,6-dimethylpyridine, 4-diethylaminopyridine, and 4,4’-bipyridyl (see Figure 4.1).

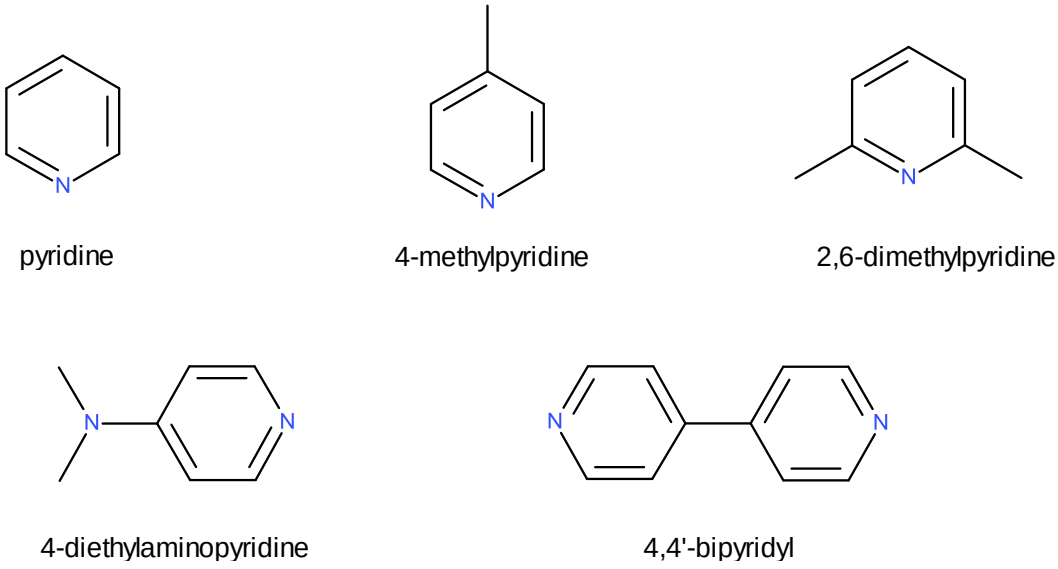

Figure 4.1 Drawings of the nitrogen-bases studied with SF_4/HF mixtures.

Excess SF_4 proved to be an effective solvent for the reaction and recrystallization of $[HNC_5H_5^+]HF_2^-\bullet 2SF_4$, $[HNC_5H_4(CH_3)^+]F^-\bullet SF_4$, $[HNC_5H_3(CH_3)_2^+]_2[SF_5^-]F^-\bullet SF_4$, $[HNC_5H_4N(CH_3)_2^+][HF_2^-]\bullet 2SF_4$, $[HNH_4C_5{-}C_5H_4N^+]F^-\bullet 2SF_4$ and $[HNH_4C_5{-}C_5H_4NH^{2+}]2F^-\bullet 4SF_4$. The products can be viewed in terms of the solvolysis of the $SF_4\bullet$*N*-base adduct by HF (Equation 2) or protonation of the free base to form a fluoride salt, followed by incorporation of SF_4 into the crystal structure (Equation 3).

$$SF_4 + NR \rightarrow SF_4\bullet NR; \qquad SF_4\bullet NR + HF \rightarrow HNR^+F^-\bullet SF_4 \qquad (2)$$

$$HF + NR \rightarrow HNR^+F^-; \qquad HNR^+F^- + SF_4 \rightarrow HNR^+F^-\bullet SF_4 \qquad (3)$$

It is likely that reaction (2) is the primary mechanism, since HF is present in the reaction system only after reaction with SF_4. In addition, the $SF_4\bullet NC_5H_4(CH_3)$ adduct was identified by both Raman spectroscopy and X-ray crystallography in an incomplete reaction mixture of SF_4, 4-methylpyridine and water. Reaction (3) could be tested by reacting nitrogen-base fluoride salts with SF_4, yet this would be

challenging because of the difficulties associated with isolating the 1:1 nitrogen-base to HF salts, due to the formation of polyfluoride anions.[10,11] When dichloromethane is used as a solvent in conjunction with nitrogen-bases, care must be taken to avoid the formation of methylenebispyridinium dichloride compounds.[14]

4.2.2 Pyridine-HF-SF_4 System

Large needle-like crystals were obtained by recrystallization of the SF_4•NC_5H_5 adduct in toluene between −60 and −80 °C. Instead of the anticipated structure of SF_4•NC_5H_5, the crystal structure of $[HNC_5H_5^+]F^-$•SF_4 was obtained. Apparently water in the toluene hydrolyzed SF_4 producing HF (see Equation 1) which then solvolyzed the SF_4•NC_5H_5 adduct. Attempts to obtain crystals of $[HNC_5H_5^+]F^-$•SF_4 were unsuccessful when SF_4 was used as a solvent. Instead, crystals of the $[HNC_5H_5^+]HF_2^-$•$2SF_4$ salt always formed, even when a deficiency of water was used. When an excess of pyridine was used, in order to ensure the selective formation of $[HNC_5H_5^+]F^-$•SF_4 and not $[HNC_5H_5^+][HF_2^-]$•$2SF_4$, a signal attributable to the SF_4•NC_5H_5 adduct was observed in the Raman spectrum. The $[HNC_5H_5^+][HF_2^-]$•$2SF_4$ salt is soluble in SF_4, whereas it is quite possible the $[HNC_5H_5^+]F^-$•SF_4 is insoluble. For the $[HNC_5H_5^+][HF_2^-]$•$2SF_4$ salt, crystals were grown by slow cooling of the pyridine, water, and excess SF_4 mixture from ambient temperature to −80 °C. Excess SF_4 and SOF_2 were removed at −90 °C.

4.2.2.1 X−ray Crystal Structures of $[HNC_5H_5^+]F^-$•SF_4 and $[HNC_5H_5^+]HF_2^-$•$2SF_4$.

Details of data collection parameters and crystallographic information for $[HNC_5H_5^+]F^-$•SF_4 and $[HNC_5H_5^+]HF_2^-$•$2SF_4$ are given in Table 4.1. Important bond

lengths, angles and contacts for $[HNC_5H_5^+]F^-\bullet SF_4$ and $[HNC_5H_5^+]HF_2^-\bullet 2SF_4$ are given in Table 4.2 and Table 4.3.

Table 4.1 Crystal Data Collection Parameters and Results of $[HNC_5H_5^+]F^-\bullet SF_4$ and $[HNC_5H_5^+]HF_2^-\bullet 2SF_4$

Compound	$[HNC_5H_5^+]F^-\bullet SF_4$	$[HNC_5H_5^+]HF_2^-\bullet 2SF_4$
File Code	MG11019	MG12051
Empirical Formula	$H_6C_5F_5NS$	$C_5H_7F_{10}NS_2$
Formula weight, g mol^{-1}	207.17	335.24
Temperature, K	153	153
Crystal System	Orthorhombic	Monoclinic
Space Group	*Pbca*	*C2/m*
Unit Cell Dimensions	*a* = 13.919 (4) Å	*a* = 16.366 (11) Å
	b = 13.681 (4) Å	*b* = 8.794 (6) Å
	c = 17.101 (4) Å	*c* = 8.842 (6) Å
		β = 116.566 (7)°
μ (mm^{-1})	0.43	0.58
Volume $Å^3$	3256.4(15)	1138.1 (13)
Z	16	4
Density (calculated), g cm^{-3}	1.690	1.956
F(000)	1664	664
Crystal Size, mm^3	1.38 × 0.36 × 0.31	0.29 × 0.12 × 0.08
Reflections Collected	35850	6509
Independent Reflections	4062 [R_{int} = 0.025]	1385 [R_{int} = 0.041]
Data/Restraints/Parameters	4062/0/225	1385/0/91
Goodness-of-fit on F^2	1.09	1.03
Refine Diff $\Delta\rho_{max}$ e $Å^{-3}$	0.23	0.86
Refine Diff $\Delta\rho_{min}$ e $Å^{-3}$	−0.37	−0.60
R_1, $I > 2\sigma(I)$[a]	0.0298	0.0466
wR_2 (F^2)[a]	0.0936	0.1089

[a] $R_1 = \Sigma||F_o| - |F_c||/\Sigma|F_o|$; w$R_2 = [\Sigma w(F_o^2 - Fc^2)^2/\Sigma w(F_o^4)]^{1/2}$.

Table 4.2 Bond Lengths (Å), Contacts (Å), and Angles (deg.) of $[HNC_5H_5^+]F^-\bullet SF_4$.

Bond Lengths and Contacts, Å			
S1−F3	1.5398(9)	S2−F7	1.5382(9)
S1−F2	1.5425(9)	S2−F6	1.5440(9)
S1−F1	1.6622(11)	S2−F5	1.6632(11)
S1−F4	1.6680(11)	S2−F8	1.6671(11)
S1---F9	2.6826(9)	S2---F9	2.8241(9)
S1---F10	2.7739(9)	S2---F10	2.6923(9)
N1(H)---F9	2.4367(13)	N2(H)---F10	2.4376(13)
		C9(H)---F9	3.290 (2)
Bond Angles, deg.			
F3−S1−F2	98.49(5)	F7−S2−F6	98.69(6)
F3−S1−F1	87.10(5)	F7−S2−F5	87.36(5)
F2−S1−F1	87.48(5)	F6−S2−F5	87.46(5)
F3−S1−F4	87.49(6)	F7−S2−F8	87.16(5)
F2−S1−F4	87.53(5)	F6−S2−F8	87.53(5)
F1−S1−F4	172.03(5)	F5−S2−F8	171.93(5)
F3−S1−F9	78.70(4)	F7−S2−F10	78.59(5)
F2−S1−F9	176.49(4)	F6−S2−F10	177.23(4)
F1−S1−F9	90.25(4)	F5−S2−F10	91.84(4)
F4−S1−F9	94.42(4)	F8−S2−F10	92.87(4)
F3−S1−F10	176.94(4)	N1−F9−S1	105.59(4)
F2−S1−F10	78.46(4)	N2−F10−S2	106.97(4)
F1−S1−F10	92.96(4)	N2−F10−S1	90.56(4)
F4−S1−F10	92.14(4)	S2−F10−S1	161.76(3)
F9---S1---F10	104.35(3)		

Table 4.3 Bond Lengths (Å), Contacts (Å), and Angles (deg.) of $[HNC_5H_5^+][HF_2^-]\bullet 2SF_4$.

Bond Lengths and Contacts, Å			
S1−F2	1.537(2)	S2−F5^{ii}	1.535(2)
S1−F2^{i}	1.537(2)	S2−F5	1.535(2)
S1−F3	1.643(3)	S2−F6	1.652(3)
S1−F1	1.648(3)	S2−F4	1.670(3)
S1---F7	2.876(3)	S2---F7	2.840(3)
N1(H)---F	2.937(5)	F7---N1	2.937(5)
F7-(H)-F7^{iii}	2.241(7)	N1−N1^{i}	1.345(6)
Bond Angles, deg.			
F2−S1−F2^{i}	99.71(17)	F5^{ii}−S2−F5	99.47(18)
F2−S1−F3	86.54(13)	F5^{ii}−S2−F6	87.14(13)
F2^{i}−S1−F3	86.54(13)	F5−S2−F6	87.14(13)
F2−S1−F1	87.80(13)	F5^{ii}−S2−F4	86.98(12)
F2^{i}−S1−F1	87.80(13)	F5−S2−F4	86.98(12)
F3−S1−F1	171.21(18)	F6−S2−F4	170.90(19)
F5^{ii}−S2−F7	174.02(12)	S2−F7−S1	172.33(11)
F5−S2−F7	76.09(12)	F7^{iii}−F7---N1	142.73(13)
F6−S2−F7	96.54(11)	S2−F7---N1	95.28(13)
F4−S2−F7	88.78(11)	S1−F7---N1	87.56(11)
F7^{iii}−F7−S2	96.70(11)	N1^{i}−N1−C2	120.85(18)
F7^{iii}−F7−S1	85.20(14)	N1^{i}−N1−F7	119.06(8)
F2−S1−F7	171.14(13)	C2−N1---F7	119.4(2)
F2^{i}−S1−F7	82.65(11)	N1−C2−C3	119.7(3)
F3−S1−F7	102.17(12)	F7---S1---F7^{iii}	93.8(1)
F1−S1−F7	83.75(12)	F7---S2---F7^{iii}	108.0(1)

Symmetry codes: (i) x, −y, z; (ii) x, −y+1, z; (iii) −x+1, y, −z+1.

The $[HNC_5H_5^+]F^-\bullet SF_4$ salt crystallizes in the orthorhombic space group, *Pbca*. The structure consists of infinite chains, along the *c*-axis, of sulfur tetrafluoride molecules linked by fluoride anions, forming S---F---S bridges (Figure 4.2).

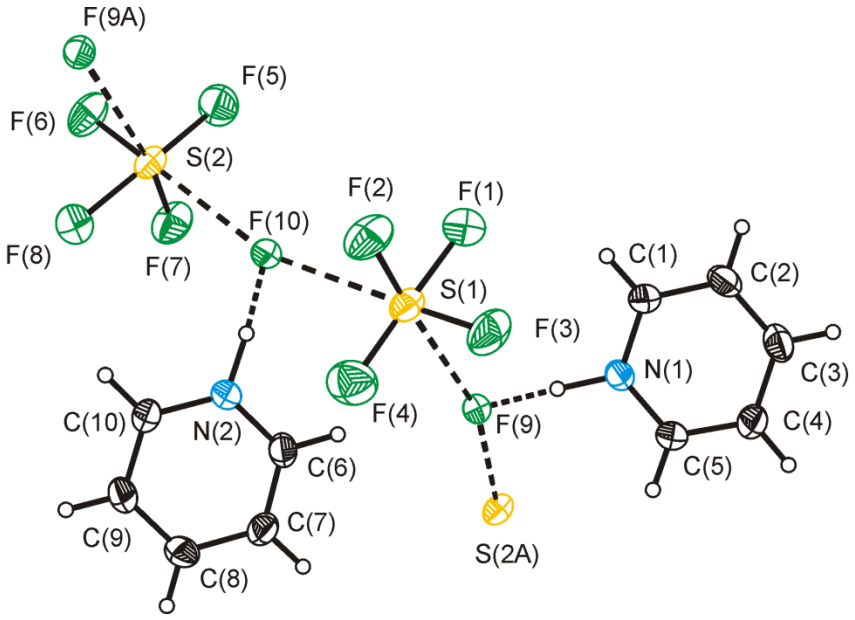

Figure 4.2 Thermal ellipsoid plot of a chain in the crystal structure of $[HNC_5H_5^+]F^-\bullet SF_4$ with thermal ellipsoids set to 50% probability.

The fluoride anions are hydrogen-bonded to pyridinium cations, which alternate positions along the chain. Sulfur tetrafluoride adopts the expected seesaw geometry and has two additional long contacts (2.6826(9) and 2.7739(9) Å) to the fluoride anions. The equatorial S−F bonds lengths (1.5398(9) and 1.5425(9) Å) are slightly longer than that of solid SF_4 (1.527(4) and 1.535(4) Å) (see Chapter 5), but shorter than those in the nitrogen-base SF_4 adduct $SF_4\bullet N(C_2H_5)_3$ (1.5555(14) and 1.5943(14) Å).[9] The axial S−F bond lengths are 1.6622(11) and 1.6680(11) Å which are significantly longer than the equatorial S−F bonds. The lone pair on sulfur lies

between the two S---F contacts, resulting in a large F---S---F contact angle of 104.35(3)°. The N1(H)---F9 distance (2.4367(13) Å) in the $[HNC_5H_5^+]F^-\bullet SF_4$ salt agrees well with that of the $C_5H_5N\bullet HF$ salt (2.472 Å).[11] Infinite chains bridged by weak fluorine bridges are quite common structural motifs with molecular species which contain open coordination sites. For example group 17 fluorides,[15] $[BrF_4^+][Sb_2F_{11}^-]$,[16] and TeF_4 form fluorine-bridges in the solid state.[17]

The $[HNC_5H_5^+][HF_2^-]\bullet 2SF_4$ salt crystallizes in the monoclinic space group *C2/m*. The structure consists of a sulfur fluoride double chain composed of alternating SF_4 and HF_2^- molecules with pyridinium cations hydrogen-bonded to a bifluoride anion. (Figure 4.3)

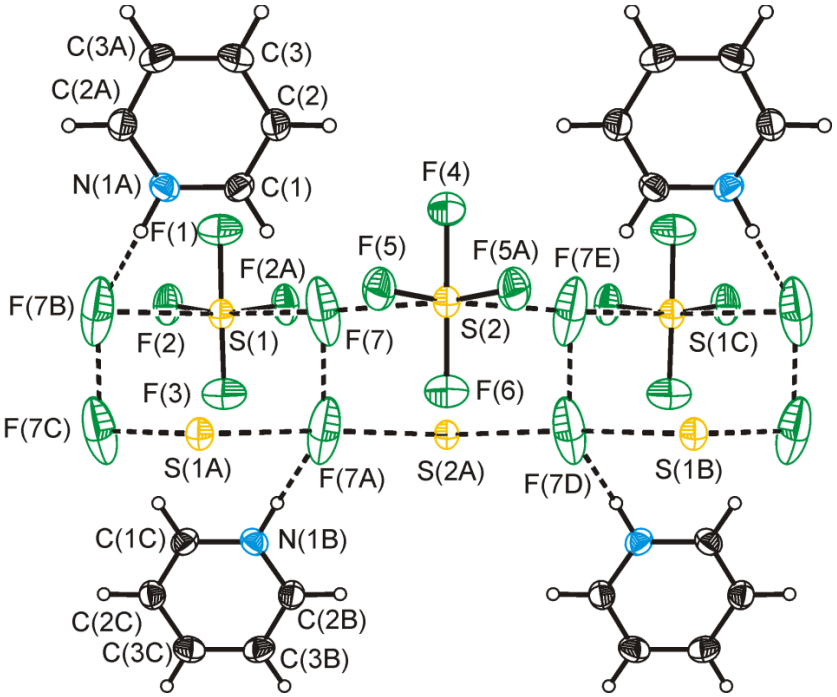

Figure 4.3 Thermal ellipsoid plot of the $[HNC_5H_5^+][HF_2^-]\bullet 2SF_4$ double chain. The fluorines bound to S(1A), S(2A) and S(1B) are omitted for clarity. Thermal ellipsoids are set to 50% probability. The pyridinium cations are disordered where half the time the ring is rotated by 60° and hydrogen bonded to adjacent bifluoride anions.

The pyridinium cation exhibits an orientational disorder where half the time it is hydrogen-bonded to one bifluoride, and the other half of the time it is shifted by 60° and hydrogen-bonded to the adjacent bifluoride. This disorder is imposed by a mirror plane, which relates the C1 and N1 atoms with a site occupancy of 50% each. The equatorial S−F bond lengths (S1−F2 = 1.537(2) Å and S2−F5 = 1.535(2) Å) in both SF_4 molecules are identical since both SF_{2ax} moieties lie in mirror planes, that bisect the SF_{2eq} angles. The axial S−F bond lengths range from 1.643(3) to 1.670(3) Å. All of the S−F bond lengths agree within experimental error with that of neat SF_4. Along the *b*-axis, the pyridine rings, bifluoride and both SF_4 molecules pack in a parallel fashion.

The N(H)---F (2.937(5) Å) and the S---F (2.840(3) to 2.876(3) Å) distances are much longer in the bifluoride structure than those found in $[HNC_5H_5^+]F^-\bullet SF_4$ ((N(H)---F = 2.4367(13) Å and S---F = 2.6826(9) Å). This agrees with the much weaker basicity of bifluoride compared to that of fluoride. These long contacts reflect the relative instability of the crystals towards loss of SF_4 which was observed when handling the crystals in the cold trough at −80 °C while selecting crystals. The N(H)---F contacts are much longer than those found in pyridinium bifluoride (2.508 Å) and also 4-methylpyridinium bifluoride (2.533(4) Å) (*vide infra*), and could be imposed by the pyridinium ring disorder. The pyridinium disorder has also an effect on the polarization of the bifluoride anion. Depending which side of the anion the pyridinium is hydrogen-bonded to, i.e., F1−H---F2---$HNC_5H_5^+$ and $NC_5H_5H^+$---F1---H−F2, the hydrogen in HF_2^- will be closer to one or the other fluorine atom. As the consequence of these two superimposed structures, the hydrogen in the bifluoride anion is supposedly disordered over two positions and could not be located in the

difference map and the thermal ellipsoids of the fluorines are elongated. The F---F distance in bifluoride is 2.241(7) Å which is shorter than the F---F distance found in pyridinium bifluoride (2.326 Å), or 4-methylpyridinium bifluoride (2.322(4) Å). The F---S---F contact angles alternate from 93.8(1) ° (S1), and 108.0(1) ° (S2). The small angle occurs between two adjacent bifluorides that are hydrogen-bonded to the same disordered pyridinium cations, while the large angle is observed when the bifluorides are hydrogen-bonded to two different pyridinium cations.

4.2.2.2 Raman Spectroscopy

Raman spectroscopy on the $[HNC_5H_5^+]F^-\bullet SF_4$ salt was unsuccessful due to the intense signals of toluene, surrounding the crystallized sample, which dominated the spectrum. The Raman spectrum of $[HNC_5H_5^+][HF_2^-]\bullet 2SF_4$ was acquired at −97 °C (Figure 4.4). The observed vibrational frequencies and their tentative assignments for $[HNC_5H_5^+][HF_2^-]\bullet 2SF_4$ can be found in Table 4.4. The assignment of Raman bands associated with the pyridinium cation is based on that previously reported for pyridinium salts.[18] Comparisons could also be made with the Raman spectrum of the $SF_4\bullet NC_5H_5$ adduct, previously assigned with the aid of computational chemistry.

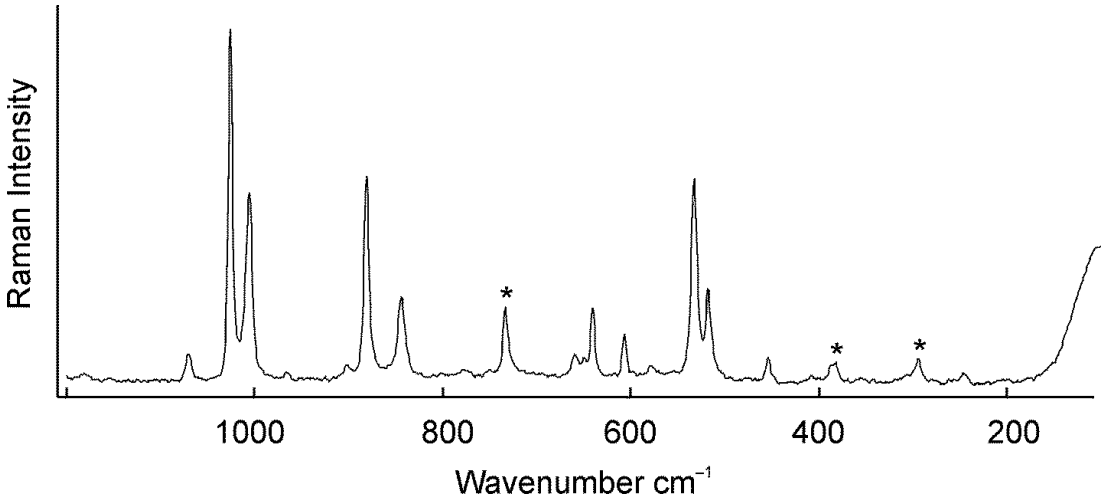

Figure 4.4 Raman spectrum of $[HNC_5H_5^+][HF_2^-]\bullet 2SF_4$. Asterisks (*) denote bands arising from the FEP sample tube.

The N−H stretching band could not be located in the Raman spectrum of $[HNC_5H_5^+][HF_2^-]\bullet 2SF_4$. The N−H stretching band in Raman spectra is known to vary greatly in intensity, broadness and frequency, depending on the counter-anion. This is because the nature of the anion determines the type of interaction between the proton and the nitrogen.[19] The most intense peak is found at 1028 cm^{-1}, which is attributable to the NC_5 ring breathing mode, and is at a higher frequency than that of neat pyridine (990 cm^{-1}), the $SF_4\bullet NC_5H_5$ adduct (1003 cm^{-1}), and the pyridinium chloride salt (1009 cm^{-1}).[18] The signals attributable to S−F stretching within SF_4 are only slightly shifted from those of neat SF_4, when compared to the shifts of SF_4 stretching bands observed for the nitrogen-base-SF_4 adducts. This reflects the weak donor properties of bifluoride compared with the relatively strong donor properties of the nitrogen bases. Despite the weak interaction of SF_4 with bifluoride, the peaks in the Raman spectrum attributable to SF_4 are sharp compared to liquid SF_4 at the same temperature.

Table 4.4 Raman Frequencies (cm^{-1}) and Tentative Assignments of $[HNC_5H_5^+][HF_2^-]\bullet 2SF_4$.

$[HNC_5H_5^+][HF_2^-]\bullet 2SF_4$[a,c]	SF_4[d]	Assignment
3092(19)		ν(C–H)
3065(7)		
2992(4)		
1631(7)		ν(C–C)/ ν(C–N)
1309(4)		
1260(4)		
1216(13)[b]		
1177(2)		
1075(4)		
1024(100)		ν_{ring}
	904(32)	SF_4 comb. band
880(7)	888(75)/880(99)	$\nu_s(SF_{2eq})$
841(13)	860sh	$\nu_{as}(SF_{2eq})$
649(19)	629(7)	$\nu_{as}(SF_{2ax})$
522(21)	536(92)/532(100)	$\nu_s(SF_{2ax})$
	524(54)	
449(4)	458(31)	$\tau(SF_2)$
367(2)		
351(3)		
	243(15)	$\delta_{sc}(SF_{2eq}) - \delta_{sc}(SF_{2ax})$

[a] Signals from the FEP sample tube were observed at: 1383(6), 1216(13) (overlap), 733(13), 595(2), 385(3), 294(3), [b] Signals overlap with those of FEP, [c] Acquired at −97 °C. [d] Solid SF_4 at −135 °C.

4.2.3 4-Methylpyridine-HF-SF_4 System

Recrystallization of the SF_4•$NC_5H_4(CH_3)$ adduct from toluene resulted in the formation of large needles. The crystals were the $[HNC_5H_4(CH_3)^+]HF_2^-$ salt which likely formed because the presence of trace amounts of water in the toluene that was used and because of a deficiency of SF_4 in this experiment, which reacted with the water to form SOF_2 and HF. Cooling of a 1:2 mixture of water to 4-methylpyridine, in excess SF_4 from room temperature to −20 °C resulted in the formation of large crystalline blocks. These crystals were shown to be of $[HNC_5H_4(CH_3)^+]F^-$•SF_4.

4.2.3.1 X−ray Crystal Structures of $[HNC_5H_4(CH_3)^+]F^-$•SF_4 and $[HNC_5H_4(CH_3)^+]HF_2^-$

Details of data collection parameters and crystallographic information for $[HNC_5H_4(CH_3)^+]F^-$•SF_4 and $[HNC_5H_4(CH_3)^+]HF_2^-$ are given in Table 4.5. Important bond lengths, angles and contacts for $[HNC_5H_4(CH_3)^+]F^-$•SF_4 and $[HNC_5H_4(CH_3)^+]HF_2^-$ are given in Table 4.6 and Table 4.7, respectively.

The compound, $[HNC_5H_4(CH_3)^+]F^-$•SF_4, crystallized in the triclinic space group, $P\bar{1}$ and consisted of 4-methylpyridinium cations hydrogen-bonded to fluoride, which forms two long contacts to the sulfur atom of SF_4 (S1---F1 = 2.632 (6) Å, S1---F1A = 2.823(6) Å) forming discrete dimers (see Figure 4.5). As expected, SF_4 adopts a seesaw geometry with the S−F_{eq} bonds (S1−F1 = 1.544(4) Å, S1−F2 = 1.543(4) Å) being shorter than the S−F_{ax} bonds (S1−F3 = 1.652(4) Å, S1−F4 = 1.650 (4) Å). The F5---S1---F5A angle of 103.69(3)° agrees well with the contact angle in $[HNC_5H_5^+]F^-$•SF_4 (104.35(3)°). Two 4-methylpyridinium rings exhibit π-stacking

(C3---C5 = 3.352(3) Å) along the *c*-axis, in which the rings are alternating, rotated by 180°.

Table 4.5 Crystal Data Collection Parameters and Results of $[HNC_5H_4(CH_3)^+]F^-\bullet SF_4$ and $[HNC_5H_4(CH_3)^+][HF_2^-]$.

Compound	$[HNC_5H_4(CH_3)^+]F^-\bullet SF_4$	$[HNC_5H_4(CH_3)^+]HF_2^-$
File Code	MG12072	MG12078
Empirical Formula	$C_6H_8F_5NS$	$C_6H_9F_2N$
Formula weight, g mol^{-1}	221.20	133.14
Temperature, K	153	153
Wavelength, Å	0.71073	0.71073
Crystal System	Triclinic P	Orthorhombic
Space Group	$P\bar{1}$	*Pnma*
Unit Cell Dimensions	*a* = 7.261 (16) Å	*a* = 19.22 (4) Å
	b = 8.419 (18) Å	*b* = 7.741 (16) Å
	c = 8.705 (19) Å	*c* = 4.74 (1) Å
	α = 61.90 (2)°	
	β = 82.15 (2)°	
	γ = 75.28 (2)°	
Volume	453.9 (17)	705 (2)
Z	2	4
ρ (calculated), g cm^{-3}	1.618	1.254
Abs. coeff. μ (mm^{-1})	0.39	0.11
F(000)	224.0	280
Crystal Size, mm^3	0.28 × 0.23 × 0.16	0.35 × 0.16 × 0.09
Reflections Collected	2101	7416
Independent Reflections	2101 [*R*int = 0.020]	869 [*R*int = 0.040]
Data/Restraints/Parameters	2101/0/119	869/0/53
Goodness-of-fit on F^2	1.02	1.02
$\Delta\rho$max (e $Å^{-3}$)	0.31	0.20
$\Delta\rho$min (e $Å^{-3}$)	−0.34	−0.14
R_1, $I > 2\sigma(I)$[a]	0.0295	0.0366
wR_2(F^2)[a]	0.0884	0.1148

[a] $R_1 = \Sigma||F_o| - |F_c||/\Sigma|F_o|$; w$R_2 = [\Sigma w(F_o^2 - Fc^2)^2/\Sigma w(F_o^4)]^{1/2}$.

Table 4.6 Bond Lengths (Å), Contacts (Å), and Angles (deg.) of $[HNC_5H_4(CH_3)^+]F^-\bullet SF_4$.

Bond Lengths and Contacts, Å			
S1−F2	1.543(4)	S1---F5A	2.823(6)
S1−F1	1.544(4)	C1−C2	1.365(3)
S1−F4	1.650(4)	C2−C3	1.376(3)
S1−F3	1.652(4)	C3−C4	1.382(3)
S1---F5	2.632(6)	C3−C6	1.488(3)
N1−C1	1.330(3)	C4−C5	1.367(3)
N1−C5	1.331(3)	N1(H1A)···F5	2.404(4)
Bond Angles, deg.			
F2−S1−F1	97.80(7)	F2−S1−F5	177.96(5)
F2−S1−F4	87.67(7)	F1−S1−F5	80.16(6)
F1−S1−F4	87.13(6)	F4−S1−F5	92.28(6)
F3−S1−F5	91.75(5)	F5---S1---F5A	103.69(3)
C1−N1−C5	119.63(15)	C2−C3−C4	117.82(16)
N1−C1−C2	121.28(17)	C2−C3−C6	121.01(17)
F2−S1−F3	88.06(7)	C4−C3−C6	121.17(18)
F1−S1−F3	86.83(6)	C5−C4−C3	119.46(17)
F4−S1−F3	172.06(6)	N1−C5−C4	121.68(16)

Table 4.7 Bond Lengths (Å), Contacts (Å), and Angles (deg.) of $[HNC_5H_4(CH_3)^+]HF_2^-$.

Bond Lengths and Contacts, Å		Bond Angles, deg.	
N1−C4^i	1.335(3)	C4^i−N1−C4	121.3(2)
N1−C4	1.335(3)	N1−C4−C3	120.33(15)
C4−C3	1.372(3)	C4−C3−C2	120.21(16)
C3−C2	1.388(3)	C3−C2−C3^i	117.6(2)
C2−C3^i	1.388(3)	C3−C2−C1	121.18(11)
C2−C1	1.496(4)	C3^i−C2−C1	121.18(11)
N1(H1)···F1	2.533(4)		
F---F	2.323(5)		
F1−H5	1.25(3)		
F2−H5	1.07(3)		

Symmetry code: (i) *x*, −*y*+1/2, *z*.

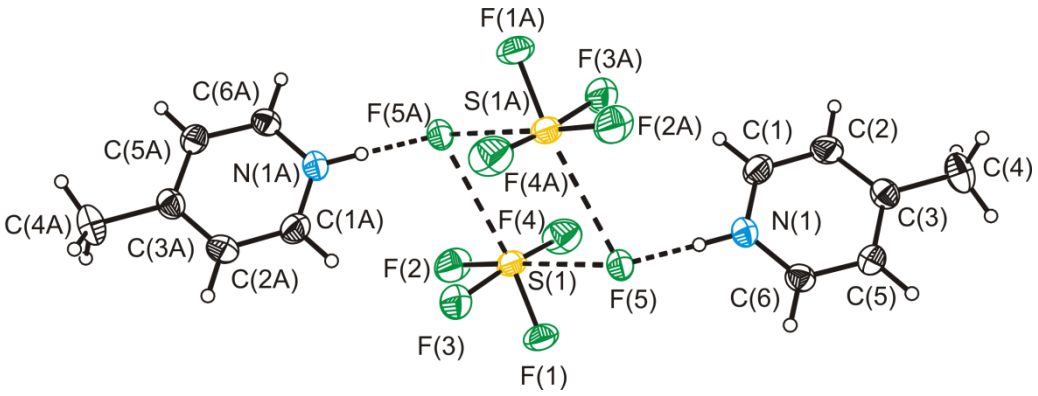

Figure 4.5 Thermal ellipsoid plot of the dimer present in the crystal structure of $[HNC_5H_4(CH_3)^+]F^-\bullet SF_4$. Thermal ellipsoids are at 50% probability.

The crystal structure is remarkably different from the extended chain structures observed with the pyridine-HF-SF_4 system. In the crystal structure of the $[HNC_5H_5^+]F^-\bullet SF_4$ salt, a fluoride is present close to the para-position (C9(H)---F9 = 3.290(2) Å) of the pyridine rings. The methyl group in the 4-position of $[HNC_5H_4(CH_3)^+]F^-\bullet SF_4$ prevents the formation of an infinite chain with a packing similar to that of $[HNC_5H_5^+]F^-\bullet SF_4$. The N1(H)---F5 distance (2.404(4) Å) is significantly shorter than the N(H)---F distance (2.4379(13) Å) in $[HNC_5H_5^+]F^-\bullet SF_4$. This is in accord with the weaker Brønsted acidity of 4-methylpyridinium (pK_a = 5.98) compared to that of pyridinium (pKa = 5.23).[20]

In the $[HNC_5H_4(CH_3)^+]HF_2^-$ salt, the 4-methylpyridinium cation is hydrogen-bonded to one of the fluorines of bifluoride (see Figure 4.6). The N1(H)---F1 distance (2.533(4) Å) is longer than the majority of the structures containing fluoride bound to SF_4 and substantially longer than the N(H)---F contact length (2.405(4) Å) of the $[HNC_5H_5^+]F^-\bullet SF_4$ salt. The F---F distance in the bifluoride anion is 2.323(5) Å, which is the same as the F---F distance of 2.326 Å found in pyridinium bifluoride.[11] The hydrogen atom was located in the difference map and refined. As

expected, the F1−H5 distance (1.25(3) Å) is longer than the F2−H5 distance (1.07(3) Å), due to the hydrogen-bonding interaction between F1 the 4-methylpyridinium cation.

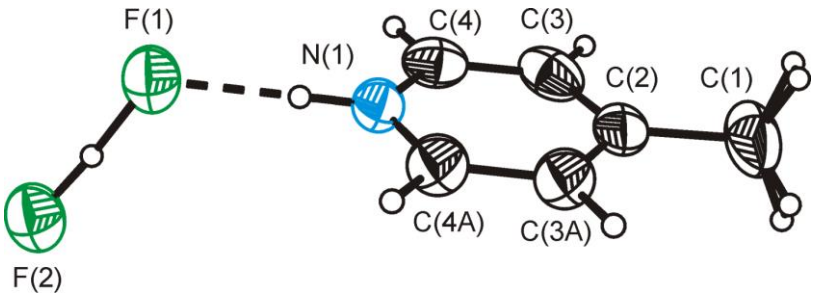

Figure 4.6 Thermal ellipsoid plot of the $[HNC_5H_4(CH_3)^+]HF_2^-$ ion pair. Thermal ellipsoids are at 50% probability.

4.2.3.2 Raman Spectroscopy

Obtaining Raman spectroscopic data on the $[HNC_5H_4(CH_3)^+]HF_2^-$ salt was unsuccessful due to the intense signals of toluene which dominated the spectrum. The Raman spectrum of $[HNC_5H_4(CH_3)^+]F^-•SF_4$ at −85 °C is shown in Figure 4.7. The Raman frequencies and tentative assignments are listed in Table 4.8. The tentative assignments were based on the Raman spectrum of the $SF_4•NC_5H_4(CH_3)$ adduct, previously assigned with the aid of computational chemistry.

Table 4.8 Raman Frequencies (cm^{-1}) and Tentative Assignments of $[HNC_5H_4(CH_3)^+]F^-\bullet SF_4$.

$[HNC_5H_4(CH_3)^+]F^-\bullet SF_4$[a]	SF_4[c]	Assignment
3097(36)		
3082(49)		ν(C–H)
3021(15)		
2967(21)		
2931(82)		
2879(12)		$\nu(CH_3)$
2736(6)		
1632(36)		
1595(8)		ν(C–C)/ ν(C–N)
1448(9)		
1380(45)[b]		
1336(21)		CH_3 deformation
1256(11)		
1222(26)		
1074(32)		$\nu_s(NC_5)$
1002(14)		
	904(32)	SF_4 comb. band
855(17)	888(75)/880(99)	$\nu_s(SF_{2eq})$
828(56)	860sh	ν_{as} (SF_{2eq})
815(13)		$\delta_{out\text{-}of\text{-}plane}$(HCC)
798(19)		$\delta_{out\text{-}of\text{-}plane}$(HCC)
788(19)		SF_2
770(55)		SF_2
665(79)		$\delta_{in\text{-}plane}$(CCC)/ $\delta_{in\text{-}plane}$(CNC)
	629(7)	$\nu_{as}(SF_{2ax})$
604(8)		
562(8)		
521(100)	536(92)/532(100)	$\nu_s(SF_{2ax})$
	524(54)	$\delta_{rock}(SF_{2eq})$
487(9)	515(72)/508(66)	$\delta_{sc}(SF_{2eq}) + \delta_{sc}(SF_{2ax})$
445(19)	458(31)	$\tau(SF_2)$
351(31)		
294(18)[b]		$\rho_r(CH_3)$
258(6)		$\rho_r(CH_3)$
238(21)	243(15)	$\delta_{sc}(SF_{2eq}) - \delta_{sc}(SF_{2ax})$

[a] Signals from the FEP sample tube were observed at: 1513(7), 1380(45) (overlap), 1303(9), 733(47), 382(16), 294(18) (overlap) [b] Signals overlap with those of FEP. [c] Acquired at −97 °C. [d] Solid SF_4 at −135 °C.

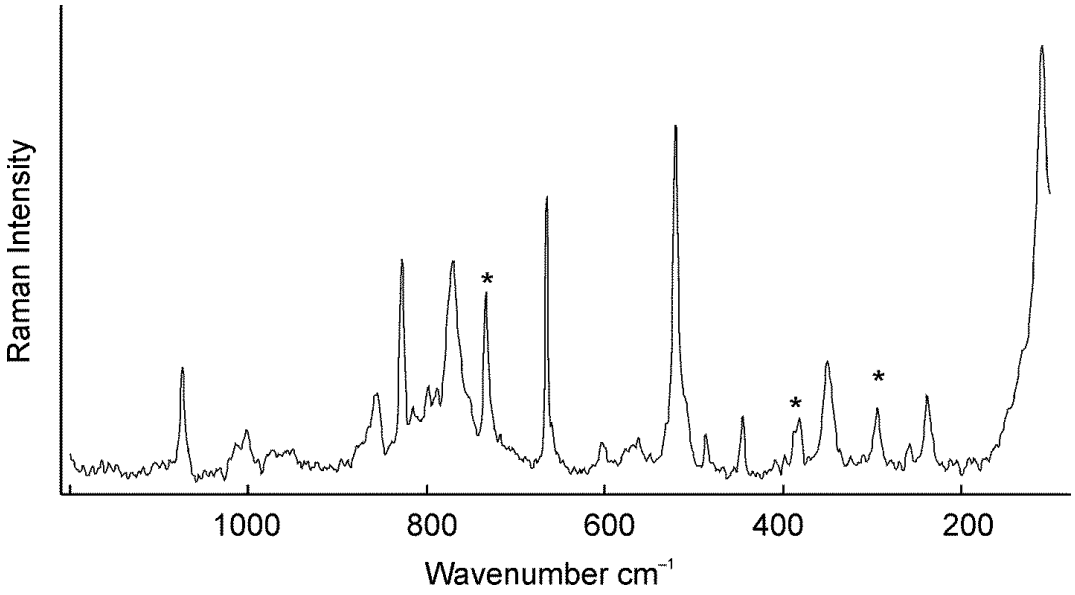

Figure 4.7 Raman spectrum of $[HNC_5H_4(CH_3)^+]F^-\bullet SF_4$. Asterisks (*) denote bands arising from the FEP sample tube.

The methyl group increases the complexity of the Raman spectrum significantly compared to that of the pyridinium salt. An intense signal at 2931 cm^{-1} is indicative of the C−H stretches on a methyl group. The most intense peak (521 cm^{-1}) can be assigned to the $\nu_s(SF_{2ax})$ stretch, which is at a lower frequency than that of neat solid SF_4 (536(92) and 532(100) cm^{-1}). The band assigned to the $\nu_s(SF_{2eq})$ mode is also at significantly lower frequency and intensity (855(17) cm^{-1}) than that of neat solid SF_4 (888(75) and 880(99) cm^{-1}), and is no longer split.

4.2.4 2,6-Dimethylpyridine-HF-SF_4 System

In an attempt to obtain crystals of SF_4-2,6-dimethylpyridine adducts, large plate-like crystals were obtained by recrystallizing the $SF_4\bullet HNC_5H_3(CH_3)_2$ adduct in toluene between −60 and −80 °C. Instead of the anticipated structure of $SF_4\bullet HNC_5H_3(CH_3)_2$, the crystal structure of $[HNC_5H_3(CH_3)_2^+]_2[SF_5^-]F^-\bullet SF_4$ was obtained. Similarly to the crystal structure of $[HNC_5H_5^+]F^-\bullet SF_4$ (*vide supra*), traces

of water in the toluene hydrolyzed SF_4 producing HF which then solvolyzed SF_4•$NC_5H_3(CH_3)_2$. Using SF_4 as a solvent and introducing stoichiometric amounts of H_2O, crystals formed which had the same unit cell as the $[HNC_5H_3(CH_3)_2^+]_2[SF_5^-]F^-$•$SF_4$ salt previously obtained. The sample, however, contained crystals with two different morphologies. A block-type crystal that was mounted on the diffractometer had different unit cell parameters than the $[HNC_5H_3(CH_3)_2^+]_2[SF_5^-]F^-$•$SF_4$ salt. This crystal contained three extra molecules of SF_4, which formed layers of SF_4, and is discussed in Section 5.2 together with the solid-state structure of SF_4.

4.2.4.1 X-ray Crystal Structure of $[HNC_5H_3(CH_3)_2^+]_2[SF_5^-]F^-$•$SF_4$

Details of data collection parameters and crystallographic information for ($[HNC_5H_3(CH_3)_2^+]_2[SF_5^-]F^-$•$SF_4$) are given in Table 4.9. Important bond lengths, angles and contacts for $[HNC_5H_3(CH_3)_2^+]_2[SF_5^-]F^-$•$SF_4$ are listed in Table 4.10. The structure of $[HNC_5H_3(CH_3)_2^+]_2[SF_5^-]F^-$•$SF_4$ consists of two 2,6-dimethylpyridinium cations hydrogen-bonded to a single fluoride anion, which is coordinated to one SF_4 molecule, and a separate SF_5^- anion (see Figure 4.8).

Table 4.9 Crystal Data Collection Parameters and Results of $[HNC_5H_3(CH_3)_2^+]_2[SF_5^-]F^-\bullet SF_4$.

Compound	$[HNC_5H_3(CH_3)_2^+]_2[SF_5^-]F^-\bullet SF_4$
File Code	MG11020
Empirical Formula	$C_{14}H_{20}F_{10}N_2S_2$
Formula weight, g mol^{-1}	470.44
Temperature, K	153
Wavelength, Å	0.71073 Å
Crystal System	Monoclinic
Space Group	$P2_1/n$
Unit Cell Dimensions	a = 7.8081 (16) Å
	b = 18.207 (4) Å
	c = 14.352 (3) Å
	β = 99.917 (2)°
μ (mm^{-1})	0.36
Volume, $Å^3$	2009.9 (7)
Z	4
Density (calculated), g cm^{-3}	1.555
F(000)	0.36
Crystal Size, mm^3	0.70 × 0.46 × 0.2
Theta Range	1.8 to 27.5
Reflections Collected	28424
Independent Reflections	4590 [R_{int} = 0.020]
Data/Restraints/Parameters	4590/24/305
Goodness-of-fit on F^2	1.03
Refine Diff Density_max	0.56
Refine Diff Density_min	−0.36
R_1, $I > 2\sigma(I)$[a]	0.038
wR_2 (F^2)[a]	0.111

[a] $R_1 = \Sigma||F_o| - |F_c||/\Sigma|F_o|$; w$R_2 = [\Sigma w(F_o^2 - Fc^2)^2/\Sigma w(F_o^4)]^{1/2}$.

Table 4.10 Bond Lengths (Å), Contacts (Å), and Angles (deg.) of $[HNC_5H_3(CH_3)_2^+]_2[SF_5^-]F^-•SF_4$.

Bond Lengths and Contacts, Å			
F1−S1A	1.506(5)	S1A−F5A	1.594(17)
F1−S1	1.586(2)	S1A−F4A	1.657(7)
S1−F4	1.663(3)	S1A−F2A	1.697(8)
S1−F3	1.698(3)	S1A−F3A	1.699(7)
S1−F2	1.709(4)	S2−F6	1.5415(11)
S1−F5	1.718(5)	S2−F8	1.5538(13)
S2−F9	1.6557(12)	S2---F10	2.5116(12)
S2−F7	1.6736(12)	N2(H2)---F10	2.5308(17)
		N1(H1)---F10	2.5396(17)
Bond Angles, deg.			
S1A−F1−S1	12.61(14)	F4A−S1A−F2A	171.1(5)
F1−S1−F4	84.28(19)	F1−S1A−F3A	83.2(3)
F1−S1−F3	87.02(13)	F5A−S1A−F3A	172.7(8)
F4−S1−F3	90.67(19)	F4A−S1A−F3A	93.7(6)
F1−S1−F2	85.9(2)	F2A−S1A−F3A	86.9(6)
F4−S1−F2	170.1(3)	F6−S2−F8	97.39(7)
F3−S1−F2	88.03(19)	F6−S2−F9	86.60(7)
F1−S1−F5	82.0(2)	F8−S2−F9	88.05(7)
F4−S1−F5	91.6(3)	F6−S2−F7	86.06(7)
F3−S1−F5	168.5(2)	F8−S2−F7	87.65(7)
F2−S1−F5	87.8(3)	F9−S2−F7	170.94(7)
F1−S1A−F5A	89.7(7)	F6−S2−F10	78.87(5)
F1−S1A−F4A	93.0(3)	F8−S2−F10	175.08(6)
F5A−S1A−F4A	85.2(8)	F9−S2−F10	88.54(6)
F1−S1A−F2A	78.2(4)	F7−S2−F10	95.23(6)
F5A−S1A−F2A	93.1(8)		

a) b)

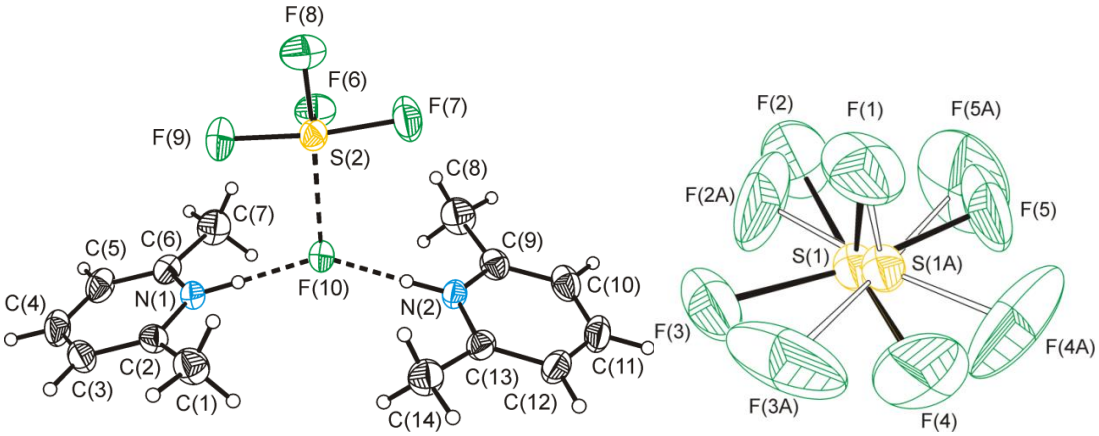

Figure 4.8 Thermal ellipsoid plot of $[HNC_5H_3(CH_3)_2^+]_2F^-\bullet SF_4[SF_5^-]$; a) the $[HNC_5H_3(CH_3)_2^+]_2F^-\bullet SF_4$ moiety and b) the disordered SF_5^- anion. Thermal ellipsoids are at 50% probability.

The 2,6-dimethylpyridinium cations exhibit long contacts to F^- (N1(H)---F10 = 2.5396(17) Å and N2(H)---F10 = 2.5308(17) Å) with an N1(H)---F10---(H)N2 angle of 146.57(6)°. The sulfur tetrafluoride adopts the expected seesaw geometry and has a S---F contact (2.5116(12) Å) with F10. The S2−F8 bond (1.5538(13) Å) in SF_4 is slightly longer than the other equatorial S2−F6 bond (1.5415(11) Å), as it is located *trans* of the Lewis basic fluoride. The SF_5^- anion adopts the expected square pyramidal structure with similar, but on average slightly longer bond lengths, compared to the SF_5^- anion in the previously reported $RbSF_5$ structure.[5] The thermal ellipsoids in the equatorial plane are elongated, suggesting some rotational motion around the S−F axis, however the actual disorder was modelled by assigning two separate SF_5^- anions which are joined by a fixed pivot point, i.e., the axial fluorine. The axial S−F bond length (1.560(2) Å) is much shorter than the equatorial S−F bond lengths (1.730(2) Å). The equatorial F−S−F bond angles range from 87.8(3) to 91.6(3)°.

The formation of the SF_5^- anion only occurs with naked fluoride. In $[HNC_5H_3(CH_3)_2^+]_2[SF_5^-]F^-\bullet SF_4$, one fluoride (F10) is not naked, since it is hydrogen-bonded to two 2,6-dimethylpyridinium cations. The F(10) fluoride does not form SF_5^- with SF_4; it forms a weak S---F^- contact of 2.5116(12) Å as observed in the structures containing the pyridinium and 4-methylpyridinium cations (*vide supra*). The second fluoride does not have any H-bonds and combines with SF_4 to form the SF_5^- anion. The N(H)---F distances are longer than those found in $[HNC_5H_5^+]F^-\bullet SF_4$ or $[HNC_5H_4(CH_3)^+]F^-\bullet SF_4$. This longer N(H)---F distance reflects the lower Lewis acidity of the 2,6-dimethylpyridinium cation. A chain structure is unlikely to form in the 2,6-dimethylpyridine system, since the two methyl groups sterically protect the fluoride, preventing the formation of multiple S---F^- contacts. The methyl groups also inhibit the formation of discrete dimers, such as the $[HNC_5H_4(CH_3)^+]F^-\bullet SF_4$ dimer.

4.2.4.2 Raman Spectroscopy

The low-temperature Raman spectrum of $[HNC_5H_3(CH_3)_2^+]_2[SF_5^-]F^-\bullet SF_4$ from toluene could not be obtained due to the intense signals of toluene which dominated the spectrum. When attempting to obtain the Raman spectrum of $[HNC_5H_3(CH_3)_2^+]_2[SF_5^-]F^-\bullet SF_4$ by use of SF_4 as a solvent, a mixture of crystals was obtained, $[HNC_5H_3(CH_3)_2^+]_2[SF_5^-]F^-\bullet SF_4$ and $[HNC_5H_3(CH_3)_2^+]_2[SF_5^-]F^-\bullet 4SF_4$. No further attempts were made to isolate the crystals of $[HNC_5H_3(CH_3)_2^+]_2[SF_5^-]F^-\bullet SF_4$.

4.2.5 The 4-Dimethylaminopyridine-HF-SF_4 System

The Lewis basicity of 4-dimethylaminopyridine is significantly greater than that of the other pyridine derivatives. As a result, the conjugate acid, 4-dimethylaminopyridinium, will be the weakest acid in this series of protonated pyridinium derivatives. Slow cooling of a 2-to-1 mixture of 4-dimethylaminopyridine and water with excess SF_4, from 3 to −20 °C, resulted in the formation of large needles, which were shown to be $[HNC_5H_4N(CH_3)_2^+][HF_2^-]\bullet 2SF_4$. In a different experiment, the $SF_4\bullet NC_5H_4N(CH_3)_2$ adduct in the presence of excess SF_4 was dissolved in dichloromethane to increase the solubility. Volatiles were removed from −80 to −60 °C which led to the formation of fine crystalline needles. These needles were $[HNC_5H_4N(CH_3)_2^+]_2[SF_5^-]F^-\bullet CH_2Cl_2$ as determined by Raman spectroscopy and X-ray crystallography. Apparently, traces of water hydrolyzed SF_4 forming HF, which protonated the basic nitrogen atoms on 4-dimethylaminopyridine.

4.2.5.1 X−ray Crystal Structures of $[HNC_5H_4N(CH_3)_2^+][HF_2^-]\bullet 2SF_4$ and $[HNC_5H_4N(CH_3)_2^+]_2[SF_5^-]F^-\bullet CH_2Cl_2$

Details of data collection parameters and crystallographic information for $[HNC_5H_4N(CH_3)_2^+][HF_2^-]\bullet 2SF_4$ and $[HNC_5H_4N(CH_3)_2^+]_2[SF_5^-]F^-\bullet CH_2Cl_2$ are given in Table 4.11. Important bond lengths, angles and contacts for $[HNC_5H_4N(CH_3)_2^+][HF_2^-]\bullet 2SF_4$ and $[HNC_5H_4N(CH_3)_2^+]_2[SF_5^-]F^-\bullet CH_2Cl_2$ are given in Table 4.12 and Table 4.13.

Table 4.11 Crystal Data Collection Parameters and Results of $[HNC_5H_4N(CH_3)_2^+][HF_2^-]\bullet 2SF_4$ and $[HNC_5H_4N(CH_3)_2^+]_2[SF_5^-]F^-\bullet CH_2Cl_2$.

Compound	$[HNC_5H_4N(CH_3)_2^+][HF_2^-]\bullet 2SF_4$	$[HNC_5H_4N(CH_3)_2^+]_2[SF_5^-]F^-\bullet CH_2Cl_2$
File Code	MG12071	MG12074
Empirical Formula	$C_7H_{12}F_{10}N_2S_2$	$C_{15}H_{24}Cl_2F_6N_4S$
Formula weight, g mol^{-1}	378.31	477.34
Temperature, K	153	153
Wavelength, Å	0.71073	0.71073
Crystal System	Monoclinic	Monoclinic
Space Group	$P2_1/c$	$P2_1/n$
Unit Cell Dimensions	a = 8.605 (6) Å b = 20.371 (15) Å c = 16.500 (12) Å β = 90.415 (9)°	a = 7.001 (5) Å b = 14.351 (10) Å c = 21.647 (15) Å β = 96.742 (8)°
Abs. coeff. μ (mm^{-1})	0.47	0.46
Volume $Å^3$	2892 (4)	2160 (3)
Z	8	4
Density (calculated), g cm^{-3}	1.738	1.468
F(000)	1520	984
Crystal Size, mm^3	0.52 × 0.22 × 0.20	0.37 × 0.09 × 0.08
Reflections Collected	32789	24526
Independent Reflections	6703 [R_{int} = 0.046]	5242 [R_{int} = 0.045]
Data/Restraints/Par	6703/0/391	5242/34/297
Goodness-of-fit on F^2	1.02	1.15
Refine Diff $\Delta\rho$max e $Å^{-3}$	0.38	0.64
Refine Diff $\Delta\rho$min e $Å^{-3}$	−0.32	−0.43
R_1, $I > 2\sigma(I)$[a]	0.0325	0.0707
wR_2 (F^2)[a]	0.0886	0.1930

[a] $R_1 = \Sigma||F_o| - |F_c||/\Sigma|F_o|$; w$R_2 = [\Sigma w(F_o^2 - Fc^2)^2/\Sigma w(F_o^4)]^{1/2}$.

Table 4.12 Selected Bond Lengths (Å), Contacts (Å), and Angles (deg.) of $[HNC_5H_4N(CH_3)_2^+][HF_2^-]\bullet 2SF_4$

Bond Lengths and Contacts, Å			
S1−F14	1.5422(14)	S3−F32	1.6497(15)
S1−F13	1.5463(14)	S3−F31	1.6726(17)
S1−F11	1.6484(15)	S3−F2	2.758(2)
S1−F12	1.6746(16)	S3−F4^{i}	2.7668(18)
S1−F1	2.6783(18)	N1(H1)---F1	2.638(2)
S1−F3i	2.8703(18)	N1A(H1A)---F3	2.632(2)
S2−F23	1.5332(15)	F2(H1B)---F1	2.284(2)
S2−F24	1.5414(13)	F4(H2B)---F3	2.291(2)
S2−F21	1.6325(15)	S4−F44	1.5357(14)
S2−F22	1.6617(16)	S4−F43	1.5458(13)
S2−F2	2.7136(18)	S4−F42	1.6539(15)
S2−F4	2.799(2)	S4−F41	1.6825(16)
S3−F34	1.5414(14)	S4−F3	2.6787(19)
S3−F33	1.5434(15)	S4−F1	2.8411(17)
Bond Angles, deg.			
F11−S1−F12	171.02(8)	F41−S4−F3	85.42(6)
F14−S1−F1	168.84(6)	F44−S4−F1	77.74(7)
F13−S1−F1	78.26(7)	F43−S4−F1	166.18(5)
F11−S1−F1	102.91(6)	F42−S4−F1	79.09(6)
F12−S1−F1	81.64(6)	F41−S4−F1	106.77(6)
F14−S1−F3^{i}	82.48(8)	F3−S4−F1	108.26(6)
F13−S1−F3^{i}	171.01(6)	F14−S1−F13	99.25(9)
F11−S1−F3^{i}	84.08(7)	F14−S1−F11	87.75(8)
F12−S1−F3^{i}	102.72(7)	F13−S1−F11	87.17(8)
F1−S1−F3^{i}	101.69(6)	F14−S1−F12	87.36(8)
F23−S2−F24	98.79(8)	F13−S1−F12	86.19(8)
F23−S2−F21	87.36(9)	F21−S2−F4	87.70(7)
F24−S2−F21	87.23(8)	F22−S2−F4	97.97(8)
F23−S2−F22	86.53(9)	F2−S2−F4	106.41(6)
F24−S2−F22	86.79(9)	F34−S3−F33	99.04(9)
F21−S2−F22	170.71(8)	F34−S3−F32	87.34(8)
F23−S2−F2	76.66(7)	F33−S3−F32	87.01(8)
F24−S2−F2	174.40(6)	F34−S3−F31	86.97(8)
F21−S2−F2	89.28(8)	F33−S3−F31	86.93(8)
F22−S2−F2	96.11(8)	F32−S3−F31	170.95(8)
F23−S2−F4	174.16(6)	F34−S3−F2	77.92(8)
F24−S2−F4	77.84(7)	F33−S3−F2	176.83(7)
F44−S4−F43	99.05(9)	F32−S3−F2	93.70(7)
F44−S4−F42	88.26(8)	F31−S3−F2	91.99(7)
F43−S4−F42	87.41(7)	F34−S3−F4^{i}	179.45(6)

Table 4.12 continued.

F44−S4−F41	87.51(8)	F33−S3−F4^{i}	80.78(8)
F43−S4−F41	86.37(7)	F32−S3−F4^{i}	93.17(7)
F42−S4−F41	171.85(7)	F31−S3−F4^{i}	92.50(7)
F44−S4−F3	171.82(6)	F2−S3−F4^{i}	102.25(7)
F43−S4−F3	76.41(7)	S1−F1−S4	115.89(6)
F42−S4−F3	98.25(6)	S2−F2−S3	118.61(6)

Symmetry code: (i) x+1, y, z.

Table 4.13 Selected Bond Lengths (Å), Contacts (Å), and Angles (deg.) of $[HNC_5H_4N(CH_3)_2^+]_2[SF_5^-]F^- \bullet CH_2Cl_2$

Bond Lengths and Contacts, Å			
S1−F5	1.553(5)	S1A−F5A	1.452(13)
S1−F2	1.696(3)	S1A−F3A	1.690(12)
S1−F3	1.707(4)	S1A−F4A	1.700(15)
S1−F1	1.728(5)	S1A−F1A	1.719(14)
S1−F4	1.749(5)	S1A−F2	1.755(11)
N3(H)---F6	2.511(4)	N1(H)---F6	2.517(4)
Bond Angles, deg.			
F5−S1−F2	85.5(2)	F3−S1−F1	168.0(4)
F5−S1−F3	83.6(3)	F5−S1−F4	83.5(3)
F2−S1−F3	90.37(19)	F2−S1−F4	169.0(3)
F5−S1−F1	84.5(4)	F3−S1−F4	88.5(3)
F2−S1−F1	90.6(2)	F1−S1−F4	88.3(3)

The structure of $[HNC_5H_4N(CH_3)_2^+][HF_2^-]\bullet 2SF_4$ contains a double chain consisting of bifluoride, each anion coordinating to four SF_4 molecules, and 4-dimethylaminopyridinium cations hydrogen-bonded to fluorine on the same side of all bifluoride anions. (Figure 4.9)

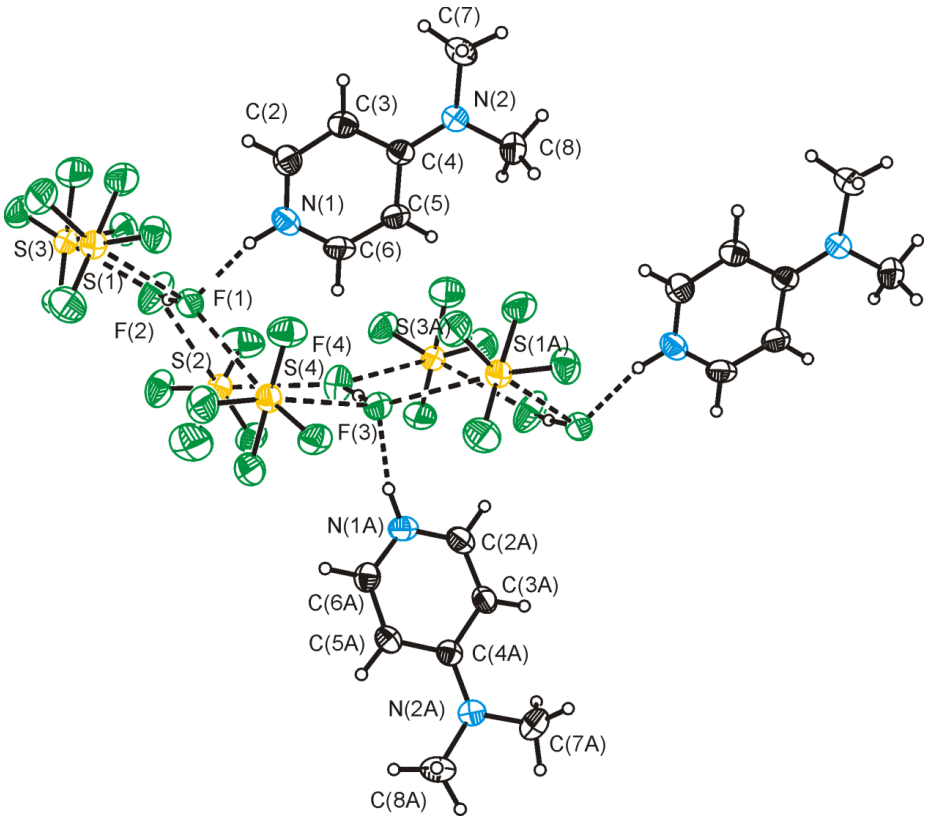

Figure 4.9 Thermal ellipsoid plot of the $[HNC_5H_4N(CH_3)_2^+][HF_2^-]\bullet 2SF_4$ double chain. Thermal ellipsoids are at 50% probability.

The structural motif is very similar to that observed for the $[HNC_5H_5^+][HF_2^-]\bullet 2SF_4$ salt as it contains a double bifluoride-SF_4 chain, except that the protonated nitrogen-base cations are not disordered as the dimethylamino group prevents rotation of the pyridinium ring while maintaining the overall packing arrangement. The 4-dimethylaminopyridinium cations are all found on one side of

the bifluoride chain, which causes polarization of the bifluoride anions. The thermal ellipsoids of SF_4 and one fluorine atom of bifluoride, which compose the half of the double chain that have contacts to the 4-dimethylaminopyridinium cations, are smaller than the thermal ellipsoids of the other half of the chain, which do not have contacts with the cations. This reflects the stabilizing effect of the hydrogen-bonded cations on the chain. The S−F_{eq} bond lengths (1.5332(15) to 1.5458(13) Å) are the same within 3σ with those of neat solid SF_4 (1.527(4) and 1.535(4) Å).

The N(H)---F contacts (2.632(2) and 2.638(2) Å) are much longer than those in all of the structures containing fluoride and pyridinium/pyridinium derivatives, but are significantly shorter than the N(H)---F contacts (2.937(5) Å) in $[HNC_5H_5^+]HF_2^-$•$2SF_4$. The N(H)---F distance is significantly longer than the N(H)---F distances found in other bifluoride salts which do not contain SF_4, such as the $[HNC_5H_5^+]HF_2^-$ salt (2.508 Å) and the $[HNC_5H_4(CH_3)^+]HF_2^-$ salt (2.534(4) Å), because the 4-dimethylaminopyridinium cation is a weaker Bronsted acid (p*Ka* = 9.5).[20] In this structure, it was possible to locate the proton in the bifluoride anion. As expected, the fluorides (F1 and F3) that are hydrogen-bonded to the cations have longer F1−H1B/F3−H2B bonds (1.28(3) and 1.25(3) Å) than the F2−H1B/F4−H2B bonds (1.01(3) and 1.05(3) Å). The F---F distances in the bifluoride anions are relatively short (2.284 (2) and 2.291 (2) Å), although it is not as short as the F---F distance of 2.213(4) Å found in the tetramethylammonium bifluoride salt that contains symmetric HF_2^- anions.[21] The S---F contacts (2.758(2) Å) are generally longer than the S---F contacts found in the other salts, particularly the structures that do not form chains. The F---S---F bond angles range from 101.69(6) to 108.26(6)°, and span a smaller range than the angles found in the $[HNC_5H_5^+][HF_2^-]$•$2SF_4$ salt.

The structure of $[HNC_5H_4N(CH_3)_2^+]_2[SF_5^-]F^-\bullet CH_2Cl_2$ consists of two protonated 4-dimethylaminopyridinium cations hydrogen-bonded to a fluoride anion, which in turn has a long contact to dichloromethane (see Figure 4.10), and also a well separated SF_5^- anion.

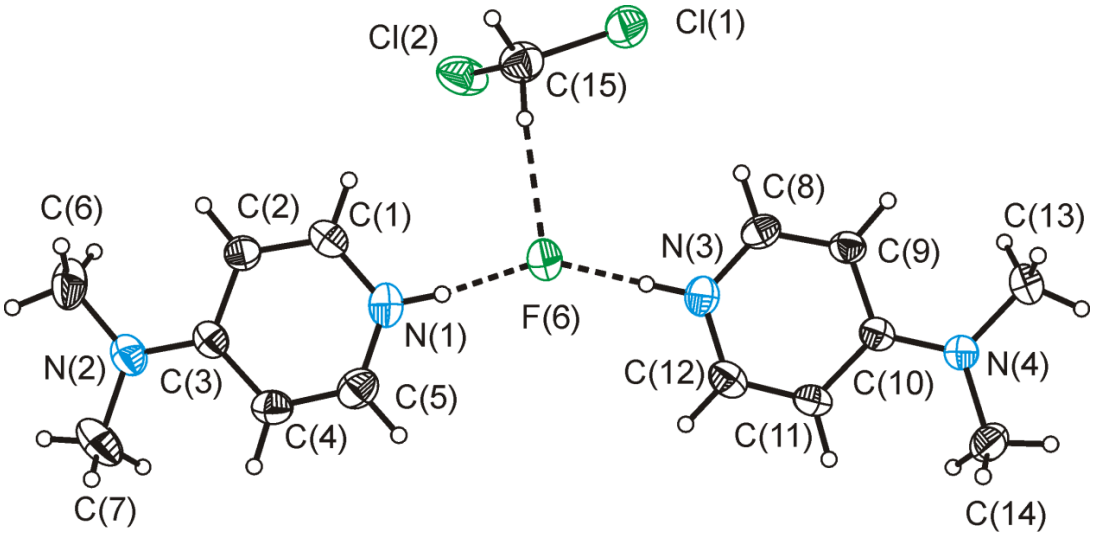

Figure 4.10 Thermal ellipsoid plot of $[HNC_5H_4N(CH_3)_2^+]_2[SF_5^-]F^-\bullet CH_2Cl_2$, excluding the SF_5^- anion. Thermal ellipsoids are at 50% probability.

The structure is similar to the structure of the $[HNC_5H_3(CH_3)_2^+]_2[SF_5^-]F^-\bullet SF_4$ salt (see Figure 4.8), except a dichloromethane molecule is found in place of an SF_4 molecule coordinated to the fluoride. The very long C---F distance of 3.106(6) Å is expected, as the Lewis acidity of CH_2Cl_2 is less than that of SF_4. The well separated SF_5^- anion exhibits a two-fold disorder (see Figure 4.11). The disorder was modeled using the same method that used for the SF_5^- anion in the $[HNC_5H_3(CH_3)_2^+]_2[SF_5^-]F^-\bullet SF_4$ salt, except for in this case the pivot point happened to be one of the equatorial fluorines, i.e., F(2).

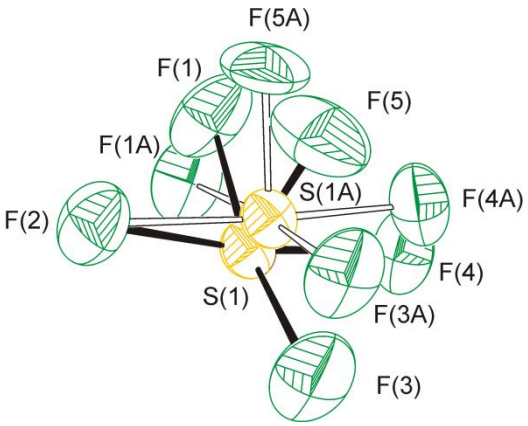

Figure 4.11 Thermal ellipsoid plot of the SF_5^- anion in $HNC_5H_4N(CH_3)_2^+]_2[SF_5^-]F^-\bullet CH_2Cl_2$. Thermal ellipsoids set at 50% probability.

The S−F_{ax} bond lengths (S1−F5 = 1.553(5) Å and S1A−F5A = 1.452(13) Å) are shorter than the S−F_{eq} bonds (1.690(12) to 1.755 (11) Å). These distances are similar to the SF_5^- anion observed in the $[HNC_5H_3(CH_3)_2^+]_2[SF_5^-]F^-\bullet SF_4$ salt (SF_{ax} = 1.586(2) and 1.594(17) Å; SF_{eq} = 1.657(7) to 1.718(5) Å).

4.2.5.2 Raman Spectroscopy

The Raman spectra of $[HNC_5H_4N(CH_3)_2^+][HF_2^-]\bullet 2SF_4$ and $[HNC_5H_4N(CH_3)_2^+]_2[SF_5^-]F^-\bullet CH_2Cl_2$ at −85 °C are depicted in Figure 4.12 and Figure 4.13. The Raman frequencies and tentative assignments are listed in Table 4.14 and Table 4.15.

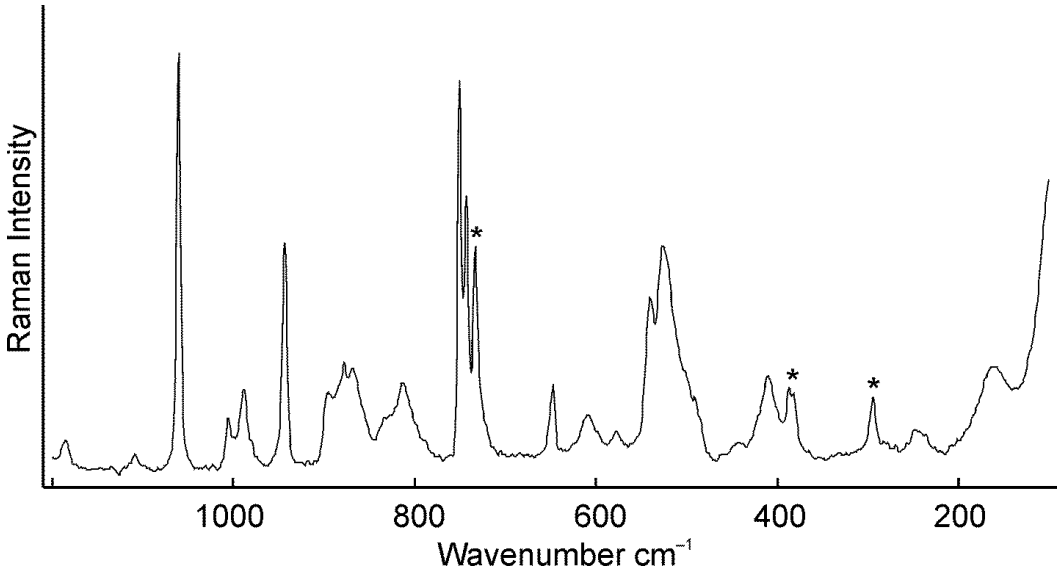

Figure 4.12 Raman spectrum of $[HNC_5H_4N(CH_3)_2^+][HF_2^-]\bullet 2SF_4$. Asterisks (*) denote bands arising from the FEP sample tube.

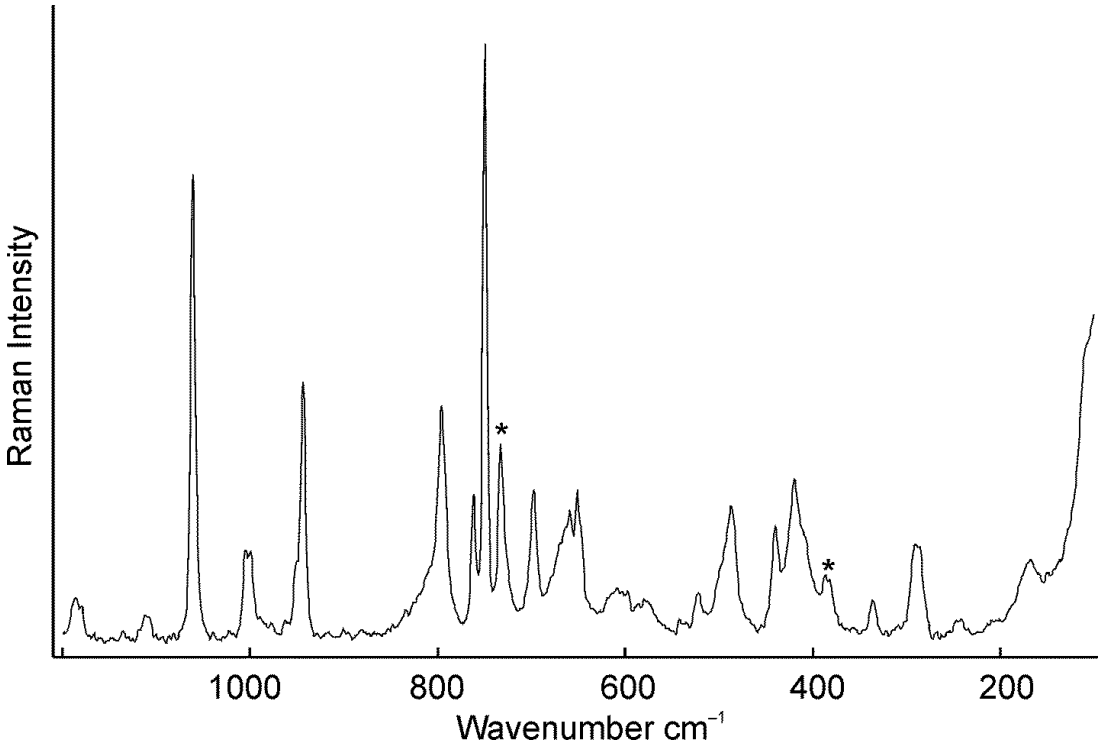

Figure 4.13 Raman spectrum of $[HNC_5H_4N(CH_3)_2^+]_2[SF_5^-]F^-\bullet CH_2Cl_2$. Asterisks (*) denote bands arising from the FEP sample tube.

Table 4.14 Raman Frequencies (cm^{-1}) and Tentative Assignments of $[HNC_5H_4N(CH_3)_2^+][HF_2^-]\bullet 2SF_4$.

$[HNC_5H_4N(CH_3)_2^+][HF_2^-]\bullet 2SF_4$[a]	SF_4	Assignment
3114(21)		ν(C–H)
3030(9)		ν(C–H)
2941(28)		$\nu(CH_3)$
2877(10)		$\nu(CH_3)$
2827(11)		$\nu(CH_3)$
1643(30)		ν (C–C)/ ν(C–N)
1566(29)		
1524(13)		
1487(7)		$\delta_{as}(CH_3)$
1469(11)		
1446(30)		
1419(9)		ν(C–C)/ ν(C–N)
1406(11)		
1336(4)		
1305(sh)		
1250(5)		$\delta_{in\text{-}plane}$(HCC)
1212(13)		
1185(7)		$\rho_r(CH_3)$
1108(4)		
1060(100)		$\nu_s(NC_5)$
1006(13)		
988(16)		DMAP $\delta_{in\text{-}plane}$(CCC)/$\delta_{in\text{-}plane}$(NCC)
943(51)		DMAP $\rho_r(CH_3)$
897(19)	904(32)	SF_4 comb.
878(24)	888(75)	$\nu_s\ SF_{2eq}$
868(23)	880(99)	$\nu_s\ SF_{2eq}$
813(20)	860sh	$\nu_{as}\ SF_{2eq}$
751(86)[b]		DMAP $\delta_{in\text{-}plane}$(CCC)/$\delta_{in\text{-}plane}$(NCC)
743(60)		
647(18)		DMAP
	629(7)	$\nu_{as}\ SF_{2ax}$
609(6)		$\nu_s\ (HF_2^-)$
540(34)	536(92)/532(100)	$\nu_s\ SF_{2ax}$
	524(54)	$\delta_{rock}\ (SF_{2eq})$
526(50)	515(72)/508(66)	$\delta_{sc}(SF_{2eq}) + \delta_{sc}(SF_{2ax})$
	458(31)	$T(SF_2)$
410(19)		DMAP
248(6)	243(15)	$\delta_{sc}(SF_{2eq}) - \delta_{sc}(SF_{2ax})$
159(19)		$\rho_r(CH_3)$

[a] Signals from the FEP sample tube were observed at: 1383(16), 1294(12), 1222(sh), 733(48), 578(4), 387(18), 294(13)

[b] Overlap with FEP signal

Table 4.15 Raman Frequencies (cm^{-1}) and Tentative Assignments of $[HNC_5H_4N(CH_3)_2^+]_2[SF_5^-]F^-\bullet CH_2Cl_2$.

$[HNC_5H_4N(CH_3)_2^+]_2[SF_5^-]$ $F^-\bullet CH_2Cl_2$	CH_2Cl_2	$CsSF_5^-$	Assignment
3111(25)			ν(C–H)
	3056(12)		CH_2Cl_2 ν(CH_2)
3025(16)			ν(C–H)
2986(18)	2987(74)		CH_2Cl_2 ν(CH_2)
2932(32)			ν(CH_3)
2876(18)			ν(CH_3)
	2827(1)		CH_2Cl_2 comb.
2823(20)			
1650(31)			ν(C–C)/ ν(C–N)
1612(14)			
1565(30)			
1524(13)			
1490(6)			$\delta_{as}(CH_3)$
1459(24)			
1446(31)			
1423(28)	1419(17)		CH_2Cl_2 δ(CH_2)
1405(11)			
1310(8)			
1296(13)[b]			
	1265(3)		CH_2Cl_2 ω(CH_2)
1248(2)			$\delta_{in\text{-}plane}$(HCC)
1220(12)[b]			
1212(10)			
	1156(8)		CH_2Cl_2 τ(CH_2)
1186(7)			
1112(4)			
1061(81)			$\nu_s(NC_5)$
1005(16)			
943(44)			DMAP $\rho_r(CH_3)$
	896(2)		CH_2Cl_2 δ(CH_2)
796(40)		796(37)	SF_5^- ν (SF_{ax})
762(23)		785(12)	SF_5^-ν (SF_{ax})
750(100)[b]			DMAP $\delta_{in\text{-}plane}$(CCC)/$\delta_{in\text{-}plane}$(NCC)
	739(10)		CH_2Cl_2, $\nu_{as}(CCl_2)$
697(21)	701(100)		CH_2Cl_2, $\nu_s(CCl_2)$
659(18)			DMAP
651(20)			
609(3)		590 sh/583(7)	SF_5^-, $\nu_{as}(SF_4)$
542(2)			
522(6)		522(27)	SF_5^- ν_s (SF_4) in phase
487(21)		512(7)	SF_5^- $\delta_s(SF_4)_{out\ of\ plane}$
440(19)		435(100)/469(100)	$SF_5^-\delta_s(SF_4)$ umbrella
420(28)		435(100)/420(12)	SF_5^- δ($F_{ax}SF_4$)

Table 4.15 continued.

336(7)		342(16)/315(7)	SF_5^- $\delta_s(SF_4)$ in plane
290(19)[b]	287(53)		CH_2Cl_2, $\delta(CCl_2)$
242(2)		241(12)/242(13)	SF_5^- $\delta_{as}(SF_4)$ in plane
168(7)			$\rho_r(CH_3)$

[a] Signals from the FEP sample tube were observed at: 1382(7), 1296(13) (overlap), 1220(12) (overlap), 750(100) (overlap), 733(30), 387(8), 290(19) (overlap)
[b] Overlap with FEP signal

The region from 1700 to 50 cm^{-1} of the Raman spectrum of the $[HNC_5H_4N(CH_3)_2^+][HF_2^-]$•$2SF_4$ salt is very complicated. The most intense peak is found at 1060 cm^{-1} and coincides with different structures containing the 4-DMAP moiety. (neat DMAP: 1064 cm^{-1}, SF_4•DMAP: 1063 cm^{-1}, $[HNC_5H_4N(CH_3)_2^+]_2[SF_5^-]F^-$•$CH_2Cl_2$: 1061 cm^{-1}). The bands assigned to the SF_{2eq} stretches of SF_4 are very broad and are found at 878(24)/868(23) cm^{-1} ($\nu_s(SF_{2eq})$) and 813(20) cm^{-1} ($\nu_{as}(SF_{2eq})$). The bands assigned to the $\nu_s(SF_{2ax})$ stretches of SF_4 are broad and found at 540(34) and 526(50) cm^{-1}. It is possible that the $\nu_{as}(SF_{2ax})$ is overlapped with a signal attributable to C−C bending at 647(18) cm^{-1}. The ν_s stretch of the bifluoride anion was assigned to the peaks at 609(6) cm^{-1} based on the Raman spectrum of the previously reported KHF_2 salt (ν_s = 610, 600 cm^{-1}).[22]

The Raman spectrum of the $[HNC_5H_4N(CH_3)_2^+]_2[SF_5^-]F^-$•$CH_2Cl_2$ salt contains signals that can be assigned to CH_2Cl_2, SF_5^-, and the 4-dimethylaminopyridinium cation, as well as a few low-intensity peaks associated with an SF_4•4-dimethylaminopyridine impurity. The intense band at 697 cm^{-1} is assigned to the $\nu_s(CCl_2)$ mode of dichloromethane and is not significantly shifted relative to neat CH_2Cl_2 (701 cm^{-1}). The band at 420(28) cm^{-1} is assigned to the $\delta(F_{ax}SF_4)$ mode of the SF_5^- anion and agrees well with the Raman spectrum of $CsSF_5$

(420(12) cm^{-1}).[6] The peaks assigned to the 4-dimethylaminopyridinium cation coincide with the peaks in the Raman spectrum of $[HNC_5H_4N(CH_3)_2^+][HF_2^-]$•$2SF_4$. The most intense peak assigned to residual SF_4•4-dimethylaminopyridine is at 796(40) cm^{-1}.

4.2.6 The 4,4'-Bipyridyl-HF-SF_4 System

Previous attempts at elucidating the structure of the product formed between 4,4'-bipyridyl and SF_4 had limited success.[23] The solubility of 4,4'-bipyridyl in neat SF_4 is low. It was hypothesized that the solubility of protonated 4,4'-bipyridyl in neat SF_4 could be higher. Slow cooling of a 1-to-2 mixture of H_2O to 4,4'-bipyridyl (1:1 HF to 4,4-bipyridyl) in excess SF_4 caused the formation of large needles ($[HNH_4C_5{-}C_5H_4N^+]F^-$•$2SF_4$). Slow cooling of a 1-to-1 mixture of H_2O to 4,4'-bipyridyl (2:1 HF to 4,4-bipyridyl) in excess SF_4 from room temperature to −80 °C resulted in the formation of large needles with the composition $[HNH_4C_5{-}C_5H_4NH^{2+}]2F^-$•$4SF_4$.

4.2.6.1 X−ray Crystal Structures of $[HNH_4C_5{-}C_5H_4N^+]F^-$•$2SF_4$ and $[HNH_4C_5{-}C_5H_4NH^{2+}]2F^-$•$4SF_4$

Details of data collection parameters and crystallographic information for $[HNH_4C_5{-}C_5H_4N^+]F^-$•$2SF_4$ and $[HNH_4C_5{-}C_5H_4NH^{2+}]2F^-$•$4SF_4$ are given in Table 4.16. Important bond lengths, angles and contacts for $[HNH_4C_5{-}C_5H_4N^+]F^-$•$2SF_4$ and $[HNH_4C_5{-}C_5H_4NH^{2+}]2F^-$•$4SF_4$ are listed in Table 4.17 and Table 4.18 respectively.

Table 4.16 Crystal Data Collection Parameters and Results of $[HNH_4C_5{-}C_5H_4N^+]F^-{\bullet}2SF_4$ and $[HNH_4C_5{-}C_5H_4NH^{2+}]2F^-{\bullet}4SF_4$

Compound	$[HNH_4C_5{-}C_5H_4N^+]F^-{\bullet}2SF_4$	$[HNH_4C_5{-}C_5H_4NH^{2+}]2F^-{\bullet}4SF_4$
File Code	MG120176	MG12086
Empirical Formula	$C_{10}H_9F_9N_2S_2$	$C_{10}H_{10}F_{18}N_2S_4$
Formula weight, g mol^{-1}	392.31	628.44
Temperature, K	153	153
Wavelength, Å	0.71073	0.71073
Crystal System	Orthorhombic	Tetragonal
Space Group	$P2_12_12_1$	$P4_2Tc$
Unit Cell Dimensions	a = 7.339 (7) Å	a = 16.530 (13) Å
	b = 10.783 (10) Å	c = 8.322 (6) Å
	c = 18.641 (17) Å	
Abs. coeff. μ, mm^{-1}	0.46	0.57
Volume	1475 (2)	2274 (3)
Z	4	4
Density (calculated), g cm^{-1}	1.783	1.836
F(000)	784	1240
Crystal Size, mm^3	0.31 × 0.15 × 0.11	0.58 × 0.08 × 0.08
Reflections Collected	17011	25142
Independent Reflections	3418 [R_{int} = 0.054]	2620 [Rint = 0.053]
Data/Restraints/Parameters	3418/0/209	2620/0/155
Goodness-of-fit on F^2	1.02	1.05
Refine Diff $\Delta\rho$max e Å^{-3}	0.41	0.23
Refine Diff $\Delta\rho$min e Å^{-3}	−0.28	−0.29
R_1, $I > 2\sigma(I)$[a]	0.0377	0.0324
$wR_2(F^2)$[a]	0.1041	0.0882

[a] $R_1 = \Sigma||F_o| - |F_c||/\Sigma|F_o|$; $wR_2 = [\Sigma w(F_o^2 - Fc^2)^2/\Sigma w(F_o^4)]^{1/2}$.

Table 4.17 Selected Bond Lengths (Å), Contacts (Å), and Angles (deg.) of $[HNH_4C_5{-}C_5H_4N^+]F^-{\bullet}2SF_4$.

Bond Lengths and Contacts, Å			
S1−F1	1.521(2)	S2−F11	1.510(2)
S1−F2	1.559(2)	S2−F12	1.553(2)
S1−F4	1.644(2)	S2−F13	1.633(2)
S1−F3	1.650(2)	S2−F14	1.651(2)
S1−N1	2.613(3)	N2(H)---F5	2.429(3)
F5---S2	2.562(3)	S1----F5^{i}	3.005(3)
Bond Angles, deg.			
F1−S1−F2	96.06(11)	F11−S2−F12	98.75(14)
F1−S1−F4	87.43(15)	F11−S2−F13	88.35(15)
F2−S1−F4	88.31(12)	F12−S2−F13	87.80(13)
F1−S1−F3	87.88(14)	F11−S2−F14	87.68(15)
F2−S1−F3	88.31(12)	F12−S2−F14	88.69(15)
F4−S1−F3	173.90(14)	F13−S2−F14	174.25(15)
F1−S1−N1	78.09(9)	F11−S2−F5	77.98(11)
F2−S1−N1	173.14(9)	F12−S2−F5	175.17(10)
F4−S1−N1	87.85(10)	F13−S2−F5	88.56(12)
F3−S1−N1	94.99(11)	F14−S2−F5	94.69(13)

Symmetry code: (i) −1/2+x, 1.5−y, 1−z

Table 4.18 Selected Bond Lengths (Å), Contacts (Å), and Angles (deg.) of $[HNH_4C_5{-}C_5H_4NH^{2+}]2F^-{\bullet}4SF_4$.

Bond Lengths and Contacts, Å			
S1−F1	1.512(3)	F9----S2^{i}	2.695(3)
S1−F2	1.534(3)	S2−F6	1.536(2)
S1−F4	1.642(3)	S2−F8	1.547(2)
S1−F3	1.643(3)	S2−F7	1.653(2)
S1---F9	2.838(3)	S2−F5	1.680(2)
S2---F9	2.658(2)	N1(H1)---F9	2.427(3)
Bond Angles, deg.			
F1−S1−F2	99.83(16)	F8−S2−F7	87.67(12)
F1−S1−F4	88.93(15)	F6−S2−F5	87.25(10)
F2−S1−F4	88.36(14)	F8−S2−F5	86.93(11)
F1−S1−F3	87.19(14)	F7−S2−F5	172.39(11)
F2−S1−F3	88.11(16)	F6−S2−F9	174.90(10)
F4−S1−F3	174.23(16)	F8−S2−F9	77.42(11)
F1−S1−F9	77.08(12)	F7−S2−F9	89.42(9)
F2−S1−F9	174.35(12)	F5−S2−F9	94.63(8)
F4−S1−F9	96.26(10)	S2−F9−S2^{i}	126.43(8)

Table 4.18 continued.

F3−S1−F9	87.03(12)	S2−F9−S1	91.12(8)
F6−S2−F8	97.97(13)	S2^{i}−F9−S1	112.96(8)
F6−S2−F7	88.19(11)	F9---S2---F9	107.11(6)

Symmetry codes: (i) y+1/2, x−1/2, z+1/2; (ii) −x+2, −y+1, z.

The structure of $[HNH_4C_5{-}C_5H_4N^+]F^-{\bullet}2SF_4$ consists of a 4,4'-bipyridyl molecule with one protonated nitrogen. The protonated nitrogen is hydrogen-bonded to a fluoride, which forms a contact to SF_4. The other nitrogen is directly coordinated to an SF_4 molecule (see Figure 4.14).

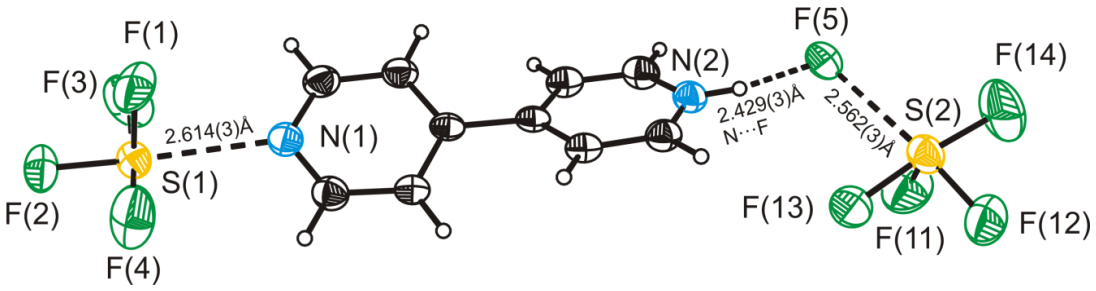

Figure 4.14 Thermal ellipsoid plot of $[HNH_4C_5{-}C_5H_4N^+]F^-{\bullet}2SF_4$ Thermal ellipsoids are at 50% probability.

The torsion angle between the rings in 4,4'-bipyridyl is 14.3(2)°, which agrees well with the angle in neat 4,4'-bipyridyl of 14.1(8)°.[24] This structure contains both F_4S---N and F_4S---(F)---HN bonding, and is therefore a link between the previously characterized SF_4-nitrogen-base adducts, and the nitrogen-base-HF-SF_4 salts. The S---N contact is 2.614(3) Å which is significantly shorter than the sum of the van-der-Waals radii (3.35 Å). The SF_4 which forms a contact with the nitrogen also has a weak contact (3.005(3) Å) with the fluoride. This contact, however, does

not distort the square pyramidal geometry of the F_4S---N moiety. The S---N (2.614(3) Å) contact is longer than the previous S---N contact in F_4S---NC_5H_5 of 2.5140(18) Å, reflecting the weaker Lewis basicity of the partially protonated 4,4'-bypyridyl ligand compared to pyridine. The equatorial S1−F2 bond (1.559(2) Å) opposite of the nitrogen atom is much longer than the other equatorial S1−F1 bond (1.521(2) Å). This increase in bond length is caused by the *trans*-effect of the nitrogen donor. The SF_{ax} bond lengths are the same within 3σ (1.644(2) and 1.650(2) Å). Similar S−F bond lengths are observed in the SF_4 molecule which is coordinated by fluoride (S---F^- = 2.562(3) Å). The *trans* S2−F12 bond (1.553(2) Å) is elongated compared with the other equatorial S−F bond (1.510(2) Å), due to *trans*-effect of the fluoride contact. The bipy rings exhibit π-π stacking, in which the proton alternates sides (C1---C10 3.522(5) Å, C2---C9 3.603(4) Å).

In the $[HNH_4C_5{-}C_5H_4NH^{2+}]2F^-{\bullet}4SF_4$ crystal structure, both nitrogen atoms of 4,4'-bipyridyl are protonated and the NH groups form hydrogen-bonds to fluoride, which is coordinated to three SF_4 molecules. (Figure 4.15) Two of the three SF_4 molecules are related by crystallographic symmetry. The asymmetric unit contains half of the protonated bipyridyl ring bound to fluoride, coordinated to two SF_4 molecules. The SF_4 and fluoride form an infinite chain, which is different from what is observed in the previous chained structures in this chapter, i.e., $[HNC_5H_5^+]F^-{\bullet}SF_4$, $[HNC_5H_5^+][HF_2^-]{\bullet}2SF_4$, and $[HNC_5H_4N(CH_3)_2^+][HF_2^-]{\bullet}2SF_4$.

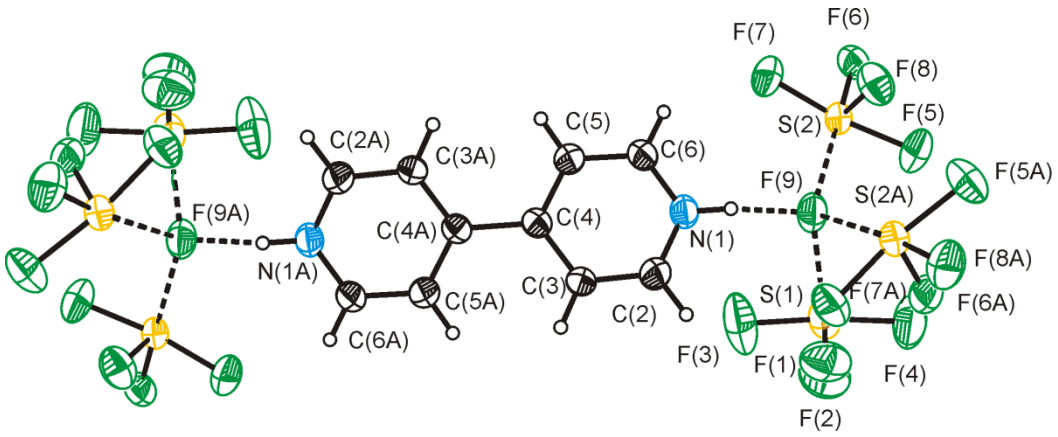

Figure 4.15 Thermal ellipsoid plot of $[HNH_4C_5{-}C_5H_4NH^{2+}]2F^{-}{\bullet}4SF_4$ with thermal ellipsoids set at 50% probability.

The chain contains two unique SF_4 molecules. One SF_4 has two comparatively short contacts (2.658(2) and 2.695(3) Å) with two fluorides and forms a similar chain to $[HNC_5H_5^{+}]F^{-}{\bullet}SF_4$. The other SF_4 molecule has a long contact (2.838(3) Å) with fluoride, and a very long contact (3.156(3) Å) with the equatorial fluorine of the first SF_4 with short S---F contacts. The thermal ellipsoids of the SF_4 with long contacts are larger, representing the greater degree of thermal motion in less coordinated SF_4. As expected, both the axial and equatorial S−F bond lengths are longer in the more strongly coordinated SF_4 molecule than in the less coordinated SF_4 molecule. The $[HNH_4C_5{-}C_5H_4NH^{2+}]2F^{-}{\bullet}4SF_4$ salt also exhibits π−π stacking (C---C = 3.520(5) and 3.547(5) Å) between the aromatic 4,4'-bipyridyl rings, which lies along the *c*-axis (see Figure 4.16).

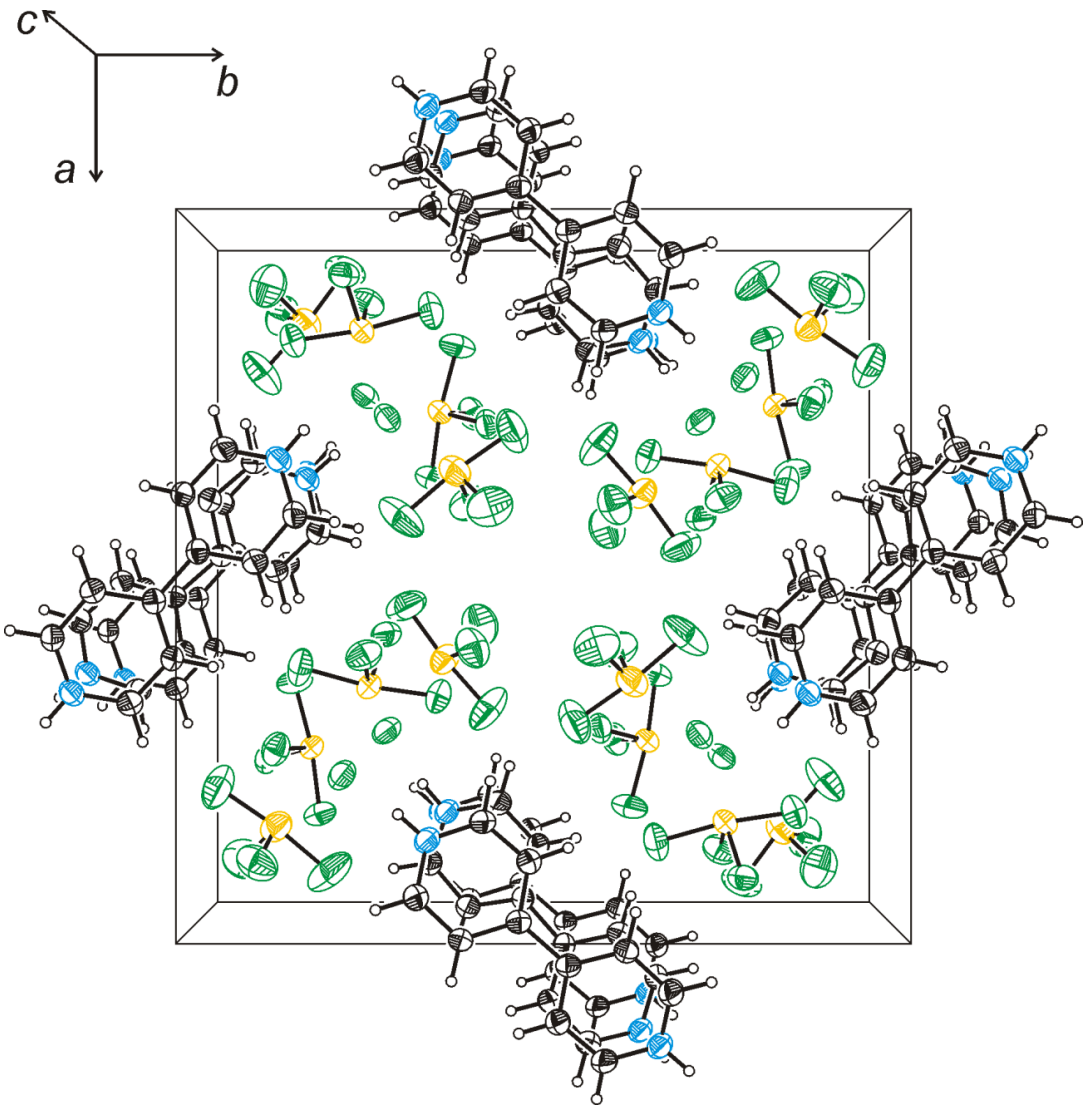

Figure 4.16 Thermal ellipsoid plot of $[HNH_4C_5{-}C_5H_4NH^{2+}]2F^{-}{\bullet}4SF_4$ packed along the *c*-axis. Thermal ellipsoids are set to 50% probability.

Along the *c*-axis, one can see that the columns of the bipyridyl moieties are completely surrounded by SF_4. The N(H)---F contacts in the partially protonated 4,4'-bipyridyl salt compared to the fully protonated bipyridyl salt are not significantly different (2.429(3) vs. 2.427(3) Å, respectively).

4.2.6.2 Raman Spectroscopy

The Raman spectrum of $[HNH_4C_5{-}C_5H_4N^+]F^-{\bullet}2SF_4$ at −85 °C and $[HNH_4C_5{-}C_5H_4NH^{2+}]2F^-{\bullet}4SF_4$ at −97 °C, are shown in Figure 4.17. The Raman frequencies and tentative assignments are shown in Table 4.19 and in Table 4.20.

The Raman spectrum of both salts contain signals associated with the 4,4'-bipyridyl moiety as well as signals associated with SF_4 moieties. The assignment of the 4,4'-bipyridyl moiety was aided by the previous assignments reported by Topaçli and Akyüz.[25] As expected, the Raman spectrum of $[HNH_4C_5{-}C_5H_4N^+]F^-{\bullet}2SF_4$ contains a significantly greater number of bands than that of $[HNH_4C_5{-}C_5H_4NH^{2+}]2F^-{\bullet}4SF_4$, due to the overall lower symmetry and different sulfur tetrafluoride crystallographic environments. The frequency of the $\nu_s(SF_{2ax})$ (534 cm^{-1}) mode does not change between the two salts, although its relative intensity varies greatly. The Raman spectrum of $[HNH_4C_5{-}C_5H_4N^+]F^-{\bullet}2SF_4$ contains two $\tau(SF_2)$ signals at 452(11) and 445(8) cm^{-1} as well as two signals attributable to the $\nu_{as}(SF_{2eq})$ stretches at 856(8) and 843(3) cm^{-1}. It is difficult to assign a signal to the two different SF_4 considering the $S{-}F_{eq}$ bond lengths are not significantly different (N---SF_4 $S{-}F_{eq}$ = 1.559(2) and 1.521(2) Å; F^----SF_4 $S{-}F_{eq}$ = 1.553(2) and 1.510(2) Å). The Raman spectrum of $[HNH_4C_5{-}C_5H_4NH^{2+}]F^-{\bullet}4SF_4$ contains only one signal attributable to the $\tau(SF_2)$ mode, at 446(6) cm^{-1}. It is therefore likely that $\tau(SF_2)$ (N---SF_4) = 452(11) cm^{-1} and $\tau(SF_2)$ (F^----SF_4) = 445(8) cm^{-1} for the $[HNH_4C_5{-}C_5H_4N^+]F^-{\bullet}2SF_4$ salt.

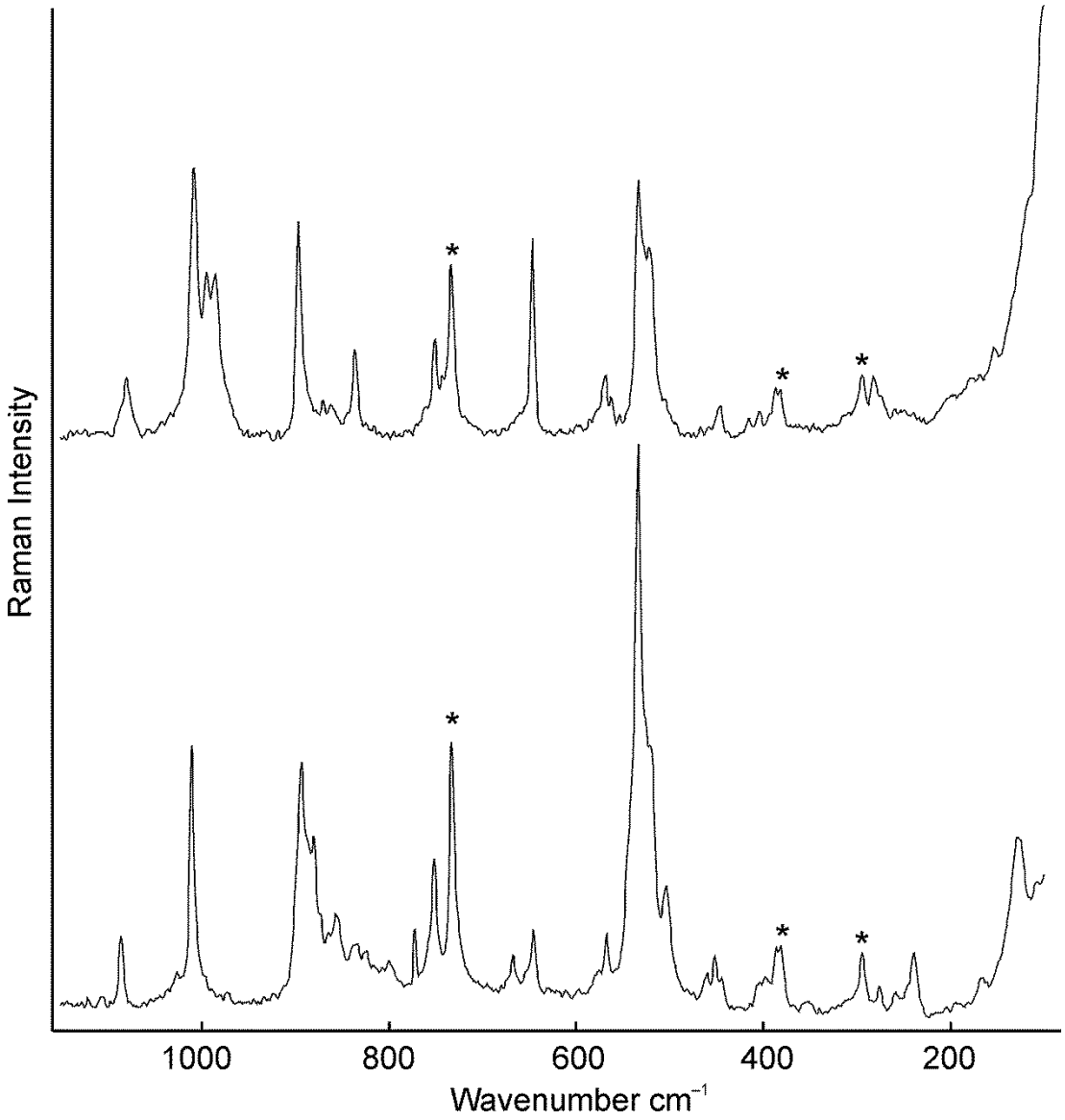

Figure 4.17 Raman spectra of $[HNH_4C_5{-}C_5H_4N^+]F^-{\bullet}2SF_4$ (top) and $[HNH_4C_5{-}C_5H_4NH^{2+}]2F^-{\bullet}4SF_4$ (bottom). Asterisks (*) denote bands arising from the FEP sample tube.

Table 4.19 Raman Frequencies (cm^{-1}) and Tentative Assignments of $[HNH_4C_5{-}C_5H_4N^+]F^-{\bullet}2SF_4$.

$[HNH_4C_5{-}C_5H_4N^+]F^-{\bullet}2SF_4$	SF_4	Assignment
3125(7)		
3107(13)		ν(C–H)
3089(6)		
1654(19)		ν(C–C)/ ν(C–N)
1639(57)		ν_{ring}
1549(12)		ν(C–C)/ ν(C–N)
1528(13)		ν(C–C)/ ν(C–N)
1394(4)		
1294(56)		
1250(20)[b]		
1243(8)		δ(CH)
1231(5)		
1122(1)		
1107(3)		
1086(13)		
1028(4)		
1011(46)		ν_{ring}
973(2)		
893(42)	904(32)	$\nu_s(SF_{2eq})$
880(29)	888(75)/880(99)	$\nu_s(SF_{2eq})$
865(2)		$\nu_s(SF_{2eq})$
856(8)	860sh	$\nu_{as}(SF_{2eq})$
834(3)		$\nu_{as}(SF_{2eq})$
824(3)		
800(3)		
772(10)		bipy γ_{ring}
752(22)[b]		bipy γ_{ring}
667(6)		
646(11)		
	629(7)	$\nu_{as}(SF_{2ax})$
567(10)		bipy γ_{ring}
	536(92)/	$\nu_s(SF_{2ax})$
534(100)	532(100)	
521(sh)	524(54)	$\delta_{rock}(SF_{2eq})$
504(21)	515(72)/508(66)	$\delta_{sc}(SF_{2eq}) + \delta_{sc}(SF_{2ax})$
460(8)		
452(11)	458(31)	$F_4S{---}F^-$ $\tau(SF_2)$
445(8)		$F_4S{---}N$ $\tau(SF_2)$
404(4)		
398(6)		

Table 4.19 continued.

381(11)		
352(3)		bipy δ_{ring}
276(4)		
259(3)		
239(12)	243(15)	$\delta_{sc}(SF_{2eq}) - \delta_{sc}(SF_{2ax})$
166(5)		
128(29)		
108(sh)		
98(sh)		

[a] Signals from the FEP sample tube were observed at: 1383(12), 1250(20), 752(22), 733(42), 386(11), 294(9).
[b] Overlap with the FEP signal.

Table 4.20 Raman Frequencies (cm^{-1}) and Tentative Assignments of $[HNH_4C_5{-}C_5H_4NH^{2+}]2F^{-}{\bullet}4SF_4$.

$[HNH_4C_5{-}C_5H_4NH^{2+}]2F^{-}{\bullet}4SF_4$	SF_4 (solid)	Assignment
3103(12)		C−H
1651(45)		ν(C–C)/ ν(C–N)
1639(46)		
1530(30)		
1294(100)[b]		ν_{ring}
1248(40)		δ(CH)
1234(16)		
1080(13)		
1008(42)		δ_{ring}
995(24)		ν_{ring}
985(24)		ν_{ring}
897(37)	904(32)	comb. band
871(3)	888(75)	SF_4 $\nu_s(SF_{2eq})$
862(3)	880(99)	SF_4 $\nu_s(SF_{2eq})$
836(15)	860sh	SF_4 $\nu_{as}(SF_{2eq})$
751(16)[b]		bipy γ_{ring}
647(33)		
	629(7)	SF_4 $\nu_{as}(SF_{2ax})$
569(10)		bipy γ_{ring}
533(42)	536(92)/532(100)	SF_4 $\nu_s(SF_{2ax})$
521(31)	524(54)	SF_4 $\delta_{rock}(SF_{2eq})$
	515(72)/508(66)	SF_4 $\delta_{sc}(SF_{2eq})$ + $\delta_{sc}(SF_{2ax})$
446(6)	458(31)	SF_4 $\tau(SF_2)$
282(7)		bipy δ_{ring}
	243(15)	SF_4 $\delta_{sc}(SF_{2eq})$ − $\delta_{sc}(SF_{2ax})$

[a] Signals from the FEP sample tube were observed at: 1384(14), 1294(100) (overlap), 751(16) (overlap), 733(28), 387(7), 294(6)
[b] Overlap with the FEP signal.

4.3 Summary and Conclusion

A large range of pyridinium and substituted pyridinium fluoride salts that incorporate sulfur tetrafluoride have been synthesized and characterized by X-ray crystallography and Raman spectroscopy at low temperatures. These structures exhibit a surprising range of bonding modalities and provide an extensive view of

SF_4 in the solid state. The structures offer the first look at F_4S---F^- contacts in contrast to the known $F_4S{-}F^-$ bonds in the SF_5^- anion. In general, weak F_4S---F^- contacts, exhibit shorter S−F bonds and larger thermal ellipsoids. These structures represent actual fluorinating agents that have been used to fluorinate organic compounds containing carbonyl and hydroxyl groups and are only stable at low temperatures.

The S---F^- contacts range from 2.5116(12) to 2.8241(9) Å and are all significantly shorter than the sum of the van-der-Waals radii (3.27 Å). The shortest S---F^- contacts occur when one fluoride is coordinated to one SF_4 molecule, *e.g.*, S---F^- of $[HNC_5H_3(CH_3)_2^+]_2[SF_5^-]F^-{\bullet}SF_4$ (2.5116(12) Å) and S---F^- of $[HNH_4C_5{-}C_5H_4N^+]F^-{\bullet}2SF_4$ (2.562(3) Å). The longest S---F^- contacts occur when sulfur has contacts with two fluoride anions, *e.g.*, S---F^- of $[HNC_5H_5^+]F^-{\bullet}SF_4$ = 2.6923(9), 2.8241(9) Å and S---F^- of $[HNC_5H_4(CH_3)^+]F^-{\bullet}SF_4$ = 2.632(6), 2.823(6) Å. The N(H)---F^- distances range from 2.404(4) to 2.5396(17) Å. These hydrogen bonds, except for the hydrogen bonds in $[HNC_5H_3(CH_3)_2^+]_2[SF_5^-]F^-{\bullet}SF_4$, can be classified as strong, according to the Steiner.[26] The N(H)---F^- distances (2.5308(17) and 2.5396(17) Å are significantly longer in the 2,6-dimethylpyridinium $[HNC_5H_3(CH_3)_2^+]_2F^-$ moiety due to the steric hindrance of the methyl groups located at the *ortho*-positions. These hydrogen bonds can be classified moderate in strength.[1]

The bifluoride anion formed in three of these reaction systems. The F---F distances of these bifluoride anions agree well with previously reported F---F distances. The 4-methylpyridinium bifluoride formed due to the presence of excess HF, and insufficient SF_4. The $[HNC_5H_5^+][HF_2^-]{\bullet}2SF_4$ and

$[HNC_5H_4N(CH_3)_2^+][HF_2^-]\bullet 2SF_4$ salts are the first examples of SF_4-bifluoride interactions in the solid state.

References

(1) Schwesinger, R.; Link, R.; Wenzl, P.; Kossek, S. *Chem. Eur. J.* **2005**, *12*, 438-445.

(2) Clark, J. H. *Chem. Rev.* **1980**, *80*, 429-452.

(3) Christie, K. O.; Wilson, W. W. *J. Fluorine Chem.* **1990**, 47, 117-120.

(4) Tunder, R.; Siegel, B. *J. Inorg. Nucl. Chem.* **1963**, *25*, 1097-1098.

(5) Bittner, J.; Fuchs, J.; Seppelt, K. *Z. Anorg. Allg. Chem.* **1988**, *557*, 182-190.

(6) Drullinger, L. F.; Griffths, J. E. *Spectrochim. Acta A* **1971**, *27*, 1793-1799.

(7) Christe, K. O.; Curtis, E. C.; Schack, C. J.; Pilipovich, D. *Inorg. Chem.* **1972**, *11*, 1679-1682.

(8) Clark, M.; Kellen-Yuen, C.; Robinson, K.; Zhang, H.; Yang, Z.-Y.; Madappat, K.; Fuller, J.; Atwood, J.; Thrasher, J. *Eur. J. Solid State Inorg. Chem.* **1992**, *29*, 809-833.

(9) Goettel, J. T.; Chaudhary, P.; Hazendonk, P.; Mercier, H. P. A.; Gerken, M. *Chem. Commun.* **2012**, *48*, 9120–9122.

(10) Olah, G. A.; Welch, J. T.; Vankar, Y. D.; Nojima, M.; Kerekes, I.; Olah, J. A. *J. Org. Chem.* **1979**, *44*, 3872-3881.

(11) Boenigk, D.; Mootz, D. *J. Am. Chem. Soc.* **1988**, *110*, 2135-2139.

(12) Schaefer, T.; Rowbotham, J. B.; Parr, W. J.; Marat, K.; Janzen, A. F. *Can. J. Chem.* **1976**, *54*, 1322-1328.

(13) Dmowski, W. *Pol. J. Chem.* **1982**, *56*, 1369.

(14) Rudine, A. B.; Walter, M. G.; Wamser, C. C. *J. Org. Chem.* **2010**, *75*, 4292-4295.

(15) Casteel, W. J.; Dixon, D. A.; LeBlond, N.; Lock, P. E.; Mercier, H. P. A.; Schrobilgen, G. J. *Inorg. Chem.* **1999**, *38*, 2340-2358.

(16) Lind, M. D.; Christe, K. O. *Inorg. Chem.* **1972**, *11*, 608-612.

(17) Kniep, R.; Korte, L.; Kryschi, R.; Poll, W. *Angew. Chem. Int. Ed. Engl.* **1984**, *23*, 388-389.

(18) Cook, D. *Can. J. Chem.* **1961**, *39*, 2009-2024.

(19) Aakeroy C, B.; Seddon, K. R. *Z. Naturforsch., B: Chem. Sci.* **1993**, *48*, 1023-1025.

(20) Andon, R.; Cox, J.; Herington, E. *Trans. Faraday Soc.* **1954**, *50*, 918-927.

(21) Wilson, W. W.; Christe, K. O.; Feng, J.-a.; Bau, R. *Can. J. Chem.* **1989**, *67*, 1898-1901.

(22) Dawson, P.; Hargreave, M. M.; Wilkinson, G. R. *Spectrochimica Acta Part A: Molecular Spectroscopy* **1975**, *31*, 1055-1063.

(23) Chaudhary, P., M.Sc. Thesis, Lethbridge, Alta.: University of Lethbridge, Dept. of Chemistry and Biochemistry, 2011.

(24) Boag, N. M.; Coward, K. M.; Jones, A. C.; Pemble, M. E.; Thompson, J. R. *Acta Crystallogr., Sect. C: Cryst. Struct. Commun.* **1999**, *55*, 672-674.

(25) Topaçli, A.; Akyüz, S. *Spectrochim. Acta, Part A* **1995**, *51*, 633-641.

(26) Steiner, T. *Angew. Chem. Int. Ed.* **2002**, *41*, 48-76.

5 Structure of Sulfur Tetrafluoride in the Solid State

5.1 Introduction

Sulfur tetrafluoride is one of the fundamental binary main-group fluorides and, since its discovery in 1929, its structure and bonding has been subject to many studies.[1,2] The structure of SF_4 has been determined in the gas phase by microwave,[3] vibrational,[4] and nuclear magnetic resonance spectroscopy,[5] as well as electron diffraction,[6] revealing the molecular seesaw geometry (C_{2v}) which is in accordance with the VSEPR rules. Vibrational spectra of liquid SF_4 have also been assigned in terms of molecular C_{2v} point symmetry.[7] Sulfur tetrafluoride in solution is one of the typical examples for a fluxional trigonal bipyramidal electron-group geometry, with rapidly exchanging axial and equatorial fluorine environments on the NMR time-scale at room temperature.[8] At low-temperature, the exchange can be slowed down, allowing the observation of two triplets in the ^{19}F NMR spectrum for the axial and equatorial fluorine environments in SF_4.

An NMR study of the temperature dependence of the ^{19}F NMR chemical shifts and ^2J coupling constants suggested the presence of labile fluorine bridging.[9] In the past, a series of structures in solutions and the solid state have been discussed (see Figure 5.1).

Structures (I) and (II) were first proposed but later discarded since the equatorial S−F bonds are more covalent than the axial S−F bonds. This renders the equatorial fluorines less fluoro-basic than the axial fluorines. The more ionic nature

of the axial fluorines would favour dimers (III) or chain-type oligomers (IV). (*vide infra*).

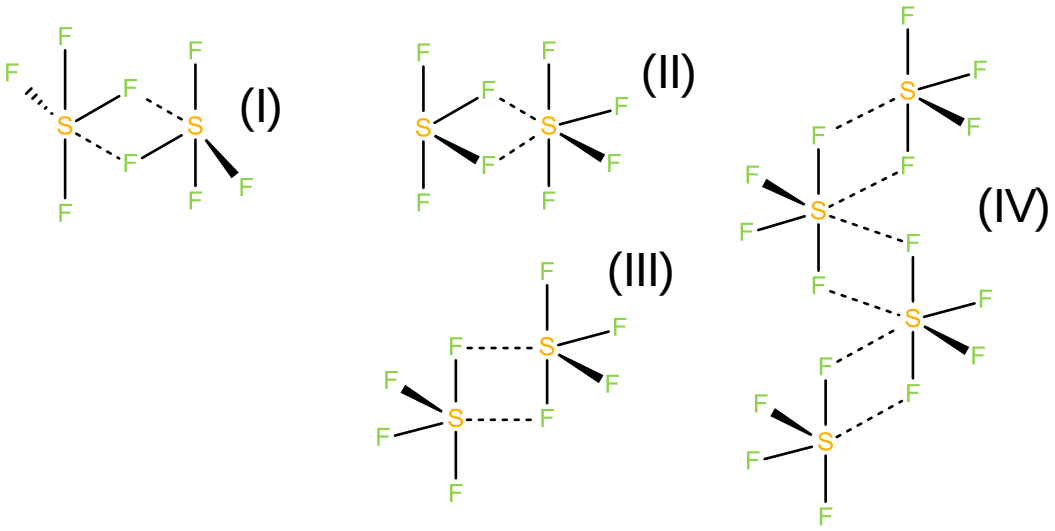

Figure 5.1 Proposed structures of SF_4 redrawn from reference 9.

The solid-state structure of SF_4 has remained elusive considering its low melting point and highly reactive nature. Raman spectroscopic data of SF_4 in the solid state have been interpreted in terms of three different polymorphs.[10] Fluorine-bridged chains were proposed for the solid-state structure of SF_4. Using miniature zone-melting techniques, crystals of SF_4 were grown, but its crystal structure has been reported to be severely disordered and no discernible structure could be determined.[11] In the same study, the crystal structures of SOF_2 and SiF_4 were obtained instead, as unintentional reaction products of SF_4 with moisture and glass, respectively.[11] The crystal structures of SeF_4 and TeF_4 have previously been obtained.[12] Tellurium tetrafluoride exists as TeF_3^+ units bridged by two fluorides,

whereas SeF_4 contains distinct distorted disphenoidal SeF_4 units connected by contacts involving the axial fluorines.

5.2 Results and Discussion

5.2.1 $[HNC_5H_3(CH_3)_2^+]_2[SF_5^-]F^-•4SF_4$

The $[HNC_5H_3(CH_3)_2^+]_2[SF_5^-]F^-•4SF_4$ salt was synthesized by the reaction of 2,6-dimethylpyridine with half an equivalent of water in the presence of a large excess of SF_4 (see Equation 1).

$$6\ SF_4 + H_2O + 2\ N(C_5H_3)(CH_3)_2 \rightarrow [HNC_5H_3(CH_3)_2^+]_2F^-[SF_5^-]•4SF_4 + SOF_2 \quad (1)$$

While mounting crystals of $[HNC_5H_3(CH_3)_2^+]_2[SF_5^-]F^-•SF_4$ (see Chapter 4), which have a lozenge-like morphology, a small number of block-shaped crystals were observed. The majority of these block-shaped crystals were found in the lower portion of the reaction vessel. The crystal structure of the block-shaped crystals was found to be related to that of $[HNC_5H_3(CH_3)_2^+]_2[SF_5^-]F^-•SF_4$, but included layers of uncoordinated SF_4. The use of a very large excess of SF_4, along with cooling to lower temperatures, exclusively yielded thick needles, which easily broke into block-shaped crystals of $[HNC_5H_3(CH_3)_2^+]_2F^-[SF_5^-]•4SF_4$. The $[HNC_5H_3(CH_3)_2^+]_2F^-[SF_5^-]•4SF_4$ salt is stable up to –90 °C, above which the crystals decompose. This compound is the only one in which layers of uncoordinated SF_4 are present.

5.2.1.1 *X-ray crystallography*

Details of data collection parameters and crystallographic information for $[HNC_5H_3(CH_3)_2^+]_2F^-[SF_5^-]\bullet 4SF_4$ are given in Table 5.1. Important bond lengths, angles and contacts for $[HNC_5H_3(CH_3)_2^+]_2F^-[SF_5^-]\bullet 4SF_4$ are listed in Table 5.2.

This salt contains two 2,6-dimethylpyridinium cations that are hydrogen-bonded to one fluoride anion, an SF_5^- anion, and four different SF_4 molecules. (Figure 5.2)

One SF_4 molecule exhibits an S---F^- contact to the fluoride and is located within a layer of the $[HNC_5H_3(CH_3)_2^+]$ cations and the F^- and SF_5^- anions (see Figure 5.3). This S---F^- contact distance (2.487(2) Å) is shorter than the S---F^- contact distance (2.5116(12) Å) in the salt which does not contain an SF_4 layer, *i.e.*, $[HNC_5H_3(CH_3)_2^+]_2[SF_5^-]F^-\bullet SF_4$. A second significantly weaker interaction (2.818(2) Å) between sulfur and a fluorine atom from the SF_5^- anion expands the coordination environment about S(1) to six.

Table 5.1 Crystal Data Collection Parameters and Results of $[HNC_5H_3(CH_3)_2^+]_2[SF_5^-]F^-\bullet 4SF_4$ and SF_4.

Compound	$[HNC_5H_3(CH_3)_2^+]_2[SF_5^-]F^-\bullet 4SF_4$	SF_4
File Code	MG12107	MG12097
Empirical Formula	$C_{14}H_{20}F_{22}N_2S_5$	F_4S
Formula weight, g mol-1	794.62	108.06
Temperature, K	133	100
Wavelength, Å	0.71073 Å	0.71073 Å
Crystal System	Orthorhombic	Orthorhombic
Space Group	$P2_12_12_1$	$P2_12_12_1$
Unit Cell Dimensions	a = 7.4597(10) Å	a = 6.773(4) Å
	b = 18.150(2) Å	b = 6.812(4) Å
	c = 21.863(3) Å	c = 13.122(8) Å
Abs. coeff. μ mm^{-1}	0.54	0.98
Volume	2960.2(7)	605.5(6)
Z	4	8
Density (calculated), g cm^{-1}	1.783	2.371
F(000)	1584	416
Crystal Size, mm^3	0.56 × 0.23 × 0.16	0.17 × 0.15 × 0.14
Reflections Collected	33934	6874
Independent Reflections	6819 [Rint = 0.033]	1387 [Rint = 0.052]
Data/Restraints/Parameters	6819/0/392	1387/0/92
Goodness-of-fit on F^2	1.04	1.18
Refine Diff $\Delta\rho$max e $Å^{-3}$	0.63	0.85
Refine Diff $\Delta\rho$min e $Å^{-3}$	−0.43	−0.67
R_1, $I > 2\sigma(I)$[a]	0.0416	0.0501
$wR_2(F^2)$[a]	0.1166	0.1117

[a] $R_1 = \Sigma||F_o| - |F_c||/\Sigma|F_o|$; $wR_2 = [\Sigma w(F_o^2 - Fc^2)^2/\Sigma w(F_o^4)]^{1/2}$.

Table 5.2 Selected Bond Lengths (Å), Contacts (Å), and Angles (deg.) of $[HNC_5H_3(CH_3)_2^+]2F^-[SF_5^-]\bullet 4SF_4$

Bond Lengths and Contacts, Å			
S1−F1	1.5447(18)	S1B---F9	2.937(2)
S1−F2	1.549(2)	S1B---F4A^{iii}	3.164(3)
S1−F3	1.6503(18)	S1C−F2C	1.502(3)
S1−F4	1.7059(18)	S1C−F1C	1.533(2)
S1---F5	2.487(2)	S1C−F3C	1.604(3)
S1---F7^{i}	2.818(2)	S1C−F4C	1.641(4)
S1A−F1A	1.530(2)	S1C---F4^{iv}	2.867(2)
S1A−F2A	1.543(2)	S1C---F4C^{v}	3.114(4)
S1A−F3A	1.658(2)	S2−F6	1.564(2)
S1A−F4A	1.668(2)	S2−F10	1.664(2)
S1A---F8	2.755(2)	S2−F9	1.719(2)
S1A---F3A^{ii}	3.036(3)	S2−F7	1.730(2)
S1B−F2B	1.500(4)	S2−F8	1.763(2)
S1B−F1B	1.546(3)	N1(H1)---F5	2.554(3)
S1B−F3B	1.619(3)	N2(H2)---F5	2.553(3)
S1B−F4B	1.640(3)		
Bond Angles, deg.			
F1−S1−F2	97.43(11)	F2B−S1B---F9	75.21(14)
F1−S1−F3	87.09(11)	F1B−S1B---F9	172.89(15)
F2−S1−F3	88.27(12)	F3B−S1B---F9	86.07(15)
F1−S1−F4	86.05(10)	F4B−S1B---F9	100.26(13)
F2−S1−F4	87.32(11)	F2B−S1B---F4A^{iii}	168.7(2)
F3−S1−F4	171.31(11)	F1B−S1B---F4A^{iii}	76.38(17)
F1−S1---F5	79.91(9)	F3B−S1B---F4A^{iii}	102.5(2)
F2−S1---F5	176.53(10)	F4B−S1B---F4A^{iii}	79.92(14)
F3−S1---F5	89.36(9)	F9---S1B---F4A^{iii}	107.83(7)
F4−S1---F5	94.69(9)	F2C−S1C−F1C	100.49(18)
F1−S1---F7^{i}	171.55(9)	F2C−S1C−F3C	87.1(2)
F2−S1---F7^{i}	81.81(10)	F1C−S1C−F3C	90.0(2)
F3−S1---F7^{i}	101.29(10)	F2C−S1C−F4C	88.2(2)
F4−S1---F7^{i}	85.50(9)	F1C−S1C−F4C	87.69(19)
F5−S1---F7^{i}	101.15(8)	F3C−S1C−F4C	174.3(3)
F1A−S1A−F2A	99.76(15)	F2C−S1C---F4^{iv}	79.99(13)
F1A−S1A−F3A	87.10(15)	F1C−S1C---F4^{iv}	179.35(14)
F2A−S1A−F3A	87.53(13)	F3C−S1C---F4^{iv}	90.48(14)
F1A−S1A−F4A	87.31(15)	F4C−S1C---F4^{iv}	91.89(14)
F2A−S1A−F4A	87.99(13)	F2C−S1C---F4C^{v}	171.49(17)
F3A−S1A−F4A	172.15(14)	F1C−S1C---F4C^{v}	84.89(15)
F1A−S1A---F8	76.09(11)	F3C−S1C---F4C^{v}	86.32(19)
F2A−S1A---F8	172.92(11)	F4C−S1C---F4C^{v}	98.66(11)

Table 5.2 continued.

F3A−S1A---F8	97.89(10)	F4^{iv}---S1C---F4C^{v}	94.68(8)
F4A−S1A---F8	86.10(10)	F6−S2−F10	86.74(13)
F1A−S1A---F3A^{ii}	168.85(12)	F6−S2−F9	85.13(13)
F2A−S1A---F3A^{ii}	78.66(11)	F10−S2−F9	89.98(13)
F3A−S1A---F3A^{ii}	103.79(8)	F6−S2−F7	85.99(15)
F4A−S1A---F3A^{ii}	81.62(11)	F10−S2−F7	90.35(13)
F8−S1A---F3A^{ii}	104.29(7)	F9−S2−F7	171.08(13)
F2B−S1B−F1B	101.8(2)	F6−S2−F8	83.96(12)
F2B−S1B−F3B	88.5(3)	F10−S2−F8	170.70(13)
F1B−S1B−F3B	87.41(18)	F9−S2−F8	88.89(10)
F2B−S1B−F4B	88.8(2)	F7−S2−F8	89.35(11)
F1B−S1B−F4B	86.03(18)	S2−F8---S1A	125.71(10)
F3B−S1B−F4B	172.2(2)	S2−F9---S1B	134.86(12)

Symmetry codes: (i) x−1, y, z; (ii) x−1/2, −y+1/2, −z+1; (iii) x+1/2, −y+1/2, −z+1; (iv) x+1, y, z; (v) x+1/2, −y+1/2, −z.

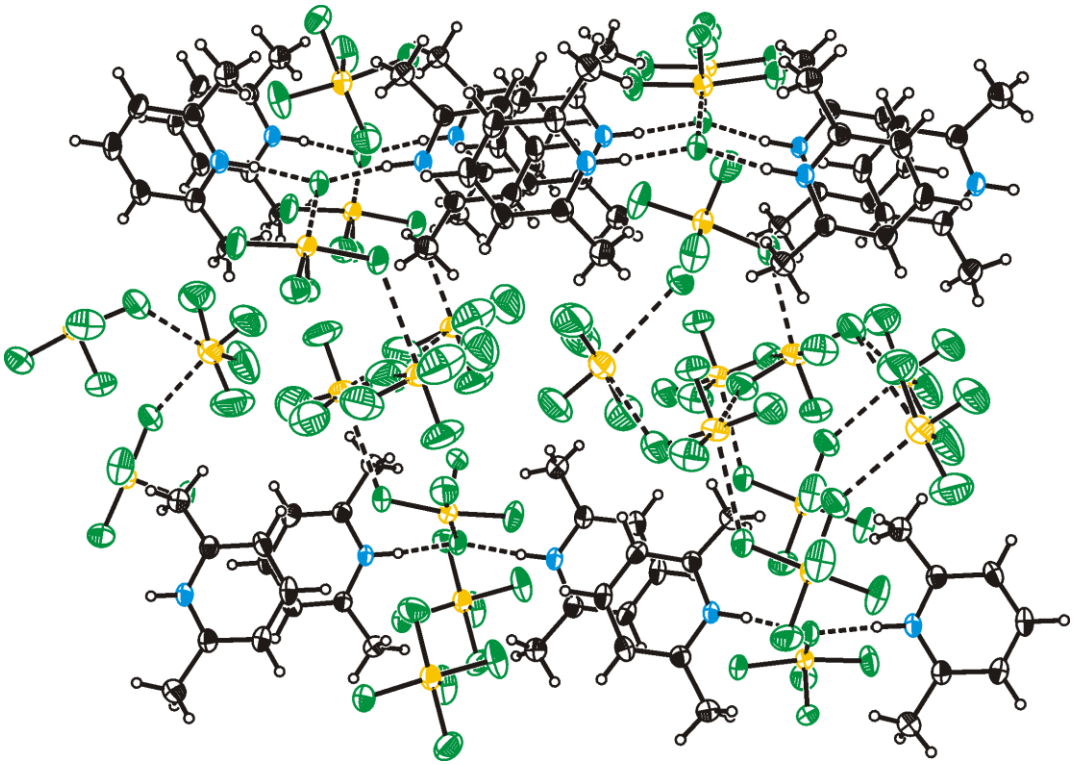

Figure 5.2 Thermal ellipsoid view along the *a*-axis of the packing of $[HNC_5H_3(CH_3)_2^+]_2F^-[SF_5^-]\bullet 4SF_4$. Thermal ellipsoids are set at 50 % probability.

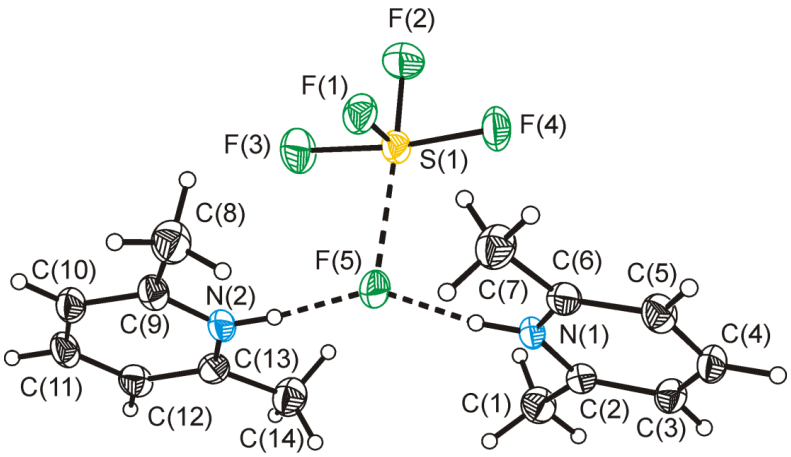

Figure 5.3 Thermal ellipsoid plot of the $[HNC_5H_3(CH_3)_2^+]_2F^-$---$SF_4$ moiety. Thermal ellipsoids are set at 50 % probability.

The 2,6-dimethylpyridinium cations form hydrogen bonds to the fluoride with N(H)---F^- distances of 2.553(3) and 2.554(3) Å, which are slightly longer than the distances in $[HNC_5H_3(CH_3)_2^+]_2[SF_5^-]F^-•SF_4$ (N1(H)---F10 = 2.5396(17) Å and N2(H)---F10 = 2.5308(17) Å).

The second fluoride ion in the structure is sufficiently naked to form the SF_5^- anion (Figure 5.4). Because three of the four equatorial fluorines of this anion form F---S contacts, the anion is locked in one position without disorder. As a consequence of the contacts the anion geometry deviates from an idealized square pyramid.

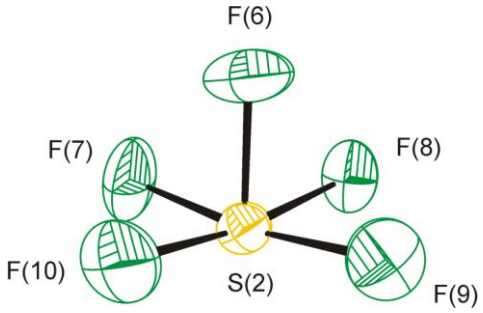

Figure 5.4 Thermal ellipsoid plot of the SF_5^- anion in $[HNC_5H_3(CH_3)_2^+]_2F^-[SF_5^-]•4SF_4$. Thermal ellipsoids are set at 50 % probability.

The axial S−F bond length (1.564(2) Å) is much shorter than the equatorial S−F bond lengths (1.664(2) to 1.763(2) Å). The three equatorial fluorines that have contacts to adjacent SF_4 molecules have significantly longer S−F bonds (1.719(2) to 1.763(2) Å) than the bond to the other equatorial fluorine, which does not form contacts. The average $S-F_{eq}$ bond length is 1.719 Å, which is in excellent agreement with the average equatorial bond length reported for $Rb[SF_5]$.[13] The fluorine of the longest most ionic bond in SF_5^- forms the strongest contact (F(8)---S and is *trans* to the shortest most covalent equatorial bond, i.e., S2−F10 (1.664(2) Å).

Three SF_4 molecules form a layer separating two ionic layers (see S1A-C in Figure 5.5). The SF_4 molecules in the layer show significantly larger thermal ellipsoids on fluorine, than those on the SF_4 coordinated to F^-. The coordination environments about sulfur in all SF_4 molecules include two S---F contacts (Figure 5.5). The S---F contacts of the three SF_4, which compose the layer, are with axial fluorines of other SF_4 molecules (2.867(2) to 3.164(3) Å) and with equatorial fluorines of the SF_5^- anion (2.755(2) and 2.937(2) Å). One of the SF_4 molecules in the layer has contacts only with axial fluorines of other SF_4 molecules. The observation of the layer of "free" SF_4 sparked interest in the solid-state structure of neat SF_4 (*vide infra*).

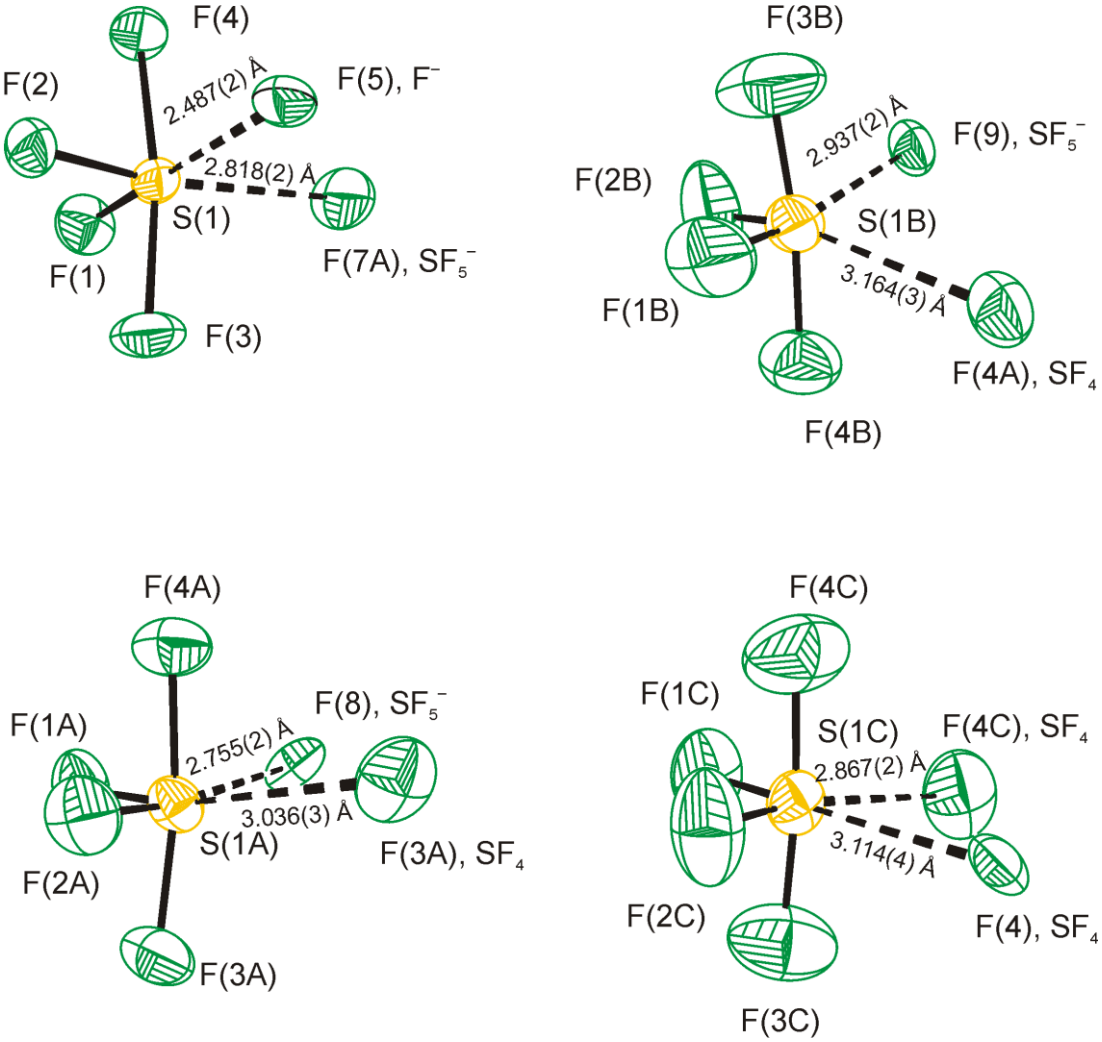

Figure 5.5 Thermal ellipsoid plot of the coordination environment about the SF4 molecules in the X-ray crystal structure of $[HNC_5H_3(CH_3)_2^+]2F^-[SF_5^-]\bullet 4SF_4$; thermal ellipsoids are drawn at the 50% probability level.

5.2.1.2 Raman Spectroscopy

The observed vibrational frequencies and their tentative assignments for $[HNC_5H_3(CH_3)_2^+]_2F^-[SF_5^-]\bullet 4SF_4$ are listed in Table 5.3. The Raman spectrum of solid SF_4 at −135 °C exhibits significant splitting as previously observed.[10] These splittings can be explained by the presence of two crystallographically different SF_4 molecules and/or by vibrational coupling between SF_4 molecules in one unit cell.

The Raman spectrum of $[HNC_5H_3(CH_3)_2^+]_2F^-[SF_5^-]\bullet 4SF_4$ at −100 °C is depicted in Figure 5.6 and contains the characteristic signals associated with the $HNC_5H_3(CH_3)_2^+$ cation and the SF_5^- anion. The latter were assigned based on the vibrational assignments previously reported for the Cs^+, $[Cs(18\text{-crown-}6)_2]^+$, and $[N(CH_3)_4]^+$ salts.[13-15] The Raman spectrum also shows several bands attributable to SF_4. Interestingly, two sets of bands in the equatorial SF_2 stretching region can be distinguished and tentatively assigned to $\nu_s(SF_{2,eq})$ of SF_4 in the layer (880 cm^{-1}), which is close to that of neat SF_4 (896, 880 cm^{-1}), and that of SF_4 coordinated by F^- (863 cm^{-1}). A Raman spectrum of solid $[HNC_5H_3(CH_3)_2^+]_2F^-[SF_5^-]\bullet 4SF_4$ recorded at −85 °C contains a broadened signal at 884 cm^{-1}, which resembles the broad signal observed in liquid SF_4. This observation corroborates the observation of significant thermal motion within the SF_4 layer and suggests the onset of decomposition via release of SF_4.

Table 5.3 Experimental Raman frequencies and Tentative Assignments for $[HNC_5H_3(CH_3)_2^+]_2F^-[SF_5^-]\bullet 4SF_4$.

$[HNC_5H_3(CH_3)_2^+]2F^-[SF_5^-]\bullet 4SF_4$[a]		SF_4 solid		SF_5^- in $CsSF_5$[b]/$[Cs(18\text{-crown-}6)_2]SF_5$[c]	
	Assignment		Assignment		Assignment
3111(6)					
3082(6)	ν(C–H)				
3015(6)					
2981(13)					
2940(66)	$\nu(CH_3)$				
2861(3)					
2757(8)					
1657(10)					
1626(20)	ν(C–C)/ ν(C–N)				
1556(7)					
1439(6)					
1420(9)					
1393(30)	CH_3 deform				
1385(31)	CH_3 deform				
1312(4)					
1293(27)	ν(C–C) / ν(C–N)				
1286sh					
1216(3)					
1174(9)					
1100(16)	$\nu_s(NC_5)$				
1089(4)					
1015(86)					
993(5)					
		904(32)	Overtone or comb. band		
880(63)	SF_4 (in layer), $\nu_s(SF_{2eq})$	888(75) 880(99)	$\nu_s(SF_{2eq})$		
863(32)	$SF_4\cdots F^-$, $\nu_s(SF_{2eq})$				
849sh 844(21)	SF_4 (in layer), $\nu_{as}(SF_{2eq})$	860sh	$\nu_{as}(SF_{2eq})$		
819(19)	$SF_4\cdots F^-$,ν_{as} (SF_{2eq})				
809(19) 803sh	SF_5^-, ν (SF_{ax})			796(37)/785(12)	ν (SF_{ax})
790sh					

Table 5.3 continued.

725(90)	$\delta_{in\text{-}plane}(CCC)$/ $\delta_{in\text{-}plane}(CNC)$				
626(3)	SF_4, $\nu_{as}(SF_{2ax})$	629(7)	$\nu_{as}(SF_{2ax})$		
580(16)[c] 574sh	SF_5^- $\nu_{as}(SF_4)$			590 sh/583(7)	$\nu_{as}(SF_4)$
561(24)	$\delta_{in\text{-}plane}(CCC)$/ $\delta_{in\text{-}plane}(CNC)$				
543sh	$\delta_{in\text{-}plane}(CCC)$/ $\delta_{in\text{-}plane}(NCC)$				
535(88)	SF_4 $\nu_s(SF_{2ax})$	536(92) 532(100)	ν_s SF_{2ax}		
527sh 514sh	SF_4, $\delta_{sc}(SF_{2eq})$ + $\delta_{sc}(SF_{2ax})$ SF_5^- $\nu_s(SF_4)$ in phase	524(54)	$\delta_{sc}(SF_{2eq})$ + $\delta_{sc}(SF_{2ax})$	522(27)/ 512(7)	$\nu_s(SF_4)$ in phase
486(16)	SF_4, $\delta_{rock}(SF_{2eq})$ SF_5^- $\nu_s(SF_4)$ out of phase[e]	515(72) 508(66)	$\delta_{rock}(SF_{2eq})$	435(100)/469(100)	SF_5^- $\nu_s(SF_4)$ out of phase[e]
459(8)	SF_4, $\tau(SF_2)$	458(31)	$\tau(SF_2)$		
440 sh	SF_5^- $\nu_s(SF_4)$ umbrella			469 sh/435(17)	$\delta_s(SF_4)$ umbrella
428(13)	$\delta_{out\text{-}of\text{-}plane}(CCH)$				
403(13)	SF_5^-, $\delta(F_{ax}SF_4)$ [e]			435(100)/420(12)	$\delta(F_{ax}SF_4)$ [e]
332(6)	SF_5^-, $\delta_s(SF_4)$ in plane			342(16)/315(7)	$\delta_s(SF_4)$ in plane
297(23)[d]	$\rho_r(CH_3)$				
244sh 238sh	SF_4, $\delta_{sc}(SF_{2eq})$ – $\delta_{sc}(SF_{2ax})$ SF_5^-, $\delta_{as}(SF_4)$ out of plane	243(15)	$\delta_{sc}(SF_{2eq})$ – $\delta_{sc}(SF_{2ax})$	269 sh/267(20)	$\delta_{as}(SF_4)$ out of plane
229(28) 222(27)	SF_5^-, $\delta_{as}(SF_4)$ in plane $\rho_r(CH_3)$			241(12)/242(13)	$\delta_{as}(SF_4)$ in plane
153(2) 126(100)	Lattice modes				

[a] Signals from the FEP sample tube were observed at 733(21), 387(4) 381(7), and 293sh cm^{-1}.
[b] From K.O. Christe, E.C. Curtis, C. J. Schack, and D. Pilipovich, *Inorg. Chem.* **1972**, *11*, 1679-1682.
[c] From M. Clark, C. J. Kellen-Yuen, K. D. Robinson, H. Zhang, Z.-Y. Yang, K. V. Madappat, J. W. Fuller, J. L. Atwood, J. S. Thrasher, *Eur. J. Solid State Inorg. Chem.* **1992**, *29*, 809-833.
[d] Overlap with the FEP signal.
[e] Assignment could be reversed.

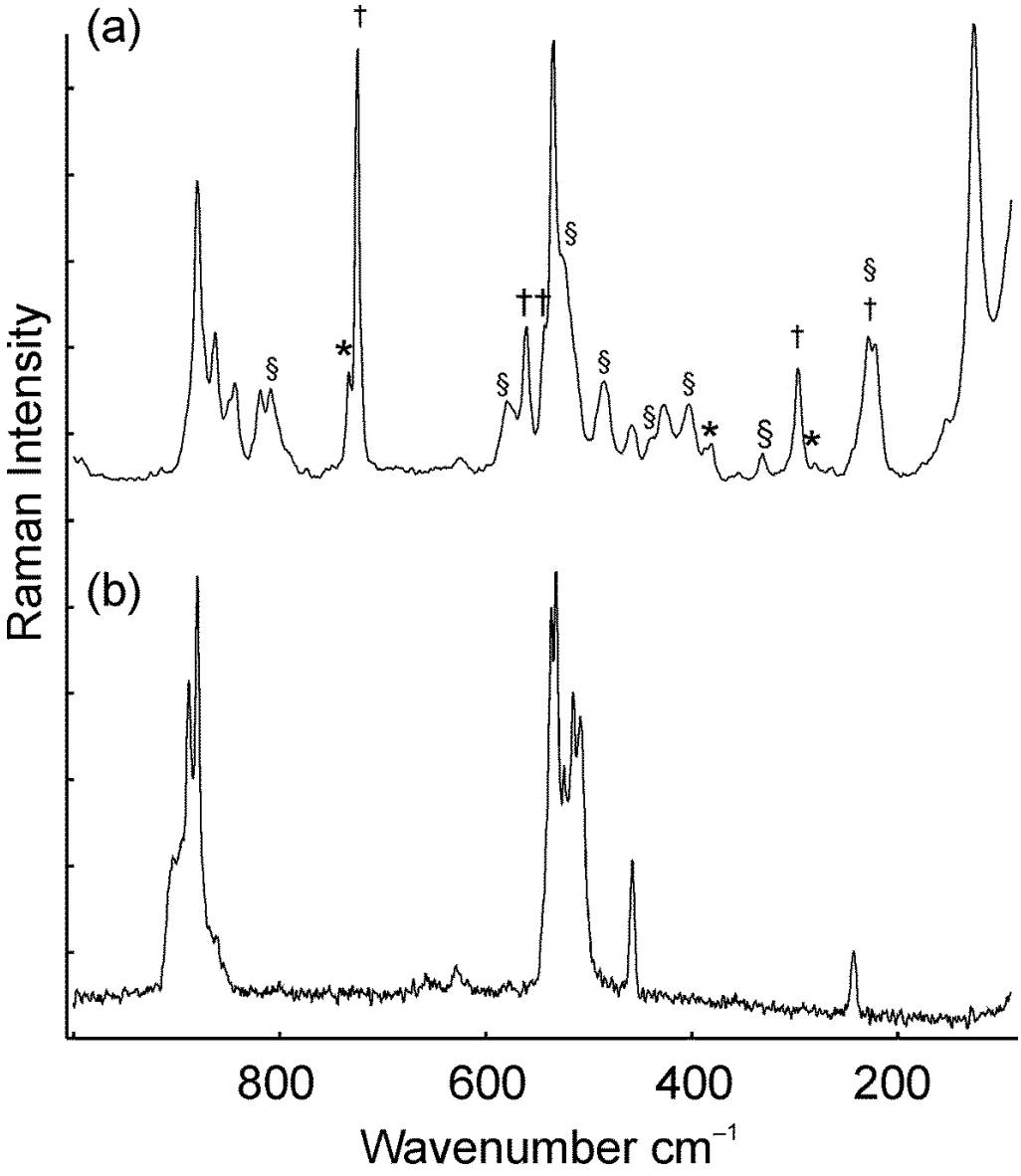

Figure 5.6 Raman spectra of (a) $[HNC_5H_3(CH_3)_2^+]_2F^-[SF_5^-]\bullet 4SF_4$ in FEP tubing and (b) of solid SF_4 in a Pyrex glass 5-mm NMR tube recorded at –100 °C and –135 °C, respectively, using 1064-nm excitation. Asterisks (*) denote signals arising from the FEP sample tube. Bands attributed to the 2,6-dimethylpyridinium cation and to the SF_5^- anion are denoted by (†) and (§), respectively.

5.2.2 Solid State Structure of SF_4

Raman spectroscopy has been reported on solid SF_4 in the past. Using matrix-isolation techniques, three different phases were observed.[10] It may be possible to obtain different "phases" using low temperature matrix-isolation and annealing

techniques, yet we observed no indications of different phases in bulk samples. The Raman spectrum at −135 °C and 1 cm^{-1} resolution exhibited splitting and shoulders which have been previously reported and assigned by Christe *et al.*[15]

Slow cooling of neat SF_4 results in the formation of a clear solid mass, which contains striations that suggest a crystalline phase. The suggested unit cell of crystals grown from neat SF_4 was tetragonal P (6.81 × 6.81 × 13.17 Å), which is different than the previously reported unit cell; cubic F: (6.761(5) Å).[11] However attempts at solving the structure in this unit cell failed. Since the use of a solvent to grow crystals could provide an ordered structure, SF_4 was crystallized from CF_2Cl_2. Ultimately the same tetragonal unit cell was obtained for crystals grown from CF_2Cl_2. The correct structural solution, however, showed that SF_4 crystallized in the orthorhombic system with twinning and two crystallographically unique ordered SF_4 molecules in the asymmetric unit (see Figure 5.7). Details of data collection parameters and crystallographic information for SF_4 are given in Table 5.1.

Important bond lengths, angles and contacts for SF_4 are listed in Table 5.4.

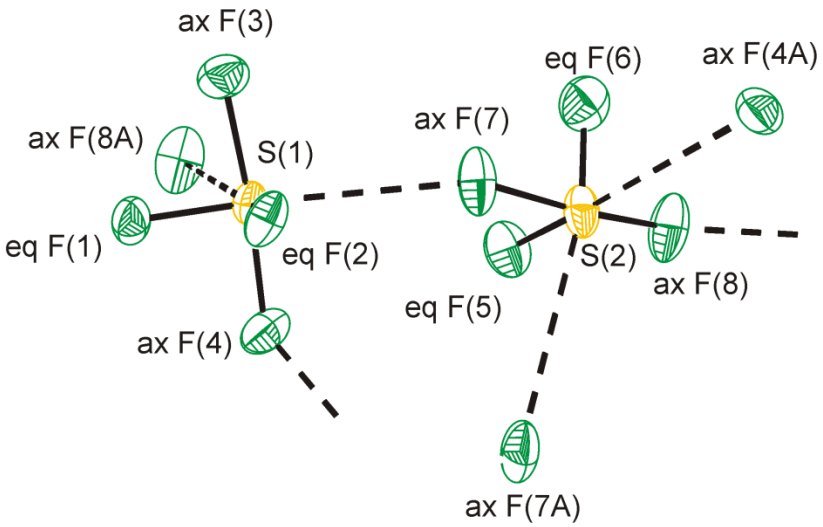

Figure 5.7 Thermal Ellipsoid Plot of the asymmetric unit of SF_4. Thermal Ellipsoids are set to 50% probability.

Table 5.4 Bond Lengths (Å), Contacts (Å), and Angles (deg.) of SF_4.

Bond Lengths and Contacts, Å			
S1−F1	1.527(4)	S2−F6	1.474(6)
S1−F2	1.535(4)	S2−F5	1.553(4)
S1−F3	1.647(5)	S2−F8	1.635(4)
S1−F4	1.676(5)	S2−F7	1.671(5)
S1---F7	2.954(5)	S2---F4^{ii}	2.975(4)
S1---F8^{i}	3.031(5)	S2---F7^{iii}	3.261(6)
Bond Angles, deg.			
F1−S1−F2	101.0(2)	F6−S2−F8	86.9(3)
F1−S1−F3	88.3(3)	F5−S2−F8	88.6(3)
F2−S1−F3	87.7(3)	F6−S2−F7	86.6(3)
F1−S1−F4	87.3(3)	F5−S2−F7	87.1(3)
F2−S1−F4	87.3(2)	F8−S2−F7	171.6(3)
F3−S1−F4	172.6(3)	F6−S2---F4^{ii}	73.8(2)
F1−S1---F7	170.4(2)	F5−S2---F4^{ii}	170.1(3)
F2−S1---F7	69.57(18)	F8−S2---F4^{ii}	83.6(2)
F3−S1---F7	92.9(2)	F7−S2---F4^{ii}	99.8(2)
F4−S1---F7	90.5(2)	F6−S2---F7^{iii}	167.3(2)
F1−S1---F8^{i}	68.4(2)	F5−S2---F7^{iii}	71.4(2)
F2−S1---F8^{i}	167.45(19)	F8−S2---F7^{iii}	101.5(3)
F3−S1---F8^{i}	85.4(2)	F7−S2---F7^{iii}	84.01(18)
F4−S1---F8^{i}	98.5(2)	F4^{ii}---S2−F7^{iii}	116.20(13)
F7−S1---F8^{i}	121.21(15)	S2−F7---S1	135.9(2)
F6−S2−F5	99.6(3)		

Symmetry codes: (i) −x+5/2, −y, z+1/2; (ii) x−1/2, −y+1/2, −z+2; (iii) x+1/2, −y+1/2, −z+2.

The structure can best be described as a network with weak intermolecular S---F contacts. The shortest S---F contact found in the structure is 2.954(5) Å. These contacts are exclusively formed by the more ionic axial fluorines to the sulfur atoms of adjacent SF_4 molecules. The geometry of the SF_4 molecules agree well with the seesaw geometry found for the gas phase with two longer, more ionic axial S–F bonds and two shorter equatorial S–F bonds. None of the equatorial fluorines form significant intermolecular contacts. This agrees very well with the more covalent nature of the S−F_{eq} bonds. Because of the location of the lone pair, the F---S---F

angles (121.2(2)° and 116.2(1)°) are significantly larger than the F_{eq}---S---F_{eq} angles (101.0(2)° and 99.6(3)°). The S2−F6 bond (1.474(6) Å) is significantly shorter than the subsequently shortest S−F bond (1.527(4) Å). This can be explained by an unfavourable steric interaction between F6 and F8, which has a distance of 2.774(1) Å, which is within the sum of the van-der-Waals radii (2.94 Å).

The S---F contacts found in solid SF_4 (2.945(4) to 3.261(6) Å) are significantly longer than the S---F^- contact (2.487(2) Å) of the fluoride bound SF_4 found in the $[HNC_5H_3(CH_3)_2^+]_2F^-[SF_5^-]•4SF_4$ structure, but are comparable to the S---$F_{eq}SF_3$ contacts found in the layer (2.867(2) to 3.164(3) Å). The S−F_{eq} of solid SF_4 bond lengths are not significantly different than the S−F_{eq} bond lengths in the layer.

The structure is very different from that of TeF_4, which forms infinite chains composed of TeF_3^+ units bridged by fluorides (Figure 5.8).

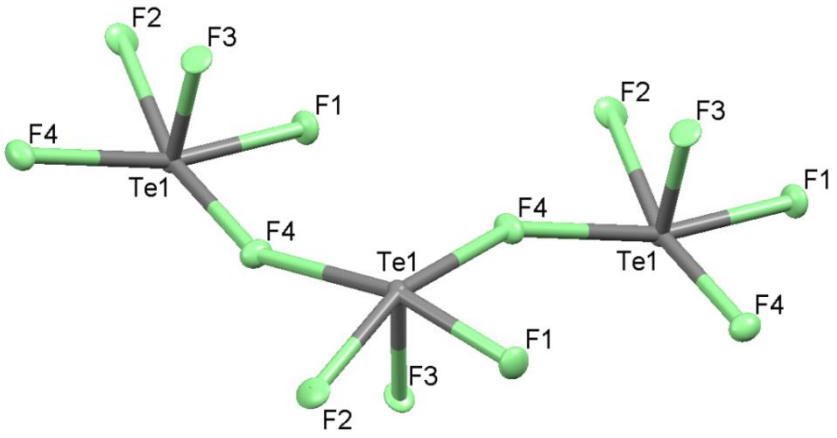

Figure 5.8 Thermal Ellipsoid Plot of the TeF_4 chain. Thermal ellipsoids are set at 50% probability. (Data from reference 12)

The structure is similar to that of SeF_4, except that SeF_4 only contains one crystallographically unique molecule and each of the axial fluorines form a contact

with an adjacent selenium atom (Figure 5.9). In SF_4, on the other hand, one of the axial fluorines (F3) has no significant contacts.

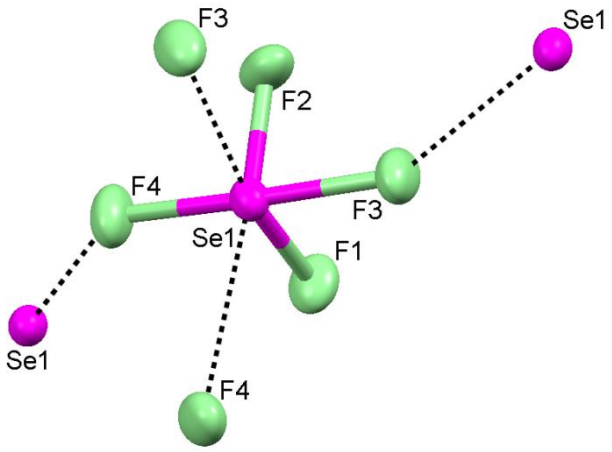

Figure 5.9 Thermal ellipsoid plot of SeF_4, showing contacts to adjacent SeF_4 molecules. Thermal ellipsoids are set to 50% probability. (Data from reference 12)

5.3 Summary and Conclusion

The $[HNC_5H_3(CH_3)_2^+]_2F^-[SF_5^-] \bullet 4SF_4$ salt was synthesized and studied at low temperatures. The structure was found to contain layers of "free" SF_4, and was characterized by X-ray crystallography and Raman spectroscopy. For the first time, the structure of SF_4 in the solid state has been elucidated. The structure can best be described as a network with weak intermolecular S---F contacts formed exclusively with the axial fluorines that exhibit more ionic character. The structure is different from TeF_4 and previous predictions of chain-type or dimeric structures, which contains two contacts between each SF_4 molecule.[9] A similar structural motif is found in the novel $[HNC_5H_3(CH_3)_2^+]_2F^-[SF_5^-] \bullet 4SF_4$ salt which contain SF_4 layers. The latter salt represents the first compound that contains a range of interaction

motifs between SF_4 and F, i.e., $F_4S{-}F^-$ (1.564(2) to 1.763(2) Å), $F_4S\cdots F^-$ (2.587(2) Å), $F_4S\cdots FSF_4^-$(1.755(2) to 2.937(2) Å), $F_4S\cdots FSF_3$ (2.867(2) to 3.164(2) Å).

References

(1) Fischer, J.; Jaenckner, W. *Angew. Chem. Int. Ed. Engl.* **1929**, *42*, 810-811.

(2) Oberhammer, H.; Shlykov, S. A. *Dalton Trans.* **2010**, *39*, 2838-2841.

(3) Tolles, W. M.; Gwinn, W. D. *J. Chem. Phys.* **1962**, *36*, 1119-1121.

(4) Dodd, R. E.; Woodward, L. A.; Roberts, H. L. *Trans. Faraday Soc.* **1956**, *52*, 1052-1061.

(5) Spring, C. A.; True, N. S. *J. Am. Chem. Soc.* **1983**, *105*, 7231-7236.

(6) Ewing, V.; Sutton, L. *Trans. Faraday Soc.* **1963**, *59*, 1241-1247.

(7) Christe, K. O.; Zhang, X.; Sheehy, J. A.; Bau, R. *J. Am. Chem. Soc.* **2001**, *123*, 6338-6348.

(8) Pavone, M.; Barone, V.; Ciofini, I.; Adamo, C. *J. Chem. Phys.* **2004**, *120*, 9167-9174.

(9) Gombler, W.; Seel, F. *J. Fluorine Chem.* **1974**, *4*, 333-339.

(10) Berney, C. V. *J. Mol. Struc.* **1972**, *12*, 87-97.

(11) Mootz, D.; Korte, L. *Z. Naturforsch., B: Anorg. Chem., Org. Chem.* **1984**, *39B*, 1295-1299.

(12) Kniep, R.; Korte, L.; Kryschi, R.; Poll, W. *Angew. Chem. Int. Ed. Engl.* **1984**, *23*, 388-389.

(13) Bittner, J.; Fuchs, J.; Seppelt, K. *Z. Anorg. Allg. Chem.* **1988**, *557*, 182-190.

(14) Drullinger, L. F.; Griffths, J. E. *Spectrochim. Acta A* **1971**, *27*, 1793-1799.

(15) Christe, K. O.; Curtis, E. C.; Schack, C. J.; Pilipovich, D. *Inorg. Chem.* **1972**, *11*, 1679-1682.

6 Sulfur Tetrafluoride Oxygen-Base Adducts

6.1 Introduction

Recently, Lewis acid-base adduct formation was conclusively shown for SF_4 and a number of nitrogen bases, *i.e.*, pyridine,[1] 4-methylpyridine,[1] 2,6-dimethylpyridine,[1] 4-dimethylaminopyridine,[1] and triethylamine.[2] Based on the ^{19}F chemical shift of SF_4 in THF (OC_4H_6) and ethyl acetate, Muetterties suggested that SF_4 does not form adducts with these two oxygen bases.[3] Azeem, on the other hand, reported that at low temperatures the changes in $\delta(^{19}F)$ and the decrease in ^2J ($^{19}F-^{19}F$) coupling of SF_4 in THF and Et_2O solvents suggest the formation of $SF_4 \bullet OC_4H_6$ and $SF_4 \bullet O(C_2H_5)_2$ adducts.[4] Two new bands in the infrared spectrum of matrix-isolated SF_4 with acetone were also interpreted in terms of the formation of a 1:1 adduct.[5] No conclusive information, however, is available about the Lewis acid-base interactions between SF_4 and oxygen bases.

The heavier chalcogen analogue, TeF_4, which is significantly more Lewis acidic than SF_4, reacts with various cyclic and acyclic ethers to form the adducts $TeF_4 \bullet$1,4-dioxane,[6] $TeF_4 \bullet (1,2\text{-dimethoxyethane})_2$,[6] $TeF_4 \bullet Et_2O$,[6] and $TeF_4 \bullet (THF)_2$,[7] which have been structurally characterized by X-ray crystallography.

6.2 Results and Discussion

6.2.1 Synthesis and Properties

The reaction of SF_4 with a series of oxygen-bases was studied by low-temperature Raman spectroscopy and X-ray crystallography. The three oxygen-bases

which formed isolable adducts with SF_4 were a cyclic ether (THF), a diether (1,2-dimethoxyethane), and a cyclic ketone (cyclopentanone) (see Figure 6.1).

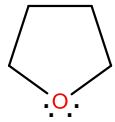

tetrahydrofuran
(OC_4H_8)

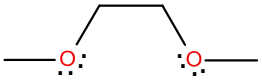

1,2-dimethoxyethane
[$(CH_3OCH_2)_2$]

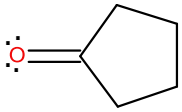

cyclopentanone
($O{=}C_5H_8$)

Figure 6.1 Structures of the oxygen-bases that form Lewis acid-base adducts with SF_4.

Unlike the nitrogen-base adducts, mixtures of SF_4 with oxygen-bases do not appear to be sensitive to the presence of traces of HF and no solvolysis products analogous to those described in Chapter 4 were observed. The SF_4•*O*-base adducts dissociate back into the Lewis acids and bases when warmed above −60 °C or placed under reduced pressure. Mixtures of SF_4 and THF in various ratios form clear colourless liquids, which have lower vapour pressures than neat SF_4 or neat THF at temperatures between −60 to −90 °C. A 1:1 mixture of SF_4 and THF freezes at −99 °C, forming a clear colourless crystalline solid whereas a 1:2 mixture of SF_4 to THF freezes at a lower temperature of −106 °C. As shown by Raman spectroscopy and X-ray crystallography, two distinct adducts were obtained from the two reagent ratios (see Equation 6.1).

$$SF_4 + nOC_4H_8 \rightleftharpoons SF_4{\bullet}(OC_4H_8)_n \quad (\text{where } n = 1, 2) \qquad (6.1)$$

A mixture of 1,2-dimethoxyethane in excess SF_4 was placed under dynamic vacuum at −90 °C for several hours. Mass balance measurements indicated that the mixture obtained after the removal of excess SF_4, corresponded to an approximate 1:1 molar ratio of SF_4 to 1,2-dimethoxyethane. This resulting mixture froze at −105 °C to form a clear colourless crystalline solid which was characterized by Raman spectroscopy and X-ray crystallography as the SF_4•$(CH_3OCH_2)_2$ adduct. (Equation 6.2) It remains solid at −83 °C, but with vigorous agitation will revert back to the liquid state.

$$SF_4 + (CH_3OCH_2)_2 \rightleftharpoons SF_4\bullet(CH_3OCH_2)_2 \qquad (6.2)$$

Cyclopentanone is miscible with an equivalent amount of SF_4 at −50 °C. It remains liquid until approximately −100 °C, when it starts to crystallize into a solid mass, which melts at −63 °C (see Equation 6.3). A crystal suitable for X-ray crystallography was isolated from the solid mass and was shown to contain a 1:2 molar ratio of SF_4 vs. cyclopentanone. The nature of the solid was also confirmed by Raman spectroscopy. No evidence of fluorination of the carbonyl was observed in the Raman spectrum under these conditions.

$$SF_4 + 2\ O{=}C_5H_8 \rightleftharpoons SF_4\bullet(O{=}C_5H_8)_2 \qquad (6.3)$$

The reaction of SF_4 with three other oxygen-bases was studied: diethyl ether, acetylacetone, and 4-methylcyclohexanone (Figure 6.2).

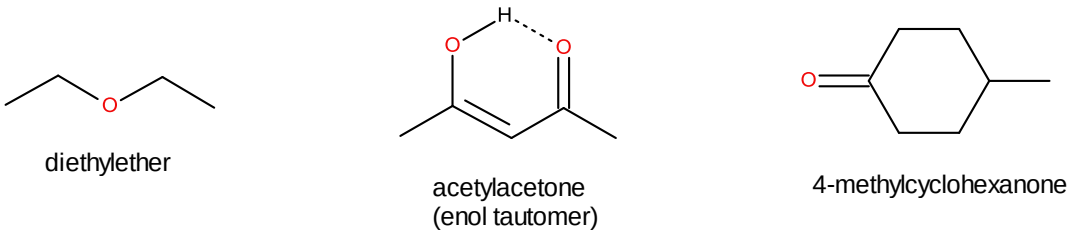

Figure 6.2 Structure of oxygen-bases that were studied and for which no SF_4 adducts could be isolated.

The melting point of a 1:1 mixture of SF_4 and Et_2O is approximately −145 °C, much lower than the melting point of Et_2O (−116 °C) or of SF_4 (−121.5 °C) and attempts at growing single crystals suitable for X-ray crystallography were unsuccessful. The formation of the proposed SF_4•OEt_2 adduct[4] could not be confirmed.

Large, plate-like crystals formed when a homogenous mixture of excess SF_4 with acetylacetone were cooled from −50 °C to −85 °C. A Raman spectrum at −97 °C showed signals attributable to acetylacetone and neat SF_4. Furthermore, X-ray crystallography of the crystals gave the structure of the enol tautomer of acetylacetone. The Lewis basicity of the enol tautomer is much lower than that of a ketone since the carbonyl oxygen forms already a hydrogen bond to the hydroxyl group, which explains the lack of evidence for Lewis-acid-base interactions with SF_4.

A 1:1 homogeneous mixture of SF_4 with 4-methylcyclohexanone had a very low freezing point of approximately −130 °C. Slow partial removal of SF_4 at −80 °C led to the formation of plate like crystals. Determination of the structure by X-ray crystallography gave 4-methylcyclohexanone without SF_4. Despite the unsuccessful attempts of isolation of SF_4 adducts with diethyl ether, acetylacetone, and 4-methylcyclohexanone, the presence of Lewis acid-base interactions between SF_4 and

these oxygen-bases cannot be excluded, but the expected lability and low dissociation temperatures of the adducts renders the isolation of any adducts difficult.

6.2.2 Crystal Structure of $SF_4•OC_4H_6$ and $SF_4•(OC_4H_6)_2$

Details of data collection parameters and crystallographic information for $SF_4•OC_4H_6$ and $SF_4•(OC_4H_6)_2$ are given in Table 6.1. Important bond lengths, angles and contacts for $SF_4•OC_4H_6$ and $SF_4•(OC_4H_6)_2$ are given in Table 6.2 and Table 6.3, respectively.

Table 6.1 Crystal Data Collection Parameters and Results of $SF_4•OC_4H_8$, $SF_4•(OC_4H_8)_2$, $SF_4•(CH_3OCH_2)_2$, and $SF_4•O=C_5H_8$.

Compound	$SF_4•OC_4H_8$	$SF_4•(OC_4H_8)_2$	$SF_4•(CH_3OCH_2)_2$	$SF_4•(O=C_5H_8)_2$
File Code	MG12088	MG13029	MG13024	MG13026
Empirical Formula	$C_4H_8F_4OS$	$C_8H_{16}F_4O_2S$	$C_4H_{10}F_4O_2S$	$C_{10}H_{16}F_4O_2S$
Formula weight, g mol^{-1}	180.16	252.27	198.18	276.29
Temperature, K	133	123	128	123
Wavelength, Å	0.71073	0.71073	0.71073	0.71073
Crystal System	Monoclinic	Triclinic	Orthorhombic	Monoclinic
Space Group	$P2_1/n$	$P\bar{1}$	$Pbcm$	$P2_1/n$
Unit Cell	a = 11.225(4) Å b = 10.798(4) Å c = 12.435(4) Å β = 97.074(4)°	a = 11.307 (2) Å b = 13.664 (4) Å c = 17.149 (3) Å α = 107.28 (4)° β = 98.74 (3)° γ = 107.83 (3)°	a = 4.6402(12) Å b = 13.168(3) Å c = 13.503(3) Å	a = 8.9081(16) Å b = 16.721(3) Å c = 9.4878(17) Å β = 116.320(2)°
Volume, $Å^3$	1495.7(8)	2320.9(9)	825.1(4)	1266.7(4)
Z	8	8	4	4
μ (mm^{-1})	0.44	0.31	0.42	0.29
Density (calc.), g cm^{-1}	1.600	1.444	1.595	1.449
F(000)	736	1056	408	576
Crystal Size, mm^3	0.50 × 0.31 × 0.15	0.22 × 0.19 × 0.10	0.67 × 0.20 × 015	0.27 × 0.16 × 0.12
Reflections Collected	16903	21104	8490	14456
Independent Reflections	3481	10599	991	2906
Data/Restraints/ Parameters	3481/0/182	10599/0/541	991/0/56	2906/0/154
Goodness-of-fit on F^2	1.05	0.93	1.13	1.00
$\Delta\rho_{max}$ (e $Å^{-3}$)	0.75	0.36	0.30	0.30
$\Delta\rho_{min}$ (e $Å^{-3}$)	−0.74	−0.28	−0.32	−0.30
R_1, $I > 2\sigma(I)$ [a]	0.0473	0.057	0.020	0.034
wR_2 (F^2) [a]	0.1193	0.133	0.058	0.085

[a] $R_1 = \Sigma||F_o| - |F_c||/\Sigma|F_o|$; $wR_2 = [\Sigma w(F_o^2 - Fc^2)^2/\Sigma w(F_o^4)]^{1/2}$.

Table 6.2 Selected Bond Lengths (Å), Contacts (Å), and Angles (°) of $SF_4 \bullet OC_4H_6$.

Bond Lengths and Contacts, Å					
S1−F2	1.5344(17)	S2−F6	1.5465(17)	S1---O6	2.7766(17)
S1−F1	1.5448(16)	S2−F5	1.5468(16)	S1---O1	2.8022(19)
S1−F4	1.6430(17)	S2−F8	1.6503(19)	S2---O6	2.7892(18)
S1−F3	1.6610(18)	S2−F7	1.6557(19)	S2---O1	2.793(2)
Bond Angles, deg.					
F2−S1−F1	98.25(10)	F6−S2−F5	98.46(10)	C5−O1−C2	108.37(18)
F2−S1−F4	88.15(11)	F6−S2−F8	87.18(10)	C5−O1−S2	116.03(18)
F1−S1−F4	87.93(10)	F5−S2−F8	87.28(10)	C2−O1---S2	118.26(15)
F2−S1−F3	88.09(11)	F6−S2−F7	87.28(11)	C5−O1−S1	110.57(17)
F1−S1−F3	87.68(10)	F5−S2−F7	87.33(10)	C2−O1−S1	123.64(14)
F4−S1−F3	173.77(11)	F8−S2−F7	171.62(11)	S2---O1---S1	77.49(5)
F2−S1−O6	79.70(8)	F6−S2−O6	79.21(8)	S1---O6---S2	77.97(4)
F1−S1−O6	175.99(8)	F5−S2−O6	176.75(8)		
F4−S1−O6	88.56(7)	F8−S2−O6	90.32(8)		
F3−S1−O6	95.66(8)	F7−S2−O6	94.81(8)		
F2−S1−O1	176.04(9)	F6−S2−O1	178.47(8)		
F1−S1−O1	79.72(8)	F5−S2−O1	80.26(9)		
F4−S1−O1	88.38(8)	F8−S2−O1	91.92(8)		
F3−S1−O1	95.20(8)	F7−S2−O1	93.49(8)		
O6---S1---O1	102.12(6)	O6---S2---O1	102.03(5)		

Table 6.3 Selected Bond Lengths (Å), Contacts (Å), and Angles (°) of $SF_4•(OC_4H_6)_2$.

Bond Lengths and Contacts, Å			
S1−F1	1.5275(19)	S2−F6	1.5341(18)
S1−F2	1.5350(19)	S2−F7	1.5454(18)
S1−F3	1.649(2)	S2−F5	1.643(2)
S1−F4	1.658(2)	S2−F8	1.653(2)
S1---O2	2.687(2)	S2---O4	2.678(2)
S1---O1	2.701(2)	S2---O3	2.737(2)
S3−F11	1.5316(19)	S4−F14	1.5352(19)
S3−F10	1.5438(19)	S4−F13	1.5457(18)
S3−F12	1.641(2)	S4−F15	1.626(2)
S3−F9	1.641(2)	S4−F16	1.641(2)
S3---O6	2.662(2)	S4---O7	2.703(2)
S3---O5	2.792(2)	S4---O8	2.731(2)
Bond Angles, deg.			
F1−S1−F2	96.68(11)	F6−S2−F7	96.50(10)
F1−S1−F3	87.14(12)	F6−S2−F5	86.20(11)
F2−S1−F3	88.07(12)	F7−S2−F5	87.60(11)
F1−S1−F4	87.42(12)	F6−S2−F8	87.93(11)
F2−S1−F4	86.53(11)	F7−S2−F8	86.45(11)
F3−S1−F4	171.84(12)	F5−S2−F8	171.12(11)
F1−S1---O2	171.09(9)	F6−S2---O4	174.42(9)
F2−S1---O2	76.05(9)	F7−S2---O4	78.00(9)
F3−S1---O2	97.63(11)	F5−S2---O4	94.41(10)
F4−S1---O2	87.00(10)	F8−S2---O4	90.79(10)
F1−S1---O1	76.21(9)	F6−S2---O3	78.17(8)
F2−S1---O1	170.96(9)	F7−S2---O3	173.03(9)
F3−S1---O1	86.03(10)	F5−S2---O3	96.45(10)
F4−S1---O1	98.56(10)	F8−S2---O3	88.85(10)
O2---S1---O1	111.52(7)	O4---S2---O3	107.25(7)
F11−S3−F10	96.73(11)	F14−S4−F13	97.07(10)
F11−S3−F12	86.29(13)	F14−S4−F15	86.99(13)
F10−S3−F12	87.80(12)	F13−S4−F15	88.35(12)
F11−S3−F9	88.37(12)	F14−S4−F16	88.42(12)
F10−S3−F9	86.94(11)	F13−S4−F16	86.48(11)
F12−S3−F9	172.02(11)	F15−S4−F16	172.63(12)
F11−S3---O6	171.15(11)	F14−S4---O7	74.95(9)
F10−S3---O6	75.96(9)	F13−S4---O7	171.42(9)
F12−S3---O6	98.25(11)	F15−S4---O7	94.29(10)
F9−S3---O6	86.28(10)	F16−S4---O7	90.09(10)
F11−S3---O5	76.16(9)	F14−S4---O8	171.02(9)
F10−S3---O5	168.69(10)	F13−S4---O8	75.35(9)
F12−S3---O5	100.33(10)	F15−S4---O8	87.95(10)
F9−S3---O5	84.11(9)	F16−S4---O8	95.82(10)
O6---S3---O5	110.24(7)	O7---S4---O8	112.86(7)

The SF_4•OC_4H_6 adduct crystallizes in the monoclinic space group $P2_1/n$, with two SF_4 and two THF molecules in the asymmetric unit. The structure consists of $(SF_4$•$OC_4H_6)_2$ dimers containing two SF_4 molecules bridged by the oxygen atoms of two THF molecules. (Figure 6.3)

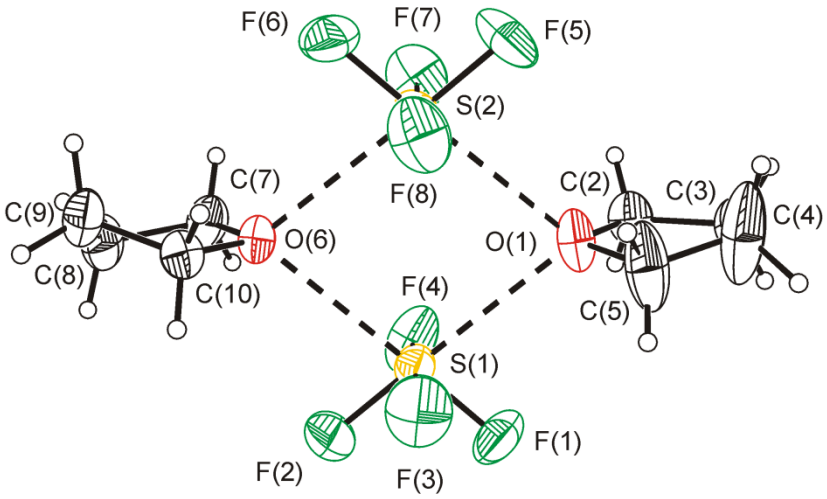

Figure 6.3 Thermal ellipsoid plot of the $(SF_4$•$OC_4H_6)_2$ dimer; thermal ellipsoids are set at 50% probability.

Each sulfur atom has two S---O contacts ranging from 2.777(2) to 2.802(2) Å. The two crystallographically different SF_4 molecules have similar bond lengths and angles. The equatorial S−F bonds range from 1.5344(17) to 1.5468(16) Å, which are significantly shorter than the axial bond lengths, ranging from 1.6430(17) to 1.6610(18) Å. The O---S---O angles are 102.12(6)° and 102.03(5)°, which is significantly higher than 90° as a result of the lone pairs on the sulfur atoms. The S---O---S angles around the oxygen atoms (S2---O1---S1: 77.49 (5) ° and S1---O6---S2: 77.97(4) °) are much smaller than the coordination angles around the sulfur atoms. Along the *a*-axis, the THF rings are stacked, rotated by 180° with respect to the adjacent rings. The thermal ellipsoids of the carbons on one THF molecule are

elongated, reflecting a high degree of thermal motion, i.e., puckering of the THF ring, which is a common occurrence with THF.

The $SF_4•(OC_4H_6)_2$ adduct crystallizes in the triclinic space group $P\bar{1}$. The asymmetric unit contains 4 molecules of SF_4 and 8 molecules of THF. In the structure, two THF molecules coordinate to one sulfur atom of each SF_4 molecule, and the oxygen atoms are essentially in the same plane as the equatorial fluorines of SF_4 (see Figure 6.4). The structure contains a large range of S---O contacts and O---S---O angles. The equatorial S−F have lengths between 1.5275(19) and 1.5457(18) Å, which are significantly shorter than the axial bonds (1.626(2) to 1.658(2) Å). The S---O contact distances lie between 2.662(2) and 2.792(2) Å, which is a larger S---O range of distances than found in the $SF_4•OC_4H_6$ adduct (2.777(2) to 2.802(2) Å). The O---S---O angles range from 107.25(7) to 112.86(7) Å, which are significantly larger than the O---S---O angles in the $SF_4•OC_4H_6$ adduct (102.12(6)° and 102.03(5)°).

The coordination of THF to sulfur is very different from that of *N*-bases to SF_4. For example, for the $SF_4•NC_5H_5$ adduct, only one pyridine coordinates SF_4, resulting in a square pyramidal geometry about sulfur.[1] The O---S bridged dimer has a higher symmetry than the F^----S bridged dimer found in $[HNC_5H_4(CH_3)^+]F^-•SF_4$ (see Chapter 4).

To the best of my knowledge, these structures represent the first examples of THF coordinating to a sulfur atom as well as the $(SF_4•OC_4H_6)_2$ dimer represents a rare structure in which an organic oxygen-base is coordinated to two non-metals. A search of the Cambridge Crystal Database for coordination complexes of oxygen to sulfur gave only one result where dioxane is coordinated to SO_3.[8] The structure of

$(OC_4H_6)_2TeF_4$ consists of monomeric units with Te---O contacts of 2.448(2) and 2.697(2) Å and is different from $(SF_4{\bullet}OC_4H_6)_2$, but similar to $SF_4{\bullet}(OC_4H_6)_2$.[7]

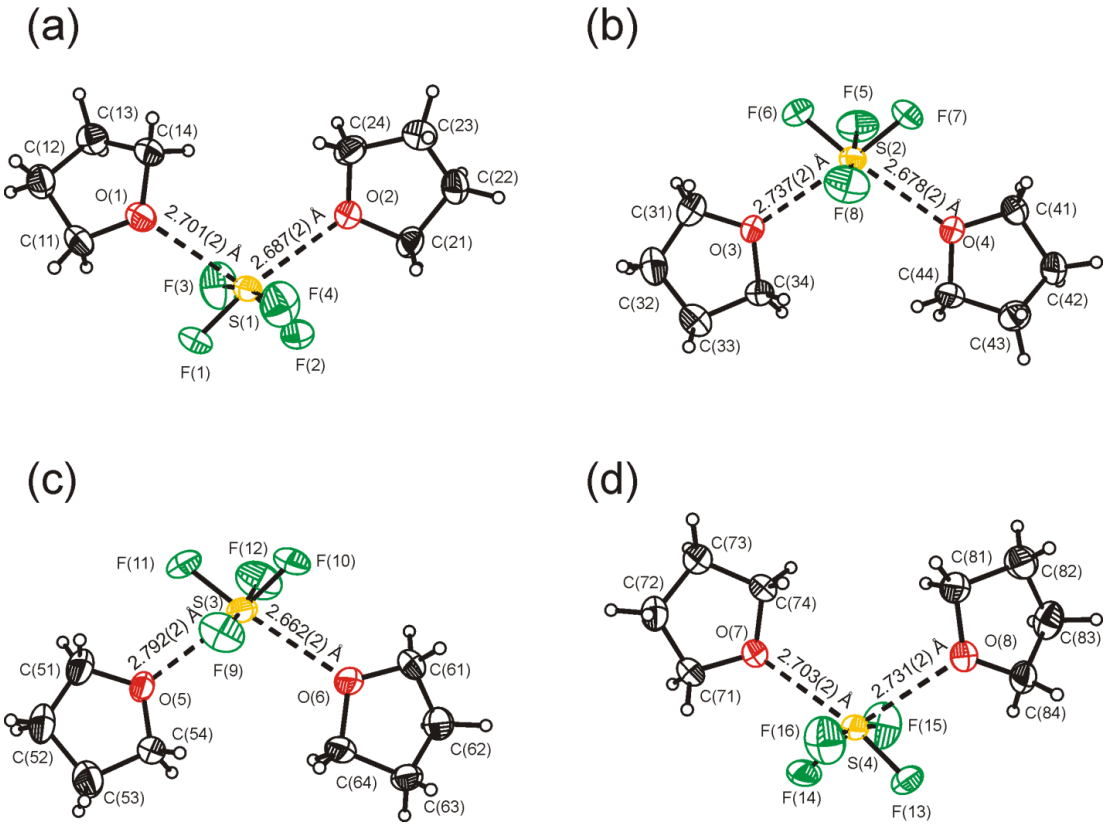

Figure 6.4 Thermal ellipsoid plots of the four crystallographically unique $SF_4{\bullet}(OC_4H_8)_2$ moieties within the asymmetric unit.

6.2.3 Raman Spectroscopy of $SF_4•OC_4H_6$ and $SF_4•(OC_4H_6)_2$

The Raman spectra of solid $SF_4•OC_4H_6$ and $SF_4•(OC_4H_6)_2$ were recorded at −107 °C, (Figure 6.5). The Raman frequencies and tentative assignments of $SF_4•OC_4H_6$ and $SF_4•(OC_4H_6)_2$ are given in Table 6.4 and Table 6.5, respectively. The assignment of Raman bands associated with the THF molecule is based on the data reported by Berthier *et al.*, who used computational chemistry to aid in the vibrational assignment.[9] The band at 848(12) cm^{-1} and several shoulders (2280, 822, and 513 cm^{-1}) in the Raman spectrum of the $SF_4•OC_4H_6$ adduct can be attributed to an impurity of $SF_4•(OC_4H_6)_2$. Most bands attributable to the THF moiety exhibit shifts relative to those of free THF. For example, for the $SF_4•OC_4H_6$ adduct, the most intense band attributable to the THF moiety (ν_s(COC)) has been shifted to a higher frequency (923(53) cm^{-1}) compared to that of neat THF (914(100) cm^{-1}). The most intense band in the Raman spectrum was assigned to the $\nu_s(SF_{2eq})$ mode at 859(100) cm^{-1}, which is at a significantly lower frequency than that of neat liquid SF_4 (896(65) cm^{-1}) reflecting the increase in ionic nature of the $S-F_{eq}$ bonds upon donation of electron density from the Lewis base. The second most intense band appears at 527(84) cm^{-1} and was assigned to the $\nu_s(SF_{2ax})$ mode. This stretching mode is only slightly shifted to lower frequency compared to that of neat SF_4 (536(100) cm^{-1}). The bands attributable to the equatorial S−F stretching modes ($\nu_s(SF_{2eq})$) have been more significantly shifted than the axial S−F stretching modes since they are located *trans* to the oxygen donor atom of THF. As expected, the equatorial SF_2 stretching bands ($\nu_s(SF_{2eq})$ 859(100) cm^{-1} and $\nu_{as}(SF_{2eq})$ 828(39)) show a less pronounced low-frequency shift compared to the SF_{eq} stretching bands found in the Raman spectrum

of the SF_4•$N(C_2H_5)_3$ adduct (ν_s 826/816 cm^{-1} and ν_{as} 691 cm^{-1}),[2] since triethylamine is a much stronger base than THF.

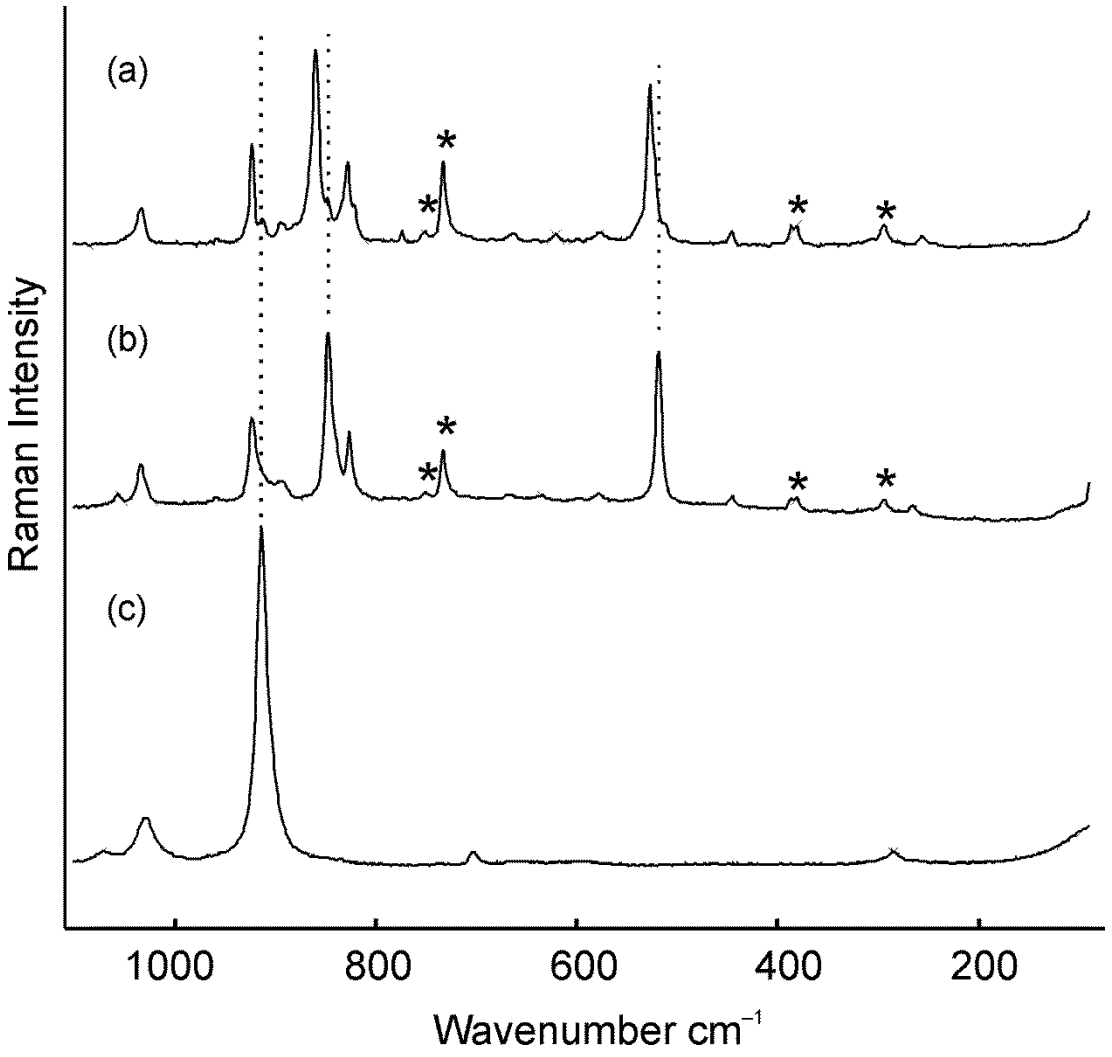

Figure 6.5 Raman spectra of a) SF_4•OC_4H_6 (at −107 °C), b) SF_4•$(OC_4H_6)_2$ (at −107 °C), and c) OC_4H_6 (room temperature). Asterisks (*) denote bands arising from the FEP sample tube.

Table 6.4 Raman Frequencies (cm^{-1}) and Tentative Assignments of $SF_4•OC_4H_6$, OC_4H_6, and SF_4.

$SF_4•OC_4H_6$[a,c]	OC_4H_6[d]	SF_4[b]	Assignment
2996(sh)	2983(sh)		
2987(43)	2962(93)		$\nu_s(CH_2)$
2975(sh)			
2956(31)			
2942(30)	2941(88)		
2917(13)	2913(sh)		$\nu_{as}(CH_2)$
2893(56)	2877(64)		
	2875(98)		
2732(1)			
2684(1)	2661(5)		
	2623(1)		
2584(2)	2575(2)		
1492(12)			$\delta(CH_2)$
1485(9)	1489(15)		
1462(14)			
1450(23)	1449(16)		
1372(10)	1365(3)		
1346(3)	1334(2)		$(CH_2)_{wag}$
1308(9)			
1246(19)			
1239(16)	1228(12)		$(CH_2)_{twist}$
1176(8)	1179(2)		
1141(2)	1070(3)		
1033(19)	1029(13)		$\rho_{rock}(CH_2)$
958(4)			
923(53)	914(100)		$\nu_s(COC)$
913(11)			$\nu_{as}(COC)$
894(9)			$\nu_s(C-C)$
880(sh)	880/866		$\nu_{as}(C-C)$
859(100)		896(65)	$\nu_s(SF_{2eq})$
828(39)		857(22)	$\nu_{as}(SF_{2eq})$
774(6)	703(5)		
663(5)			ring bend
621(4)			
578(5)			ring bend
527(84)		536(100)	$\nu_s(SF_{2ax})$
446(8)		461(16)	$\tau(SF_2)$
381(10)			
295(11)	286(4)		ring pucker
256(6)		237(12)	$\delta_{sc}(SF_{2eq}) - \delta_{sc}(SF_{2ax})$

[a] Signals from the FEP sample tube were observed at: 1383(11), 1297(sh), 1216(4), 751(6), 733(40), 386(10), 295(11) cm^{-1}. Signals from the $SF_4•(OC_4H_6)_2$ impurity were observed at: 2880(sh), 848(12), 822(sh), and 513(sh) cm^{-1}. [b] The Raman spectrum was recorded in a ¼-in. FEP tube at −110°C. Signals from the FEP sample tube were observed at 294(8), 385(12), 733(53), 1216(2), 1306(1), 1382(2) cm^{-1}. Bands at 1382(19), 804(9), 772(11) cm^{-1} were observed for ν(S–O) SOF_2, ν(S–F) SOF_2 and ν(S–F) SF_6 respectively. [c] Acquired at −107 °C. [d] Acquired at room temperature.

Table 6.5 Raman Frequencies (cm^{-1}) and Tentative Assignments of $SF_4•(OC_4H_6)_2$, OC_4H_6, and SF_4.

$SF_4•(OC_4H_6)_2$[a]	$(OC_4H_6)_2$[d]	SF_4[c]	Assignment
2983(63)	2983(sh)		$\nu_s(CH_2)$
	2962(93)		
2940(59)	2941(88)		$\nu_{as}(CH_2)$
	2913(sh)		
2879(70)	2875(98)		
2726(8)	2718(12)		
	2661(5)/		
2669(4)	2623(1)		
2582(2)	2575(2)		$\delta(CH_2)$
1493(16)	1489(15)		
1462(16)			
1448(32)	1449(16)		
1369(8)			
1342(4)	1365(3)		$(CH_2)_{wag}$
1306(4)	1334(2)		
1244(19)	1228(12)		$(CH_2)_{twist}$
1176(7)	1179(2)		
1056(8)	1070(3)		
1033(25)	1029(13)		$\rho_{rock}(CH_2)$
959(3)			
923(49)	914(100)		$\nu_s(COC)$
894(10)			$\nu_s(C-C)$
847(100)		896(65)	$\nu_s(SF_{2eq})$
826(41)		857(22)	$\nu_{as}(SF_{2eq})$
773(2)			
666(3)	703(5)		
634(3)			
579(5)			ring bend
518(91)		536(100)	$\nu_s(SF_{2ax})$
445(7)		461(16)	$\tau(SF_2)$
381(9)			
294(9)[b]	286(4)		ring Pucker
266(6)		237(12)	$\delta_{sc}(SF_{2eq}) - \delta_{sc}(SF_{2ax})$

[a] Signals from the FEP sample tube were observed at FEP: 1383(8), 751(3), 733(28), 387(9), 294(9) cm^{-1}. [b] Overlaps with FEP signals. [c] The Raman spectrum was recorded in a ¼-in. FEP tube at −110°C. Signals from the FEP sample tube were observed at 294(8), 385(12), 733(53), 1216(2), 1306(1), 1382(2) cm^{-1}. Bands at 1382(19), 804(9), 772(11) cm^{-1} were observed for ν(S–O) SOF_2, ν(S–F) SOF_2 and ν(S–F) SF_6 respectively. [d] Sample recorded at room temperature in 5-mm glass NMR tube.

The most intense band in the Raman spectrum of $SF_4•(OC_4H_6)_2$ appears at 847(100) cm^{-1} and was assigned to the $\nu_s(SF_{2eq})$ mode. The second most intense peak (518(91) cm^{-1}) was assigned to the $\nu_s(SF_{2ax})$ mode. These observations agree very well with the expected trend for the sequence neat SF_4, $SF_4•OC_4H_6$, $SF_4•(OC_4H_6)_2$. The more electron density is donated to the sulfur atom on SF_4, the more ionic and weaker the S−F bonds are expected to become, resulting in lower stretching frequencies. The vibrational frequencies of the $\nu_s(SF_{2eq})$ decrease from 896(65) cm^{-1} (SF_4) to 859(100) cm^{-1} ($SF_4•OC_4H_6$), and 847(100) cm^{-1} ($SF_4•(OC_4H_6)_2$). The vibrational frequencies attributable to the $\nu_{as}(SF_{2eq})$ mode are also significantly different from neat liquid SF_4 (860sh cm^{-1}) but the difference between $SF_4•OC_4H_6$ (828(39) cm^{-1}) and $SF_4•(OC_4H_6)_2$ (826(41)cm^{-1}) is not significantly different.

6.2.4 Crystal Structure of $SF_4•(CH_3OCH_2)_2$

Details of data collection parameters and crystallographic information for $SF_4•(CH_3OCH_2)_2$ are given in Table 6.1. Important bond lengths, angles and contacts for $SF_4•(CH_3OCH_2)_2$ are given in Table 6.6.

The adduct, $SF_4•(CH_3OCH_2)_2$, crystallizes in the orthorhombic space group *Pbcm*. The structure of $SF_4•(CH_3OCH_2)_2$ consists of 1,2-dimethoxymethane, in which one Lewis basic oxygen atom is coordinated to one sulfur atom of SF_4 and the second oxygen is coordinated to a second SF_4 molecule. (Figure 6.6) The sulfur atom in SF_4 has two equivalent contacts (2.8692(9) Å) with oxygen atoms of different 1,2-dimethoxyethane molecules, which increase the coordination environment around sulfur to 6.

Table 6.6 Selected Bond Lengths (Å), Contacts (Å), and Angles (°) of $SF_4•(CH_3OCH_2)_2$

Bond Lengths and Contacts, Å			
S1−F1	1.5474(7)	S1---O	2.8692(9)
S1−F1^{i}	1.5474(7)	S1---O1^{i}	2.8692(9)
S1−F2	1.6602(10)	C1−O1	1.4203(13)
S1−F3	1.6736(10)	O1−C2	1.4275(12)
		C2−C2^{ii}	1.498(2)
Bond Angles, deg.			
F1−S1−F1^{i}	99.03(5)	F1−S1−O1^{i}	75.69(3)
F1−S1−F2	87.49(4)	F1^{i}−S1−O1^{i}	168.37(3)
F1^{i}−S1−F2	87.49(4)	F2−S1−O1^{i}	81.98(3)
F1−S1−F3	86.94(4)	F3−S1−O1^{i}	102.93(3)
F1^{i}−S1−F3	86.94(4)	O1---S1---O1^{i}	107.49(4)
F2−S1−F3	171.41(5)	C1−O1−C2	110.98(8)
F1−S1---O1	168.37(3)	C1−O1---S1	106.59(6)
F1^{i}−S1---O1	75.69(3)	C2−O1−S1	126.25(6)
F2−S1−O1	81.98(3)	O1−C2−C2^{ii}	109.98(7)
F3−S1−O1	102.93(3)		

Symmetry codes: (i) x, y, −z+1/2; (ii) x, −y+1/2, −z+1.

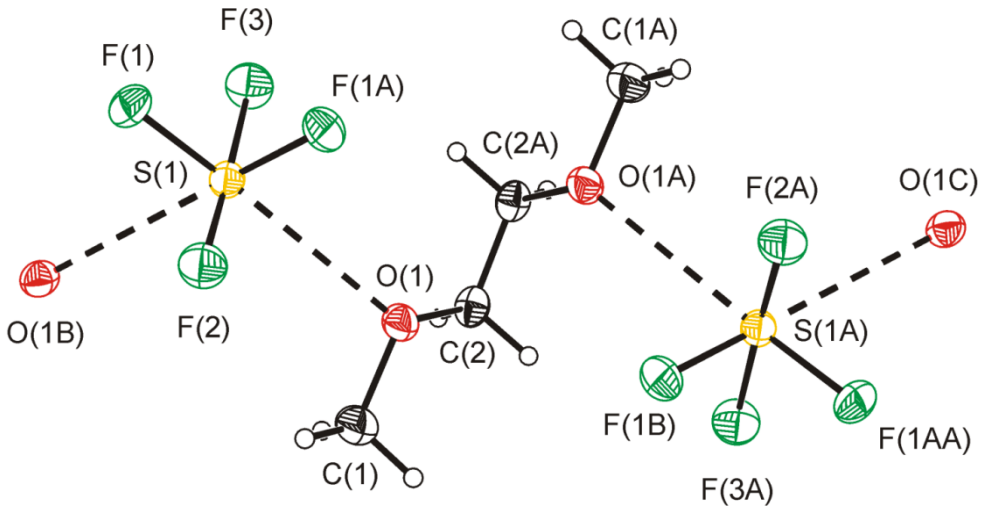

Figure 6.6 Thermal ellipsoid plot of the $SF_4•(CH_3OCH_2)_2$ adduct; thermal ellipsoids are set at 50% probability.

These contacts result in infinite chains along the *c*-axis. The axial fluorine atoms and the sulfur of SF_4 lie in a crystallographic mirror plane, and therefore the equatorial S−F bonds are symmetry-related. As expected, the axial S−F bonds (S1−F2 = 1.6602(10) Å and S1−F3 = 1.6736(10) Å) are significantly longer than the equatorial bonds (S1−F1 = 1.5474(7) Å). The difference in the length of the axial S−F bonds is likely due to packing effects, since both of the axial fluorines form no significant contacts. The O1---S1---O1^{i} contact angle is 107.49(4)°, which is much larger than the F_{eq}−S−F_{eq} angle (99.03(5)°), because of the location of the lone pair on sulfur. The 1,2-dimethoxyethane molecule lies on a C_2-axis, thus half of the molecule is related by symmetry and the 1,2-dimethoxyethane molecule adopts the stable gauche conformation.[10] The view along the *c*-axis shows the two different orientations of adjacent SF_4-1,2-dimethoxyethane chains (see Figure 6.7).

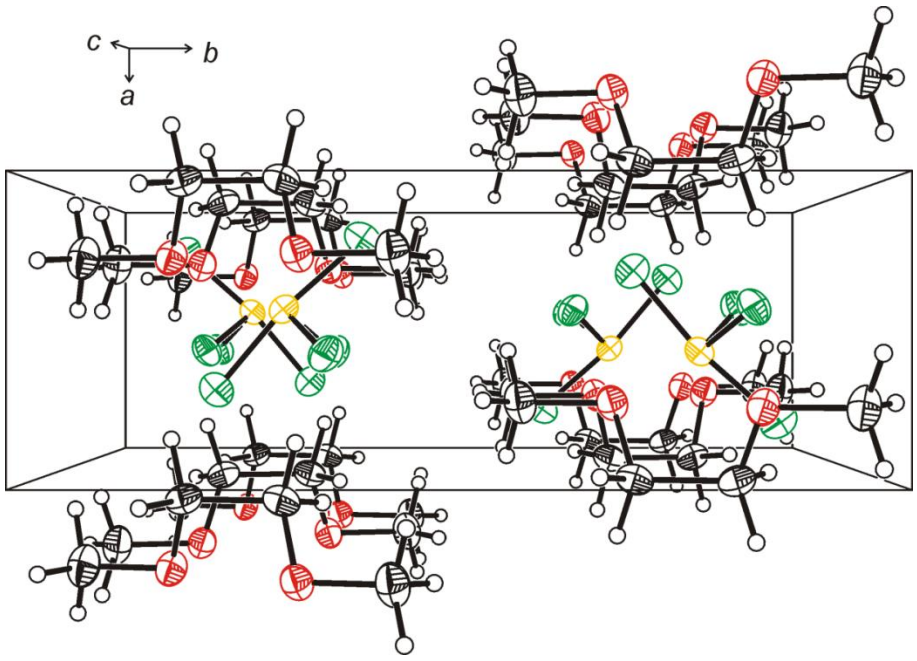

Figure 6.7 View along the *c*-axis of the thermal ellipsoid plot of SF_4•$(CH_3OCH_2)_2$. Thermal ellipsoids set at 50% probability.

It was hypothesized that 1,2-dimethoxyethane could act as a bidentate ligand towards sulfur, as seen towards metal complexes and TeF_4.[11,12] A bidentate coordination may be geometrically disfavoured because of the smaller size of sulfur compared to tellurium. It is interesting to note that TeF_4 forms an adduct in which two 1,2-dimethoxyethane ligands coordinate to Te in a bidentate fashion. The resulting coordination number of 9 about Te is possible because of its much larger radius.

6.2.5 Raman Spectroscopy of SF_4•$(CH_3OCH_2)_2$

The Raman spectrum of SF_4•$(CH_3OCH_2)_2$ at −107 °C is shown in Figure 6.8. The Raman frequencies and tentative assignments are listed in Table 6.7. The Raman spectrum at −107 °C contains bands associated with the SF_4 and 1,2-dimethoxyethane moieties, and low-intensity signals associated with residual neat liquid SF_4. The assignment of Raman bands associated with the 1,2-dimethoxyethane is based on the previous assignments by Yoshida and Matsuura using DFT calculations.[13]

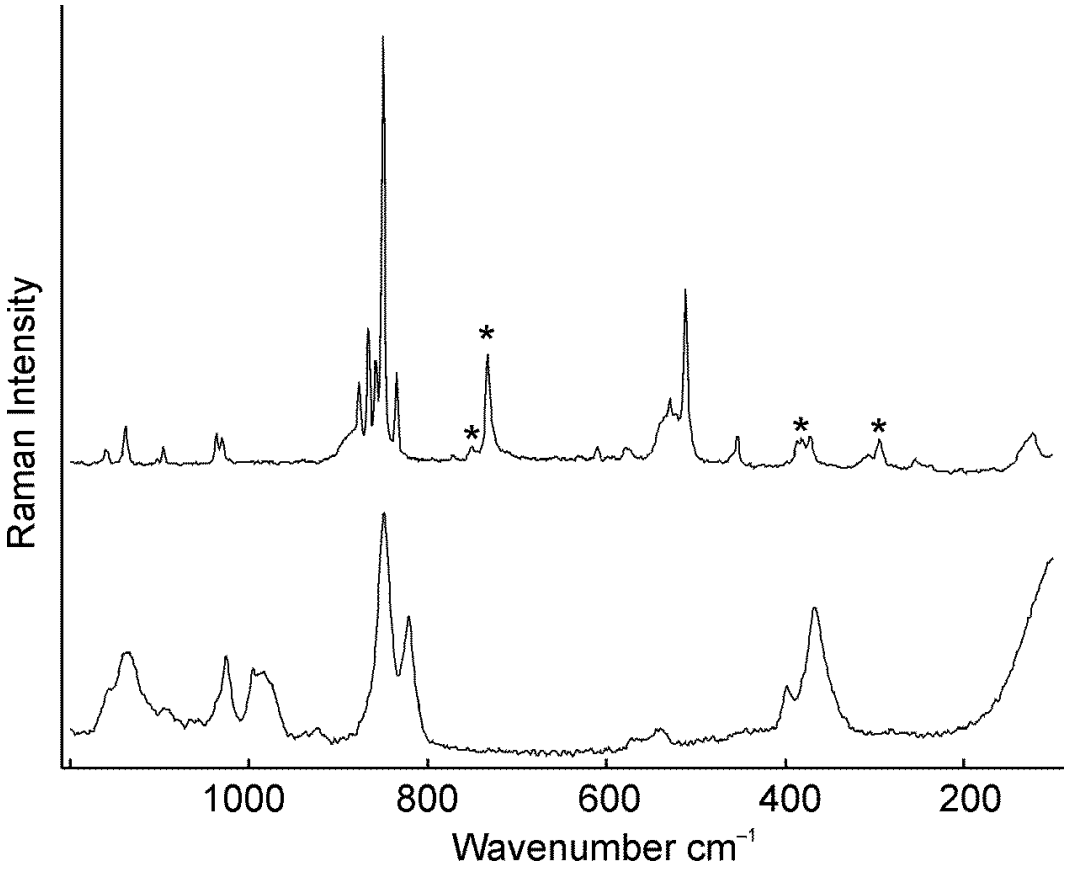

Figure 6.8 Raman Spectrum of $SF_4 \bullet (CH_3OCH_2)_2$ (top) and neat 1,2-dimethoxyethane (bottom). Asterisks (*) denote bands arising from the FEP sample tube.

Table 6.7 Raman Frequencies (cm^{-1}) and Tentative Assignments of $SF_4•(CH_3OCH_2)_2$, $(CH_3OCH_2)_2$, and SF_4.

Vibrational Frequencies, cm^{-1}			
$SF_4•(CH_3OCH_2)_2$[a,e]	$(CH_3OCH_2)_2$[d]	SF_4[c]	Assignments
3000(21)	2984(39)		
2960(10)	2945(51)		
2934(13)			
2916(22)	2922(52)		
2903(19)	2890(70)		ν(C−H)
2884(9)			
2855(14)	2842(74)		
2824(24)	2818(100)		
2811(sh)			
2800(sh)			
2732(4)	2719(10)		
1479(29)	1472(24)		CH_2 $_{scis}$, CH_3 asym def.
1460(15)			CH_3 asym def, CH_2 scis.
1454(8)			CH_3 sym def, CH_2 scis.
1447(6)	1451(30)		
1418(4)			CH_2 wag, C–C str, CH_3 def.
1306(4)			
1289(12)	1286(7)		CH_2 twist
1250(3)	1251(3)		CH_2 twist, CH_3 rock
1160(3)			CH_3 rock
1138(10)	1135(7)		CH_3–O str, C–O str
1096(4)			CH_2 rock, CH_3 rock
1036(8)			CH_2 rock, CH_3–O str, C–O str
1030(7)	1026(7)		CH_3–O str, C–C str
	995(5)		
	984(5)		
877(19)			
866(31)		896(65)	$\nu_s(SF_{2eq})$
858(24)	849(24)		
850(100)			C–O str, CH_2 rock, C–C Str
835(22)	821(13)	857(22)	$\nu_{as}(SF_{2eq})$
773(1)			
610(4)			
579(3)	539(1)		CCO def, δ(COC) , CH_2 rock
529(16)			
522(12)		536(100)	$\nu_s(SF_{2ax})$
512(40)			
453(7)		461(16)	$\tau(SF_2)$
381(6)	398(4)		
372(8)	367(12)		COC bend, CCO def
308(2)			COC bend, CCO def
294(7)[b]			CCO def, COC bend, C–C tor
255(3)		237(12)	$\delta_{sc}(SF_{2eq}) - \delta_{sc}(SF_{2ax})$
123(8)			C–C tor, CH_3–O

[a] Signals from the FEP sample tube were observed at: 1383(6), 1214(1), 733(24), 751(3), 294(7), 387(6). [b] Signals overlap with those of FEP. [c] The Raman spectrum was recorded in a ¼–in FEP tube at −110°C. Signals from the FEP sample tube were observed at 294(8), 385(12), 733(53), 1216(2), 1306(1), 1382(2) cm^{-1}. Bands at 1382(19), 804(9), 772(11) cm^{-1} were observed for ν(S–O) SOF_2, ν(S–F) SOF_2 and ν(S–F) SF_6 respectively. [d] Sample recorded at room temperature in 5-mm glass NMR tube.

The majority of the peaks associated with the 1,2-dimethoxethane remain un-shifted relative to the neat liquid. The bands in the Raman spectrum of $SF_4•(CH_3OCH_2)_2$ attributable to the $\nu_s(SF_{2eq})$ mode are at lower frequency (877(19) and 866(31) cm^{-1}) than that of neat liquid SF_4 (896(65) cm^{-1}). The band attributable to the $\nu_{as}(SF_{2eq})$ mode is found at 835(22) cm^{-1} which has also a lower frequency than that of neat SF_4 (857(22) cm^{-1}). The symmetric $S-F_{ax}$ stretch (529(16), 522(12) cm^{-1}) are at significantly lower frequencies than that of solid neat SF_4 ($\nu_s(SF_{2ax})$ = 536(92), 532(100) cm^{-1}). The shift to lower frequencies of these stretches of the adduct relative to that of neat SF_4 is a result of the longer and weaker S−F bonds in the adduct.

6.2.6 Crystal Structure of $SF_4•(O=C_5H_8)_2$

Details of data collection parameters and crystallographic information for $SF_4•(O=C_5H_8)_2$ are given in Table 6.1. Important bond lengths, angles and contacts for $SF_4•(O=C_5H_8)_2$ are listed in Table 6.8.

The structure consists of discrete units of SF_4 with two long contacts (S1---O1 = 2.7880(12) Å and S1---O2 = 2.7592(12) Å) to the oxygen atoms on two crystallographically unique cyclopentanone molecules. (Figure 6.9) Both cyclopentanone molecules have essentially the same bond lengths and angles and are not significantly different from that of neat cyclopentanone.[14]

Table 6.8 Selected Bond Lengths (Å), Contacts (Å), and Angles (°) of SF_4•$(O=C_5H_8)_2$

Bond Lengths and Contacts, Å					
S1−F1	1.5455(10)	O1−C1	1.2151(18)	O2−C6	1.2157(19)
S1−F2	1.5478(10)	C1−C2	1.507(2)	C6−C7	1.509(2)
S1−F3	1.6579(10)	C1−C5	1.507(2)	C6−C10	1.510(2)
S1−F4	1.6674(10)	C2−C3	1.527(2)	C8−C7	1.525(2)
S1---O2	2.7592(12)	C3−C4	1.528(2)	C8−C9	1.532(2)
S1---O1	2.7880(12)	C4−C5	1.525(2)	C9−C10	1.527(2)
				O2−C6	1.2157(19)
Bond Angles, deg.					
F1−S1−F2	98.24(6)	C1−O1---S1	120.80(10)	C6−O2---S1	118.73(10)
F1−S1−F3	87.70(6)	O1−C1−C2	125.16(14)	O2−C6−C7	125.04(14)
F2−S1−F3	87.24(6)	O1−C1−C5	125.92(14)	O2−C6−C10	126.08(14)
F1−S1−F4	87.21(6)	C2−C1−C5	108.92(13)	C7−C6−C10	108.88(13)
F2−S1−F4	87.19(6)	C1−C2−C3	104.91(12)	C7−C8−C9	103.93(13)
F3−S1−F4	171.85(6)	C2−C3−C4	103.98(13)	C6−C7−C8	105.23(12)
O2---S1---O1	105.46(4)	C5−C4−C3	103.57(13)	C10−C9−C8	103.76(13)
		C1−C5−C4	104.50(13)	C6−C10−C9	104.30(13)
		F1−S1---O1	177.00(5)	F1−S1---O2	77.41(5)
		F2−S1---O1	78.83(5)	F2−S1---O2	173.57(5)
		F3−S1---O1	91.51(5)	F3−S1---O2	87.85(5)
		F4−S1---O1	93.25(5)	F4−S1---O2	97.24(5)

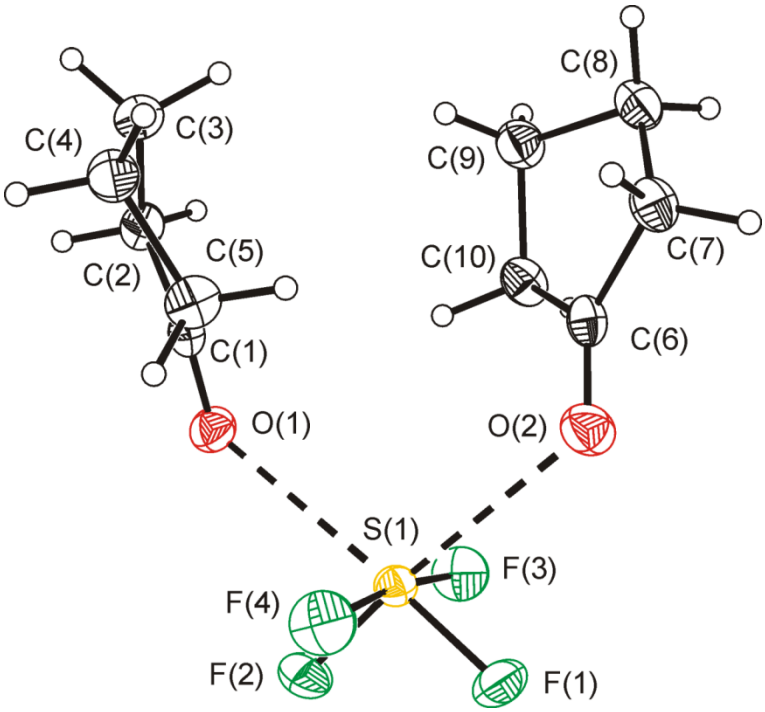

Figure 6.9 Thermal ellipsoid plot of the SF_4•$(O{=}C_5H_8)_2$ adduct; thermal ellipsoids are set at 50% probability.

As in neat SF_4 and the other SF_4•*O*-base adducts, the S−F_{eq} bond lengths (1.5455(10) and 1.5478(10) Å) are shorter than the S−F_{ax} bond lengths (1.6579(10) and 1.6674(10) Å). The lone pair on sulfur resides directly in between both S---O contacts which form an O---S---O angle of 105.46(4)°. The small size of the carbon thermal ellipsoids suggests less thermal motion in the carbon ring of cyclopentanone than that found in the THF ring of the SF_4•OC_4H_6 adduct. The C=O lengths of the cyclopentanone molecules in the SF_4 adduct (1.2151(18) and 1.2157(19) Å) are not significantly different from those of the neat cyclopentanone (1.2109(15) and 1.2148(15) Å)) reflecting the weakness of the acid-base interaction.[14]

6.2.7 Raman Spectroscopy of SF_4•$(O=C_5H_8)_2$

The Raman spectrum of solid SF_4•$(O=C_5H_8)_2$ recorded at −107 °C is shown in Figure 6.10. The Raman frequencies and tentative assignments are listed in Table 6.9. The Raman spectrum contains peaks associated with the SF_4 and cyclopentanone moieties. The assignment of Raman bands associated with cyclopentanone are based on the previously reported assignments by Cataliotti and Paliani.[15] A number of the peaks associated with the cyclopentanone ring are shifted and exhibit extra splittings presumably because of vibrational coupling of the two $O=C_5H_8$ molecules in the adduct. The signals associated with SF_4 are significantly shifted and are much sharper than that of neat SF_4 at the same temperature. For example, the $\nu_s(SF_{2eq})$ mode is a single band shifted to 872(88) cm^{-1} from that of neat liquid SF_4 (896(65) cm^{-1}).

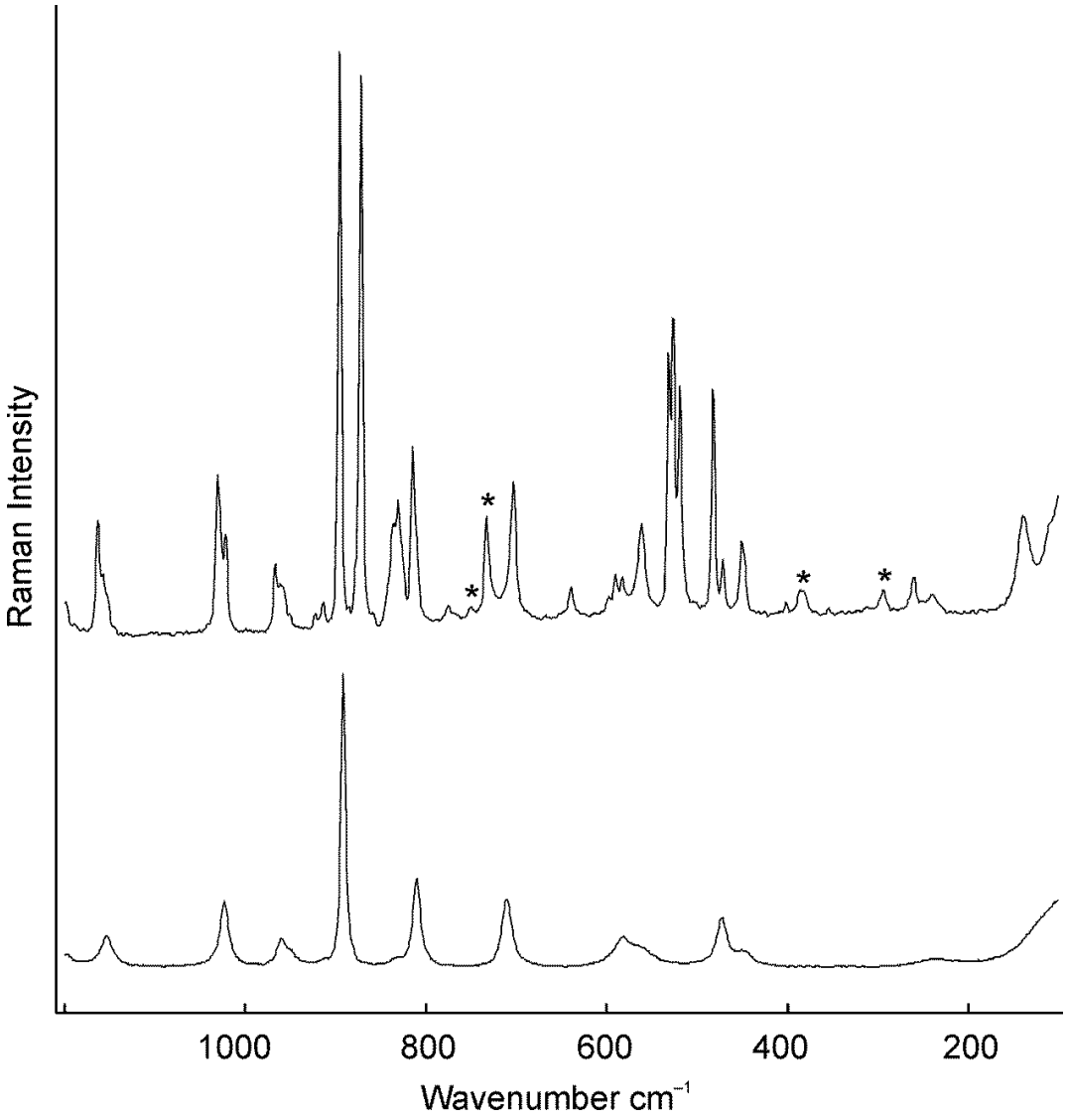

Figure 6.10 Raman spectra of $SF_4 \bullet (O=C_5H_8)_2$ (top) and neat cyclopentanone ($O=C_5H_8$) (bottom). Asterisks (*) denote bands arising from the FEP sample tube.

Table 6.9 Raman Frequencies (cm^{-1}) and Tentative Assignments of $SF_4•(O=C_5H_8)_2$ (−107 °C), $O=C_5H_8$, and SF_4.

$SF_4•(O=C_5H_8)_2$[a]	$O=C_5H_8$[b]	SF_4[c]	Assignments
2978(100)	2969(100)		ν(C−H)
2969(82)			
2957(42)			
2941(19)			
2918(sh)			
2914(58)			
2906(53)	2902(84)		
2901(55)			
2890(sh)			
2886(56)	2883(95)		
2787(3)	2802(7)		
2616(3)	2606(3)		
1724(16)	1743(18)		ν(C–O)
1712(34)	1728(18)		
1507(1)			
1474(8)	1470(11)		CH_2 def.
1470(3)			
1459(25)	1455(22)		
1453(38)			
1403(35)	1410(23)		
1319(6)	1309(2)		
1286(12)	1278(8)		CH_2 wag
1275(12)	1268(8)		CH_2 wag
1242(22)	1231(9)		CH_2 twist
1232(10)			
1198(4)	1197(2)		
1163(18)			
1158(sh)			CH_2 rock
1152(sh)	1153(9)		
1030(25)	1023(20)		
1021(20)			
967(12)			Ring mode
961(8)	960(8)		Ring mode
922(3)			CH_2 rock
914(4)			
895(89)	892(88)		Ring mode
872(88)		896(65)	$\nu_s(SF_{2eq})$
836(18)			Ring mode
831(21)		857(22)	$\nu_{as}(SF_{2eq})$
814(29)	810(27)		Ring mode
775(2)			
703(23)	711(20)		Ring mode
639(5)			
590(4)	581(10)		Ring mode
583(4)			
561(14)			Ring mode
532(41)	538(30)		
526(47)		536(100)	$\nu_s(SF_{2ax})$
519(36)			
482(36)		461(16)	$\tau(SF_2)$

Table 6.9 continued

471(8)	473(15)		C–O def
450(12)	451(sh)		C–O def
401(2)			
382(3)			
355(1)			
260(5)		237(12)	$\delta_{sc}(SF_{2eq}) - \delta_{sc}(SF_{2ax})$
239(3)	236(2)		
139(14)			
97(21)			

[a] Signals from the FEP sample tube were observed at: 1384(3), 751(1), 733(18), 598(1), 386(3), 294(4) cm^{-1}. [b] Sample acquired at room temperature in a 5-mm glass NMR tube. [c] The Raman spectrum was recorded in a ¼–in FEP tube at −110°C. Signals from the FEP sample tube were observed at 294(8), 385(12), 733(53), 1216(2), 1306(1), 1382(2) cm^{-1}. Bands at 1382(19), 804(9), 772(11) cm^{-1} were observed for ν(S–O) SOF_2, ν(S–F) SOF_2 and ν(S–F) SF_6 respectively.

6.3 Summary and Conclusion

For the first time, SF_4•oxygen-base adducts have been synthesized, isolated, and structurally characterized. Adduct formation was observed with the oxygen bases: THF, 1,2-dimethoxethane, and cyclopentanone at low temperatures. It was crucial to handle these adducts at temperatures below −60 °C to avoid dissociation because of the weakness of their Lewis-acid-base interaction. The adducts were characterized by low-temperature Raman spectroscopy and X-ray crystallography. Each structure contains sulfur atoms which are coordinated by two Lewis-basic oxygens, increasing the coordination environment about sulfur in SF_4 from 4 to 6. This observation is in contrast to SF_4•*N*-base adducts in which only one nitrogen base coordinates to sulfur tetrafluoride to form a square pyramidal geometry about sulfur.[1,2] The S---N contacts lengths (2.141(2) to 2.5140(18) Å, for F_4S•4-$NC_5H_4N(CH_3)_2$ and SF_4•NC_5H_5, respectively)[1] in the SF_4•*N*-base adducts are much shorter than the S---O contact lengths (2.663(3) to 2.8692 (9) Å). The stronger Lewis acid-base interaction in the SF_4•*N*-base adducts results in donation of electron density to sulfur and, as a consequence, a lowering of the Lewis acidity of sulfur in SF_4, and in addition, a closer proximity with the nitrogen base. Therefore, both electronic and steric arguments likely contribute in preventing further coordination of another nitrogen base.

Whereas sulfur tetrafluoride exclusively formed hexacoordinated adducts with oxygen-bases, and pentacoordinated adducts with nitrogen-bases, both types of coordination geometries are observed for fluorides (see Chapter 4). The contact lengths between the SF_4•*O*-base adducts are on average longer than those in the SF_4•F^-(H)*N*-base adducts. The S---F^- contact lengths and the F^----S---F^- angles have

a much larger range than the S---O contact lengths and the O---S---O bond angles in the SF_4•*O*-base adducts since the basicity of F^- greatly depends on the strength of the hydrogen bond to the protonated N-base. In SF_4•F^-(H)*N*-base adducts which form chain-type structures or dimers, the sulfur atom has a coordination environment of 6, the same as the SF_4•*O*-base adducts. In other cases, such as the $[HNC_5H_3(CH_3)_2^+]_2[SF_5^-]F^-$•$SF_4$ salt, only one significant S---F^- contact (2.5116(12) Å) with SF_4 is present, yielding a square pyramidal geometry about the sulfur atom. The sulfur atom in this SF_4 has an additional contact (2.900(5) Å) with one of the fluorine atoms on the SF_5^- anion; however, it does not distort the square pyramidal geometry to a noticeable extent (see Chapter 4). The extreme case, which is most dissimilar to the SF_4•*O*-base adducts, is when naked fluoride coordinates to sulfur tetrafluoride to form the square pyramidal SF_5^- anion.

This is the first report of the coordination of oxygen-bases to SF_4. Particularly, the characterization of the SF_4•ketone adduct (SF_4•$O{=}C_5H_4$) is of great significance, since SF_4 can serve as a fluorinating agent towards carbonyl groups. It is, however, postulated that SF_3^+•ketone adducts are the intermediates in the fluorination reaction.

These adducts offer the first extensive view of dative O---S(IV) bonds. A summary of trends in structure and vibrational frequencies of these adducts can be seen in Table 6.10. All of O---S contacts are within the sum of van-der-Waals radii (3.32 Å). The longest S---O contacts are found in the SF_4•$(CH_3OCH_2)_2$ adduct (2.8692(9) Å). Despite the fact that THF is the strongest donor, the 1:1 adduct SF_4•OC_4H_8 has relatively long contacts since one oxygen donor atom bridges two Lewis acidic sulfur atoms. As expected, the 2:1 adduct (SF_4•OC_4H_8) has the shortest contact (2.663(3) Å).

Quantification of Lewis basicity is difficult, since it depends on the nature of the Lewis acid.[16] The most extensive list of Lewis basicity values is that for the BF_3 affinity scale.[16] Although BF_3 is a harder acid than SF_4, it was found that the trends in BF_3 affinity values are in agreement with the current observations. The higher frequencies (877(19) and 866(31) cm^{-1}) of the $\nu_s(SF_{2eq})$ stretch in the $SF_4•(CH_3OCH_2)_2$ adduct agrees well with the weak donor properties of 1,2-dimethoxyethane (74.67(19) kJ mol^{-1} (BF_3)) when compared with the stronger donor properties of THF (90.40(28) kJ mol^{-1} (BF_3)).[17]

It is possible that cyclopentanone is not basic enough to act as a donor towards two SF_4 molecules, as observed with THF, but the 1:1 adduct ($SF_4•O=C_5H_8$) cannot be excluded based on my results. The oxygen is not sterically confined; therefore, one would expect it would have the geometrical abilities to interact with more than one SF_4, if it were electronically favourable.

Table 6.10 Selected Structural and Vibrational Data in isolated SF_4•*O*-Base Adducts.

Compound	$SF_4•OC_4H_8$	$SF_4•(OC_4H_8)_2$	$SF_4•(CH_3OCH_2)_2$	$SF_4•(O=C_5H_8)_2$
S---O (Å)	2.7892(18) 2.8022(19)	2.662(2) 2.792(2)	2.8692(9)	2.7592(12) 2.7880(12)
O---S---O (°)	102.03(5) 102.12(6)	107.25(7) 112.86(7)	107.49(4)	105.46(4)
S−F_{eq} (Å)	1.5344(17) 1.5448(16)	1.5275(19) 1.5457(18)	1.5474(7)	1.5455(10) 1.5478(10)
S−F_{ax} (Å)	1.6430(17) 1.6610(18)	1.626(2) 1.658(2)	1.6602(10) 1.6736(10)	1.6579(10) 1.6674(10)
$\nu_s(SF_{2eq})$ (cm^{-1})	859(100)	847(100)	877(19), 866(31)	872(88)
Donor Strength[a]	90.40(28)	90.40(28)	74.67(19)	77.44(45)

[a] Donor strength (kJ mol^{-1}) using the BF_3 affinity scale, from 17.

References

(1) Goettel, J. T.; Chaudhary, P.; Hazendonk, P.; Mercier, H. P. A.; Gerken, M. In *95th Canadian Chemistry Conference* Calgary, Alberta, Canada 2012, Abstract #353.

(2) Goettel, J. T.; Chaudhary, P.; Hazendonk, P.; Mercier, H. P. A.; Gerken, M. *Chem. Commun.* **2012**, *48*, 9120–9122.

(3) Muetterties, E. L.; U.S. Patent 2,729,663: 1959.

(4) Azeem, M. *Pak. J. Sci. Ind. Res.* **1967**, *10*, 10-12.

(5) Sass, C. S.; Ault, B. S. *J. Phys. Chem.* **1985**, *89*, 1002-1006.

(6) Shlykov, S. A.; Giricheva, N. I.; Titov, A. V.; Szwak, M.; Lentz, D.; Girichev, G. V. *Dalton Trans.* **2010**, *39*, 3245-3255.

(7) Lentz, D.; Szwak, M. *Angew. Chem. Int. Ed.* **2005**, *44*, 5079-5082.

(8) Richtera, L.; Toužín, J. *Chemické listy* **2004**, 633-633.

(9) Cadioli, B.; Gallinella, E.; Coulombeau, C.; Jobic, H.; Berthier, G. *J. Phys. Chem.* **1993**, *97*, 7844-7856.

(10) Jaffe, R. L.; Smith, G. D.; Yoon, D. Y. *J. Phys. Chem.* **1993**, *97*, 12745-12751.

(11) Belli Dell'Amico, D.; Bradicich, C.; Labella, L.; Marchetti, F. *Inorg. Chim. Acta* **2006**, *359*, 1659-1665.

(12) Shlykov, S. A.; Giricheva, N. I.; Titov, A. V.; Szwak, M.; Lentz, D.; Girichev, G. V. *Dalton Trans.* **2010**, *39*, 3245-3255.

(13) Yoshida, H.; Matsuura, H. *J. Phys. Chem. A* **1998**, *102*, 2691-2699.

(14) Yufit, D. S.; Howard, J. A. K. *Acta Crystallogr., Sect. C: Cryst. Struct. Commun.* **2011**, *67*, o104-o106.

(15) Cataliotti, R.; Paliani, G. *Chem. Phys. Lett.* **1973**, *20*, 280-283.

(16) Laurence, C.; Gal, J. F. *Lewis Basicity and Affinity Scales*; John Wiley and Sons: Chichester, 2010.

(17) Maria, P. C.; Gal, J. F. *J. Phys. Chem.* **1985**, *89*, 1296-1304.

7 Summary and Directions for Future Work

7.1 Conclusions

The chemistry of sulfur tetrafluoride was significantly extended in the present work. The previously known [$ReO_2F_4^-$], [$IO_2F_4^-$], and [IOF_4^-] anions were synthesized in one-step reactions of SF_4 with the oxo-anions ReO_4^-, IO_4^-, and IO_3^-, respectively. These reactions gave excellent yields and were easy to separate from the by-product, SOF_2 and solvents (CH_3CN or aHF). These reactions are the first reported use of SF_4 as a selective fluorinating agent towards oxo-anions to form oxide-fluoride anions.

A large range of compounds were synthesized from mixtures of pyridine and pyridine derivatives with HF and SF_4. These compounds exhibit a wide range of bonding modalities in the solid state, and provide a detailed view into the interaction between SF_4 and fluoride.

The solid-state structure of SF_4 was, for the first time, fully elucidated. The structure can best be described as a network with weak intermolecular S---F contacts formed exclusively with the axial fluorines, which are more ionic in nature. A similar structural motif was observed in the novel $[HNC_5H_3(CH_3)_2^+]_2F^-[SF_5^-]\bullet 4SF_4$ salt which contains layers of SF_4.

For the first time, adducts between sulfur tetrafluoride and oxygen bases were isolated and structurally characterized. These adducts exhibit two long S---O contacts per SF_4 molecule, characteristic of the lower Lewis basicity of the oxygen bases compared to that of the nitrogen bases or fluoride. These compounds offer the first look at S(IV)---OR_2 interactions in the solid state. The $SF_4\bullet(O{=}C_5H_8)_2$ adduct proves

that carbonyl groups interact with SF_4, which could be the first step in mechanism of fluorination of carbonyl groups by SF_4.

7.2 Directions for Future Work

The chemistry of sulfur tetrafluoride with other oxo-anions should be explored. The reaction of SF_4 with main-group oxo-anions such as ClO_x^-, BrO_x^-, SO_4^{2-}, PO_4^{3-}, NO_3^- and CO_3^- could possibly result in clean efficient methods for obtaining oxide-fluoride species.

The introduction of organic compounds containing carbonyl, hydroxyl and carboxylic acid substituents to the SF_4-HF-nitrogen base mixtures at low-temperatures is the next step for elucidating the mechanism of fluorination of these respective groups by SF_4 in the presence of nitrogen-bases. For example, addition of cyclopentanone to $[HNC_5H_4(CH_3)^+]F^-\bullet SF_4$ in the presence of excess SF_4 could reveal interesting Lewis acid-base interactions in the solid state at low temperature.

Adducts between other oxygen-bases (acetone, dioxanes, esters) should be characterized by Raman and X-ray crystallography. Computational chemistry should be used to confirm the geometries and Raman frequencies of these adducts. Also molecules containing both nitrogen-bases and oxygen-bases should be used, such as the reaction of SF_4 with caffeine, in light of the possibility of forming two contacts between sulfur and two different atoms.

Finally, exploring the chemistry of sulfur fluorides as ligands towards transition-metal complexes should be further pursued, such as the reaction of sulfur fluorides with tungsten carbonyl complexes. Although no conclusive evidence was

obtained for the formation of these species in this study, it is likely that these species can be isolated in a variety of systems, and their pursuit is worthwhile.